CHEMICAL INCORPORATION OF POLYHEDRAL OLIGOMERIC SILSESQUIOXANE INTO THERMOSET MATRICES

By

Hosouk Cho

A Dissertation
Submitted to the Faculty of
Mississippi State University
in Partial Fulfillment of the Requirements
for the Degree of Doctor of Philosophy
in Organic Chemistry
in the Department of Chemistry

Mississippi State, Mississippi

August 2006

CHEMICAL INCORPORATION OF POLYHEDRAL OLIGOMERIC

SILSESQUIOXANE INTO THERMOSET MATRICES

By

Hosouk Cho

Approved:

Charles U. Pittman, Jr. Professor of Chemistry (Director of Dissertation)	Hossein Toghiani Associate Professor of Chemical Engineering (Committee Member)
Keith T. Mead Professor of Chemistry Department Head (Committee Member)	Michael E. Koscho Assistant Professor of Chemistry (Committee Member)
Gloria Thomas Assistant Professor of Chemistry (Committee Member)	Stephen C. Foster Associate Professor of Chemistry (Graduate Coordinator of the Department of Chemistry)

Philip B. Oldham
Dean of the College of Arts & Science

Name: Hosouk (Jenny) Cho

Date of Degree: August 5, 2006

Institution: Mississippi State University

Major Field: Organic Chemistry

Major Professor: Dr. Charles U. Pittman, Jr.

TITLE OF STUDY: CHEMICAL INCORPORATION OF POLYHEDRAL OLIGOMERIC SILSESQUIOXANE INTO THERMOSET MATRICES

Pages in Study: 232

Candidate for Degree of Doctor of Philosophy

A new class of organic-inorganic hybrid nanocomposites containing well-defined polyhedral oligomeric silsesquioxane (POSS) monomers, which have been copolymerized with organic monomers, were synthesized.

Poly(isobutyl methacrylate-co-butanediol dimethacrylate-co-3-methacrylylpropyl-heptaisobutyl(T_8)polyhedral oligomeric silsesquioxane) (P(iBMA-co-BDMA-co-MA-POSS)) nanocomposites with different crosslink densities (BDMA loadings of 1, 3 and 5 wt%) and different MA-POSS percentages (5, 10, 15, 20 and 30 wt%) have been synthesized by radical-initiated terpolymerization. Linear P(iBMA-co-MA-POSS) copolymers were also prepared. Viscoelastic properties and morphologies were studied by DMTA (dynamic mechanical thermal analysis) and TEM (transmission electron microscopy).

Two types of inorganic-organic hybrid polyhedral oligomeric silsesquioxane (POSS) / vinyl ester (VE) nanocomposites were synthesized. The first type contained a

mixture of T_8, T_{10} and T_{12} cages, each multifunctionalized with 3-methacrylylpropyl groups. The second type contained octa(3-methacrylylpropyldimethylsiloxyl)(T_8)POSS. VE/POSS samples with weight ratios of 99/1, 97/3, 95/5, 90/10, 85/15 and 80/20 were prepared of each type. The nanocomposites were characterized by DMTA, TEM, scanning electron microscopy (SEM), X-ray energy dispersive spectroscopy (X-EDS), swelling, extraction and FT-IR.

Three classes of inorganic-organic hybrid phenolic resin/polyhedral oligomeric silsesquioxane (POSS) nanocomposites were also synthesized via condensation polymerization. The POSS macromers employed included multifunctional dichloromethylsilylethylheptaisobutyl(T_8)POSS, trisilanolheptaphenyl-POSS, and poly(phenylsilsesquioxane) uncured POSS. A nonfunctional octaisobutyl(T_8)POSS was blended into the uncured phenolic resin followed by curing under the same conditions as those used for the other three nanocomposites classes. Phenolic/POSS samples with weight ratios of 99/1, 97/3, 95/5 and 90/10 were prepared of each type.

Octaaminophenyl(T_8)POSS and dodecaaminophenyl(T_{12})POSS were synthesized, characterized and then incorporated into two types of thermoset resins: (1) the bisphenol-F-based cyanate ester resin, PT-15, and (2) epoxy (Epon 828, Shell Chemical Corp.)/ 4,4'-diaminodiphenylmethane (DDM) resin, respectively, to make two series of nanocomposites. The sum of amino groups in both DDM and POSS were held in a 1:1 mole ratio to the epoxy groups. EPON-828/POSS/DDM (78.63/0/21.37, 77.48/5/17.52, 76.34/10/13.66, 74.05/20/5.95 and 72.28/27.72/0 wt/wt/wt compositions for both series) was prepared. PT-15/POSS composites (99/1, 97/3 and 95/5 wt/wt compositions for both types) were also prepared.

DEDICATION

I would like to dedicate this dissertation to my parents; Siho Cho and Kihyo Ko

ACKNOWLEDGMENTS

I would like to express my sincere gratitude to Dr. Charles U. Pittman, Jr. for his guidance, advice, suggestions and the tough time that he gave me.

Sincere appreciation is extended to my graduate committee members Dr. Hossein Toghiani, Dr. Keith T. Mead, Dr. Michael E. Koscho, Dr. Gloria Thomas, Dr. Andrzej Sygula and Dr. Tingyu Li for their constant and continued assistance, encouragement, helpful suggestions, and discussions. All professors in the Department of Chemistry are also thanked for their insights and guiding during my studies.

Special thanks go to Dr. Guizhi Li, Dr. Lichang Wang, Dr. Aihua Zhou, Dr. Dinesh Mohan, Dr. Mitra Yoonessi and Dr. Kaiwen Liang for their valuable help.

Appreciation is also expressed to Sang Ho Lee, Moses G. Njugo, Gang Huang, Guozhong Ye, Yingquan Song, Yongcheng Zhang, Sidika Polat Cakir, Chengli Zhu, and all other colleagues and friends for their friendship and valuable help.

Finally, I would like to extend my most grateful thanks to my family for everything they brought to my life and their endless love.

TABLE OF CONTENTS

CHAPTER Page

CHAPTER Page

CHAPTER Page

LIST OF TABLES

LIST OF FIGURES

FIGURE Page

FIGURE Page

FIGURE Page

FIGURE Page

FIGURE Page

FIGURE Page

CHAPTER I

INTRODUCTION

Nanocomposites

Engineering applications of polymers often exhibit major problems due to low stiffness, low strength and low thermal stability of the available polymers. Therefore, new technology needs to be developed to meet new requirements, such as high use temperatures, high resistance to oxidation, reduced flammability and improved mechanical properties [1].

The development of composites is one approach to this problem. A composite is a material consisting of two or more physically distinct phases, the purpose of which is to achieve better properties than can be obtained by a single homogenous material [2]. Generally, composites are composed of a filler (reinforcing material) and a continuous matrix, which adheres to and binds the filler. Any combination of two or more materials, such as metallic, organic or inorganic, might be used to construct composites.

Recently, nanocomposites containing an organic binding matrix and an inorganic nanoparticle (reinforcing filler) have attracted considerable attention. In conventional organic/inorganic hybrid composites, the reinforcement particles are on the order of a few microns or larger in size. The properties of these composites are simply the volume-normalized sum of properties of each component [3]. However, in organic/inorganic

hybrid nanocomposites, where the dispersed phase component sizes approach molecular levels (a few nanometers), interfacial interactions between the organic matrix and the nanoparticles influence global properties. This might result in non-linear or exponential improvement in composite properties [4-12]. In this respect, inorganic nanoparticles have been incorporated into common polymers to generate a new class of composites that combine the desirable properties of inorganic nanoparticles (e.g. high strength, electrical conductivity, and thermal stability) with the advantages of polymers (e.g., ease of processing, flexibility, and toughness) [4-12].

These nanocomposites are defined as polymers reinforced with nanoparticles. They comprise a variety of 1-, 2- and 3-dimensional materials whose components are mixed at the nanometer scale [10-14]. The properties of nanocomposites depend on the properties of their individual components and also on their interfacial interactions [4-8]. Due to very large surface areas and the high aspect ratios of nanophases involved, the interaction between the polymer matrix and nanophases is much greater when compared with their traditional composites counterparts at the same volume fraction. In other words, a certain level of improvement can be achieved at a much lower volume fraction of nanophases when compared with conventional composite materials. Also, the dispersion of nanophases into the polymer matrix is more uniform over a given microsized volume element owing to the nanoparticles' very small sizes. Therefore, nanocomposites are promising materials for use as high-performance and lightweight matrix composites for many applications including spacecraft structures, automobile structures, sporting goods and general customer goods [4-8, 15-16].

Nanoparticles as reinforcement agents

There are three categories of nanoparticle-reinforced composites depending on how many dimensions of dispersed nanophases are in the nanometer range. These nanophases include: 3-dimensional nanophases such as nanosilica and polyhedral oligomeric silsesqiuoxanes (POSS) [38-47]; 2-dimensional nanophases, such as carbon nanofibers [22-29] and carbon nanotubes [30-37]; and 1-dimensional nanophases, such as layered silicates (nanoclays) [17-21].

Layered silicates are the best examples of 1-dimensional nanoreinforcement agents where one of the dimensions is in the nanometer scale. Montmorillonite, saponite and synthetic mica are commonly used layered silicates [15]. Among them, montmorillonite is normally referred to as nanoclay when it is nanodispersed (exfoliated or intercalated) in a matrix phase. Montmorillonite is the most common type of smectite clay. It consists of stacks of platelet sheets and their interlayers (galleries) which are the spacings between the platelets that allow molecules such as water, solvents, and polymers to enter into the clay. Each platelet is composed of one alumina octahedral layer sandwiched between two external silica tetrahedron layers. The silicon atoms share oxygen ions with aluminum atoms in the central octahedral layer [17]. There are hydroxy groups at the edge of each platelet as shown in Figure 1.1 [17]. A single montmorillonite platelet has a thickness of 1 nm and lateral dimensions of 20 nm to 2000 nm. Separating individual platelets results in high aspect ratios. Typical montmorillonites have net charges distributed within their platelets, generated by isomorphous substitutions in either the octahedral layer (where Mg^{2+} or Fe^{2+} substitutes for Al^{3+}) or the tetrahedral layer (where Si^{4+} is replaced by Al^{3+}).

These substitutions cause negative charges to occur within platelets. Positively charged ions cannot penetrate to these negatively charged sites. These negative charges in montmorillonite are balanced by interlayer counterions such as Na^+, K^+, Ca^{2+} or Mg^{2+}. These hold the platelets together in stacks.

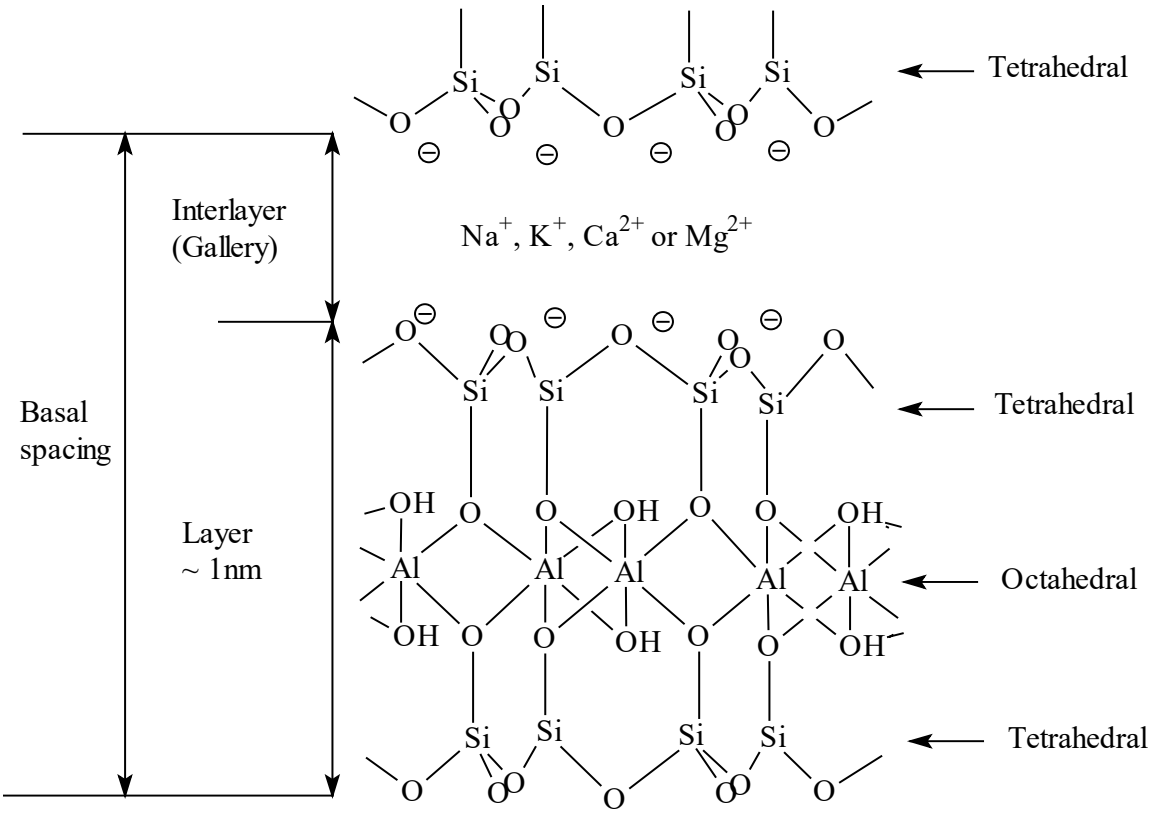

Figure 1.1 Structure of montmorillonite clay [17]

Montmorillonite is extremely hydrophilic. The lack of affinity between hydrophilic nanoclays and hydrophobic organic polymers prevents the polymer from diffusing into the galleries and cleaving clay particles into smaller and smaller particles (called tactoids). Thus, the clay particles remain aggregated within the polymer matrix, and the size distribution of the clay within the polymer resembles the size distribution purchased

(micron size range). Therefore, chemical modification of the original clay is required to make montmorillonite compatible with the organic polymer matrix. For example, cation exchange reactions have been used to replace the cations in the galleries of montmorillonite (e.g., Na^+, K^+, Ca^{2+}, Mg^{2+}, etc) with alkylammonium or alkylphosphonium ions in order to change the nanoclay from a hydrophilic substance to more a hydrophobic material [12-14, 18-21]. Exchange of alkyl ammonium ions causes the nanoclay to become more compatible with organic monomers.

There are three general types of clay nanocomposites (aggregated, intercalated and exfoliated) as illustrated in Figure 1.2. An aggregated nanocomposite is formed when the clay is not compatible with the polymer matrix. Mechanical action may reduce the particle size during mixing. Intercalated or exfoliated nanocomposites can sometimes be obtained if the clay is compatible with the polymer matrix. An intercalated structure is formed when the polymer chain is inserted between the layers and the platelets move apart but are still exhibiting in a regular ordered structure. An exfoliated structure is obtained when the individual platelets are separated and randomly dispersed in a continuous polymer matrix.

Improvements in stiffness, strength, moduli and thermal stability occur with highly intercalated or highly exfoliated composites because the platelets are separated and the polymer matrix interacts with the platelet surfaces, giving a very large interfacial interaction area.

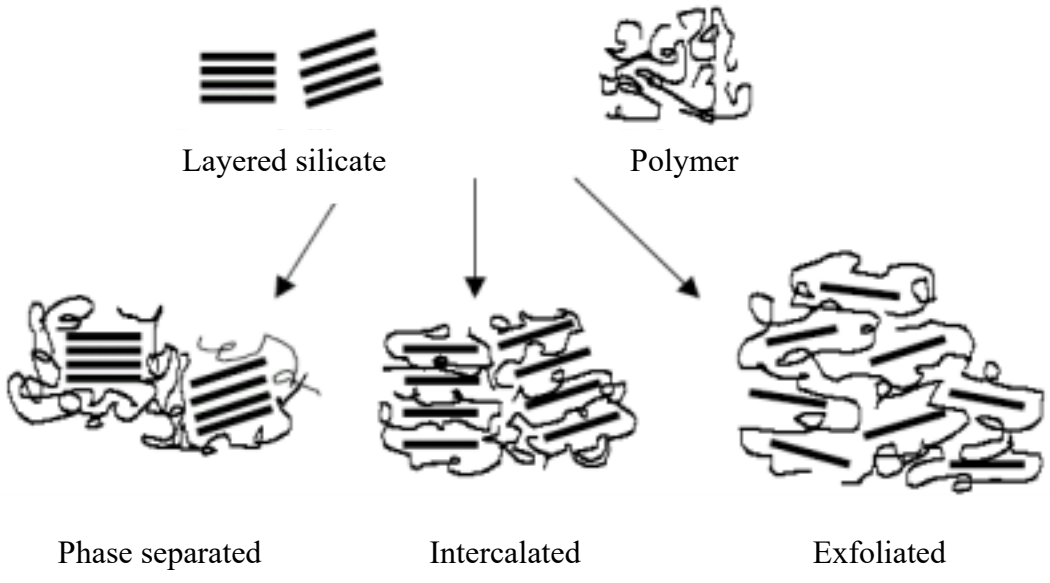

Figure 1.2 Three types of composites obtained when layered clay is mixed with polymer

Carbon nanofibers and nanotubes are examples where two of the dispersed phase's dimensions are on the nanometer size scale. Vapor grown carbon nanofibers (VGCNFs) are produced by the catalytic decomposition of a hydrocarbon gas (methane, ethane or benzene) on iron particles in the presence of hydrogen at high temperatures around 1100-1300 °C [22-24]. In this process, iron particles act as nucleation points for rapid fiber growth which occurs as the particles flow downstream with the gas. Carbon graphitic sheets are formed which wrap around to form multi-walled, conically-canted, nanotube-like fibers [25]. A multicentered "stacked cup" morphology grows to give diameters from the tens of nanometers to a few hundred nanometers and lengths from 1 micron to a few centimeters depending on the production conditions. This forms the primary filament. Continued pyrolysis deposites concentric layers of pyrolytic graphite in an "onion ring-like" or turbostratic geometries over the inner filament to create the final thickened fiber

[26-28]. This unique structure gives the carbon fibers excellent physical properties including high tensile strengths and tensile moduli, high electrical conductivities and high thermal conductivities [29]. Two general kinds of carbon nanofibers (Pyrograph I and Pyrograph III) produced by Applied Science, Inc. (ASI) are commercially available. A variety of Pyrograph I grades are available based on subsequent heat and surface chemical treatments.

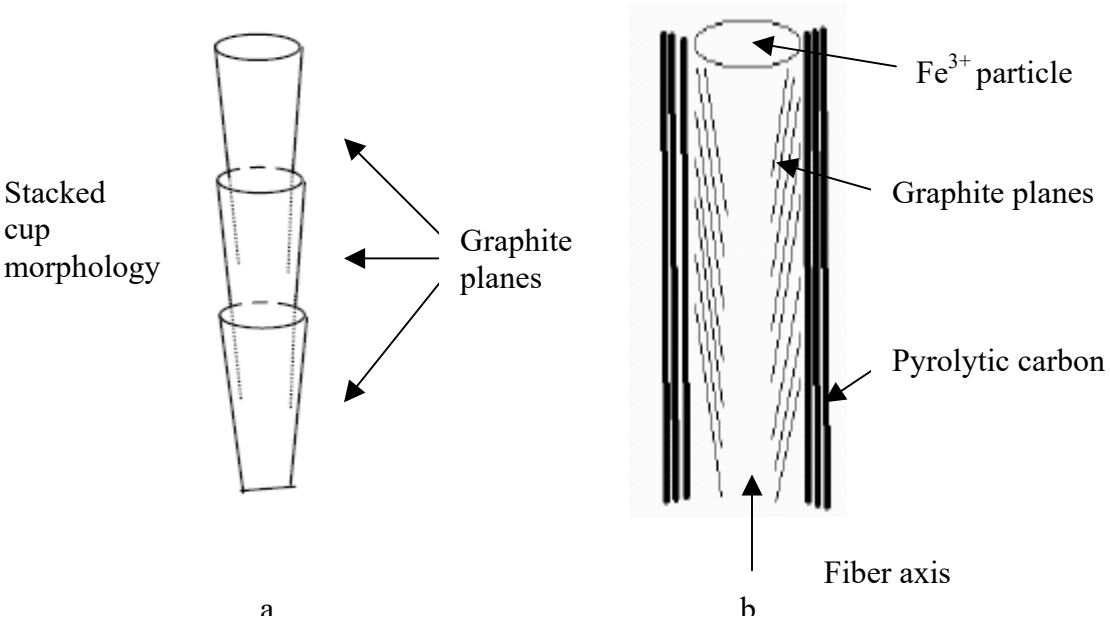

Figure 1.3 Growth stages of carbon nanofibers. A) Lengthening. Carbon adsorbed into the iron particle forms a multi-walled nanotube like filament with a "stacked cup" morphology. The small cone ends terminate at the inner portion of the hollow tube cylinders. The angle of these cones is oblique to the tube axis and the cant angle varies with the production process. B) Thicked by CVD of carbon, the diameter increases and produces a tree-ring morphology in very large fibers (eg Pyrograph III)

Carbon nanofibers are relatively cheap and readily available. However, the fibers tend to curve and aggregate. Thus, dispersing them into polymers remains still a key

problem. In addition, many challenges associated with processing and characterization of nanofiber/polymer nanocomposites exist due to poor fiber/matrix adhesion and fiber nesting.

A carbon nanotube (CNT) is a hexagonal network of carbon atoms rolled into a seamless, hollow cylinder, with each end capped with half of a fullerene molecule [30]. Both single-walled nanotubes (SWNTs) and multi-walled nanotubes (MWNTs) exist. SWNTs are individual cylinders of 1-2 nm in diameter. MWNTs are collections of several concentric graphene cylinders ranging from ~1.4 to at least 100 nm in diameter, where weak van der Waals forces, operating over their high aspect ratios (up to 1000), bind the tubes together [30]. Carbon nanotubes have high Young's moduli and high tensile strengths. For instance, experimental values of the Young's moduli and tensile strengths for SWNTs in the literature were 1-2 TPa and 50-100 GPa [31-33] respectively. Furthermore, the density-normalized tensile modulus and tensile strength of SWNT are, ~19 and ~56 times that of steel wire and ~2.4 and ~1.7 times that of silicon carbide nanorods [34-35]. Therefore, nanotubes are expected to serve as mechanical reinforcements for lightweight composite systems with possible multifunctional uses. However, they are very expensive and often exhibit the problem of nanotube aggregation due to strong interactions (0.5 eV/nm) between the pristine nanotubes and weak interaction with the surrounding matrix [36-37].

Polyhedral oligomeric silsesquioxane (POSS)

Polyhedral oligomeric silsesquioxanes (POSS) are excellent examples of a 3-dimensional nanophase where all these dimensions are in the nanometer range. The name

silsesquioxane comes from the “sesqui”, which means one and a half. This is derived from the general formula, $(RSiO_{1.5})_n$ where 1.5 oxygens are present for each silicon. The suffix “ane” represents a hydrocarbon group, R where R is hydrogen or any alkyl, alkylene, aryl, arylene or organofunctional derivatives of alkyl, alkylene, aryl or arylene groups. Other examples exist where R = $-OSiR_3$ etc. The term polyhedral indicates the cage or polyhedron nature of the $(RSiO_{1.5})_n$ core.

Various types of silsesquioxanes exist including random structures [38], ladder structures [39-41], cage structures [42-44], and partial cage structures [45]. These are illustrated in Figure 1.5. Among them, polyhedral oligomeric silsesquioxanes (POSS) are those classes with well-defined cage structures, which contain a silicon/oxygen cage (inorganic portion) and hydrocarbon functional groups (organic portions) attached to corner Si molecules. Completely and incompletely condensed POSS cages are available as shown in Figure 1.5 (structures c-f). The first closed-cage POSS compounds, $(CH_3SiO_{1.5})_n$ were isolated by Scott [46] in 1946 and open-cage POSS ‘triol’ was characterized by Brown and Vogt [47] in 1965. Much more attention has been paid to specific cage structures in the past fifteen years.

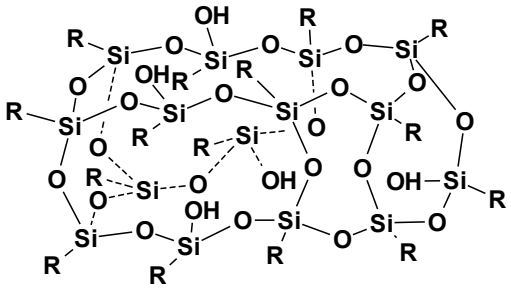

(a)
Random structure

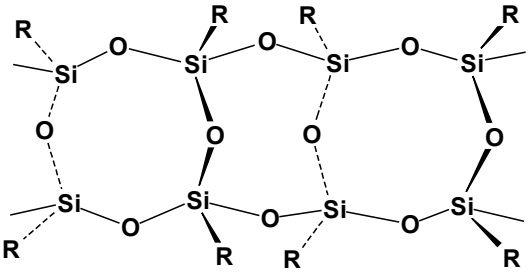

(b)
Ladder sructure

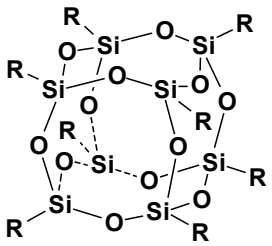

(T_8)
(c)

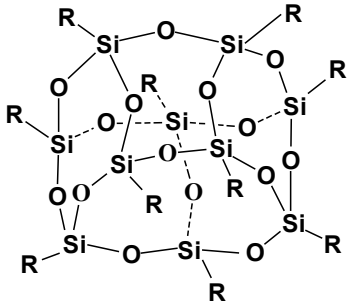

(T_{10})
(d)

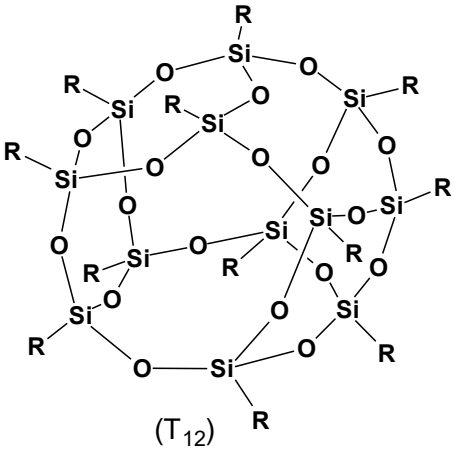

(T_{12})
(e)

Cage structures

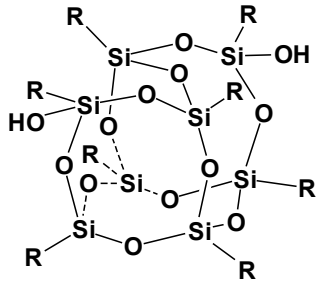

(f)
Partial cage structure

Figure 1.4 Structure of silsesquioxanes [92]

POSS nanophases have been utilized for preparing lightweight, high-performance hybrid nanocomposites. The performance region of POSS-reinforced nanocomposites is thought to be between polymers and ceramics as illustrated in Figure 1.6 [48]. POSS has two unique characteristics: First, its chemical composition is a hybrid, intermediate ($RSiO_{1.5}$) between that of silica (SiO_2) and silicone (R_2SiO). Secondly, POSS molecules span the approximate 1-3 nm size range. This size domain is physically quite large and this volume is nearly equivalent in size to most polymer segments and many polymer coils, leading to molecular level reinforcements of polymer matrices [48].

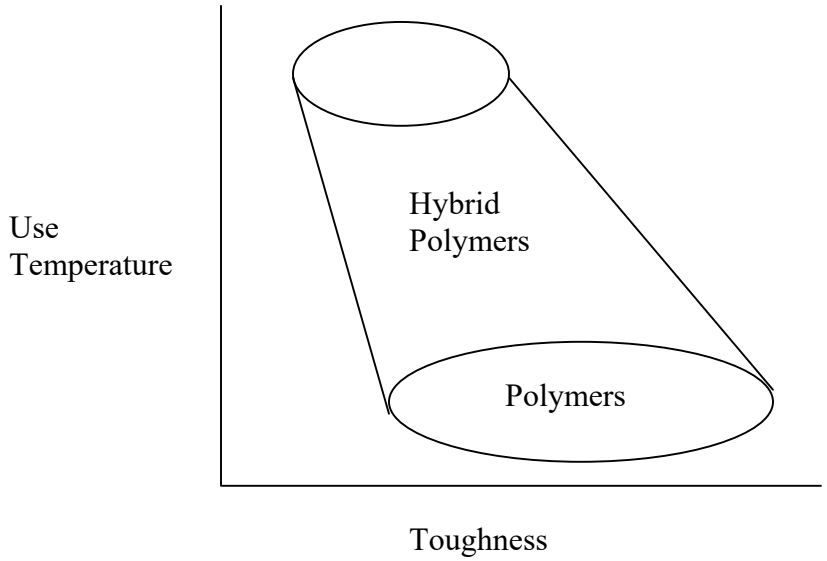

Figure 1.5 Use temperature of ceramics, polymers and hybrid polymers [48]

Typical POSS molecules contain inorganic silicon and oxygen cages, $(SiO_{1.5})_{8,10\ or\ 12}$, which are referred to as T_8, T_{10} and T_{12} cages, respectively. They can also contain organic functional groups, which can either be classic organic moieties (phenyl; isobutyl etc.) or inorganic/organic hybrids (e.g. $–OSiMe_2OPh$). POSS molecules can be thought of

as analogues of the smallest possible of silica particles. However, unlike silicas, silicones or other nanofillers, each POSS molecule contains either (1) unreactive organic functions, which help POSS molecules become soluble in, and compatible with, polymers, or (2) reactive organic functions, which make POSS molecules more suitable for polymerization or grafting.

A large-scale process for the synthesis of POSS chemicals [49-53] has been developed by a group at Edwards Air Force Base, CA. Currently, a number of POSS reagents have become commercially available from Hybrid Plastics Company, Fountain Valley, CA. and Hattiesburg, MS. [85].

Various POSS chemicals have been made that contain one or more reactive organic functions. Therefore, POSS molecules can be incorporated into conventional polymers via copolymerization [54-57], grafting [54, 58], or blending [54, 58-59]. POSS-reinforced nanocomposites have been reported with higher use temperatures [59-60], oxidation resistance [58], surface hardening [58], mechanical properties [61-62], decreased flammability [62-63], reduced heat evolution [64] and lower processing viscosities [65]. The properties of both thermoplastics and thermosets, including methacrylates [66], styrene [67], norbornene [68], ethylenes [69], epoxides [70], and siloxanes [57, 71] have been improved.

Clays and carbon nanofibers/nanotubes are most often physically dispersed into polymer matrices. In contrast, POSS chemicals can be chemically incorporated into organic resins. In other words, they can be a part of copolymer chain macromolecules. Furthermore, POSS monomers can be dissolved into other monomers and then

copolymerized. Hence the processing of POSS into plastics, using POSS monomers, is very simple conceptually, as long as these monomers are soluble in the monomer mixture. When polymerization occurs, the entropy of mixing term decreases and POSS derivatives may phase separate or partially phase separate before being reacted into the polymer structure. Also, POSS units along polymer chains may preferentially aggregate, forming POSS domains (similar to phase separation in block copolymer systems).

Synthesis of polyhedral oligomeric silsesquioxanes

The methods for synthesizing POSS compounds were covered in a review by Voronkov and co-workers in 1982 [72]. Feher et al. reviewed the recent progress on POSS synthesis in 2000 [73]. An excellent review by Li et al. published in 2001 described the synthesis of monofunctional and multifunctional POSS monomers and polymers [74]. There are two major ways to synthesize POSS and its derivatives [47, 75-77]. The first approach is to form new Si-O-Si bonds with subsequent assembly of the polyhedral cage framework. In this case, the polyhedral silsesquioxanes can be made from monomers of the $XSiY_3$ type, where X is a chemically stable substituent (such as CH_3, phenyl, or vinyl etc) and Y is a highly reactive substituent (such as Cl, OH, or OR). (Equation 1-1).

$$nXSiY_3 + 1.5nH_2O \rightarrow (XSiO_{1.5})n + 3nHY \qquad (1\text{-}1)$$

The second general route is to manipulate the substituents at the silicon atom, keeping the silicon-oxygen cage in tact. The organic functions attached to corner Si molecules can be varied to give non-reactive or reactive POSS molecules. A large number of substituents, such as alcohols and phenols, alkoxysilanes, chlorosilanes,

epoxides, esters, fluoroalkyls, halides, isocyanates, methacrylates and acrylates, alkyl and cycloalkyl groups, nitriles, norbornenyls, olefins, phosphines, silanes, silanols, and styrenes, have been attached to the silicon oxygen cages $[R(SiO_{1.5})]_{8,\ 9\ or\ 12}$ by Hybrid Plastics Co.

Monofunctional POSS synthesis

Monofunctional POSS derivatives can be synthesized by the hydrolysis and condensation of commercially available organochlorosilanes. Incompletely condensed silsesquioxanes are the major products of the hydrolysis/condensation. The condensation of the incompletely condensed silsesquioxanes with reactive organosilicon monomers follows, generating POSS derivatives [78]. For example, the controlled hydrolysis/condensation of cyclohexyl-trichlorosilane is illustrated in Figure 1.7 [78]. In this reaction, 45% of the heptameric siloxane containing three SiOH functions was obtained along with 40% of a hexamer and 15% of an octameric closed-cube silsesquioxane. The incompletely closed heptameric siloxane was easily separated from the other compounds due to its different solubility. Then, the three remaining hydroxy groups of the heptamer were used to form fully condensed POSS cage by reactions with reactive organosilicon monomers such as triethoxylsilanes $[R\text{-}Si(OEt)_3]$. Specific reactive corner R functions attached with silicon in this method include hydride, chloride, hydroxide, nitirles, amines, isocyanates, styryls and olefins. (Figure 1.7) [79-85].

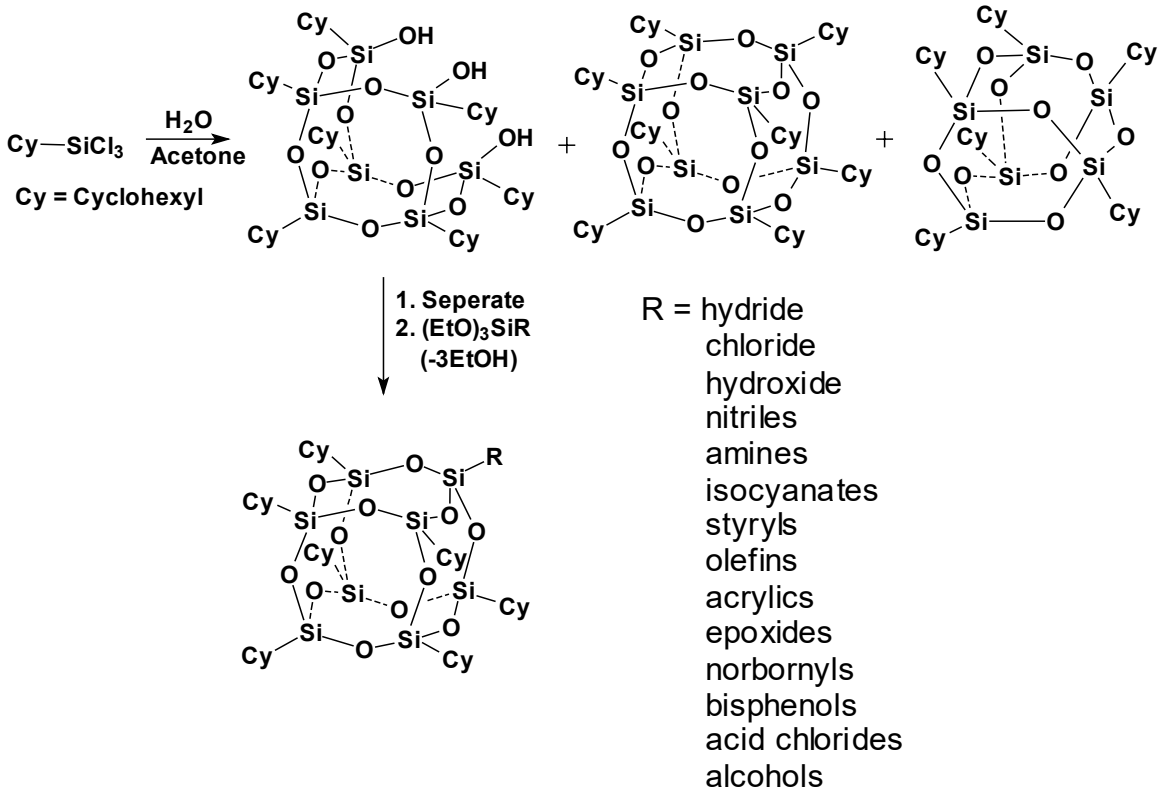

Figure 1.6 Synthesis and structures of monofunctional POSS molecules [78]

Multifunctional POSS synthesis

Multifunctional POSS derivatives can be made by hydrolysis and condensation of either trialkoxysilanes ($R'Si(OR)_3$) or trichlorosilanes ($R'SiCl_3$). R′ is a group containing a functional group which can be used later. This reaction generates an octa-functional POSS, $R'_8(SiO_{1.5})_8$ [72]. For example, octaallylsilsesquioxane was synthesized by hydrolysis and condensation of allyltrimethoxysilane ($CH_2CHCH_2Si(OCH_3)_3$) by Lee et al (Figure 1.8) [86]. Another approach involves functionalizing POSS cages that have already been formed. This can be accomplished via Pt-catalyzed hydrosilylation of alkenes or alkynes with $(HSiO_{1.5})_8$ and $(HMe_2SiOSiO_{1.5})_8$ cages [72, 87-88] (shown in

Figure 1.9). In this case, $(HMe_2SiOSiO_{1.5})_8$ was synthesized following modified literature procedures [89-90].

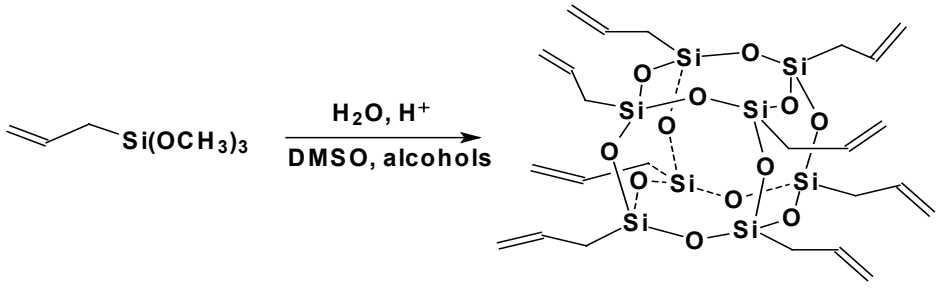

Figure 1.7 Synthesis of octaallylsilsesquioxane [86]

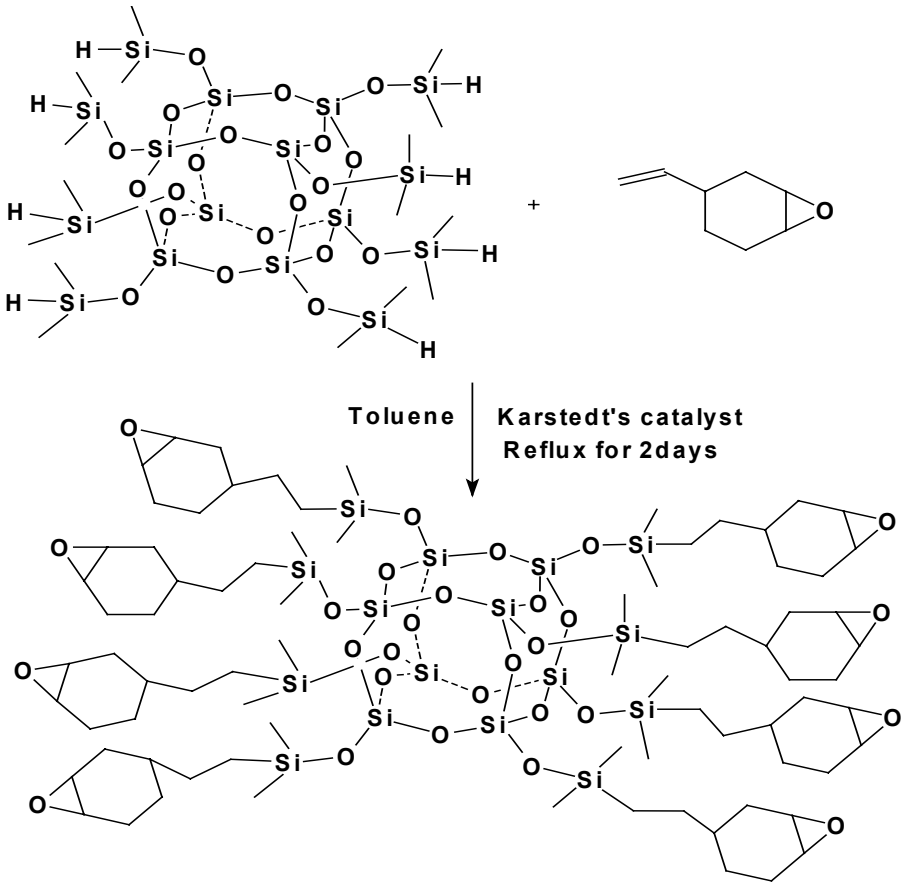

Figure 1.8 Synthesis of octa(ethylcyclohexylepoxidedimethylsiloxy)silsesquioxan [88]

Nanocomposites with POSS dispersed phases

POSS-modified nanocomposites have attracted special attention mainly due to their processing simplicity and their excellent mechanical and thermal properties [90-118]. In general, three types of POSS-modified polymers exist including non-functional POSS dispersed in polymers, monofunctional POSS modified-polymers and multifunctional POSS modified-polymers. Depending on the type and reactivity of functional groups on POSS molecules, POSS cages can be incorporated into polymer matrices by the methods of chemical copolymerization and physical blending.

POSS molecules are dispersed physically into organic polymer matrices without a covalent bonding during physical blending. POSS-POSS interactions almost always dominate resulting in various states of POSS aggregation instead of dissolution [91]. However, POSS compounds form covalent bonds with organic monomers to become part of the polymer during copolymerization. The POSS-polymer interactions still compete with POSS-POSS interactions. Pendant POSS groups may still aggregate while attached to polymer chains. This behavior is much like block copolymers exhibit microphase separation. The properties of POSS-modified nanocomposites are strongly affected by the organic substituents on POSS cages, which control the POSS/polymer miscibility. Thus, increasing the enthalpic interactions between functional groups on the POSS cage and the other monomer segments of the polymer can increase T_g and modulus [59-62]. If this interaction is weak and POSS aggregates form, the T_g and modulus can still increase because the POSS aggregates act like noncovalent crosslinks (Figure 1.10). The greatest improvement in properties comes with multifunctional POSS modified-polymers. Each

POSS moiety contains several functional groups which can form covalent bonds with the matrix. Thus, the POSS cage becomes a crosslinking center in the matrix.

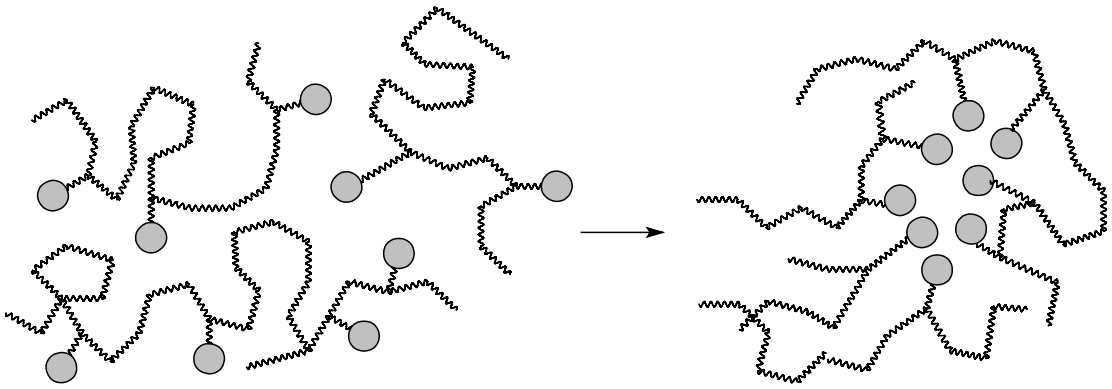

Figure 1.9 POSS aggregates act like noncovalent crosslinks

Nanocomposites with non-functional POSS dispersed phases

There are many studies on direct dispersion of non-functional POSS monomers in polymer matrices by melting blending. They simply will give dispersed POSS aggregates because of unfavorable miscibility of those silsesquioxanes with organic polymers.

Fu et al. [92] investigated the effect of octamethyl(T_8)POSS (shown in Figure 1.10) on the crystallization of isotactic polypropylene (PP) at quiescent and shear conditions. The addition of POSS molecules increased the crystallization rate of i-PP by acting as a nucleating agent in quiescent conditions. However, the i-pp crystallization rate decreased at a POSS content of 30 wt% due to the molecular dispersion of POSS in the matrix. The crystallization rate under shear conditions was significantly higher than under quiescent conditions even at higher POSS content. Molecularly dispersed POSS molecules, which have a limited role under shear conditions, are postulated to act as weak crosslinkers in polymer melts. Therefore, they increase the relaxation time of i-PP chains after shear.

Thus, chain segments can remain in oriented state for longer times after shear, resulting in a higher i-PP crystallization rate.

Li et al. [93] prepared two vinyl ester (VE) nanocomposites with non-reactive octa-i-butyl(T_8)POSS and dodecaphenyl(T_{12})POSS (Figure 1.11). Incorporation of both POSS molecules into VE did not change the T_g. However, the storage modulus of dodecaphenyl(T_{12})POSS/VE nanocomposites increased due to the favorable interaction of phenyl rings of dodecaphenyl(T_{12})POSS with abundant phenyl rings in VE resins. These interactions inhibited segmental motion and increased the modulus.

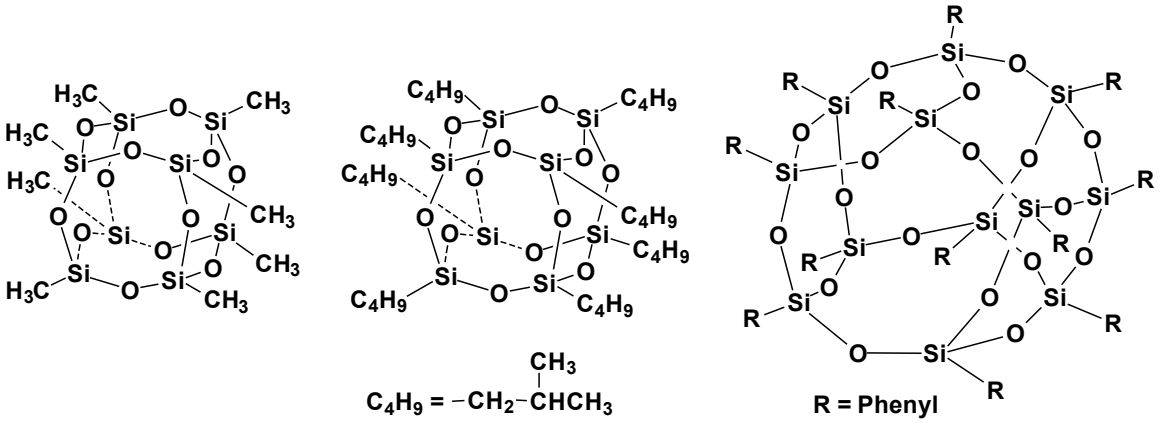

Figure 1.10 Nonfunctional POSS: octamethyl(T_8)POSS, octa-i-butyl(T_8)POSS and dodecaphenyl(T_{12})POSS

Copolymerized monofunctional POSS nanocomposites

Monofunctional POSS molecules have been used as comonomers to prepare many copolymer systems. The synthesis and properties of many such copolymers, including styryl-POSS [67], methacrylate-POSS [66], norbornyl-POSS [68], epoxy-POSS [70] and siloxane-POSS copolymers [57] have been reported.

Haddad et al [67] synthesized the mono styryl-substituted POSS, $R_7(Si_8O_{12})(CH_2CH_2C_6H_4CH{=}CH_2)$ (where R is cyclopentyl) and then prepared 4-methylstylene-co-styryl POSS copolymers by AIBN-initiated free radical polymerization of 4-methylstyrene with the monofunctional styryl-POSS monomers (Figure 1.12). The incorporation of styryl-POSS monomers into polymethylstyrene increased the glass transition temperature (T_g) and decomposition temperature (T_d). For example, the T_g and T_d values for these copolymers became higher than those of pure polymethylstyrene (T_g = 119 ^oC and T_d = 388 ^oC) when more than 8 mol % of the styryl-POSS was present. The T_g and T_d values increased steadily with a further increase in styryl-POSS content [67].

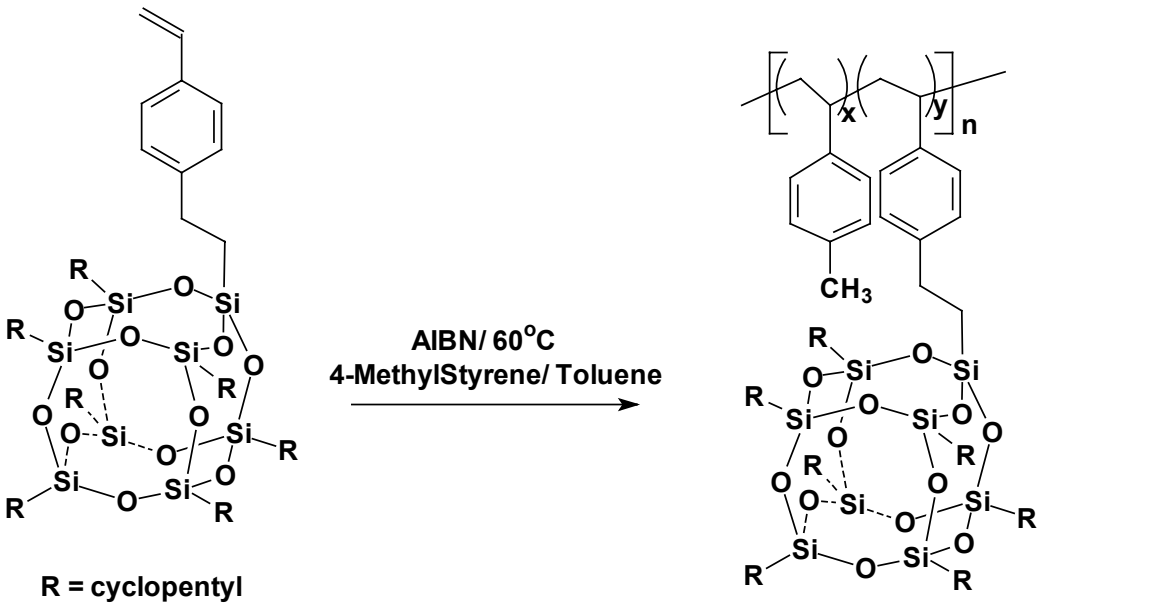

Figure 1.11 Copolymerization of styryl-POSS and 4-methylstyrene [67]

Lee and coworkers [70] incorporated the monofunctional epoxy POSS, $(cC_6H_{11})_7Si_8O_{12}(CH_2CHCH_2O)$ (shown in Figure 1.13), into an epoxy resin to study the thermal property enhancements of cured epoxy resins. The glass transition region was observed to broaden with an increase in POSS content (≤10%). Also the T_g increased with increasing POSS loading. These observations were ascribed to the massive POSS cages, which hinder the segmental motion of molecular chains.

Zhang et al [94] synthesized random copolymers of methyl methacrylate (MMA) with 3-methacrylylpropyl heptacyclopentyl-POSS, $(c\text{-}C_5H_9)_7Si_8O_{12}(C_2H_6OCOCHCH_2)$, (Figure 1.13). These copolymers were blended with PS and PMMA homopolymers to investigate the effects of the pendant POSS moieties on the phase separation. These random copolymers were efficient at compatibilizing immiscible PS/PMMA polymer blends. Compatibilization of the two homopolymers occurred when the POSS copolymers were added. When POSS was grafted onto the PMMA backbone favorable interactions existed between the cyclopentyl ring on POSS cage and the PS homopolymers [94]. The consequences of this compatibilization were shown to be reduced domain size, increased interfacial width and greatly improved fracture toughness.

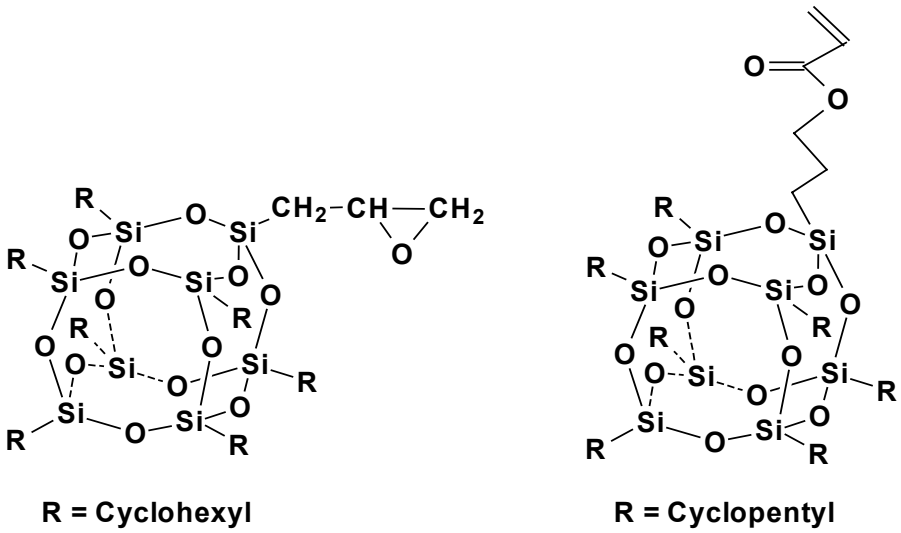

Figure 1.12 Monofunctional POSS monomers [70, 94]

Multifunctional POSS reinforced nanocomposites

Mutifunctional POSS derivatives have been used to modify thermoset systems. Most published work is related to epoxy resin networks [96-100]. Subtle changes in the functional groups attached to the POSS molecules have been shown to cause drastic changes in the properties of the resulting composites. When a multifunctional POSS is employed, several covalent bonds can be formed from the POSS cage into the matrix, forming 3-D cross-linked networks.

VE/POSS nanocomposites

Li et al [93] prepared vinyl ester (VE) nanocomposites (shown in Figure 1.14) containing the chemically bonded, multifunctional POSS monomer, $[(C_6H_5CHCHO)_4(Si_8O_{12})(CH{=}CHC_6H_5)_4]$, in VE/POSS ratios of 95/5 and 90/10 wt/wt. The viscoelastic and mechanical properties of these VE/POSS composites were studied.

A small amount of POSS (≤10 wt%) incorporation exhibits almost no influence on T_g or the glass transition range. However, the storage moduli, E', of VE/POSS composites were higher than those of the neat VE resins over entire temperature range (20-180 ^oC). Low POSS contents (5 wt%) markedly improved thermal dimensional stabilities. The flexural moduli and hardnesses of VE resins were improved by POSS incorporation.

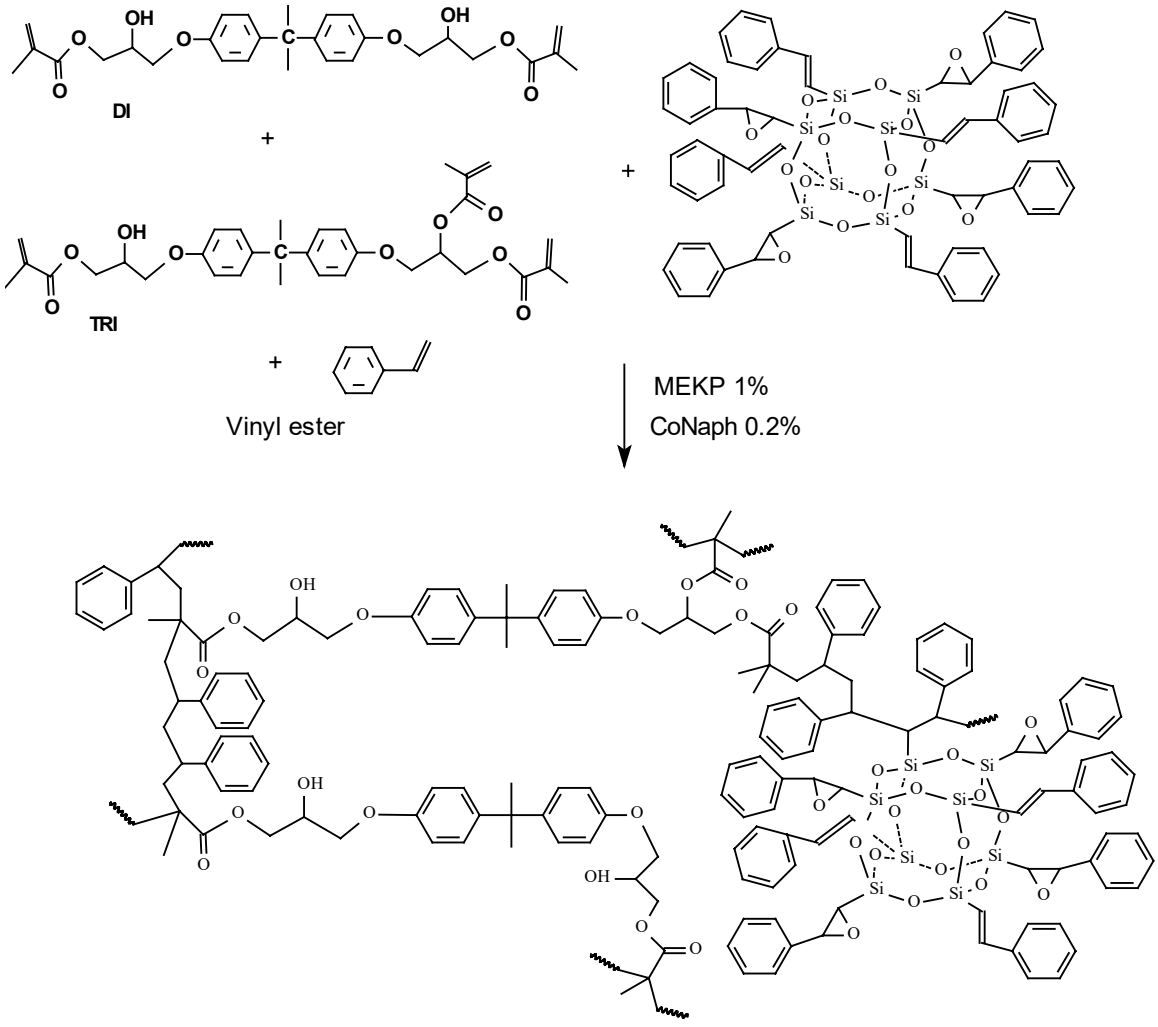

Figure 1.13 Synthesis of Vinyl ester/POSS composites [93]

Lee et al reported that multifunctional vinyl POSS cage mixtures (POSS mixtures with cages of 8, 10 and 12 Si atoms) could be used to modify thermal and flammability properties of vinyl ester resins [95]. The incorporation of 15 wt% of the mixed vinyl POSS macromers increased the ignition times of these VE/POSS nanocomposites, and also reduced the overall heat release rates. The T_g values of Derakane 441–400, Dow Chemical Corporation's vinyl ester resin (VE), and its 15 wt% mixed cage vinyl POSS composites were 118 °C and 125 °C, respectively. Their heat distortion temperatures were 245 °F, and 257 °F, respectively. The decomposition temperature (T_d) of the neat VE was substantially increased from 360 °C to 411 °C in its 15 wt% POSS composite. The residual char values increased sharply from 8 % to 34 %, respectively [95]. This incorporation of the vinyl POSS mixture into vinyl ester resins certainly improved the thermal and fire-retardant properties. However, there was very little change of their tensile strengths, tensile moduli, elongations, flexural strengths and flexural moduli [95].

Epoxy/POSS nanocomposites

Li and coworkers [96] dispersed multifunctional POSS $[(C_6H_5CHCHO))_4(Si_8O_{12})(CH{=}CHC_6H_4)_4]$ into an aliphatic epoxy resin in two wt/wt ratios (epoxy/POSS 95/5 and 75/25) and cured these systems. The POSS units appeared molecularly dispersed into epoxy network even at high POSS content (25 wt%) based on TEM observations at a magnification of 800,000. It was observed that the epoxy/POSS 95/25 composite, cured only to 120 ^oC, exhibited a lower T_g and lower storage modulus at $T<T_g$ than the neat epoxy resin cured to this same temperature. The lower reactivity of

epoxy groups on POSS cages result in an incomplete cure at this low cure temperature, accounting for this result. Higher temperature curing (150 ^{o}C) increased reactions between residual epoxy groups of the POSS and amine groups, enhancing the T_g and E' values of epoxy/POSS 95/25 sample. Incorporation of POSS into the epoxy network broadened the glass transition range in the resulting composites but had no influence on the T_g values. However, the storage moduli of epoxy composites at $T>T_g$ were higher than those of the neat epoxy resin and increased with POSS content.

Laine et al [97-98] prepared epoxy nanocomposites reinforced by a series of octafunctionalized(T_8)POSS ($R_8Si_8O_{12}$) with aminophenyl and dimethylsiloxypropyl glycidyl ether moieties. For example, epoxy composites containing octaglycidyldimethylsiloxy-octahedralsilsesquioxane, [(glycidyl-$Me_2SiOSiO_{1.5})_8$], were made. This POSS derivative is designated as OG. OG/diaminodiphenylmethane (DDM) composites were synthesized at different OG/DDM ratios and curing conditions [97]. The epoxy resin, glycidyl ether of biphenol A (eg. DGEBA), was used a reference material for comparative studies. The number of organic tether links between POSS cages was varied by changing the amine to epoxy ratio (N) to control the architecture of the resulting epoxy nanocomposites. Both OG/DDM and DGEBA/DDM composites exhibited maximum crosslink densities at N = 0.5 (NH_2: epoxy = 0.5). The OG/DDM composites had high mechanical rigidity and their thermal degradation stabilities were similar to DGEBA/DDM under similar conditions. It was possible to prepare nanocomposites with a defined nanoarchitecture and different properties by varying OG/DDM ratios.

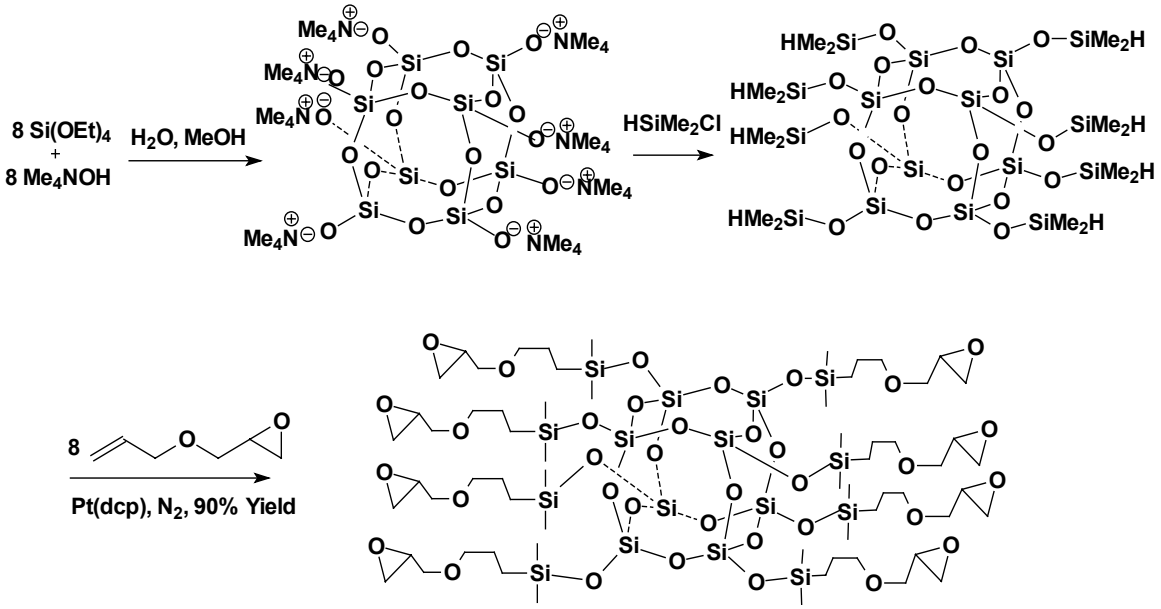

Figure 1.14 Synthesis of octaglycidyldimethylsiloxy-octasilsesquioxane (OG) [97]

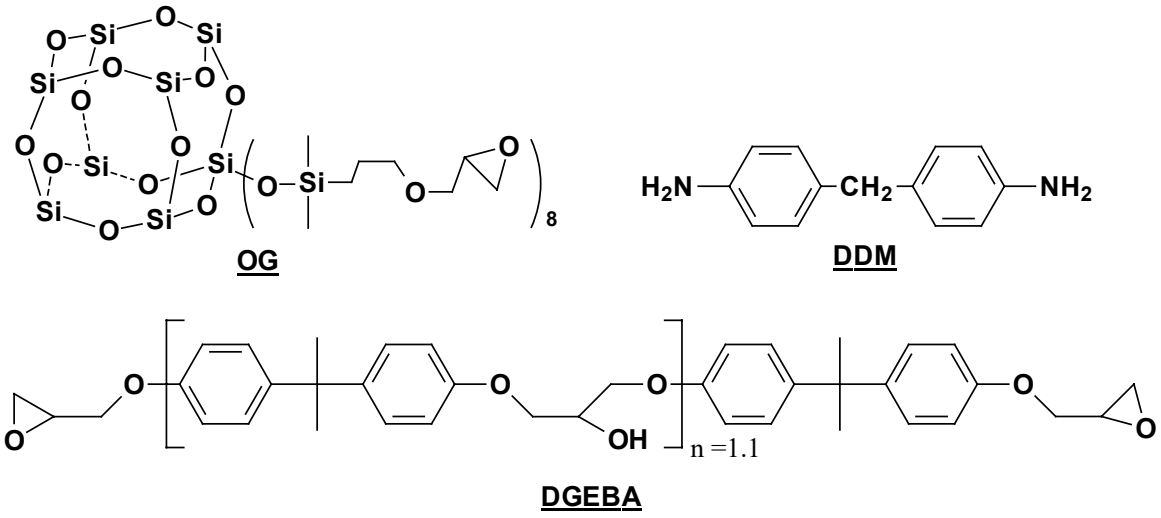

Figure 1.15 Octaglycidyldimethylsiloxy-octasilsesquioxane (GO), diaminodiphenyl-methane (DDM) and glycidyl ether of biphenol A (DGEBA) [97]

Ni et al [99] have dispersed octanitrophenyl(T_8)POSS [$(C_6H_4NO_2)_8(SiO_{1.5})_8$] and octaaminophenyl($T_8$)POSS [$(C_6H_4NH_2)_8(SiO_{1.5})_8$] (Figure 1.17) into the DGEBA epoxy

resin, respectively, by in-situ polymerization in the presence of DDM. POSS-rich phases (<0.5 μm in diameter) were found in the first case that were uniformly dispersed into the continuous epoxy matrix. These phases were detected by scanning electron microscopy (SEM) only in the composites containing octanitrophenyl(T_8)POSS. However, the nanocomposites containing octaaminophenyl(T_8)POSS exhibited a homogeneous morphology. The glass transition temperatures of both POSS-modified epoxy composites were lower than that of the controlled epoxy resin. However, the storage moduli of these composites were significantly higher than that of the controlled resin at $T<T_g$. The octaaminophenyl(T_8)POSS/epoxy nanocomposites exhibited higher thermal stabilities than the octanitrophenyl(T_8)POSS/epoxy nanocomposites in thermogravimetric analysis (TGA) studies. This was attributed to the nano-scaled dispersion of octaaminophenyl(T_8)POSS cages and their chemical bonding to the matrix. Each POSS B molecule serves as a crosslink hub because these eight amino groups can react with epoxy functions.

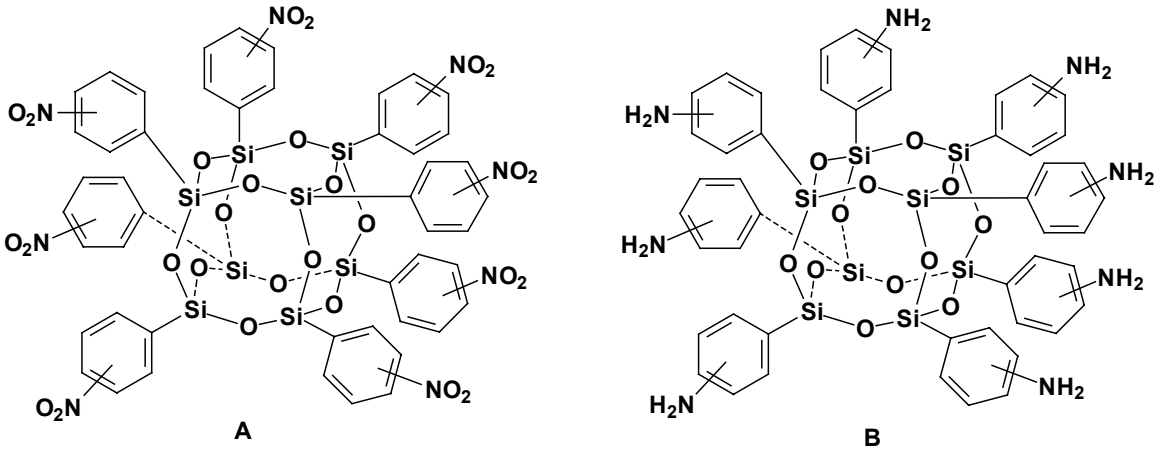

Figure 1.16 (A) Octanitophenyl(T_8)POSS and (B) octaaminophenyl(T_8)POSS [98]

Zheng and coworkers [100] have prepared epoxy nanocomposites containing up to 40 wt% of octa(propylglycidyl ether)(T_8)POSS, [glycidyl-$C_3H_6SiO_{1.5})_8$]. The homogeneous POSS dispersion in the epoxy network was observed by scanning electronic microscopy (SEM), transmission electronic microscopy (TEM) and atomic force microscopy (AFM). The storage moduli of octa(propylglycidyl ether)(T_8)POSS/DGEBA/DDM composites were significantly higher than those of the neat epoxy resin over the entire temperature range (-150 to 250 ^oC). Incorporating these POSS macromers increased thermal dimensional stability. The increased oxidation resistance of these composites was obtained due to the molecular level dispersion of POSS units and the formation of crosslinking network of POSS cages with epoxy matrix.

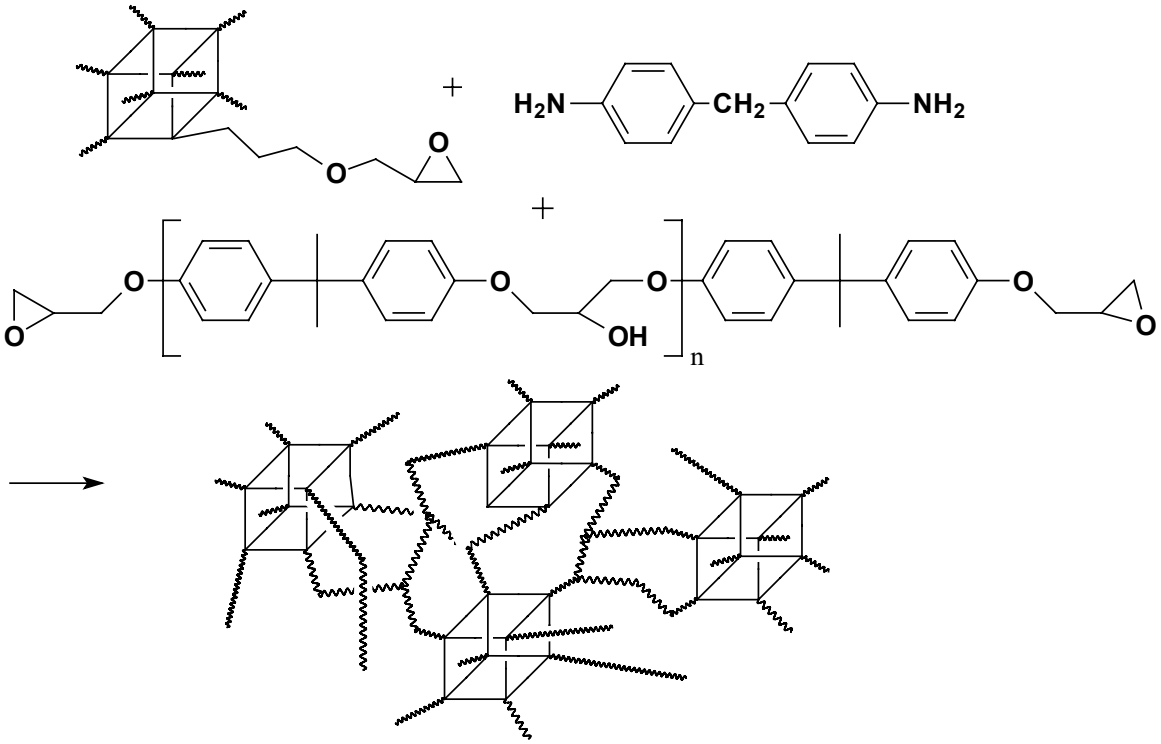

Figure 1.17 Synthesis of epoxy nanocomposites containing octa(propylglycidyl ether)(T_8)POSS [100]

Research objectives

Polyhedral oligomeric silsesquioxanes (POSS) have been used as nanoreinforcement agents that can, in specific cases, be molecularly dispersed within polymer matrices. POSS derivatives have the ability to be copolymerized into polymeric chains, when the POSS contains appropriate functional groups. Matrix properties can be improved upon adding a small amount of POSS to polymers. Therefore, POSS chemicals are good candidates for nanoreinforcement agents.

The objective of this study is to synthesize a new class of organic-inorganic hybrid nanocomposites containing well-defined polyhedral oligomeric silsesquioxane (POSS) monomers which have been copolymerized with organic monomers. Thus, POSS phases ~1nm in diameter will be molecularly dispersed and chemically bonded throughout the organic polymers. Matrix resins will be used in this work (thermosets) instead of thermoplastics. iBMA/BDMA, vinyl esters, phenolics, epoxides and cyanate esters will be the marices investigated in this study. Both monofunctional and multifunctional POSS derivatives will be employed as nanoreinforcement agents. POSS nanophases can enhance oxidation resistance and erosion resistance and they can stabilize surface regions exposed to high temperature gradients. Pyrolysis of POSS macromers produces SiO_xC_y chars on the way to ceramic materials and these chars protect the eroding surface. Direct exposure to flame generates a surface barrier layer of SiO_2 protecting the surface region [101-104]. POSS units should also improve mechanical properties of the resulting thermoset composites by increasing modulus and hardness while maintaining the stress and strain characteristics of the base resins.

However, all of the property changes will depend on how the POSS derivatives are dispersed and bonded into the matrix and on the degree of POSS aggregation within the matrix structure. Our goals are to investigate the kinetic race between molecular dispersion of POSS into the polymer network versus phase separation into POSS aggregates during the curing process in which the crosslinked resin is formed. Then, the effects of POSS nanoreinforcement on thermal and mechanical properties of various matrix resins will be evaluated.

References

[1] Swartz, M. M, Composite Materials Handbook, McGraw-Hill Book Company, 1984, New York.

[2] Richardson, T., Composites: A Design Guide, Industrial Press New York, 1987, Chapter 1.

[3] Winder, E. J., Ellis, A. b., Lisensky, G. C., Thermoelectric devices: solid-state refrigerators and electrical generators in the classroom. *J. Chem. Educ*. 7998, 73 (10), 940.

[4] Nawala, H. S., Handbook of Organic-Inorganic Hybrid Materials and Nanocomposites, American Scientific Publishers, 2003, Stevenson Ranch, CA.

[5] Gomez-Romero, P., Sanchez, C., Functional Hybrid Materials, Wiley-VCH, 2003, Wienheim, Germany.

[6] Mark, J. E., Lee, C. C-Y., Bianconi, P. A., Hybrid Organic-Inorganic Composites, American Chemical Society, May 1995, Washington D.C.

[7] Komareni, S., Roy, R., Selvaraj, U., Malla, P. B., Breval, E., *J. Mater. Res*., 1993, 8, 3163.

[8] Mark, W. E., Douglas, L. G., *Polym. News*, 1999, 24, 10, 331.

[9] Matsumura, T., Ochi, M., Nakata, *K., J. Appl. Polym. Sci*., 2003, 90, 7, 1980.

[10] Vaia, R. A., Giannelis, E. P., *MRS Bulletin*, 2001, 26, 5, 394.

[11] Lawton, G., *Chemistry and Industry*, 2001, 6, 174.

[12] Cantor, B., *Mater. Res. Soc. Symp. Proc*., 2000, 586, 287.

[13] Estroff, L. A., Hamiton, A. D., *Chem. Mater*., 2001, 13, 3227.

[14] Brown, J. M., Curliss, D. Vaia, R. A., *Chem. Mater*., 2000, 12, 3376.

[15] Thostenson, E. T., Li, C., Chou, T. W., *Compo. Sci. Technol.* 2005, *65*, 491.

[16] Breuer, O., Sundararaj, U., *Polym. Comps*, 2004, 25, 630.

[17] Wang, Z., Pinnavaia, T. J., *Chem. Mater*., 1998, 10, 1820.

[18] Giman, J. W., Jackson, C. L., Morgan, A. B., Harris, R. Jr., Manias, E., Giannelis, E. P., Wuthenow, M., Hilton, D., *Chem, Mater*., 2000, 12, 1866.

[19] Zhu, J., Wilkie, C. A., *Polym. Int*., 2000, 49, 1158.

[20] Osman, M. A., Ewing, G. E., *J. Phys. Chem. B*., 2001, 105, 23, 5434.

[21] Zanetti, M. Camino, G., Canavese, D., Morgan, A. B., Lamelas, F. J., Wilke, C. A., *Chem. Mater*. 2002, 14, 189.

[22] Brandl, W., Marginean, G., Chirila, V., Warschewski, W., *Carbon*, 2004, 42, 5.

[23] Tibbetts, G. C., Doll, D. W., Gorliewicz, J. J., Moleski, T. A. Perry, C. J. Dasch, C. J., Balogh, M. P., *Carbon*, 1993, 31, 1039.

[24] Endo, M., Koyama, T., Hishiyama, Y. M., Jap. *J. Appl. Phys*., 1976, 15, 2073.

[25] Tibbettis, G. C., Beetz, Jr. C. P., *J. Physics D*, 1987, 20, 292.

[26] Anderson, D. P., Ting, J. M., Lake, M. L., Alig, R. L., 22nd Biennial Conference on Carbon, American Carbon Society, July 1995, 304.

[27] Alig, R., Ting, J., The European Carbon Conference "Carbon 96", New castle, UK, 1996.

[28] Tibbetts, G. C., Devour, M. G., Rodda, E. J., *Carbon*, 1987, 25, 367.

[29] Tibbetts, G. C. et al., *Carbon*, 1993, 31, 1039.

[30] Dresselhaus, M. S., Lin, Y. M.; Rabin, O., Jorio, A., Saito, R., *Mater. Sci. Eng.*, 2003, C23, 129.

[31] Yu, M. F., Files, B. S., Arepalli, S., Ruo, R. S., *Phys. Rev. Lett*., 2000, 84, 5552.

[32] Krishman, A. Dujardin, E., Ebbesen, T. W., Yialios, P. N., Treacy, M. *J., Phys Rev. B*, 2001, 58, 14013.

[33] Demczyk, B. G., Wang, Y. M., Cumings, J., hetman, M., Han, W., Zettl, A., Richie, R. O., *Mater. Sci. Eng. A*, 2002, 334, 173.

[34] Baughman, R. H., Zakhidov, A. A., Heer, W. A., *Science*, 2002, 297, 787.

[35] Wong, E. W., Shennhan, P. E., Lieber, C. M., *Science*, 1997, 227, 1971.

[36] Cooper, C. A.; Cohen, S. R.; Barber, A. h.; Wagner, H. D. *Appl. Phys. Lett.*, 2002, *81*, 3873.

[37] Gojny, A.; Nastalczyk, J.; Roslaniec, Z.; Schulte, K. *Chem. Phys. Lett.*, 2003, *370*, 820.

[38] Pyun, J., Matyjaszewski, K., Wu, J., Kim, G. M., Chun, S. B., Mather, P. T., *Polymer*, 2003, 44, 2739.

[39] Unno, M., Suto, A., Takada, K., Matsumoto, H., *Bull. Chem. Soc. Jpn.*, 2000, 73, 215.

[40] Xie, P., Zhang, R., *Polym. Adv. Technol.*, 1997, 8, 649.

[41] Xu, H., Xie, P., Zhang, R., *Europ. Polym. J.*, 2001, 37, 2397.

[42] Lichtenhan, J. D., *Comments Inorg. Chem.*, 1995, 17, 115.

[43] Lichtenhan, J. D., Polymeric Material Encyclopedia; Salamone, J. C. Ed; CRC Press, New York, 1996, 10, 7768.

[44] Feher, F. J.; Budzichowski, T. A., *Polyhedron*, 1995, 14, 3239.

[45] Deng, J., Polidan, J. T., Hottle, J. R., Farmer-Creely, C. E., Viers, B. D., Esker, A. R., *J. Am. Chem. Soc*., 2002, 124, 15194.

[46] Scott, D. W., *J. Am. Chem. Soc*., 1946, 68, 356.

[47] Brown, J. F., Vogt, L. H., *J. Am. Chem. Soc*., 1965, 87, 4313.

[48] http://www.hybridplastics.com/posstech.html

[49] Lichtenhan, J. D., Schwab, J. J., Feher, F. J., Soulivong, D., U. S. Patent, 1999, 5942638.

[50] Lichtenhan, J. D., *Comments Inorg. Chem.*, 1995, 17, 115.

[51] Voigt, A., *Organometallics*, 1996, 15, 5097.

[52] Feher, F. J., Weller, K. J., *Inorg. Chem*., 1991, 30, 880.

[53] Ellsworth, M. W., Gin, D. L., *Polym. News*, 1999, 24, 331.

[54] Lichtenhan, J. D., Schwab, J. J., *Int. SAMPE Technol. Conf.*, 2000, 32, 185.

[55] Mather, P. T., Jeon, H. G. T., Haddad, T. S., *Polym. Prepr.*, 2000, 41, 528.

[56] Haddad, T. S., Choe, E., Lichtenhan, J. D., *Mater. Res. Soc. Symp. Proc.*, 1996, 435, 25.

[57] Haddad, T. S., Stapleton, R., Jeon, H. G., Mather, P. T., Lichtenhan, J. D., Phillips, S. H., *Polym. Prepr.*, 1999, 40, 496.

[58] Phillips, S. H., Blanski, R. L., Svejda, S. A., Haddad, T. S. Lee, A., Lichtenhan, J. D., Feher, F. J., Mather, P. T., Hsiao, B. S., *Mater. Res. Soc. Symp. Proc.*, 2000, 628, CC4.6.1

[59] Blanski, R. L., Phillips, S. H., Chaffee, K., Lichtenhan, J. D., Lee, A., Geng, H. P., *Polym. Prepr.*, 2000, 41, 585.

[60] Xu, H. Y., Kuo, S. W., Lee, J. Y., F. C. Chang, *Polymer*, 2000, 43, 5117.

[61] Pellice, S. A., Fasce, D. P., Williams, R. J. J., *J. Polym. Sci. Part B: Polym. Phys.* 2003, 41, 1451.

[62] Lee, A., *Mater. Res. Soc. Symp. Proc.*, 1999, 576, 343.

[63] Philips, S. H., Gonzalez, R. I., Chaffee, K. P., Haddad, T. S., Hoflund, G. B., Hsiao, B. S., Fu, B. X., *SAMPE* 2000, 45, 1921.

[64] Huang, J. C., He, C. B., Xiao, Y., Mya, K. Y., Dai, J., Siow, Y. P., *Polymer*, 2003, 44, 4491.

[65] Fu, B. X., Namani, M., Lee, A., *Polymer*, 2003, 44, 7739.

[66] Lichtenhan, J. D., Otonari, Y. A., Carr, M. J., *Macromolecules*, 1995, 28, 8435.

[67] Haddad, T. S., Lichtenhan, J. D., *Macromolecules*, 1996, 29, 7302.

[68] Bharadwaj, R. K., Berry, R. J., Farmer, B. L., *Polymer*, 2000, 41, 7209.

[69] Tsuchida, A., Bolln, C., Sernetz, F. G., Frey, H., Mulhaupt, R., *Macromolecules*, 1997, 30, 2818.

[70] Lee, A., Lichtenhan, J. D., *Macromolecules*, 1998, 31, 4970.

[71] Pan, G., Mark, J. E., Schaefer, D. W., *J. Appl. Polym. Sci. B*. 2003, 41, 3314.

[72] Voronkov, M. C., Lavrent'yev, V. I., *Topics Curr. Chem*., 1982, 102, 199.

[73] Feher, F. J., Terroba, R., Jin, R., Wyndham, K. O., Lucke, S., Brutchey, R., Nguyen, F., *Polm. Mater. Sci. Eng.*, 2000, 82, 301.

[74] Li, G., Wang, L., Ni, H., Pittman, C. U., *J. Inorg. Organomet. Polm.* 2001, 11, 123.

[75] Frye, C. L., Collins, W. T., *J. Am. Chem. Soc*., 1970, 92, 5586.

[76] Sprung, M. M., Guenther, F. O., *J. Am. Chem. Soc.*, 1995, 77, 3390.

[77] Sprung, M. M., Guenther, F. O., *J. Am. Chem. Soc.*, 1995, 77, 3396.

[78] Fesh, F. J., Newman, D. A., Walzer, J. F., *J. Am. Chem. Soc*., 1989, 111, 1741.

[79] Lichtenhan, J. D., Vu, N. Q., Cater, J. A., Gillman, J. W., Feher, F. J., *Macromolecules*, 1993, 26, 2141.

[80] Haddad, T. S., Oviatt, H. W., Schwab, J. J., Mather, P. T., Chaffee, K. p., Lichtenhan, J. D., *Polm. Prepr. Am. Chem. Soc. Div. Polym. Chem*., 1998, 39, 611.

[81] Lichtenhan, J. D., Otonari, Y. A., Carr, M. J., *Macromolecules*, 1995, 28, 8435.

[82] Schwab, J. J., Lichtenhan, J. D., *Appl. Organometal. Chem*., 1998, 12, 707.

[83] Xiao, J., Feher, F. J., *Polymeric Materials Science and Engineering*, 2002, 86, 171.

[84] Gillman, j. W., Schlitzer, D. S., Lichtenhan, J. D., *J. Appl. Polym. Sci*., 1996, 60, 591.

[85] Feher, J., Weller, K. J., *Organometallics*, 1990, 9, 2638.

[86] Lee, L. H., Chen, W. C., *Polymer*, 2005, 46, 2163.

[87] Sellinger, A., Laine, R. M., *Macromolecules*, 1996, 29, 2327.

[88] Huang, J., He, C., Liu, X., Xu, J., Tay, C. S. S., Chow, S. Y., *Polymer*, 2005, 46, 7018.

[89] Hasegawa, I., *J. Sol-Gel Sci. Technol*., 1993, 1, 57.

[90] Hasegawa, I.,Motojima, D., *J. Organomet. Chem*., 1992, 441, 373.

[91] Matĕjka, L., Strachota, A., *Macromolecules*, 2004, 37, 9449.

[92] Fu, B. X., Yang, L., Somani, R. H., Zong, S. X., Hsiao, B. S., Phillips, S., Blanski, R., Ruth, P., *J. Polm. Sci. Part. B: Polym. Phys*., 2001, 39, 2727.

[93] Li, G. Z., Wang, L., Toghiani, H., Dalton, T. L., Pittman, C. U. Jr., *Polymer*, 2002, 43, 4167.

[94] Zhang, W., Fu, B. X., Seo, Y., Schrag, E., Hsiao, B., Mather, P. T., Yang, N., Xu, D., Ade, H., Rafailovich, M., Sokolov, J., *Macromolecules*, 200, 35, 8029.

[95] Lee, A., POSS Nanotechnology Conference, 2002, Sept, Huntington Beach, CA. 25.

[96] Li, G. Z., Wang, L., Toghiani, H., Pittman, Jr. C.U., Daulton, T. L., Koyyama, K, *Macromolecules*, 2001, 34, 8686.

[97] Choi, J., Harcup, J., Yee, A. F., Zhu, Q., Laine, R. M, *J. Am. Chem. Soc*., 2001, 123, 11420.

[98] Choi, J., Kim, S. G., Laine, R. M., *Macromolecules*, 2004, 37, 99.

[99] Ni, Y., Zheng, S., Nie, K., *Polymer*, 2004, 45, 5557.

[100] Liu, Y., Zheng, S., Nie, K., *Polymer*, 2005, 46, 12016.

[101] Lichtenhan, J. D., Mantz, P., Jones, P., Gillman, G., Chaffee, K., Ismail, I., Bumiester, M., *Polymer. Prints*, 1995, 36, 334.

[102] Lichtenhan, J. D., Mantz, P., Jones, P., Gillman, G., Chaffee, K., Ismail, I., Bumiester, M., *Chem, Mater*., 1996, 8, 1250.

[103] Feher, F., Weller, K., *Chem. Mater*., 1994, 06, 7.

[104] Lee, S., *J. Am. Chem. Soc*., 1994, 116, 11819.

.

CHAPTER II

DYNAMIC PROPERTIES OF VISCOELASTIC MATERIALS

Amorphous polymers

The amorphous polymers have randomly coiled chains (Figure 2.1). Therefore, the movement of a chain in a polymeric system is highly restricted due to entanglements with other chains.

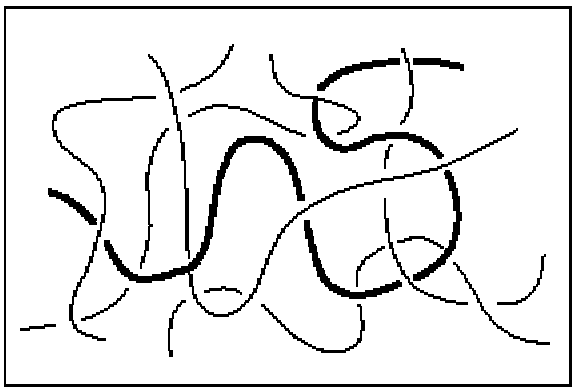

Figure 2.1 An entangled polymer

Molecular motion in amorphous polymers is generated by bond rotations within chains, which is possible only if the temperature is high enough to allow the rotational energy barriers in the chain to be overcome by thermal energy. Cooperative rotations must occur and free volume may not always be available to many segments so these motions are restricted and guided by adjacent segments of other chains. When a polymer's temperature increases, the additional thermal energy results in faster rates of

molecular motion. Therefore, the sample passes from a glass state to and through a rubber-like state when heated until finally it becomes a viscous liquid.

The physical state of a polymer is related to the extent of the molecular motion in the sample, which is governed by the chain mobility and the temperature of the system [1]. Depending on the polymer structure, four viscoelastic regions are found over a given temperature range for each specific linear amorphous polymer. These regions depend on the extent and rate of molecular motion within polymeric system. This gives rise to the four domains of viscoelastic behavior. (Figure 2.2) [1].

(1) Glassy region. In the glassy state, a relatively low temperature results in frozen chains. Therefore, segmental motion along the chain is frozen, causing the material to respond like an elastic solid to stresses.

(2) Transition region. This is the transition area where the modulus drops sharply. The glass transition temperature T_g is located here. In this region, segmental cooperative motions occur but while the modulus is still dropping molecular motion leading to displacements is still slow.

(3) Rubbery state. This is the region where the modulus curve begins to flatten out into the plateau region due to the fact that long polymer molecules are entangled. Over the whole scale, translational motions of polymer chains relative to each other are forbidden. If placed under a stress, elastic deformation may be followed by a slower, time dependent strain in which some relative disentanglement can occur with some permanent elongation occurring through “creep”. The rate of this process is highly temperature dependent as we shall see later.

(4) Flow region. This is the region where molecular motion is so extreme that even chain entanglements are no longer effective in preventing the flow of one molecule past another and a liquid-like behavior is realized. Here, flow occurs when the polymer is stretched or when subjected to some sort of stress.

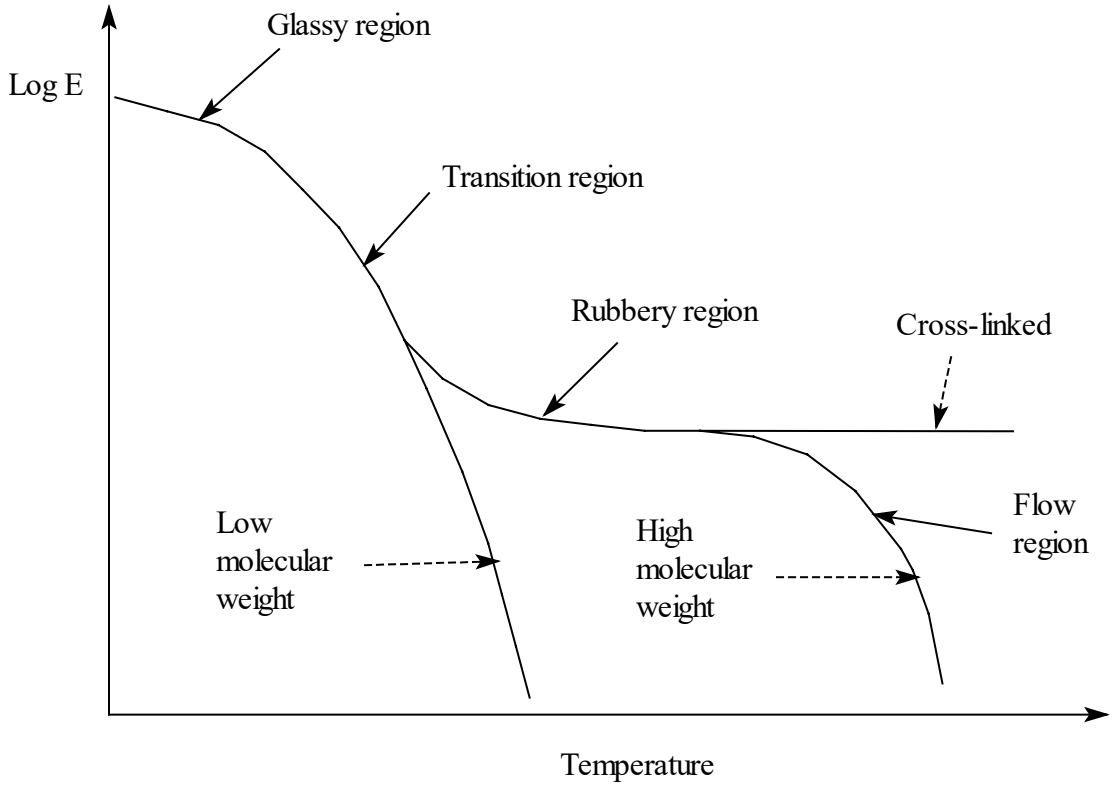

Figure 2.2 Four regions of viscoelasticity [1]

The modulus-temperature behavior of a polymer can be changed by various circumstances such as molecular weight variation, formation of crystalline regions and cross-linking [1]. Longer, high molecular weight chains have more entanglements on average than shorter ones. Thus, the onset of the rubbery flow region goes to higher temperature at quite high molecular weight. This is an effect of serious chain

entanglements which take more molecular motion to undo (Figure 2.2). A cross-linked polymer does not exhibit a flow region because cross-linking creates a permanent restriction to flow. Increasing temperature does not change this restriction because chemical bond must break to separate one chain from the crosslinked mass.

Molecular understanding of amorphous polymers

In the amorphous state, the distribution of polymer chains in the matrix is random. No structures are encountered where crystallites exist having partial crystallinity which locks adjacent chains in place. This allows the onset of molecular motion in amorphous polymers to take place at temperatures below the melting temperature of such crystallites if they were present [2]. The amorphous polymers can be in the glassy state, rubbery state or molten state upon going from low to high temperature because segmental and chain mobility increase as temperature increases.

Glassy state

When a linear amorphous polymer is in the glassy state, the segmental motions are "frozen" in place because not enough thermal energy is available to activate these motions. An amorphous polymer in this state has been thought as a plate of frozen spaghetti. If a small stress is applied to a polymer glass, it exhibits an instantaneous elastic response and recovers its original shape when a stress is released (Figure 2.3). The sample in this state has no way to dissipate a large applied stress, other than by bond rupture, and so a polymeric glass is prone to brittle fracture.

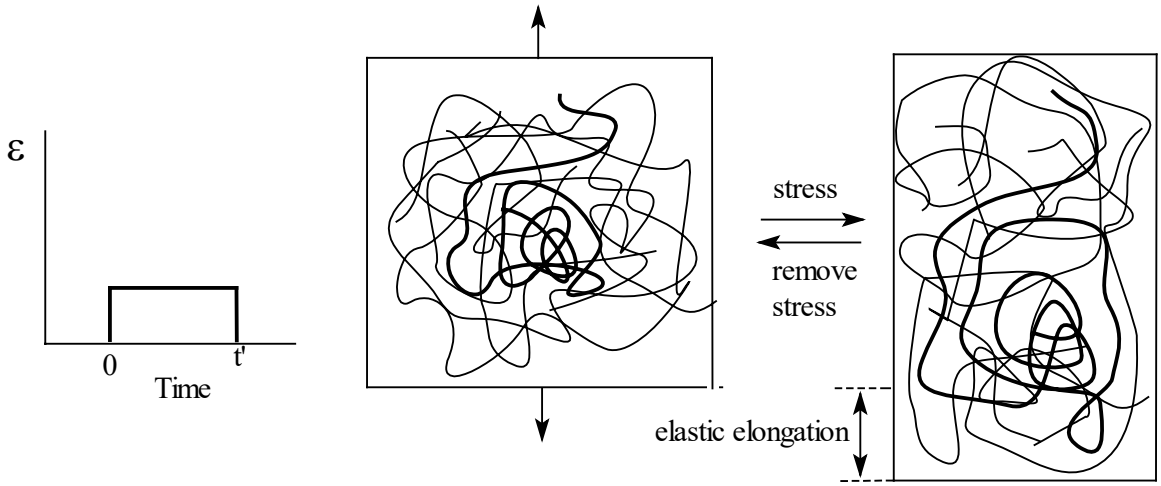

Figure 2.3 Strain (ε) vs time curves and molecular motion in the glassy region

Glass transition state

When sufficient thermal energy is supplied to the system to allow the chain segments to move cooperatively, a transition from the glass to the rubber-like state begins to take place. Molecular motion is still restricted at this stage. However, a large number of chain segments begin to move with greater freedom as the temperature increases. This glass transition can be thought as the transformation of a strong or stiff spring to a weaker spring [2]. Since weak springs can only store a smaller amount of the potential energy, other energy is lost as heat, which can be detected as mechanical damping. As the temperature increases, all the chains behave like weak springs all the time. Therefore, the material's modulus drops much lower, as does the damping. Damping passes through a maximum in the vicinity of T_g. This maximum appears because the polymer is passing from the low damping glassy state, through the high-damping transition region, to the lower-damping rubber-like state.

The transition from a glass to a rubber is a function of molecular motion [2]. Molecular motions depend on the polymer's structure, the magnitude of chain-chain attractions (Van der Walls forces, dipole-dipole attractions, H-bonding etc), the rotational barriers of various bonds along the main chain, excluded volume effects and pendant group structures etc. Rigid rod structures (long cylinder-like structures) can more readily rotate about the main chain axis but will have a hard time tumbling end over end (Figure 2.4) (like pieces of unlocked spaghetti in a random pile which rotate easily around the long axis but can't tumble).

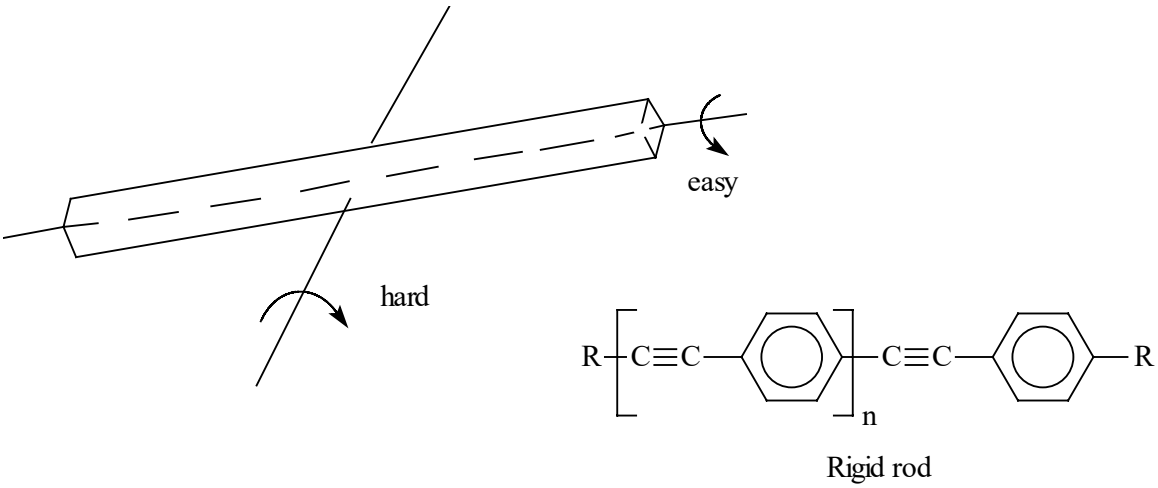

Figure 2.4 An example of a rigid rod and its rotation about the main chain

In an amorphous random coil (or a group of random entangled coils), segments near regions of free volume undergo segmental motion more rapidly and easily at a given temperature and they have a lower onset temperature for segmental motion (Figure 2.5). All sorts of segment sizes can be activated while entanglements between chains remain. As temperature rises some disentanglements occur but many remain which require more

complex relative translations of chains to undo. Therefore, as temperature rises, segmental motions go from glass-like to rubber-like activation. This takes place progressively over a temperature range. It is not sharply defined like the melting point or boiling point of water.

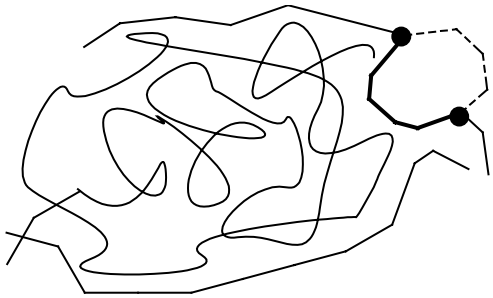

Figure 2.5 Free volume: The darkened segment (for example 5 to 20 carbons) can have a jumprole like segmental motion since the motion is not impeded by other chains in that volume element.

Rubbery state

The rubber region lies at a temperature above T_g. The rotations occurring along the chain allow the chain to assume lots of available conformations, without significant chain disentanglement taking place on the specific time scale discussed. The majority of these overall chain conformations will be compact coils simply because there are a far greater number of these conformations possible, so the probability that such a conformation is present is far higher. Therefore, their occurrence is thermodynamically favorable. When all conformations possible for a large group of chains is present, the disorder is greater (higher entropy) than when this same large group of chains is present in a smaller group of more elongated conformations (more order, lower entropy) (Figure 2.6) [2].

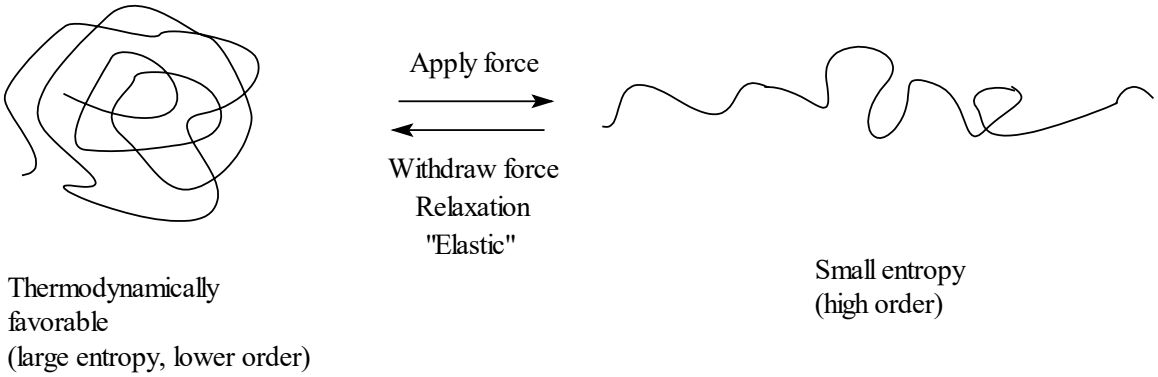

Figure 2.6 Representation of elasticity in the rubbery state [2]

When a polymer is in the rubbery state it will elongate in the direction of an applied stress due to some relative disentanglement. If the stress is applied for a short time, then removed, the sample snaps back to its original, far more probable, length. This will always be true of a single polymer molecule with no neighbors. But, if the stress is maintained on a real polymeric material with many entangled polymer molecules for a long time, then a relaxation process takes place allowing permanent deformation through "creep" [3]. The molecules are initially in highly coiled and entangled conformations but application of a force causes rotation about the chemical bonds along the chains. These rotations produce more staggered butane-like conformations enabling an elongation of the molecules in the direction of the stress (Figure 2.7). This produces a less probable distribution of chain conformations. Since this is an unstable state, the chains will rapidly recoil when the stress is released for short periods of stress. However, if the stress is maintained for a long time, there is a general tendency for chains to slip past one another into a new position where segments can relax and regain a stable coiled form (Figure 2.8) [3].

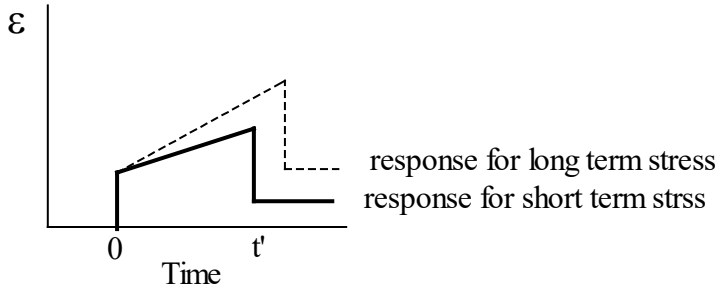

Figure 2.7 Strain vs time curves in the rubbery region

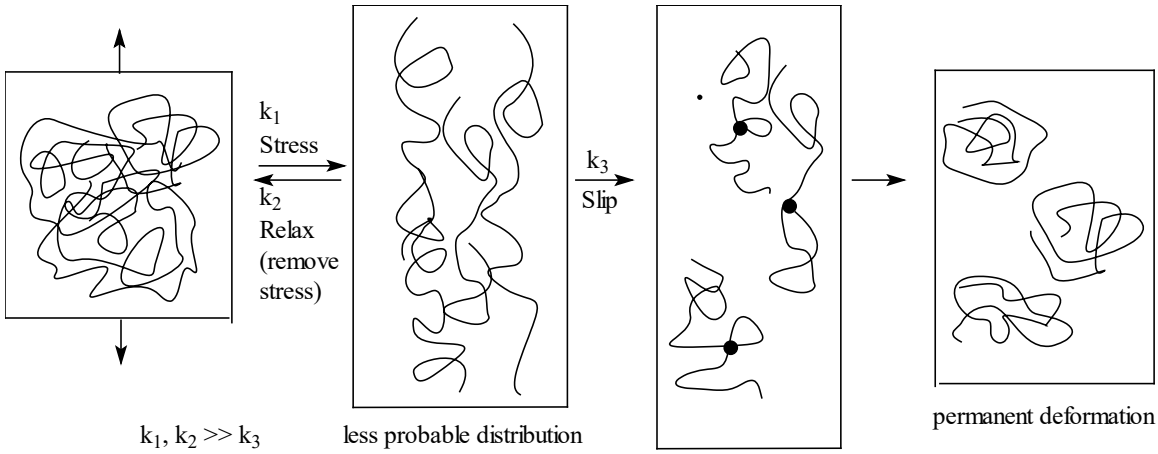

Figure 2.8 Representation of permanent deformation in the rubbery state

Flow state

When polymer chains are forced to move in the melt state, entanglements must be overcome by cooperative segmental motions and reptation motions (Figure 2.9). Reptation motions are like those of a single snake tangled in a ball of snakes as that single snake moves within the tangled ball. Heating will cause a polymer sample's volume to expand, thereby creating more free volume for movement of each kinetic unit and the application of a stress in a particular direction will encourage flow by a combination of reptation and segmental motions in the direction of the stress.

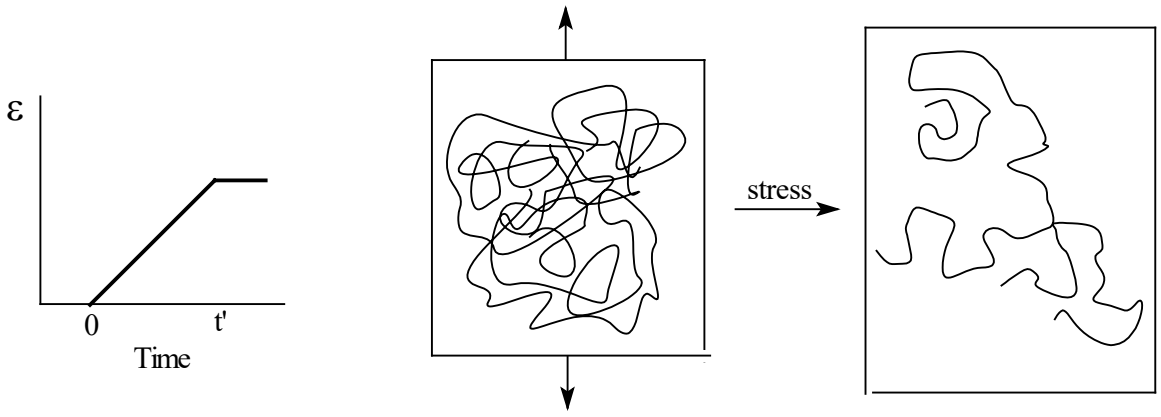

Figure 2.9 Strain vs time curves and molecular motion in the flow state

The movement of a polymer in the melt state has been successfully explained by the reptation model approach (Figure 2.10) [2]. The term "reptation" refers to the motion of a polymer in a highly entangled state. Since linear polymers are entangled with each other like spaghetti, the effect of surrounding chains on the test chain can be simplified by considering the walls of a tube in this model. The tube can be thought of as a random twisted and coiled pipe. Linear polymers can be represented as a single chain confined inside this coiled and a twisted tube-like region where the linear chain can move forward and backward within the tube. The tube acts as a confining barrier that hinders any perpendicular motion of the chain outside the tube's walls. This snake-like sliding motion is called "reptation". When the temperature is high enough in the flow state, the polymer chain reptation takes place fast enough that disentanglement of entangled chains occurs. Then each polymer molecule can move past (translate by) other polymer molecules and also become unknotted (disentangled) in the process.

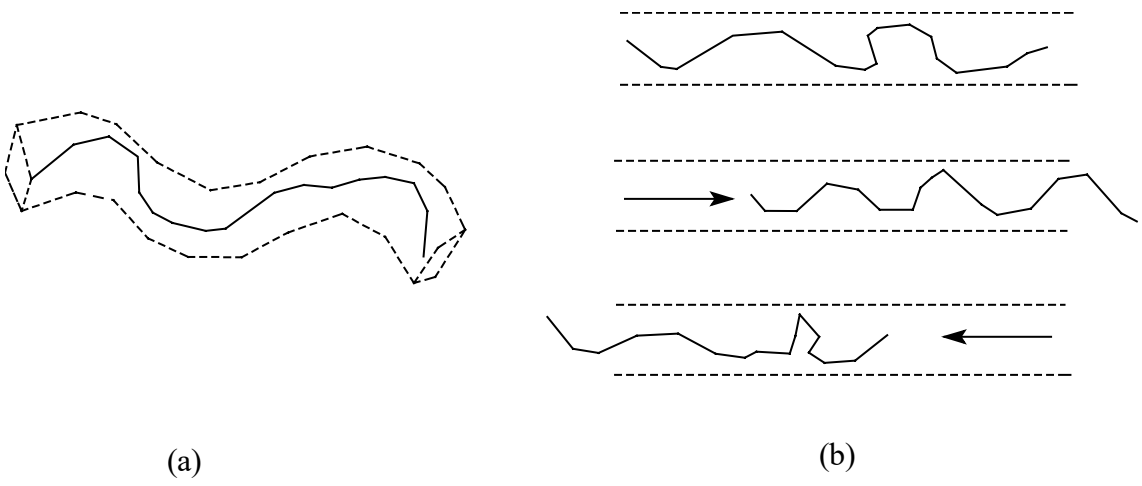

(a) (b)

Figure 2.10 (a) tube model and (b) polymer chain reptation [2]

A single polymer molecule may drag along several others during flow. Energy dissipation is then a combination of the friction between the chain, plus those which are entangled and the neighboring chains as they slip past each other. This reptation model is successful in predicting viscous properties of entangled polymer melts.

Overall polymer molecular structure

The molecular structure of a fully polymerized polymer can be classified according to one of three major types: linear, branched, or crosslinked polymers [3].

Linear polymers become entangled and twisted together, much like a bowl of cooked spaghetti. The number of entanglements is increased as the molecular weight (i.e. the length) of the polymer molecule is increased. Also, the effect of all secondary bonding forces (Van der Walls forces, dipole-dipole attractions, H-bonding, etc) between molecules is increased as the molecular weight is increased. Thus, the elastic stiffness of a bulk polymer is related to the molecular weight, increasing until a characteristic

molecular weight is achieved. After this molecular weight is reached, the solid state properties don't change much more with further increases in chain length.

In branched polymers, relatively short side chains are covalently bonded to the primary backbone of the macromolecule. The stiffness of a branched polymer is related to both the molecular weight and the number of entanglements. Since the branches greatly increase the number of certain types of entanglements, the stiffness of a branched polymer can be greater than that of a linear polymer of identical molecular weight if free volume fractions are equal.

If a linear or branched polymer is heated, the average distance between individual molecular chains is increased as temperature is increased due to the increase in thermal energy and free volume. An increase in molecular motion occurs along with a decrease in secondary bonding forces and stiffness. When a temperature is reached at which the polymeric molecules can slide rapidly past each other, the bulk polymer melts. Sharp melting points do not exist. Instead, the viscosity of the material steadily decreases until molecular motion is fast enough for flow to occur on some defined time scale. Such polymer that can be melted is called a thermoplastic [3].

Crosslinked polymers are themselves linked together by covalent bonds. Therefore, the entire molecular network can be considered as a single molecule. In contrast to thermoplastics, crosslinked polymers cannot be melted because the crosslinks do not allow unrestricted molecular motion between chain segments. If the temperature is raised high enough, the covalent bonds that form the crosslinks, as well as the backbone of the

molecular chains, are broken. Therefore, chemical degradation occurs and the polymer is destroyed. This type of polymer that cannot be melted is called a thermoset [3].

Viscoelasticity

All polymeric materials, except single crystals, exhibit some viscoelastic properties. Viscoelasticity can be defined as material response that exhibits characteristics of both an elastic solid and a viscous fluid under an influence of an applied stress or strain [4].

For an ideal solid, the mechanical properties can be described by Hooke's law, which states that the applied stress, σ, is proportional to the strain ε, and the proportionality constant is the elastic modulus E. Therefore, $\sigma = E \varepsilon$ (Equation 2.1) [4]. The elastic solid model can be represented by the spring (Figure 2.11); the response is instantaneous, without any time dependency, and the recovery after release of the stress is also instantaneous and complete (Figure 2.11).

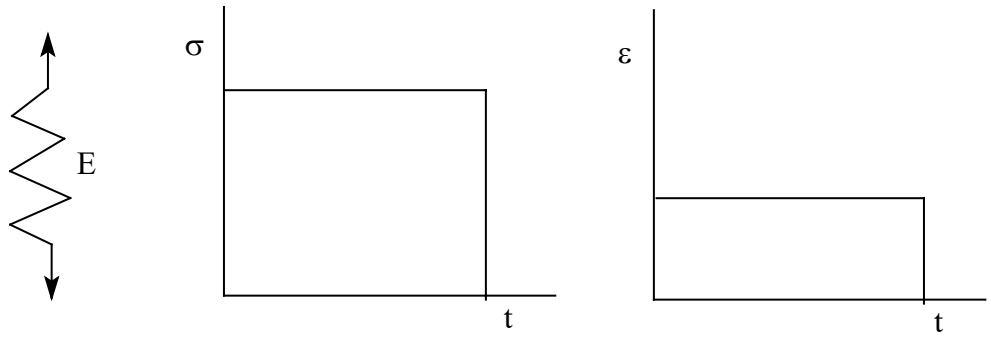

Figure 2.11 Response of an ideal elastic solid

For an ideal liquid, the mechanical properties can be described by Newton's law, which states that the stress is proportion to the rate of the strain $d\varepsilon/dt = \dot{\varepsilon}$ (Equation 2.2),

and the proportionality constant is the viscosity η, so $\sigma = \eta\varepsilon$ (Equation 2.3) [4]. The viscous flow can be represented by a dashpot which is a loose fitting piston in a cylinder containing a liquid of viscosity η (Figure 2.12). In this model, there is no instantaneous response; the strain is proportional to time, and no recovery takes place (Figure 2.12)

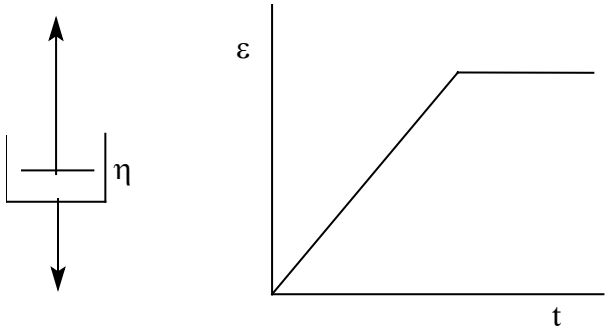

Figure 2.12 Response of an ideal liquid

Polymers exhibit the characteristics of a viscous liquid and an elastic solid. Therefore, the mechanical behavior is governed by viscoelastic phenomena.

Viscoelastic behavior of polymeric materials subjected to the stress or strain

A viscoelastic material will not respond instantaneously when stresses are applied, or the stresses will not respond instantaneously to any imposed deformation [5]. This delayed response between cause and effect is fundamental to the observed viscoelastic behavior. There are three examples of this delayed effect: (1) creep, where there is a delayed strain response after the rapid application of a stress; (2) stress-relaxation, in which the material is quickly subjected to a strain and a relaxation of stress is observed, and (3) dynamic response of a material to a steady sinusoidal stress, which produces a strain oscillating with the same frequency as, but out of phase with, the stress [5].

Mechanical models describing viscoelasticity

The viscoelastic properties of polymers can be obtained by analyzing the stress or strain response of mechanical models using a spring as the elastic element and a dashpot as the viscous element [5].

Maxwell model

The Maxwell model is the combination of a spring and a dashpot in series (Figure 2.13) [5]. The deformation rate is equal to the sum of the individual deformation rates in this model, so $\varepsilon = \varepsilon_{elast} + \varepsilon_{visc}$ (Equation 2.4). Expressing this as the differential equation leads to the equation of motion of a Maxwell unit

$$d\varepsilon/dt = (1/E)d\sigma/dt + \sigma/\eta \quad (2.5)$$

The Maxwell model can be used to explain the mechanical behavior of materials such as creep and stress-relaxation.

(1) Stress Relaxation Experiment

Stress relaxation occurs when the strain (deformation) is kept constant [5]. At $t = 0$ the model is deformed to a strain ε. The instantaneous response is a stress $\sigma_o = E\varepsilon$; the spring is strained, the dashpot does not yet respond. The dashpot is, at $t = 0$, subjected to the same stress, so it starts flowing, while it takes over an increasing part of the imposed strain so that the strain in the spring decreases. At time t, $\sigma = \sigma_o \exp(-(E/\eta)t) = \sigma_o \exp(-t/\tau)$ (Equation 2.6) where $t = \eta/E$, the relaxation time. This shows that the stress will relax exponentially with time when a Maxwell model is held at a fixed strain. (Figure 2.13).

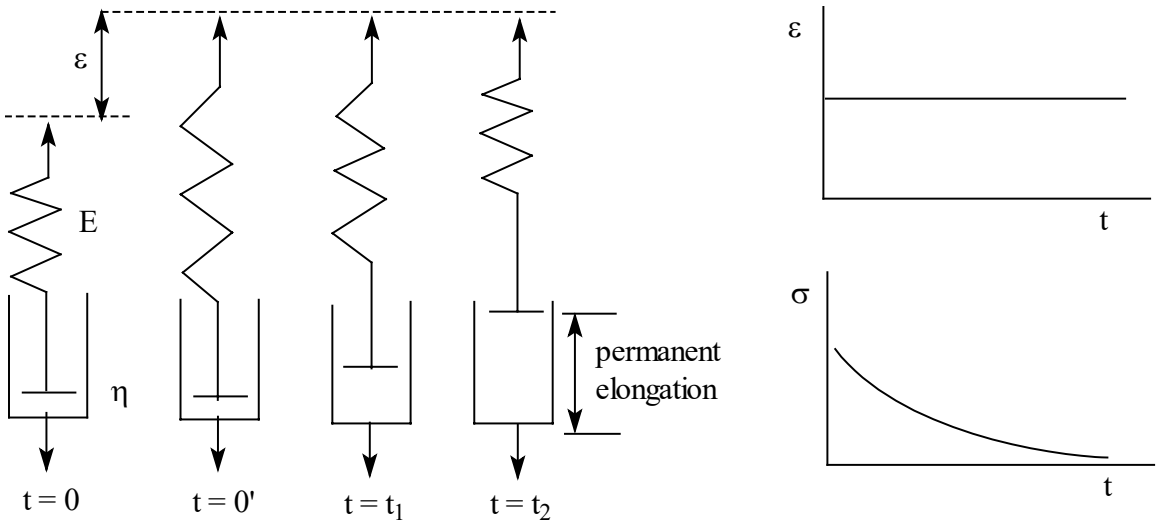

Figure 2.13 Stress relaxation of a Maxwell model

(2) Creep Experiment

Creep is a slow, progressive deformation of a material under constant stress (σ) [5]. The strain under constant stress is the sum of that of its two components, which is a spontaneous elastic deformation (ε_1) which returns when σ =0, plus permanent flow (ε_2) (Figure 2.14).

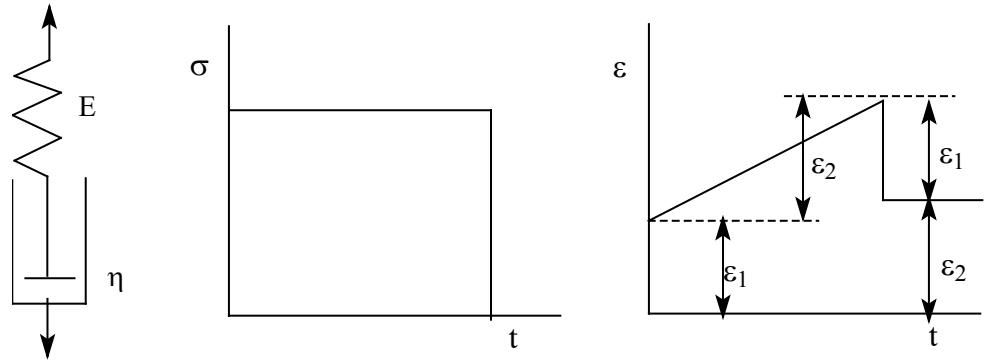

Figure 2.14 Creep of a Maxwell model

The Maxwell model can describe the phenomena of creep recovery, permanent deformation and stress relaxation observed with real materials. Moreover, the Maxwell model exhibits relaxation of stresses after a step strain deformation and continuous deformation as long as the stress is maintained. These are characteristic of liquid-like behavior. Therefore, the Maxwell model represents a viscoelastic fluid.

Voigt model

The Voigt model is a parallel array of a spring and a dashpot (Figure 2.15) [5]. This model does not allow instantaneous deformation of the dashpot thus it does not show stress relaxation. At a constant stress it exhibits creep. At $t = 0$, $\varepsilon = 0$; at time t its strain is $\varepsilon(t) = \sigma/E[1-\exp(-t/\tau)]$ (Equation 2.7) with $\tau = \eta/E$. When the stress is released the creep recovery proceeds asymptotically to $\varepsilon = 0$. The initial portion of the strain recovery is due to the elastic contribution while full recovery is delayed to longer times due to the viscous contribution (Figure 2.15)

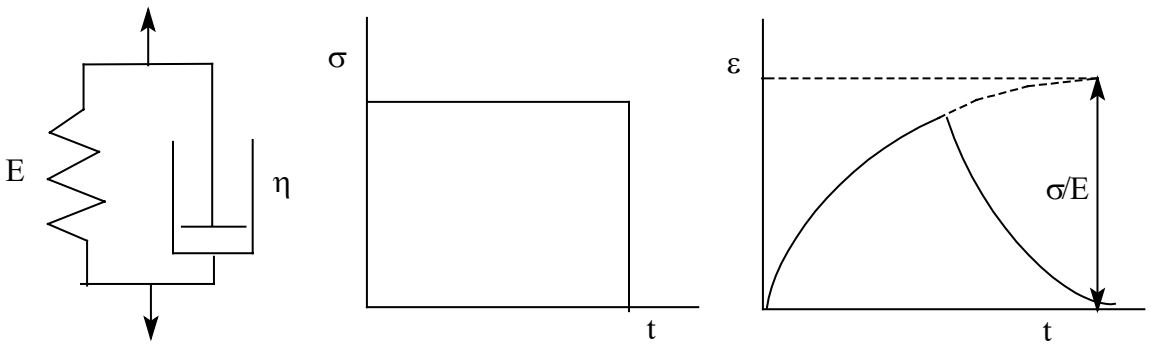

Figure 2.15 Creep of a Voigt model

The Voigt model does not continue to deform as long as stress is applied, rather it reaches an equilibrium deformation. It does not exhibit any permanent elongation. These resemble characteristics of solid-like behavior. Therefore the Voigt element represents a viscoelastic solid.

Both the Maxwell element and Voigt element are limited in their representation of the real viscoelastic behavior because the Maxwell model is able to describe stress relaxation, but only irreversible flow whereas the Voigt model can represent creep, but it cannot explain stress relaxation without instantaneous deformation. A combination of both models, Burger's model, offers more possibilities. It is well suited for a description of creep.

Burger's model

Burger's model (Figure 2.16) is composed of a spring with E_1 and a dashpot with η_2, in series with a Voigt element with E_2 and η_1, and can be used to describe the creep behavior of a polymeric material [5]. It is a Maxwell element tied in series to a Voigt element. A Schematic representation of a creep curve is shown in Figure 2.17. This curve can be represented by four element models. The changes a and a' correspond to the elastic response of the polymer and can be represented by a spring. The Voigt model produces the changes b and b'. The final changes c and c' represent viscous flow and can be represented by a dashpot.

The initial deformation (increment a) corresponds to portion OA of the curve. This rapid response is followed by a region of creep, A to B, initially fast but eventually slowing down to a constant rate represented by the section B to C due to viscous

resistance. When the stress is removed the instantaneous elastic response OA is completely recovered and the curve drops from C to D. There follows a slower recovery in the region D to E, which is never complete. This is a measure of the viscous flow experienced by the sample and is a completely non-recoverable response.

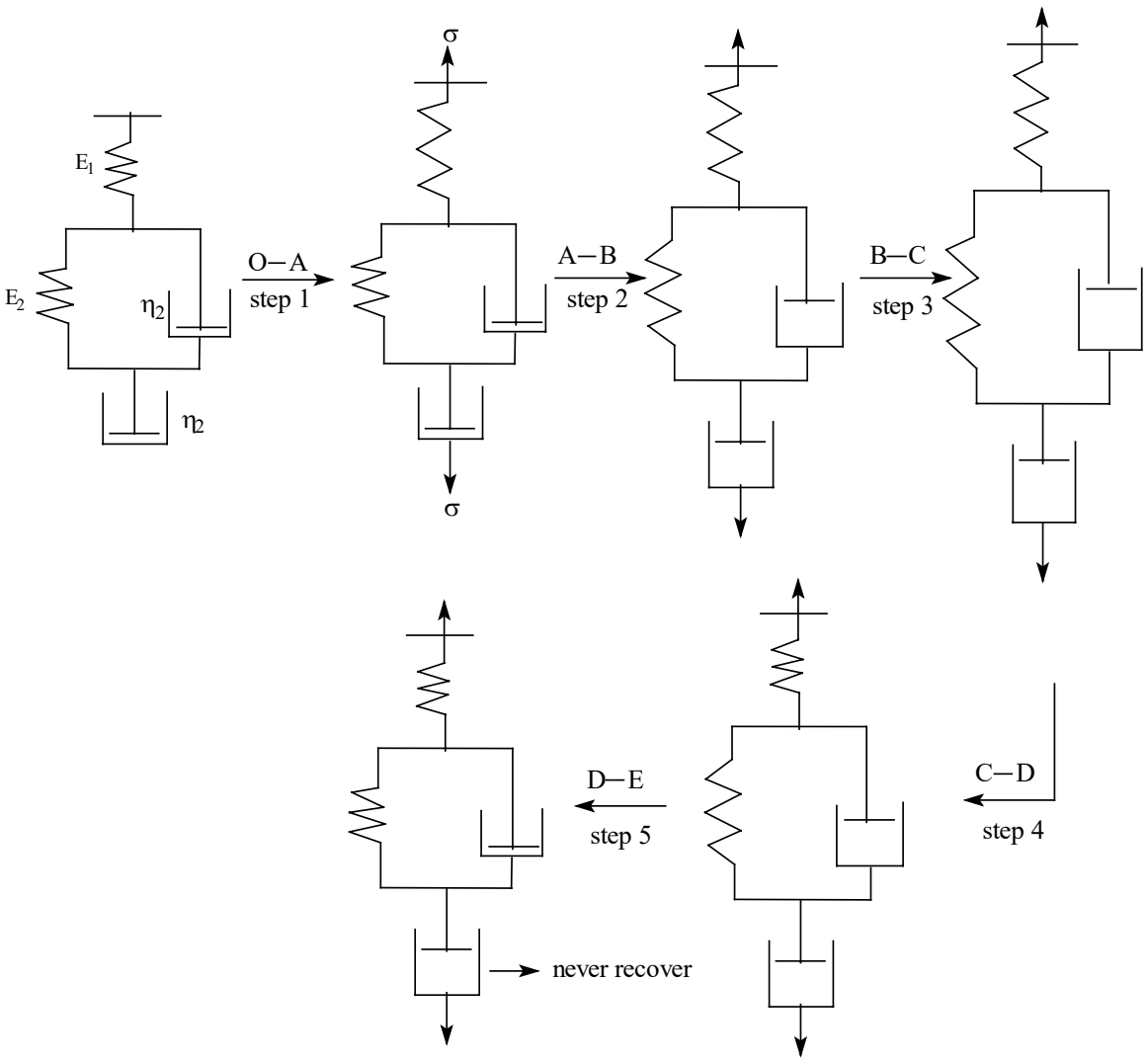

Figure 2.16 Burger's model to describe the creep behavior of a polymer material [5]

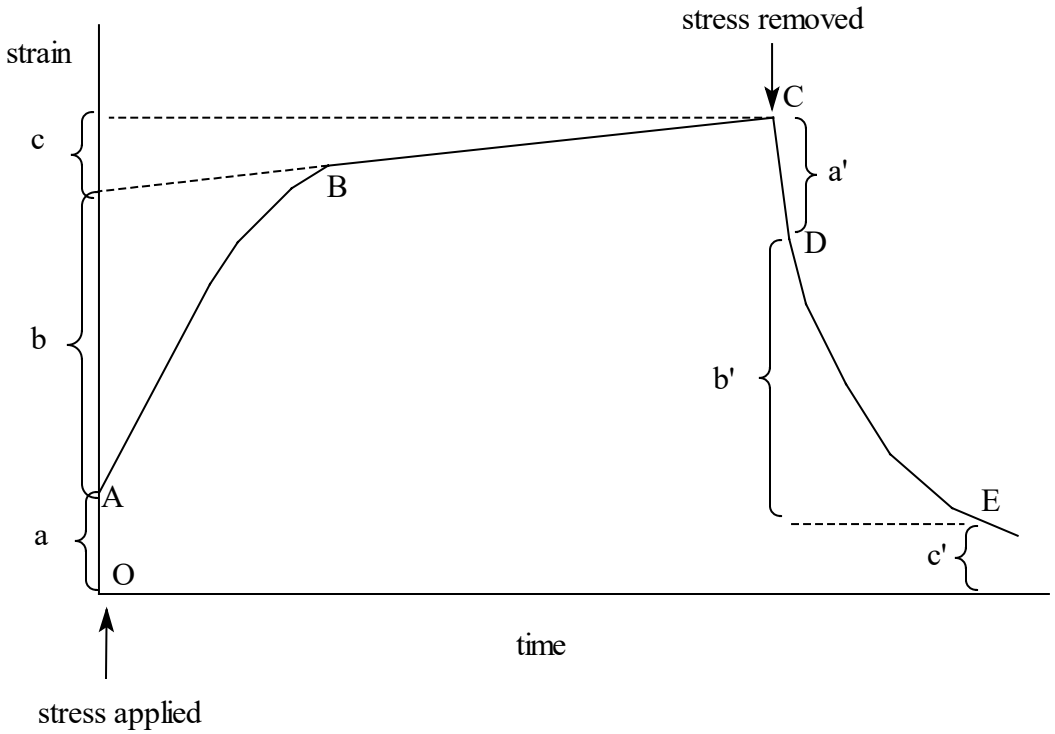

Figure 2.17 A creep curve: a, initial elastic response; b, region of creep; c, irrecoverable viscous flow. This curve can be represented by the Burger's model [5]

The creep behavior in a polymer can be explained by following a series of steps (Figure 2.16), as well as molecular pictures (Figure 2. 18). When the stress is applied to this model, in step (1) the spring E_1 extends by an amount of σ/E_1. This is followed by a decreasing rate of creep with a progressively increasing amount of stress being carried by E2 until eventually none is carried by η_1 and E_2 is fully extended in step (2). When spring E_2 is fully extended the creep attains a constant rate corresponding to movement in the dashpot η_1. Viscous flow continues and the dashpot η_2 is deformed until the stress is removed in step (3). In step (4) E_1 recovers quickly along section a' when the stress is removed and a period of slow recovery (b') follows. During this time spring E_2 forces the

dashpot plunger in η_1 back to its original position. As no force presents on η_2 it remains in the extended state, and corresponds to the non-recoverable viscous flow in step (5).

These three models described so far provide a qualitative illustration of the viscoelastic behavior of polymers. These simple models are not powerful enough to account for the behavior of a real polymer because they use a single relaxation time. This results in the prediction of a single transition in modulus and compliance, whereas high molecular weight polymers exhibit two major transitions (glass to rubber and rubber to liquid transition). This situation may be remedied by considering combinations of elements.

Multielement models

The Maxwell-Wiechert's model is a parallel combination of multiple Maxwell elements (Figure 2.18) [4]. In this model, the strains on each Maxwell element are equal and the stresses experienced by each Maxwell element are additive. Generally, the stress-relaxation modulus of a Maxwell-Wiechert model consisting of n Maxwell elements can be written as

$$E(t) = \sum_{i} Ei\, e^{-t/\tau i} \tag{2.8}$$

i.e., the time dependent moduli for each element sum to give the total modulus of the model.

The Voigt-Kelvin model [4] consists of a series arrangement of Voigt elements. For N elements, the creep compliance can be written as a summation

$$D(t) = \sum_{i} Di\,(1-e^{-t/\tau i}) \tag{2.9}$$

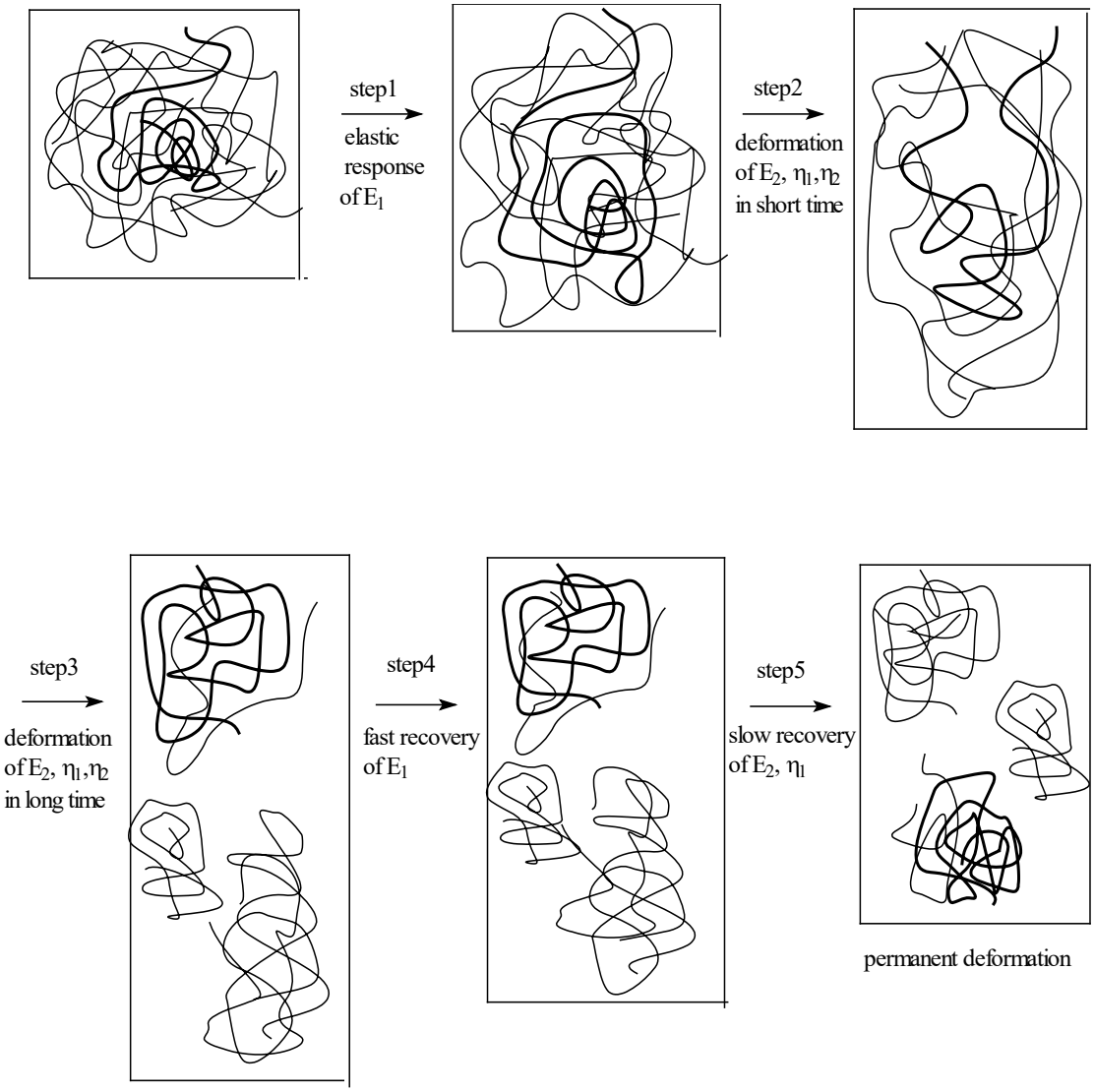

Figure 2.18 Molecular pictures of creep behavior in Burger's model

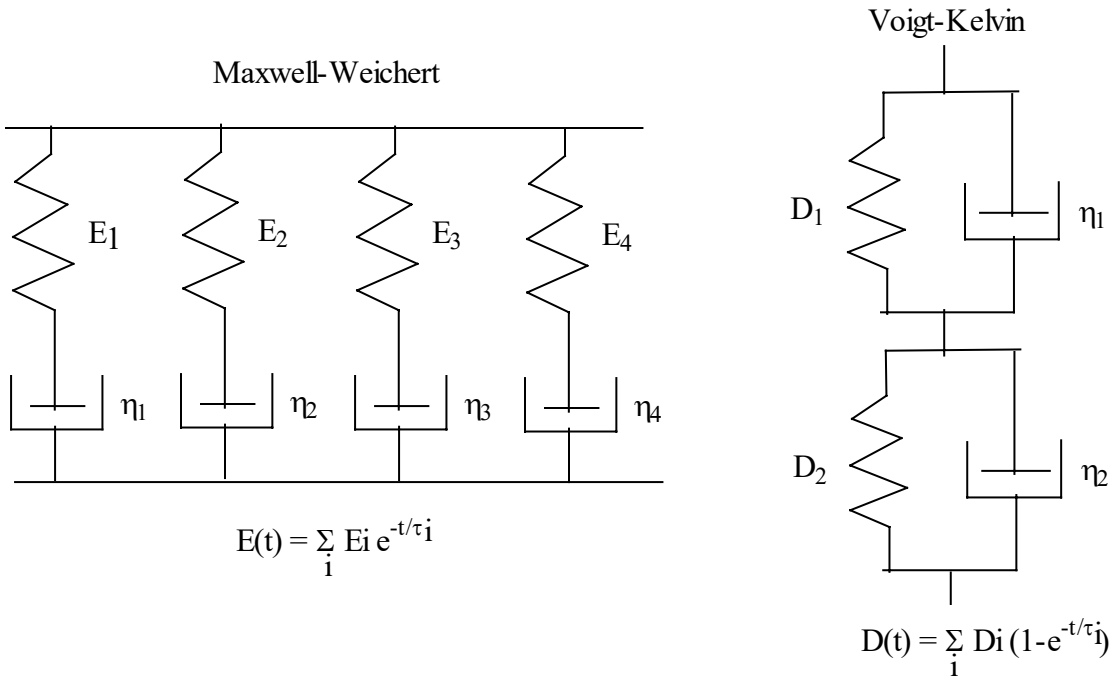

Figure 2.19 Maxwell-Wiechert and Voigt-Kelvin models [4]

Time-temperature superposition

The measurement of a full stress-relaxation or creep behavior at a given temperature can take years. Fortunately, it is possible to shift data taken over shorter time periods but at different temperatures to construct a master curve covering a broad time scale. The principle that allows horizontal shifting of data is called time-temperature superposition [4]. Information from each of these different temperature curves may be combined to yield a master curve at a single temperature by horizontally shifting each curve along the log time scale. In this procedure, the master curve is plotted as stress–relaxation modulus or creep compliance versus reduced time, t/a_T. The shift factor, a_T, is defined as the ratio of real time to reach a particular value of modulus at some

temperature to the reference-scale time coordinate, t_r, corresponding to the same value of modulus in the master curve at the reference temperature, T_r.

$$a_T = t/t_r \tag{2.10}$$

The dependence of the shift factor, a_T, on temperature is given by the Williams-Landel-Ferry (WLF) relationship

$$\log a_T = -C_1(T-T_r)/C_2 + T-T_r \tag{2.11}$$

where C_1 and C_2 are constants for a given polymer and T_r is the reference temperature. When T_r is taken to be the T_g, C_1 and C_2 may be approximated by the universal values of 17.44 and 51.6, respectively. However, these values vary from polymer to polymer.

Creep, stress-relaxation and dynamic mechanical measurements can be simplified by the general applicability of the time-temperature superposition principle; temperature changes are reflected as time scale changes and vice versa.

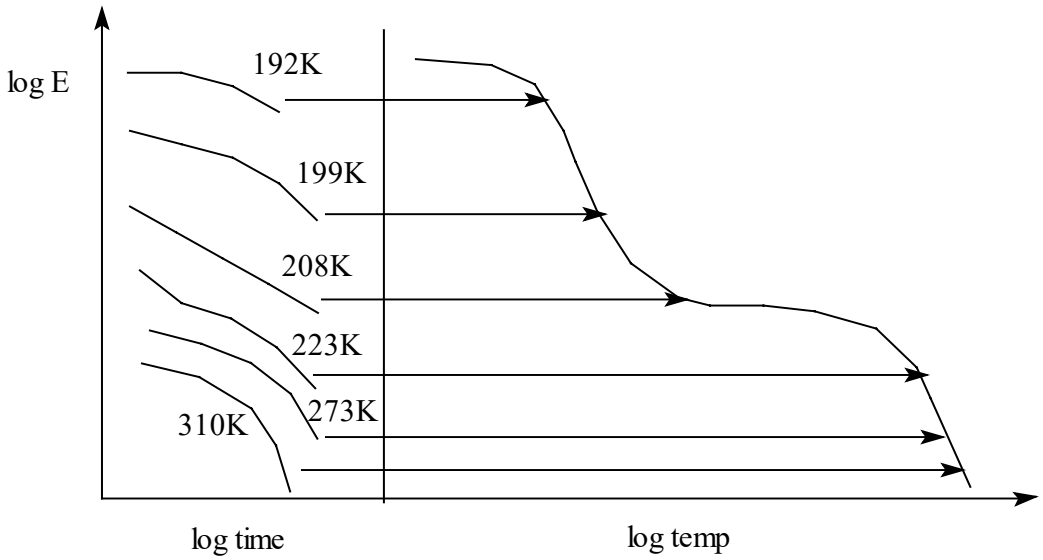

Figure 2.20 Stress-relaxation modulus as a function of time and corresponding master curve at 25 ^{o}C [4]

Dynamic properties of viscoelastic materials

Dynamic mechanical properties of viscoelastic materials can be measured by applying a periodic sinusoidal oscillation to a sample as a function of time and temperature rather than subjecting the material to a step change in stress or strain [5]. If the polymer is treated as a classic harmonic oscillator, both the elastic modulus and the damping characteristics can be obtained. Elastic materials convert mechanical work into potential energy which is recoverable. For example, an ideal spring, if deformed by a stress, stores the energy and uses it to recover its original shape after removal of the stress. No energy is converted into heat during the cycle and so no damping is occurring. Liquids, on the other hand flow, if subjected to a stress. They do not store the energy but dissipate it almost as heat and thus possess high damping properties. Viscoelastic materials exhibit both viscous and elastic behavior. Thus if a sinusoidal stress is applied to a linear viscoelastic material, the resulting stress will also be sinusoidal, but will be out of phase when there is energy dissipation or damping in the polymer. Figure 2.21 shows how various types of materials subjected to a sinusoidal stress behave in the time domain.

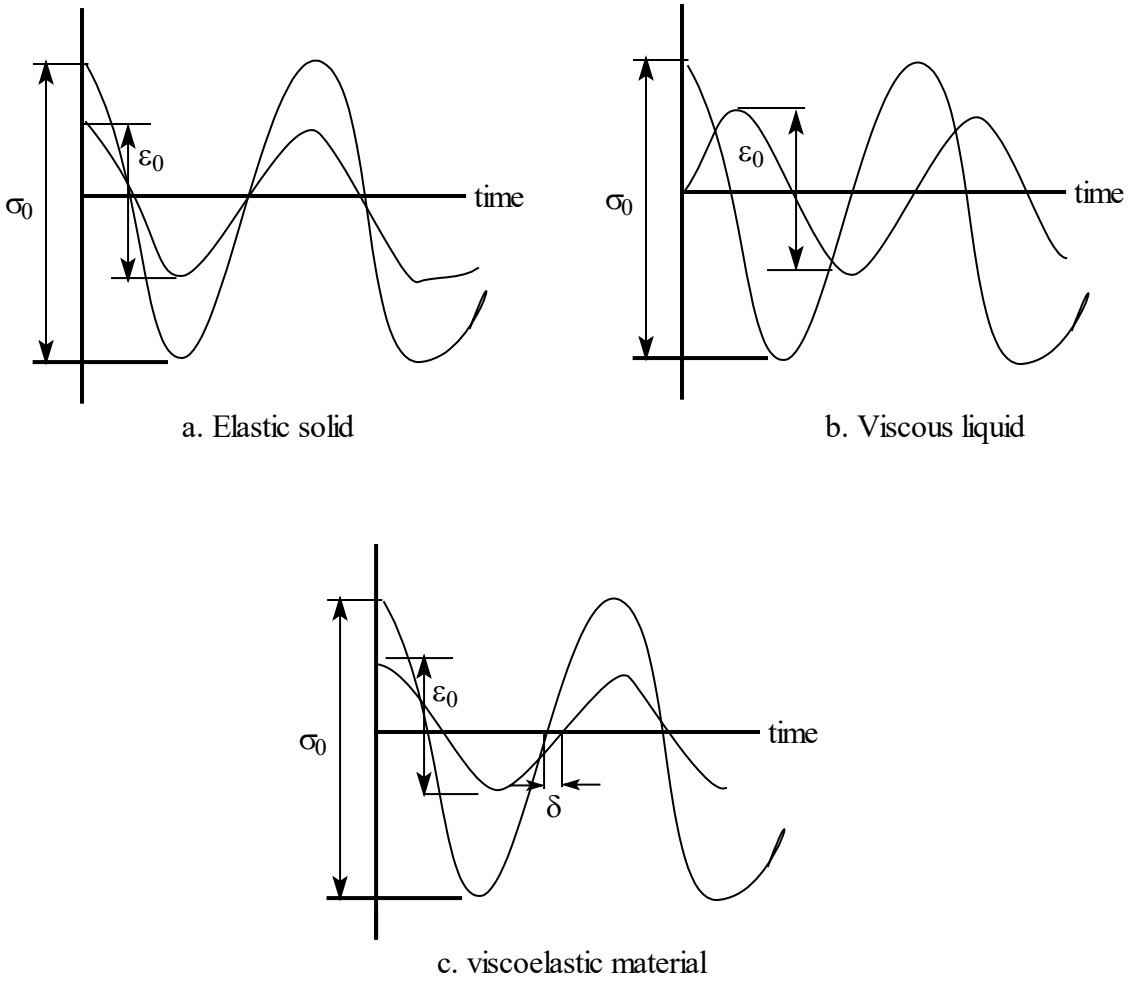

Figure 2.21 Stress and strain curves vs. time for various materials [5]

When a sinusoidal stress is applied to a purely elastic solid, the material stores the mechanical energy without dissipation and strain is in phase with the applied stress. When stress is applied to a liquid, it dissipates all the energy and deformation lags 90^{o} out of phase with the applied stress. If a sinusoidal stress is applied to viscoelastic materials neither perfectly elastic nor totally liquid behavior is observed. Some of the energy stored in a viscoelastic system is recovered upon removal of the stress, and the remainder is dissipated in the form of heat. The strain lags behind the stress by an angle, δ, where

$\delta<90^{o}$. Phase lags results from the time requirement for molecular rearrangements and is related to molecular relaxation phenomena. For a viscoelastic material, the modulus is represented by a complex quantity [5].

$$E^* = E' + iE'' \tag{2.12}$$

The real part of this complex term (storage modulus, E′) relates to the elastic behavior of the material, and defines the stiffness. The imaginary component (loss modulus, E″) relates to the material's viscous behavior, and defines the energy dissipative ability (damping property) of the material. The ratio of the energy lost to the energy stored is defined as tanδ (loss factor). Tanδ, which represents the amount of energy absorbed by a material, is closely related to the resilience of a material. A tanδ value of 0 would indicate perfect elasticity and high resilience. The higher the tanδ value, the higher the energy absorption, and the lower the resilience. The peak of the tanδ output reflects the glass transition temperature. This is the temperature where the molecular chains of a material have obtained enough energy to allow intermolecular bond rotation. Under these conditions, a material transforms from a frozen, glasslike condition with limited mobility to a more mobile system that achieves thermodynamic equilibrium.

The onset of molecular motion in a polymer sample is reflected in the behavior of E′ and E″. Figure 2.22 shows schematic diagrams of the variation of E′ and E″ as a function of temperature (a) and time (b). It is not surprising that the time dependency of E′ resembles the temperature dependency, which follows time-temperature superposition principle that is used to transform material properties from the time domain to temperature domain. Viscoeastic materials exist in various states over the broad

temperature ranges in which they are used and behave differently on which region they exist.

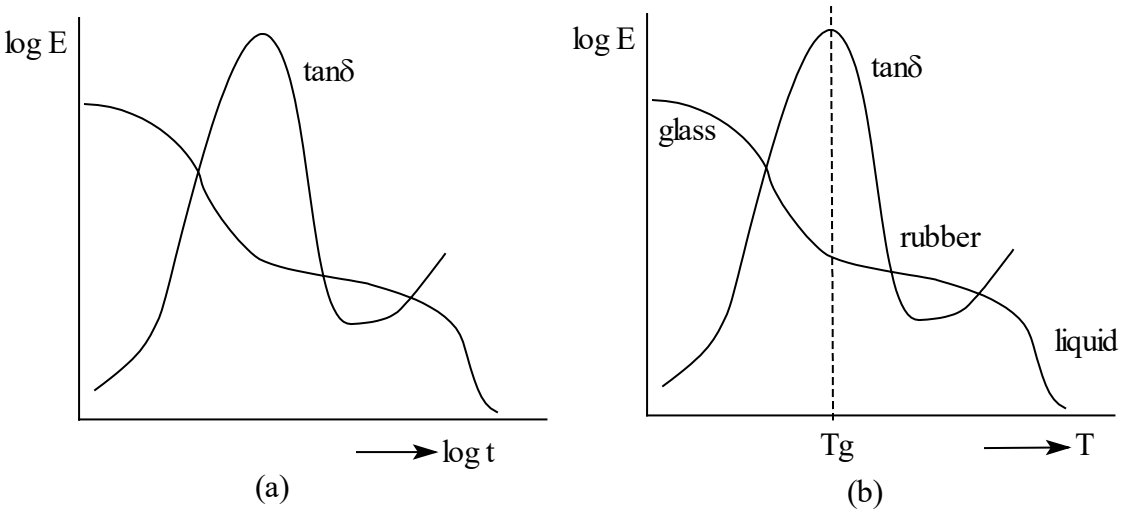

Figure 2.22 Variation of storage modulus and loss factor of a viscoelastic material with time (a) and temperature (b)

In the glassy region, polymer chain motions are so small that they hardly give rise to energy losses (spring-dashpot models: the dashpot hardly moves and the whole deformation is taken up by the spring) because the segmental motions are cooperatively immobile and effectively frozen in position. Hence stiffness, E′, is at its highest for the material in this region, and damping levels are typically low. In the transition region, the material is transforming from a glassy to a rubbery-like state. It is in this area that the viscoelastic material goes though its most rapid change in the magnitude of stiffness per unit change in temperature. This region also possesses the polymer's highest level of damping performance. The long molecular chains of the polymer are in a semi-rigid and semi-flow state, and are able to rub against adjacent chains. These frictional effects result

in the mechanical damping characteristic of viscoelastic materials. In the rubbery region, the rates of deformation are so small that the energy dissipation is low though the viscosity plays a role. Thus the material reaches a lower plateau in stiffness. Damping is also reduced.

The use of DMTA in polymer research

DMTA (dynamic mechanical thermal analysis) gives information about molecular mobility and damping properties. It is widely used to determine compatibility of blends, the degree of cross-linking, mechanical behavior as a function of thermal history and T_g dependence on molecular weight [5].

In this dissertation, DMTA was used to investigate the effect of cross-linking on mechanical and thermal properties of organic-inorganic hybrid nanocomposites containing POSS reinforcements. DMTA was also used to investigate the effect of very large polyhedral oligomeric silsesquioxane monomers (or fillers) introduced into crosslinked thermoset. When a polymer is cross-linked, an increase in the glass transition can occur or the T_g can disappear. As free volume disappears, the segmental motion in the sample is restricted and T_g rises. The storage modulus decreases when temperature increases and shows a substantial drop at T_g for lightly cross-linked materials such as rubbers. A broadening of the loss factor peak is another effect of cross-linking. Highly cross-linked materials have no glass transition at all since the motion of long segments of the main chain is not possible.

References

[1] Billmeyer, Jr., F.W., Text Book of polymer Science, John Wiley & Sons., 1984, New York

[2] Ferry, J.D., Viscoelastic Properties of Polymers. 1980, Jhon Wiley & Sons, New York

[3] Mccrum, N. G., Buckley, C. P., Bucknall, C. B., Principle of polymer engineering. Oxford Science Publication, 1988, New York

[4] Fried, J. R., Polymer Science and Technology, Prentice Hall PTR, Englewood Cliffs, 1995, New Jersey

[5] Cowie, J. M. G., "Polymers: Chemistry and Physics of Modern Materials", Intertext Books, Aylesbury, 1973, UK

CHAPTER III

SYNTHESIS AND PROPERTIES OF POLY(ISOBUTYL METHACRYLATE-CO-BUTANEDIOL DIMETHA-CRYLATE-CO-METHACRYL POSS) NANOCOMPOSITES

Introduction

Nanocomposites containing one or more phases with ultrafine (1-100 nm) dimensions have attracted considerable interest as researchers strive to enhance material properties via nanoscale reinforcement in contrast to the conventional particulate-filled microcomposites [1-2]. Polyhedral oligomeric silsesquioxane (POSS) modified nanocomposites have attracted special attention [3-18]. POSS compounds have sizes from 1 to 3 nm in diameter and are unique inorganic-organic hybrid reagents. Their inorganic cage framework is made up of silicon and oxygen $(SiO_{1.5})_n$ (n=8, 10, or 12). This inorganic cage is externally covered by organic substituents, which can enhance their solubility in organic media. One or more of these substituents may contain polymerizable functional groups. In addition, POSS monomers have been copolymerized with other common monomers [3]. This provides a means of manipulating many properties of established polymer systems [4-14].

The synthesis and properties of many monofunctional POSS copolymers have been reported [3]. Examples include styrene-co-styrylPOSS [4], 4-methylstyrene-co-styrylPOSS [5-6], methacrylatePOSS-b-n-butylacrylate-b-methacrylatePOSS [7], norbornene-co-norbornylPOSS [8-9], ethylene-co-norbornylPOSS [10-11], propylene-co-norbornylPOSS [10], ethylene-co-vinylPOSS [12], propene-co-vinylPOSS [12] and POSS-siloxane copolymers [13-14].

Both monofunctional and multifunctional POSS monomers have been used to modify thermoset network systems. The monofunctional epoxy-substituted POSS, [(c-$C_6H_{11})_7Si_8O_{12}(CH_2CHCH_2O)$], was incorporated into an epoxy resin by Lee and Lichtenhan [15]. This resin's glass transition region was broadened with an increase in POSS content (≤10 wt%) but there was no change of the onset temperature of the glass transition [15]. Pittman et. Al. incorporated the multifunctional POSS, $[(C_6H_5CHCHO)_4(Si_8O_{12})(CH{=}CHC_6H_5)_4]$, with 8 reactive functional groups, including four β-substituted styrenes and four epoxidized styrenes, into both epoxy [17] and vinyl ester resins [18]. This POSS unit dispersed extremely well in the epoxy network (on the molecular scale) based on TEM observations even at a high POSS content (25 wt%) [17]. The glass transition temperature range was broadened upon cocuring this POSS macromer into the epoxy resin at 120 and 150 °C, but the T_g values (the tanδ peak temperature from DMTA curves) remained unchanged. Incorporating small amounts of this same multifunctional POSS (≤10 wt%) into vinyl ester networks had almost no influence on T_g or the glass transition region [18]. However, both epoxy/POSS and

VE/POSS composites exhibited higher storage moduli at $T>T_g$ than those of the neat epoxy or vinyl ester resins, respectively.

In this dissertation, the monofunctional 3-methacrylylpropylheptaisobutyl-T_8-polyhedral oligomeric silsesquioxane (MA-POSS) was terpolymerized with isobutyl methacrylate (iBMA) and butanediol dimethacrylate (BDMA) to generate poly(isobutyl methacrylate-co-butanediol dimethacrylate) (e.g., P(iBMA-co-BDMA)) crosslinked networks by radical-initiated terpolymerization. The crosslinking density of these networks was controlled by changing amount of difunctional BDMA. Viscoelastic properties and morphology were measured by DMTA. Changes in viscoelastic behavior and morphology upon incorporating MA-POSS into P(iBMA-co-BDMA) networks at different crosslinking densities were investigated. The viscoelastic properties of linear P(iBMA-co-MA-POSS) copolymer nanocomposites were also studied and compared with those of poly (isobutyl methacrylate) and crosslinked P(iBMA-co-BDMA-co-MA-POSS) nanocomposites.

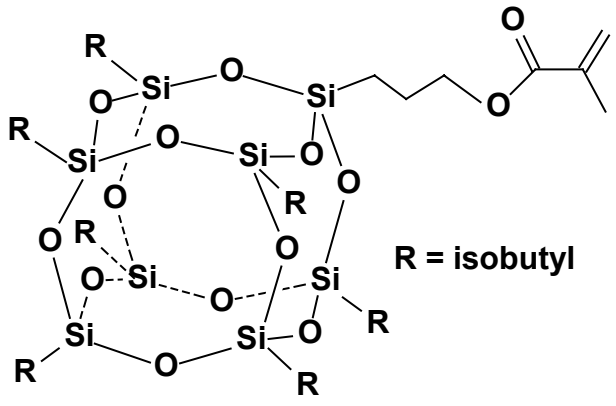

MA–POSS

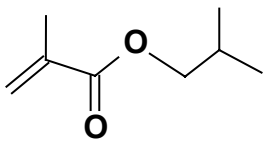

iBMA

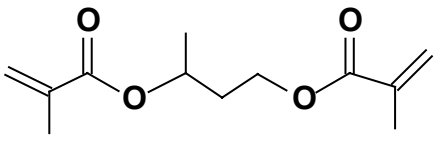

BDMA

Experimental

Materials

MA-POSS (MW=942) is a T_8 polyhedral oligomeric silsesquioxane (POSS) with seven isobutyl groups and one 3-methacrylylpropyl function on the eight corner silicone cage atoms. MA-POSS is a white powder. It was purchased from Hybrid™ Plastics Co. and used as received. Isobutyl methacrylate (iBMA) (F.W.142.2, b.p.155°) and 1,3-butanediol dimethacrylate (BDMA) (F.W.226.28, b.p.290°) were purchased from Aldrich Chemical Company Inc. and used without further purification. Methyl ethyl ketone peroxide (MEKP) solution (~35 wt%) in 2,2,4-trimethyl-1,3-pentanediol diisobutyrate was also purchased from Aldrich Chemical Company Inc. Cobalt naphthanate (CoNap) was bought from the Dow Chemical Company. MEKP and CoNap were employed in all cases as the free radical initiator/catalyst system.

Preparation of Copolymers and Terpolymer Nanocomposites

MA-POSS portions (0.5, 1, 1.5, 2 and 3 g) were added to iBMA (9.5, 9, 8.5, 8 and 7 g), respectively. At low MA-POSS contents (≤15 wt%), the white MA-POSS powder completely dissolved into iBMA, giving transparent solutions at room temperature. However, at high MA-POSS contents (20 or 30 wt%), the MA-POSS/iBMA mixture is translucent at room temperature. Then, the 0.5 wt% MEKP solution and 0.1 wt% CoNap were added into each of these monomer mixtures, followed by curing in air (88 °C/72 h) and post-curing (100 °C/24 h) to produce iBMA-co-MA-POSS linear copolymers. After curing, all these copolymers (5, 10, 15, 20 and 30 wt% MA-POSS) are transparent.

Heating at 88 °C during curing improves MA-POSS solubility in iBMA monomer and leads to good transparency for the 20 and 30 wt% MA-POSS copolymers. PiBMA was prepared using identical conditions to serve as a control sample with which to compare the copolymers.

BDMA and iBMA mixtures with 99/1, 97/3, and 95/5 weight ratios were prepared. Then, the 0.5 wt% MEKP solution and 0.1 wt% CoNap were added into each of these monomer mixtures. Transparent mixtures were obtained on shaking. After curing in air at 88 °C for 72 h, P(iBMA-co-BDMA) crosslinked network solids were made. All P(iBMA-co-BDMA) samples were post-cured at 100 °C for 24 h. P(iBMA-co-BDMA) samples with 3 wt% and 5 wt% BDMA were bent after the curing process at 88 °C/72 h and 100 °C/24 h. Therefore, the samples containing 3 wt%, and 5 wt% BDMA were also post-cured at 120 °C/2 h, and 130 °C/2 h under a small pressure (1.54 psi).

MA-POSS was weighed into various iBMA and BDMA mixtures (iBMA/BDMA/MA-POSS wt. ratios are shown in Table 3.1). MA-POSS dissolved in the iBMA and BDMA mixtures to give transparent solutions for 5, 10 or 15 wt% MA-POSS. The iBMA/BDMA/MA-POSS mixtures appeared translucent when 20 or 30 wt% MA-POSS was present. Then, 0.5 wt% MEKP solution and 0.1 wt% CoNap were added and all samples were cured at 88 °C for 72 h followed by a post-curing at 100 °C for 24 h. The nanocomposites with BDMA contents ≥3 wt% were bent after curing at 88 °C/72 h and 100 °C/24 h, similar to that observed with P(iBMA-co-BDMA) resin. Therefore, these samples were also post-cured at 120 °C/2 h and 130 °C/2 h under a pressure of 1.54 psi, respectively, to produce straight samples. P(iBMA-co-1 wt% BDMA-co-MA-POSS)

nanocomposites with 5, 10, 15, 20 and 30 wt% MA-POSS are transparent like the P(iBMA-co-MA-POSS) copolymers. However, phase-separation occurred at high BDMA loadings (3 or 5 wt%). Some visible white particles, in range of from several microns to ~0.5 mm, were formed during curing.

P(iBMA-co-3 wt% BDMA-co-MA-POSS) nanocomposites with 5, 10, 15 and 20 wt% MA-POSS are translucent while the 30 wt% POSS composite is opaque. The number of white particles (POSS-rich phase) increases with an increase of POSS content. Two layers were formed during the curing of the P(iBMA-co-5 wt% BDMA-co-MA-POSS) composites containing 5, 10, 15, 20 and 30 wt% MA-POSS. The upper layer was slightly translucent while the bottom layer was opaque with many white particles. Thus, phase-separation becomes more pronounced as the crosslinking density increases.

Measurements

The bending dynamic storage modulus (E') and loss factor (tanδ) were measured using a Polymer Laboratories DMTA MK3 instrument. Small amplitude bending oscillations (both 1 and 10 Hz) were used at a gap setting of 8.00 mm. The measurements were carried out from 30-32 °C to 150-155 °C at a rate of 2 °C/min. All samples were approximately 2.7-3.2 mm thick, 6.0-7.1 mm wide and 40 mm long.

The densities of P(iBMA-co-MA-POSS)copolymers and P(iBMA-co-BDMA-co-MA-POSS) nanocomposites were measured using an Electronic Densimeter (ED-120T) at 25.5 °C.

Each of the P(iBMA-co-BDMA-co-MA-POSS) nanocomposites (~0.5 cm^3) was immersed in THF at room temperature. The maximum swelling volumes for the 1 wt% BDMA nanocomposites with 5, 10, 15, 20 and 30 wt% MA-POSS, and P(iBMA-co-BDMA) resins with 1 and 3 wt% BDMA were measured after swelling equilibrium was reached. The swelling volume ratio was defined as this equilibrium (maximum) volume divided by the initial volume before swelling. The sample with high crosslink density exhibits lower swelling volume ratio. However, the P(iBMA-co-BDMA-co-MA-POSS) composites with 3 or 5 wt% BDMA and the P(iBMA-co-5 wt% BDMA) resin fractured into many small pieces during THF swelling, so these equilibrium swelling volumes couldn't be measured. The THF solutions, containing small amount of extracted linear copolymers, were coated on KBr plates to obtain their FT-IR spectra on an FT-IR instrument (MIDAC Corporation).

A JEM-100 CXII transmission electron microscope (TEM) (JEOL USA Inc.) operating at 60 KV was used to characterize phase morphology of some selected P(BMA-co-BDMA-co-MA-POSS) nanocomposites. Specimens for this measurement were microtomed to ~75 nm thickness and set on copper grid.

Results and Discussion

Synthesis of nanocomposites

P(iBMA-co-BDMA) networks and P(iBMA-co-BDMA-co-MA-POSS) nanocomposites were prepared by free radical initiation in bulk monomer mixtures. Formation of the MA-POSS nanocomposites is illustrated in Figure 3.1. Linear P(iBMA-

co-MA-POSS) copolymer nanocomposites were prepared for comparison. The viscoelastic properties, E', T_g and tanδ, and the swelling behavior were studied and compared.

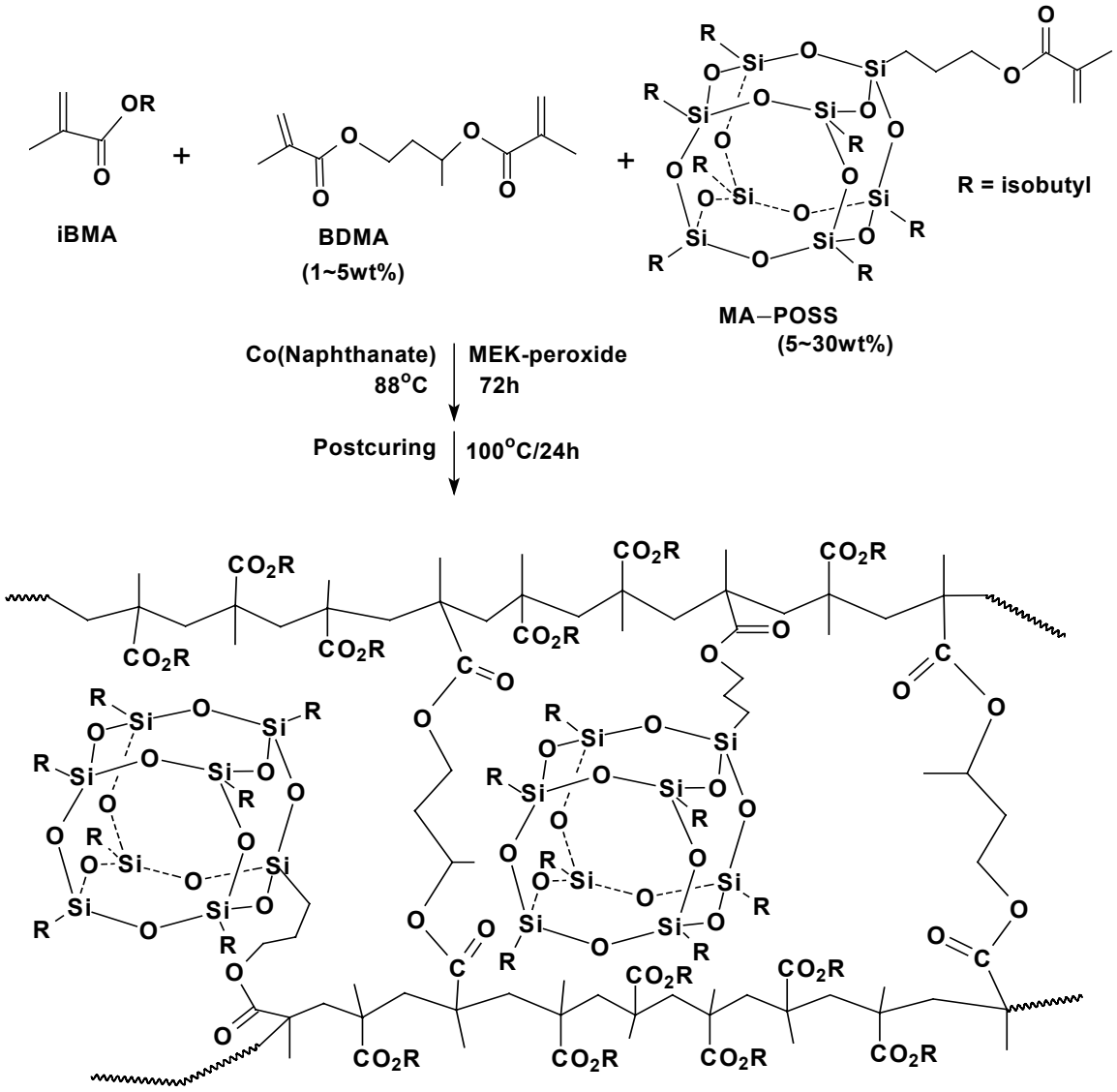

Figure 3.1 Synthesis of P(iBMA-co-BDMA-co-MA-POSS) nanocomposites

Viscoelastic properties of P(iBMA-co-BDMA) resins

The bending E' and tanδ versus temperature curves at 1 Hz for pure PiBMA and P(iBMA-co-BDMA) resins (Figure 3.2) show that the T_g and E' values increase as the BDMA content increases from 1 wt% to 3 wt% and 5 wt%. Their T_g values (tanδ peak temperature) are 85.4 °C (PiBMA), 87.3 °C (1 wt% BDMA), 90.1 °C (3 wt% BDMA) and 92.8 °C (5 wt% BDMA). PiBMA exhibits a weaker bending tanδ peak (1 Hz) than P(iBMA-co-1 wt% BDMA). The intensities decrease gradually as the BDMA content increases from 1 wt% to 3 and 5 wt%. E' values at 35 °C ($T<T_g$) of pure PiBMA and its BDMA resins with 1, 3, and 5 wt% BDMA are 0.87, 1.00, 1.04 and 0.94 GPa, respectively. In the rubbery region ($T>T_g$), E' values of all the resins are higher than those of the pure PiBMA and they increase with the BDMA content as expected. E' values of PiBMA and its BDMA resins with 1, 3 and 5 wt% BDMA at 145 °C ($T>T_g$) are 0.33, 0.42, 0.72 and 0.78 MPa, respectively.

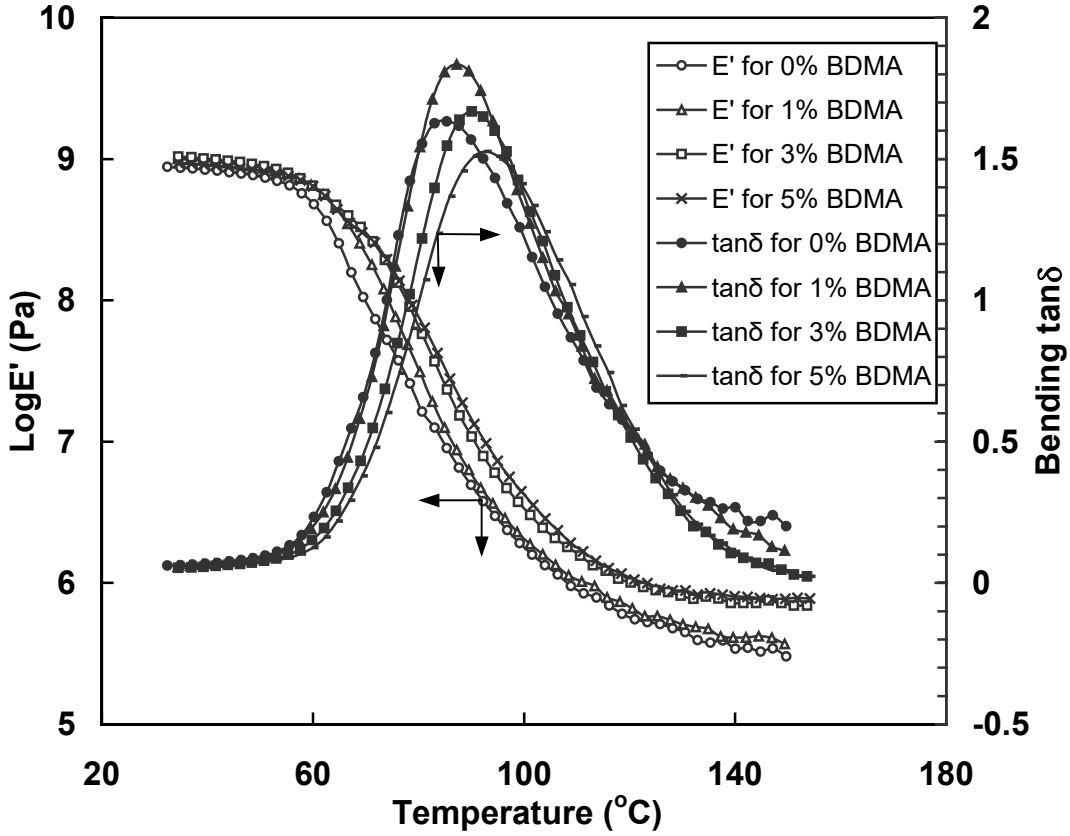

Figure 3.2 Bending storage modulus and tanδ versus temperature curves at 1 Hz of P(iBMA-co-BDMA) with 0, 1,3 and 5 % BDMA loadings

The swelling volume ratios (in THF) of P(iBMA-co-BDMA) resins with 1 and 3 wt% BDMA (shown in Table 3.1) are 4.46 and 2.60, respectively, but the swelling ratio for P(iBMA-co-5 wt% BDMA) was not measured because of fracturing. The swelling ratios decrease due to higher crosslinking as the BDMA content increases from 1 to 3 wt%. Crosslink density for the P(iBMA-co-BDMA) resins increases with an increase in BDMA loading. This is the reason why the T_g and E' values in the rubbery region for these crosslinked network increase with BDMA content.

Viscoelastic prperties of P(iBMA-co-MA-POSS) linear copolymers

P(iBMA-co-MA-POSS) linear copolymers were also synthesized for later comparison with P(iBMA-co-BDMA-co-MA-POSS) crosslinked networks with varying crosslink densities. Bending E' and tanδ curves of these linear copolymers are shown in Figure 3.3. The 5 wt% (0.79 mole%), 10 wt% (1.65 mole%) and 15 wt% (2.59 mole%) MA-POSS copolymers have slightly higher E' values than PiBMA both at $T<T_g$ and $T>T_g$. However, the copolymers with 20 wt% and 30 wt% (3.64 and 6.07 mole%) MA-POSS exhibit lower E' values than PiBMA. The values of E' at 35 °C ($T<T_g$) for PiBMA and its copolymers with 5, 10, 15, 20 and 30 wt% MA-POSS are 0.87, 0.92, 1.00, 0.89, 0.86 and 0.67 GPa, respectively. The corresponding E' values at 145 °C ($T>T_g$) are 0.33, 0.37, 0.41, 0.33, 0.30 and 0.25 MPa. The 10 wt% MA-POSS copolymer exhibits the highest E' values over the entire temperature range. In both the glassy region and rubbery regions, the E' values decrease with an increase of POSS content from 10, 15, 20 to 30 wt%.

Table 3.1 Properties of P(iBMA-co-MA-POSS) Copolymers and P(iBMA-co-BDMA-co-MA-POSS) Nanocomposites

Sam-ple No.	iBMA/BDMA/MA-POSS wt ratios	mole ratios	ρ	T_g (°C)	E' at 35°C (GPa)	E' at 145°C (MPa)	Swelling volume ratios in THF
1	100/0/0	100/0/0	1.047	85.4	0.87	0.33	----
2	95/0/5	99.21/0/0.79	1.052	85.5	0.92	0.37	----
3	90/0/10	98.35/0/1.65	1.057	83.0	1.00	0.41	----
4	85/0/15	97.41/0/2.59	1.061	84.7	0.89	0.33	----
5	80/0/20	96.36/0/3.64	1.065	80.8	0.86	0.30	----
6	70/0/30	93.93/0/6.07	1.073	80.2	0.67	0.25	----
7	99/1/0	99.37/0.63/0	1.051	87.3	1.00	0.42	4.46
8	94/1/5	98.55/0.66/0.79	1.054	84.8	1.01	0.40	4.32
9	89/1/10	97.65/0.69/1.66	1.059	87.6	1.01	0.40	3.31
10	84/1/15	96.67/0.72/2.61	1.063	85.2	0.93	0.40	3.82
11	79/1/20	95.59/0.76/3.65	1.067	84.2	0.78	0.46	4.25
12	69/1/30	93.05/0.85/6.10	1.076	82.7	0.88	0.28	3.57
13	97/3/0	98.09/1.91/0	1.052	90.1	1.04	0.72	2.60
14	92/3/5	97.21/1.99/0.80	1.053	92.1	0.82	0.62	Fractured
15	87/3/10	96.24/2.09/1.67	1.060	91.7	0.98	0.64	Fractured
16	82/3/15	95.18/2.19/2.63	1.046	91.9	0.84	0.73	Fractured
17	77/3/20	94.01/2.30/3.69	1.057	87.5	0.79	0.67	Fractured
18	67/3/30	91.26/2.57/6.17	1.076	85.9	0.76	1.23	Fractured
19	95/5/0	96.80/3.20/0	1.057	92.8	0.94	0.78	Fractured
20	90/5/5	95.85/3.35/0.80	1.034	92.3	0.75	1.48	Fractured
21	85/5/10	94.81/3.51/1.68	1.040	93.0	0.87	1.54	Fractured
22	80/5/15	93.67/3.68/2.65	1.062	91.0	0.87	1.73	Fractured
23	75/5/20	92.41/3.87/3.72	1.070	89.7	0.96	1.62	Fractured
24	65/5/30	89.45/4.32/6.23	1.085	89.9	0.64	1.64	Fractured

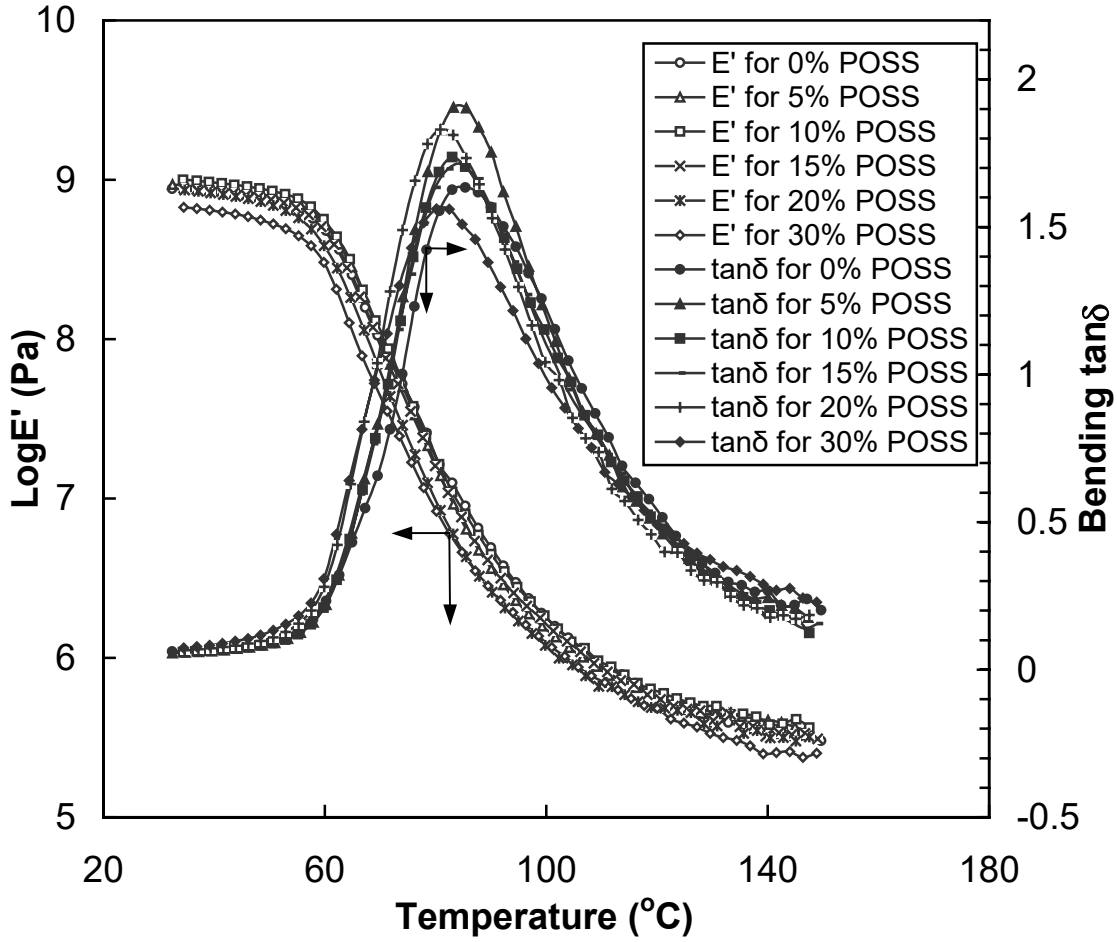

Figure 3.3 Bending storage modulus and tanδ versus temperature curves at 1 Hz of P(iBMA-co-MA-POSS) copolymers

PiBMA displays a weaker tanδ peak in the glass transition region than the P(iBMA-co-MA-POSS) copolymers with 5, 10, 15 and 20 wt% POSS. The tanδ peak intensities drop steadily for MA-POSS loadings of 5, 10, 15 and 30 wt%. But, the 20 wt% MA-POSS copolymer's tanδ peak is more intense than those of the 10 and 15 wt% POSS copolymers. Their T_g values are 85.4 °C (PiBMA), 85.5 °C (5% MA-POSS), 83.0 °C (10 % MA-POSS), 84.7 °C (15% MA-POSS), 80.9 °C (20% MA-POSS) and 80.2 °C (30%

MA-POSS), respectively. The tendency toward a drop in T_g at higher MA-POSS contents is illustrated by the 20 and 30 wt% MA-POSS samples.

Viscoelastic properties of P(iBMA-co-BDMA-co-MA-POSS) nanocomposites

P(iBMA-co-BDMA-co-MA-POSS) terpolymer nanocomposites (Figure 3.1) contain pendant MA-POSS units along the segments between crosslink sites in the P(iBMA-co-BDMA) networks. As the BDMA content increases, the mean segment lengths decrease. The E' values at 35 °C and 145 °C, and T_g values of all the linear copolymers and the crosslinked resins are shown in Table 3.1.

DMTA analysis of P(iBMA-co-1wt%BDMA-co-MA-POSS) nanocomposites (Figure 3.4) found only minor changes in E' at $T<T_g$ and $T>T_g$ with 5, 10 and 15 wt% MA-POSS (Table 3.1). The 20 wt% POSS nanocomposite has lower E' values than P(iBMA-co-1 wt% BDMA) at $T<T_g$, but slightly higher E' values at $T>T_g$. The 30 wt% POSS nanocomposite exhibits lower E' values over the entire temperature range. At 35 °C ($T<T_g$), P(iBMA-co-1 wt% BDMA) and its 5, 10, 15, 20 and 30 wt% MA-POSS nanocomposites exhibit E' values of 1.00, 1.01, 1.01, 0.93, 0.78 and 0.88 GPa, respectively. At 145 °C ($T>T_g$), the corresponding values are 0.42, 0.40, 0.40, 0.40, 0.46 and 0.28 MPa. The T_g values of P(iBMA-co-1 wt% BDMA) and its MA-POSS nanocomposites (the peak tanδ temperature) don't vary substantially until high MA-POSS levels which induce a drop in T_g: 87.3 °C (0% MA-POSS), 84.8 °C (5% MA-POSS), 87.6 °C (10% MA-POSS), 85.2 °C (15% MA-POSS), 84.2 °C (20% MA-POSS) and 82.7 °C (30% MA-POSS). The 5 wt% POSS nanocomposite exhibits a slightly more

intense tanδ peak than that of P(iBMA-co-1 wt% BDMA) while the 10, 15, 20 and 30 wt% MA-POSS samples have less intense peaks which decrease with an increase in MA-POSS (see Figure 3.4). The P(iBMA-co-1 wt%BDMA-co-20 wt% MA-POSS) nanocomposite exhibits a more intense tanδ peak than those of the 10 and 15 wt% MA-POSS nanocomposites, a similar trend to that observed for the linear P(iBMA-co-MA-POSS) copolymers.

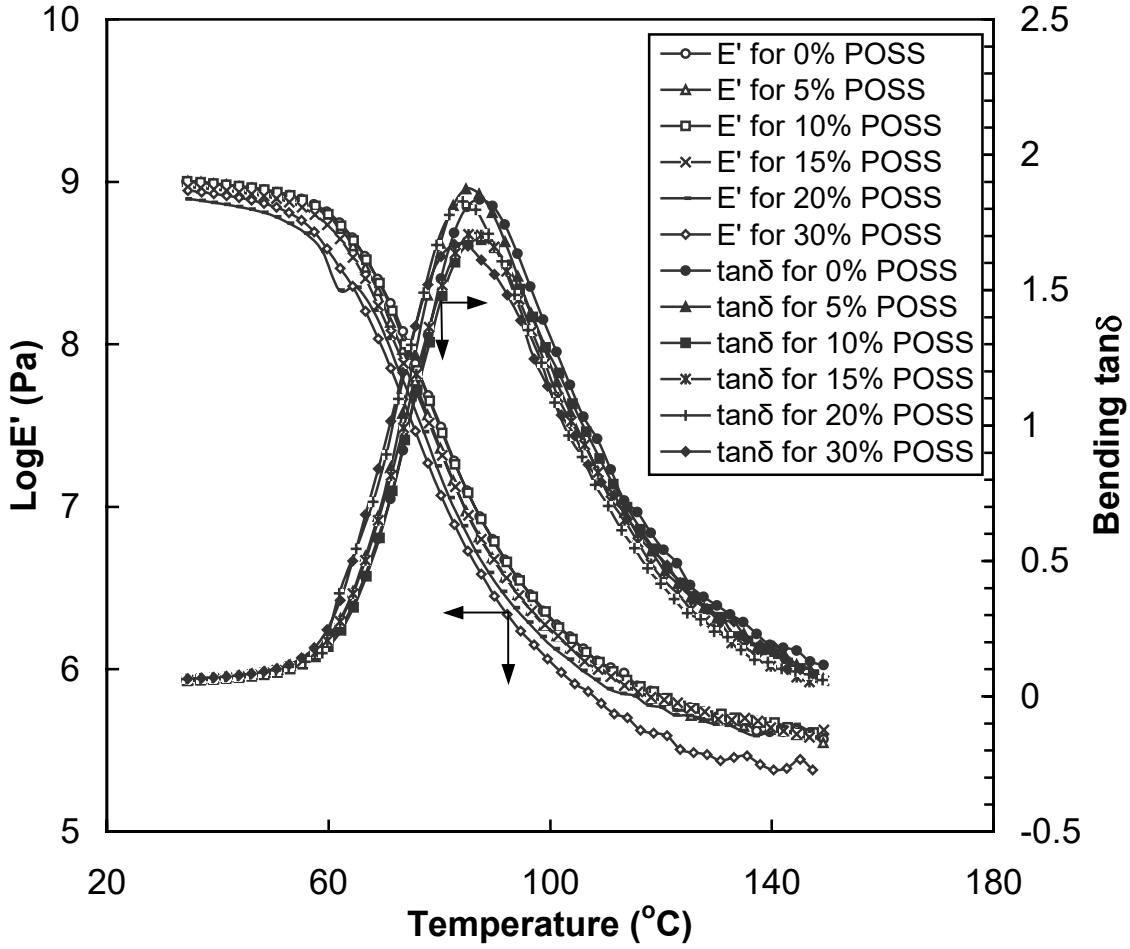

Figure 3.4 Bending storage modulus and tanδ versus temperature curves at 1 Hz of the P(iBMA-co-1 wt% BDMA-co-MA-POSS) nanocomposites

Increasing the crosslink density by using 3 wt% BDMA raises the E' values at T> T_g above those of all the 1 wt% BDMA samples (Table 3.1 and Figure 3.5). In contrast to the 1 wt% BDMA series, the 30 wt% MA-POSS/3 wt% BDMA sample has a high temperature modulus (145 °C, 1.23 MPa) which is much higher than the other samples in this group (0.72-0.62 MPa). In the glassy region, however, this same sample exhibits the lowest E' values (i.e. 0.76 GPa at 35 °C) of this 3 wt% BDMA series (1.04 to 0.79 GPa). At 35 °C ($T<T_g$), the E' values for P(iBMA-co-3 wt% BDMA) and its 5, 10, 15, 20 and 30 wt% MA-POSS nanocomposites are 1.04, 0.82, 0.98, 0.84, 0.79 and 0.76 GPa, respectively. At 145 °C ($T>T_g$), the corresponding E' values are 0.72 MPa (0% MA-POSS), 0.62 MPa (5% MA-POSS), 0.64 MPa (10% MA-POSS), 0.73 MPa (15% MA-POSS), 0.67 MPa (20% MA-POSS) and 1.23 MPa (30% MA-POSS).

The T_g of the P(iBMA-co-3 wt% BDMA-co-MA-POSS) nanocomposites with 5, 10 and 15 wt% POSS remain almost constant (92.1, 91.7 and 91.9 °C, respectively) and close to that of P(iBMA-co-3 wt% BDMA) resin (90.1 °C). However, at higher MA-POSS loadings, the T_g value drops in this 3 wt% BDMA series: 87.5 °C (20% MA-POSS) and 85.9 °C (30% MA-POSS). Figure 4 illustrates the drop in tanδ peak intensities for the P(iBMA-co-3 wt% BDMA-co-MA-POSS) nanocomposites with an increase in MA-POSS contents. This result contrasts with the behavior of P(iBMA-co-MA-POSS) copolymers and the P(iBMA-co-1 wt% BDMA-co-MA-POSS) nanocomposites. In addition, a minor drop in the bending storage moduli occurs between 61 and 69 °C ($T<T_g$) (Figure 3.5) for each of the 5, 15, 20 and 30 wt% MA-POSS nanocomposites containing 3 wt% BDMA.

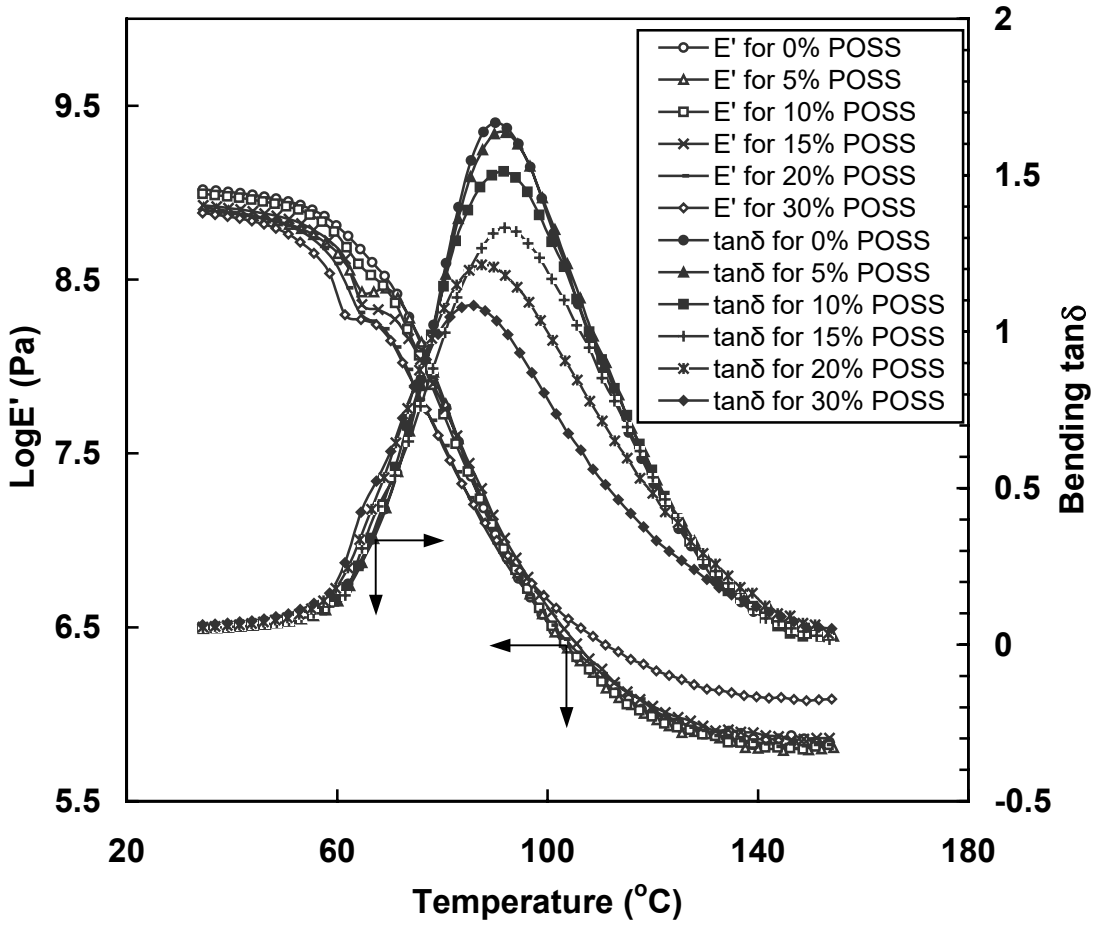

Figure 3.5 Bending storage modulus and tanδ versus temperature curves at 1 Hz of the P(iBMA-co-3 wt% BDMA-co-MA-POSS) nanocomposites

Very weak shoulders in bending tanδ curves are also observed corresponding to these E' drops. This phenomenon disappeared completely in the second heating. These sub-T_g transitions might be related with MA-POSS aggregation state changes occurring in these networks.

The DMTA curves of the P(iBMA-co-5 wt% BDMA-co-MA-POSS) series (0 to 30 wt% MA-POSS) are given in Figure 3.6. Only the 20 wt% MA-POSS sample has higher E' values than the parent P(iBMA-co-5 wt% BDMA) resin at both $T<T_g$ and $T>T_g$. The

other nanocomposites exhibit lower E' values at $T<T_g$. However, above T_g, all the E' values are higher than those of the reference resin. Adding from 5-30 wt% MA-POSS approximately doubles the bending moduli in the rubbery region. T_g values are very similar for the 5 wt%, 10 wt% and 15 wt% POSS nanocomposites (92.3, 93.0 and 91.0 °C) and close to that of P(iBMA-co-5 wt% BDMA) (92.8 °C). T_g values decrease slightly for the 20 and 30 wt% POSS nanocomposites (89.7 and 89.9 °C). The tanδ peak intensities drop steadily as the MA-POSS content goes up in this 5 wt% BDMA series. This behavior was also found in the 3 wt% BDMA series. The 5 and 10 wt% MA-POSS nanocomposites (5 wt% BDMA) exhibited a small but abrupt drop in E' in the 67~77 °C temperature range and very weaker shoulders in their tanδ curves (Figure 3.6). This phenomenon disappeared on the second heating, as was observed for the 3 wt% BDMA nanocomposites.

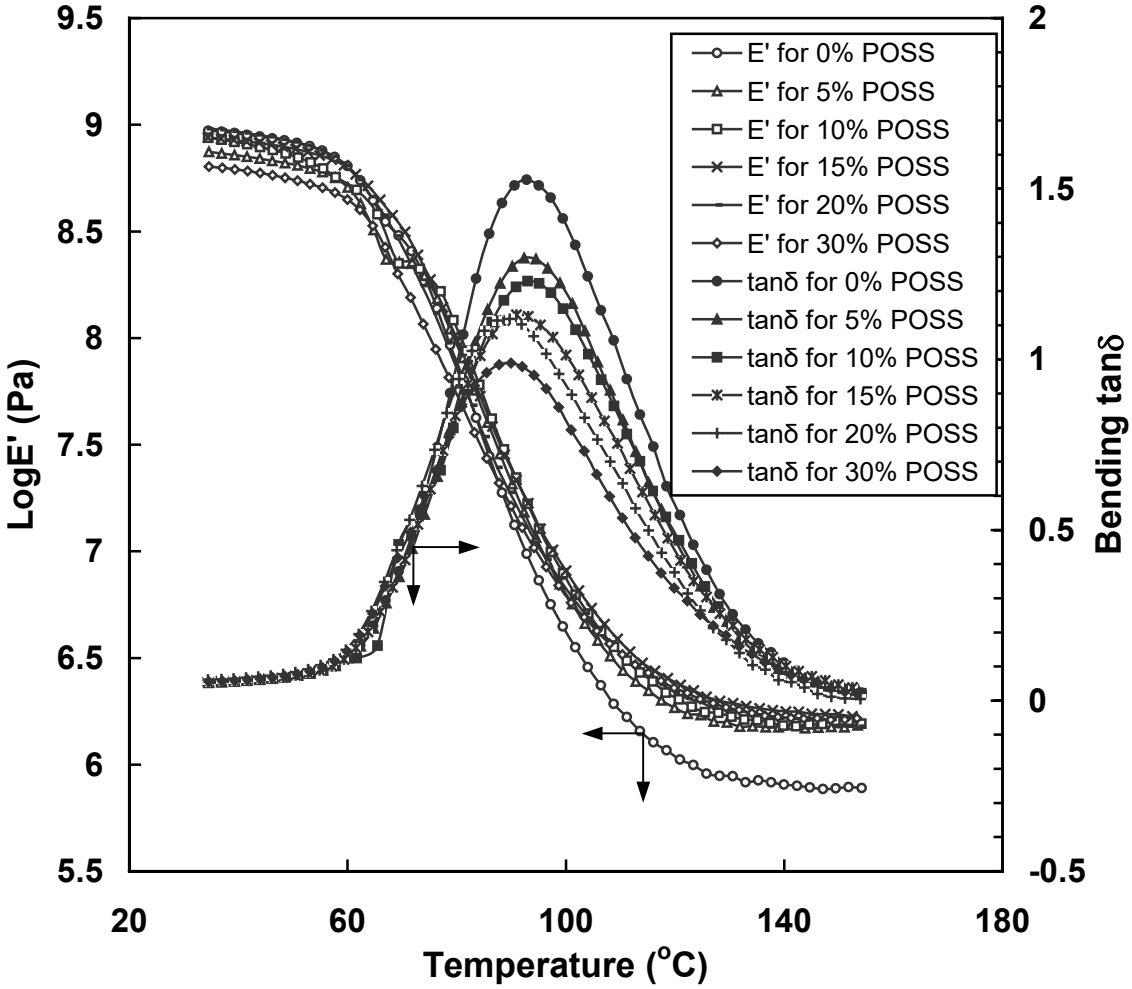

Figure 3.6 Bending storage modulus and tanδ versus temperature curves at 1 Hz of the P(iBMA-co-5 wt% BDMA-co-MA-POSS) nanocomposites

In summary, incorporating MA-POSS into P(iBMA-co-BDMA) crosslinked resins effects the viscoelastic properties in different ways at different crosslink densities. At low BDMA loading (1 wt%), the nanocomposites with 5, 10, and 15 wt% MA-POSS exhibit E' values similar to those of the P(iBMA-co-1 wt% BDMA) resin both below and above T_g while the 20 wt% and 30 wt% POSS nanocomposites' E' values are slightly lower. This effect is similar to that observed for linear P(iBMA-co-MA-POSS) copolymers. At 3

wt% BDMA, all nanocomposites show lower E' values at $T<T_g$ than those of the parent P(iBMA-co-3 wt% BDMA) resin and E' decreases with an increase of MA-POSS from 10 wt% to 15, 20 and 30 wt%. However, in the rubbery region ($T>T_g$), little difference occurs in E' between P(iBMA-co-3 wt% BDMA) and its MA-POSS nanocomposites until the MA-POSS content reaches 30 wt%, where E' increases substantially. As crosslinking increases (5 wt% BDMA), higher E' values are found in the rubbery region when MA-POSS is present versus those of the P(iBMA-co-5 wt% BDMA) resin. However, all these nanocomposites show slightly lower E' values than those of the P(iBMA-co-5 wt% BDMA) resin in the glassy region (except the 20 wt% MA-POSS sample). The T_g values of all nanocomposites with 5, 10 and 15 wt% MA-POSS are similar to those of their parent P(iBMA-co-BDMA) resins (having equivalent wt %s of BDMA) while the 20 wt% and 30 wt% MA-POSS nanocomposites exhibit slightly lower T_g values than those of their corresponding parent resins.

Effect of heating history on viscoelastic properties

Heating history has little influence on either P(iBMA-co-MA-POSS) copolymers or P(iBMA-co-BDMA-MA-POSS) nanocomposites. Representative examples are displayed in Figures 3.7 and 3.8. P(iBMA-co-1 wt% BDMA-co-15 wt% MA-POSS) exhibits slightly lower E' values and a slightly less intense tanδ peak in the second heating (Figure 3.7). The drop in E' values and a weak shoulder in the tanδ peak at 61.5~67.5 °C during the first heating disappeared completely during the second heating for P(iBMA-co-3 wt% BDMA-co-30 wt% MA-PSOS) (Figure 3.8). Furthermore, the tanδ peak

intensity in the second heating of this nanocomposite is slightly smaller than those in the first heating. The E' values of P(iBMA-co-3 wt% BDMA-co-30 wt% MA-POSS) are slightly higher at $T<T_g$ and slightly lower at $T>T_g$ in the second heating than they are in the first heating.

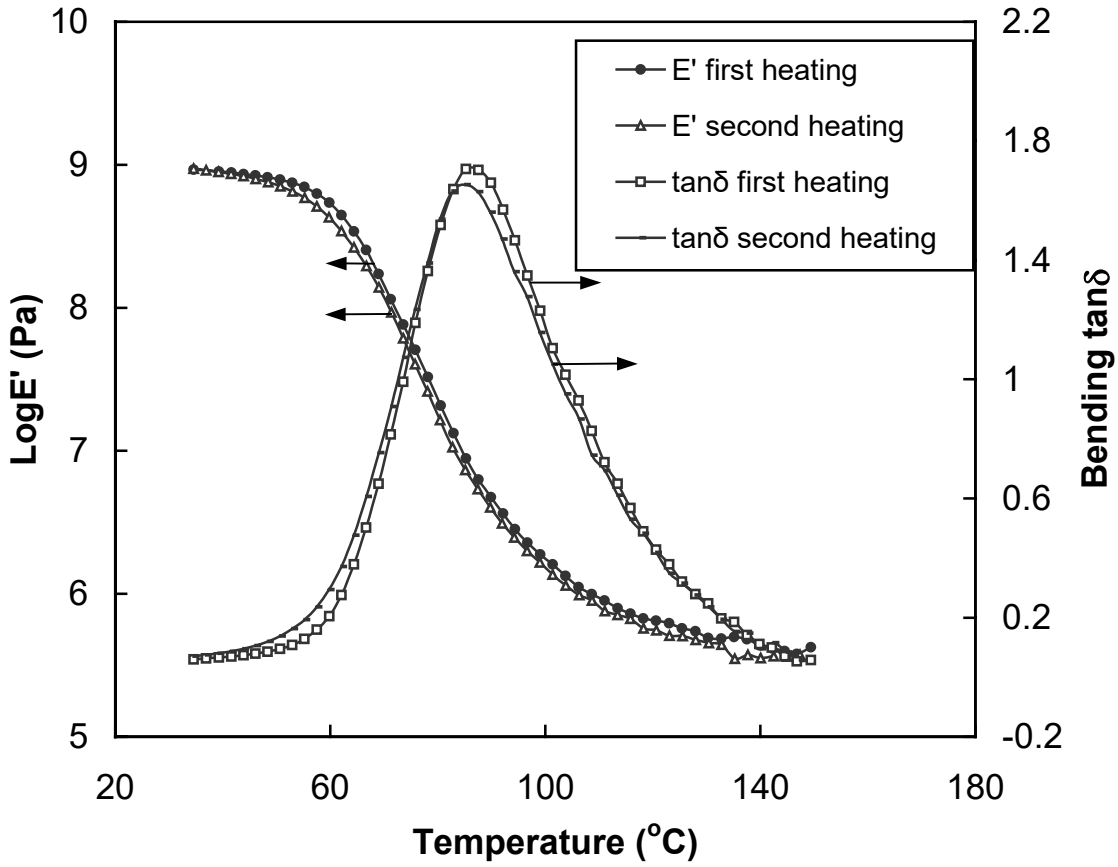

Figure 3.7 DMTA curves at 1 Hz of the P(iBMA-co-1 wt% BDMA-co-15 wt% MA-POSS) nanocomposite at the first and second heating

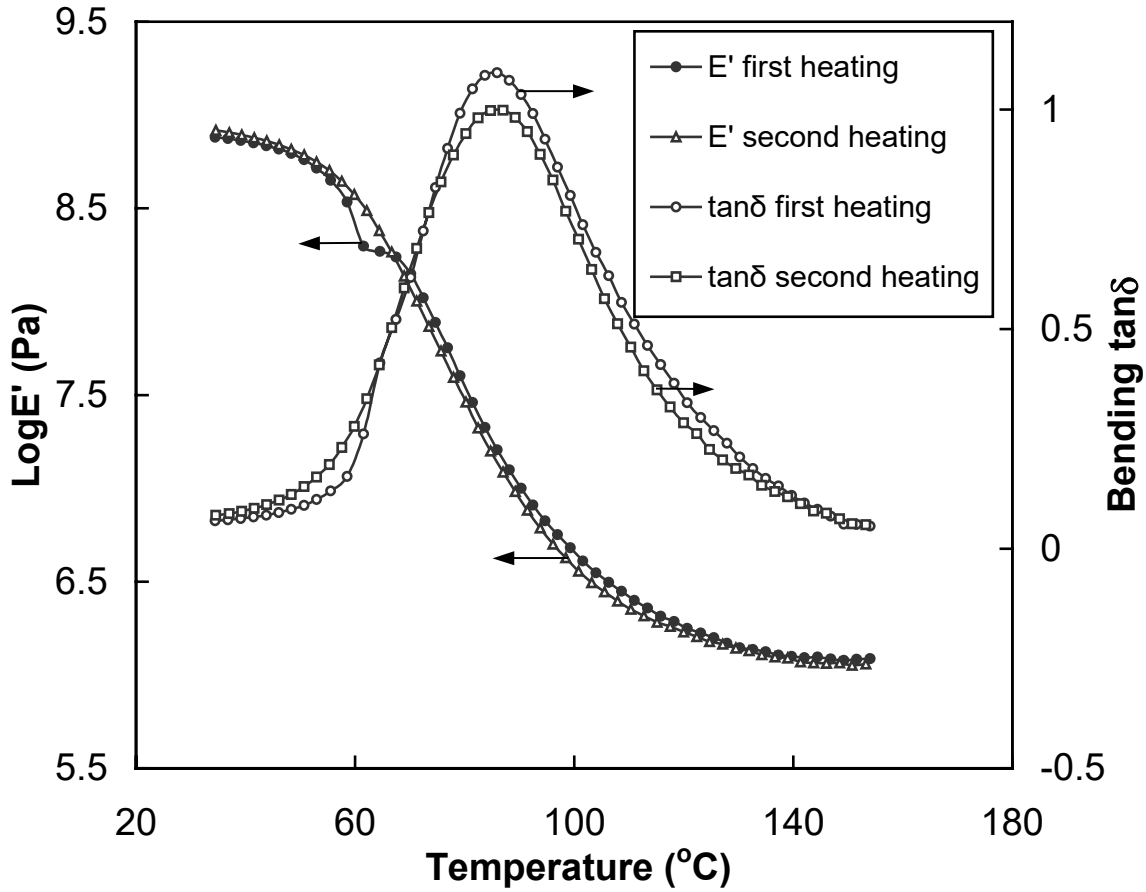

Figure 3.8 DMTA curves at 1 Hz of the P(iBMA-co-3 wt% BDMA-co-30 wt% MA-POSS) nanocomposite at the first and second heating

Properties of linear P(iBMA-co-MA-POSS) copolymers and P(iBMA-co-BDMA-co-MA-POSS) nanocomposites

Table 3.1 summarizes DMTA data (T_g, E' values at 35 °C and 145 °C), densities (ρ), and volume swelling ratios in THF of the linear copolymers and the P(iBMA-co-BDMA-co-MA-POSS) nanocomposites. P(iBMA-co-MA-POSS) and P(iBMA-co-BDMA-co-MA-POSS) nanocomposites, at each level of BDMA (1, 3 and 5 wt%) with POSS contents ≤15 wt%, exhibit T_g values similar to those of PiBMA and the parent

P(iBMA-co-BDMA) resins at equivalent BDMA loadings. However, copolymers and nanocomposites with 20 wt% and 30 wt% POSS have slightly lower T_g values than those of PiBMA and their corresponding P(iBMA-co-BDMA) resins. It is clear that large T_g increases are not achieved by having these massive, anchor-like, pendant POSS functions attached to a fraction of the segmental chains between crosslinks or to the linear polymer chains.

Haddad et al [4] reported the T_g values of three types of linear P(styrene-co-monostyryl-POSS) copolymers, where the other seven substituents on the cage silicon atoms of monostyryl-POSS were either isobutyl, cyclopentyl or cyclohexyl groups. The styryl-POSS mole percents were 4.6% (isobutyl), 4.3% (cyclopentyl) and 3.9% (cyclohexyl) in these copolymers. The T_g values (tanδ peak temperatures) of polystyrene and these three POSS copolymers are 129 °C, 120 °C, 131 °C and 138 °C, respectively. E' values for these three P(styrene-co-styryl-POSS) copolymers are all lower than those of pure PS in the glassy region ($T<T_g$). Furthermore, the E' values of the styrene/isobutyl styryl-POSS copolymers were also slightly lower than those of PS in the rubbery region ($T>T_g$) [4]. In contrast, the cyclopentyl and cyclohexyl styryl-POSS/styrene copolymers exhibited modestly higher E' values than those of PS in the rubbery region ($T>T_g$). Clearly, the alkyl group has a major effect on the bulk properties of these styryl-POSS copolymers [4]. MA-POSS contains one 3-methacryloxypropyl functional group and seven isobutyl groups. This structure is similar to isobutyl styryl-POSS. By analogy, it appears reasonable that incorporating MA-POSS into PiBMA copolymers and the

P(iBMA-co-BDMA) resins has little influence on T_g values when MA-POSS contents are ≤15wt% (<4 mole%) and slightly reduces T_g values at 20 and 30 wt% POSS.

The densities of all P(iBMA-co-MA-POSS) copolymers and the P(iBMA-co-1 wt% BDMA-co-MA-POSS) nanocomposites are higher than those of PiBMA and P(iBMA-co-1 wt% BDMA) (Table 3.1). The densities increase with an increase of POSS contents. In contrast, density does not increase with higher MA-POSS loadings in the systems with 3 and 5 wt% BDMA. For an example, P(iBMA-co-3 wt% BDMA-co-15 wt% MA-POSS) and P(iBMA-co-5 wt% BDMA-co-MA-POSS) with 5 and 10 wt% POSS, have lower densities than those of the corresponding P(iBMA-co-BDMA) resins. Visible phase-separation occurred in the P(iBMA-co-BDMA-co-MA-POSS) nanocomposites with 3 and 5 wt% BDMA loadings. POSS aggregation might influence the densities. The free volume content is likely to vary with MA-POSS addition. All P(iBMA-co-1 wt% BDMA-co-5 to 30 wt% MA-POSS) systems exhibited slightly lower swelling ratios than that of the parent P(iBMA-co-1 wt% BDMA) resin. However, this does not seem to influence their E' or T_g values.

IR spectra of the residues isolated from the THF extractions of the P(iBMA-co-BDMA-co-MA-POSS) nanocomposites exhibit –Si-O- absorptions around 1111-1120cm^{-1}, characteristic of the T_8 POSS cage. Thus, a small fraction of MA-POSS was incorporated into linear iBMA copolymers, which has not been crosslinked into the network structure during the cure. The relative intensities of –Si-O- absorptions for the extracted linear copolymers increased with an increase of MA-POSS in the polymerization.

At higher crosslink densities, the average segment length between two BDMA crosslinks is shorter. Also slightly more MA-POSS moieties are pendant along these shorter segments than in the nanocomposites which have equal wt% of MA-POSS but lower crosslinking density (lower BDMA content). This is due to the lower mole percent of iBMA. This composition difference is illustrated in two-dimensions in Figure 3.9.

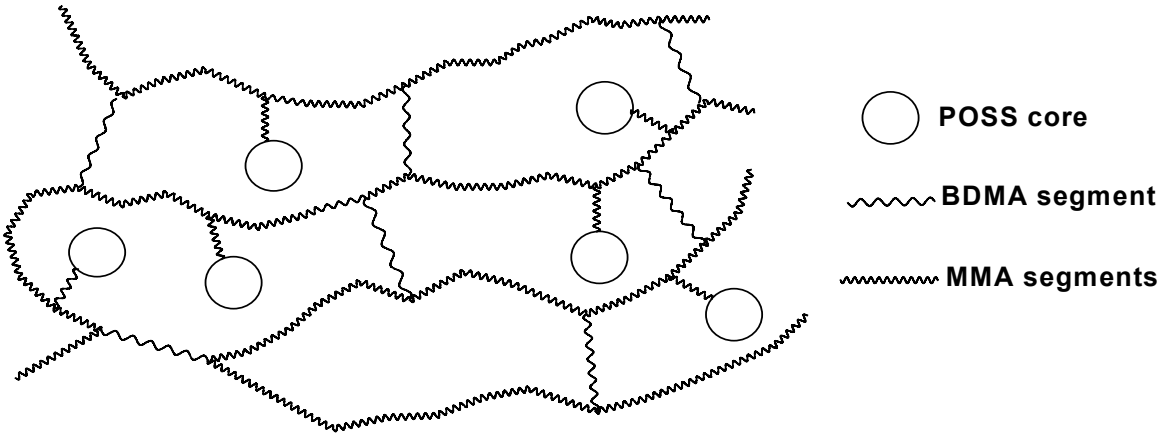

Crosslinking network at low crosslinking density

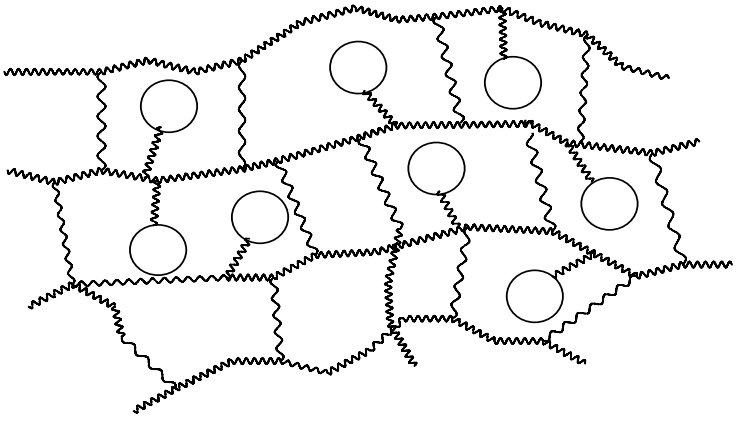

Crosslinking network at high crosslinking density

Figure 3.9 Nanocomposite networks at low and high crosslink densities

High crosslink densities act to restrict the motion of MA-POSS cores. Thus, pendant POSS units, in turn, might more effectively restrict some modes of iBMA backbone segmental motion at higher BDMA loadings. This might explain why the P(iBMA-co-5 wt% BDMA-co-MA-POSS) nanocomposites exhibit slightly higher E' values at $T>T_g$ than those of pure P(iBMA-co-5 wt% BDMA), whereas the reverse is found at lower BDMA contents (1 or 3 wt%). Pendant MA-POSS groups have a high molecular weight (901) and occupy a large volume. Thus, MA-POSS functions hinder the segmental motion of the segments to which they are attached at both low and high crosslink densities. They are analogous to an anchor attached to a jump rope, where the jump rope handles represent the segment ends where crosslinks are present. However, one must recognize that the MA-POSS mole percentages in these nanocomposites are low in all cases. In the 1 wt% BDMA series, the MMA-POSS mole percentages range from 0.79 to 6.07% (5 to 30 wt%). Similarly, in the 5 wt% BDMA series, MA-POSS mole contents range from 0.80 to 6.23% (5 to 30%). Therefore, many chain segments can exist without a POSS moiety appended to it. Their segmental motions would not be retarded by POSS "anchors". The bulky heptaisobutyl (T_8) POSS systems may also disrupt some chain packing features of the parent P(iBMA-co-BDMA) resins thereby introducing more free volume. This would lead T_g to lower temperatures.

Figure 3.9 is a highly idealized picture which cannot be extrapolated to the macroscale. It does not account for any phase separation of POSS separation of POSS moieties in the crosslinked/cured nanocomposites. The following section discusses the observed

morphology. After considering the morphology observed, a discussion of the postulated role that phase separation plays during crosslinking will be given.

Morphology of P(iBMA-co-BDMA-co-MA-POSS) nanocomposites

POSS aggregation, is another phenomenon known to occur in thermoplastic polymers [10-11] and thermosetting resins [18] containing pendant POSS groups. Coughlin et al [10-11] showed that pendant POSS moieties, randomly incorporated in polyethylene, could aggregate during solidification of copolymer melts or on precipitation of the copolymer from solutions. Highly ordered POSS domains formed in sizes and shapes which were restricted by the attached polyethylene chains and the aggregation kinetics. In P(iBMA-co-BDMA-co-MA-POSS) systems with 3 and 5wt% BDMA, micro-sized POSS aggregation were observed by the naked eye. Variations in MA-POSS aggregation within these crosslinked matrices could also have unexpected effects on the viscoelastic behavior.

P(BDMA-co-1 wt% BDMA-co-MA-POSS) nanocomposites are completely transparent. However, some MA-POSS nanocomposites containing 3 wt% or 5 wt% BDMA exhibited white visible particles.

No particles could be observed for the transparent, 1% BDMA [P(BMA-co-1 wt% BDMA-co-MA-POSS)] nanocomposites with 5, 15 and 30 wt% MA-POSS by TEM at magnifications as high as 20,000. In contrast, POSS-rich particles in the 3 wt% and 5 wt% BDMA composites were observed by TEM. A low density of particles were scattered within the P(BMA-co-3 wt% BDMA-co-5 wt% MA-POSS) sample (Figure3.10 (a)). The largest particle found had a diameter of ~0.8 μm. These features appeared to

have darker and denser particles inside their boundaries. P(BMA-co-3 wt% BDMA-MA-POSS) samples with 15 and 30 wt% MA-POSS, exhibited irregular POSS-rich particles (Figure 3.10 (b) and (c) and (d)). The particles in the 15 wt% MA-POSS sample (Figure3.10 (b)) have diameters of ~0.9-1.1 μm. Many POSS-rich particles are formed in the irregular phase separated regions of this 15 wt% POSS sample, where the biggest irregular dark phase is about 2 μm (Figure 3.10 (c)). The sample with 30 wt% POSS (Figure3.10 (d)) shows a much bigger dark phase (about 4 μm). The size of POSS-rich particles or phases (dark features) in the (PBMA-co-3 wt% BDMA-co-MA-POSS) composites increases with the wt% POSS.

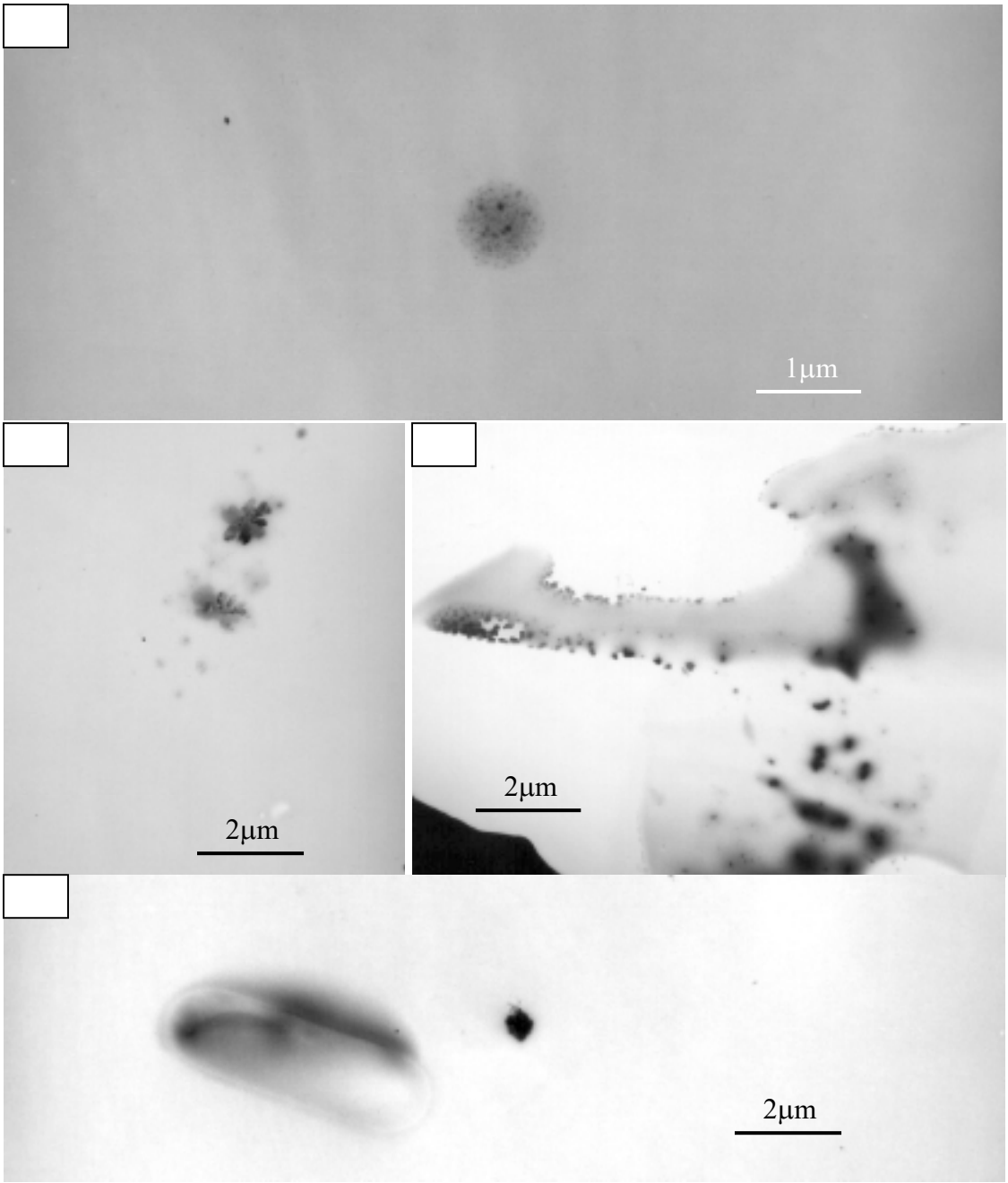

Figure 3.10 TEM micrographs of (1) P(BMA-co-3%BDMA-co-5%MA-POSS) ((a)), (2) P(BMA-co-3%BDMA-co-15%MA-POSS) ((b) and (c)), and (3) P(BMA-co-3%BDMA-co-30%MA-POSS) ((d))

POSS-rich phases were also observed in samples with 5 wt% of the crosslinkeing agent (BDMA) using TEM (Figure 3.11) in samples with 5, 15 and 30 wt% MA-POSS. The particle shown in Figure 3.11 (a) within the 5 wt% POSS sample is about 1.3 μm in diameter. The big particle in Figure 3.11 (b) of the same sample is 1.6 μm and a second aggregate ~0.5 μm is also seen nearby. The diameters of the larger particles in Figure 3.11 (c) and (d) for the 15 wt% POSS sample are 1.1 μm and 1.9 μm, respectively. As the POSS loading rises to 30 wt% while holding the BDMA content at 5 wt%, increasingly bigger particles (1.3 μm particle in Figure3.11 (e) and 2.9 μm particle in Figure 3.11 (f)) appear. The average size of POSS-rich particles increases with an increase in POSS contents in the composites with 5 wt% BDMA, similar to the trend found with 3 wt% BDMA.

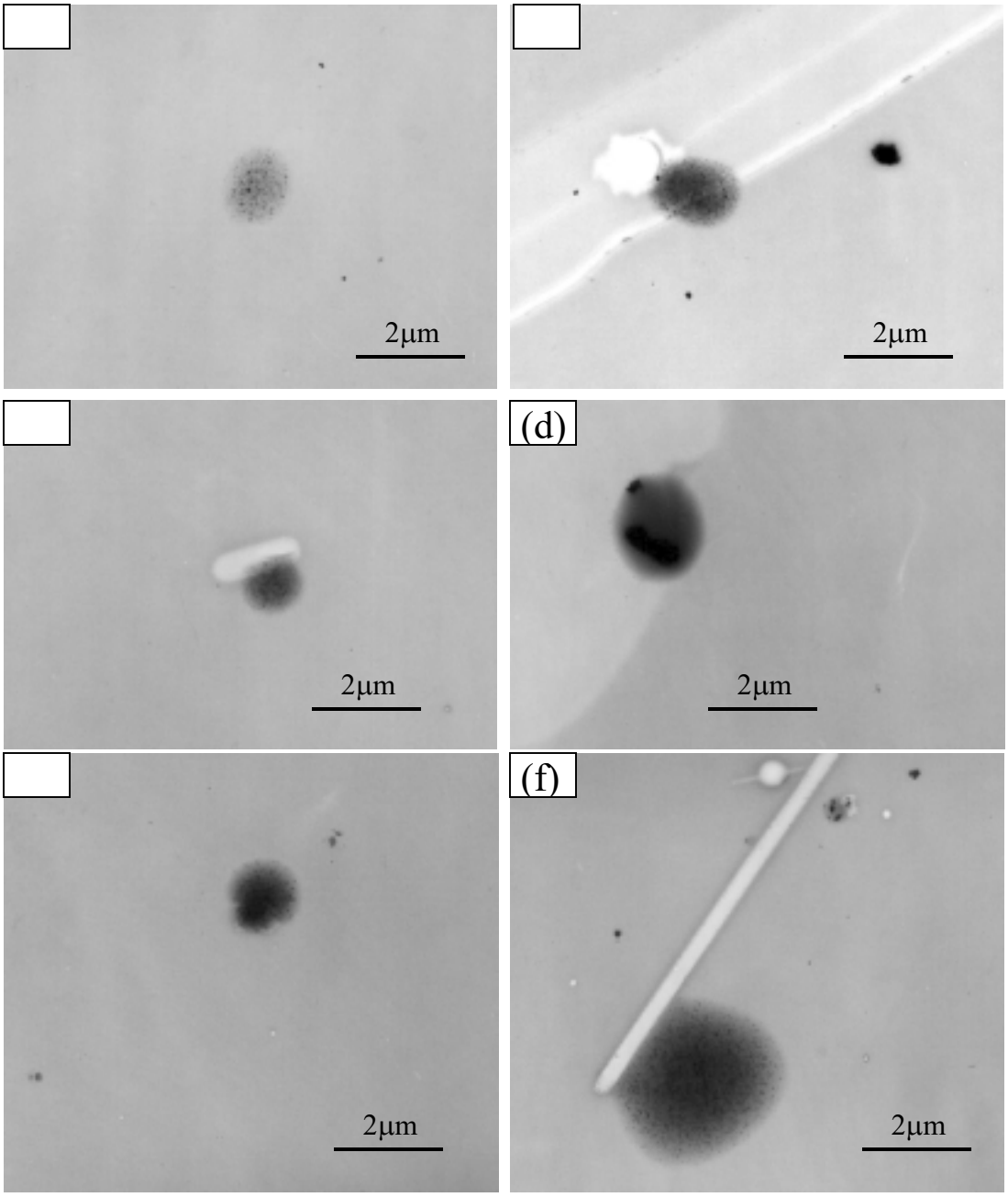

Figure 3.11 TEM micrographs of (1) P(BMA-co-5%BDMA-co-5%MA-POSS) ((a) and (b)), (2) P(BMA-co-5%BDMA-co-15%MA-POSS) ((c) and (d)), and (3) P(BMA-co-5%BDMA-co-30%MA-POSS) ((e) and (f))

Conclusions

Chemically incorporating 3-methacrylylpropylheptaisobutyl (T_8) POSS into the P(iBMA-co-BDMA) crosslinked resin network influences the viscoelastic properties of the resulting nanocomposites. The effects depend on the crosslink density, determined by the BDMA loading. At 1 wt% BDMA loading, the P(iBMA-co-BDMA-co-MA-POSS) nanocomposites exhibit a variation of viscoelastic properties versus MA-POSS content similar to those of linear P(iBMA-co-MA-POSS) copolymers. The P(iBMA-co-1 wt% BDMA-co-10 wt% MA-POSS) nanocomposite exhibited the highest E' values of all the systems examined (higher than those of P(iBMA-co-1 wt% BDMA) resin). These E' values decreased with an increase of MA-POSS from 10 wt% to 30 wt%. Some compositions of the copolymers and nanocomposites have higher E' values than the pure PiBMA and P(iBMA-co-1 wt%BDMA) resin. However, at higher BDMA loadings (3 wt% and 5 wt%), almost all nanocomposites exhibit lower E' values in the glassy region than those of the corresponding P(iBMA-co-BDMA) resins.

The P(iBMA-co-3 wt% BDMA-co-MA-POSS) nanocomposites with 15 wt% and 30 wt% MA-POSS exhibited higher E' values than those of the P(iBMA-co-3 wt% BDMA) resin in the rubbery region. The E' values of all P(iBMA-co-5 wt% BDMA-co-MA-POSS) nanocomposites in the rubbery region ($T>T_g$) are higher than those of the P(iBMA-co-5 wt%BDMA) resin and increase with an increase of POSS contents. This perhaps is due to retardation of segmental motions by pendant MA-POSS groups. These restrictions become more serious at high crosslink density (shorter average segment lengths).

The linear P(iBMA-co-MA-POSS) copolymers and all P(iBMA-co-BDMA-co-MA-POSS) nanocomposites (1, 3 and 5 wt% BDMA) with ≤15 wt% MA-POSS exhibit T_g values similar to those of the corresponding P(iBMA-co-BDMA) resins. The 20 wt% and 30 wt% MA-POSS copolymers or nanocomposites exhibit slightly lower T_g values than those of PiBMA or the corresponding P(iBMA-co-BDMA) resins. Heating history has a little influence on viscoelastic properties of P(iBMA-co-BDMA) linear copolymers and P(iBMA-co-BDMA-co-MA-POSS) nanocomposites.

POSS aggregates are not observed in the P(BMA-co-1 wt% BDMA-co-MA-POSS) nanocomposites by TEM. However, POSS-rich particles are formed in the POSS nanocomposites with 3 wt% and 5 wt% BDMA. POSS-rich particles of several microns diameter are presented in the 3 or 5wt% BDMA composites (TEM) and their size increases as the POSS contents increase. MA-POSS is soluble in iBMA and BDMA solutions. As polymerization and crosslinking proceed, the MA-POSS solubility decreases, in part due to entropy of mixing factors. Thus, a competition between incorporation into the developing polymer matrix and phase separation (followed by polymerization in the separated phases) occurs. The phase-separated regions can have varying amounts of iBMA and BDMA in them. A complex dependence on MA-POSS loading and crosslinking (BDMA loading) exists.

References

[1] Giannelis, E.P., *Adv. Mater.*, 1996, 8, 29.

[2] Alexandre, M., Dubois, P., *Mater. Sci. Eng.*, 2000, 28, 1.

[3] Li, G.Z., Wang, L., Ni, H., Pittman, C.U., *J. Inorganic and Organometalic Polymers*, 2001, 11(3), 123.

[4] Haddad, T.S., Viers, B.D., Phillips, S.H., *J. Inorganic and Organometallic Polymers*, 2001, 11(3), 155.

[5] Haddad, T.S., Lichtenhan, J.D., *Macromolecules*, 1996, 29(22), 7302.

[6] Romo-Uribe, A., Mather, P.T., Haddad, T.S., Lichtenhan, J.D., *J. Polym. Sci. B Polym. Phys.*, 1998, 36, 1857.

[7] Pyun, J., Matyjaszewski, K., *Macromolecules*, 2000, 33, 217.

[8] Mather, P.T., Jeon, H.G., Romo-Uribe, A., *Macromolecules*, 1999, 32(4), 1194.

[9] Bharadwaj, B.K., Berry, R.J., Farmer, B.L., *Polymer*, 2000, 41, 7209.

[10] Zheng, L., Farris, R.J., Coughlin, E.B., *Macromolecules*, 2001, 34, 8034.

[11] Zheng, L., Waddon, A.J., Farris, R.J., Coughlin, E.B., *Macromolecules*, 2002, 35, 2375.

[12] Tsuchida, A., Bolln, C., Sernetz, F.G., Frey, H., Mulhaupt, R., *Macromolecules*, 1997, 30(10), 2818.

[13] Lichtenhan, J.D., Vu, N.Q., Carter, J.A., Gilman, J.W., Feher, F.J., *Macromolecules*, 1993, 26, 2141.

[14] Mantz, R.A., Jones, P.F., Chaffee, K.P., Lichtenhan, J.D., Gilman, J.W., Ismail, I.M.K., Burmeister, M.J., *Chem. Mater.*, 1996, 8, 1250.

[15] Lee, A., Lichtenhan, J.D., *Macromolecules*, 1998, 31, 4970.

[16] Lee, A., Lichtenhan, J.D., Reinerth, W.A.Sr., *Polym. Mater. Sci. Eng.*, 2000, 82, 235.

[17] Li, G.Z., Wang, L., Toghiani, H., Daulton, T.L., Koyama, K., Pittman, C.U., *Macromolecules*, 2001, 34(25), 8686.

[18] Li, G.Z., Wang, L., Toghiani, H., Pittman, C.U., Daulton, T.L., *Polymer*, 2002, 43(15), 4167.

CHAPTER IV

VINYL ESTER/MULTIFUNCTIONAL METHACRYLOXY POSS INORGANIC-ORGANIC HYBRID NANO-COMPOSITES: SYNTHESIS, VISCOELASTIC PROPERTIES AND MORPHOLOGY

Introduction

The reinforcement of polymers using organic or inorganic fillers is common in the production of modern composites [1-2]. Polymeric nanocomposites represent a radical alternative to these conventional filled polymers or polymer blends. In contrast to conventional systems where noncontinuous reinforcement particles are on the order of a few microns, the polymeric nanocomposites are exemplified by discrete constituents on the scale of a few to ~100 nanometers. The development of polymer-inorganic hybrid nanocomposites with improved properties has attracted significant attention in the past few years [3-25] and extensive reviews are available [3-7]. Polyhedral oligomeric silsesquioxane (POSS) reagents combine a hybrid inorganic-organic composition, $R_n(SiO_{1.5})_n$, with inorganic nanosized cages having dimensions comparable to those of most polymeric segments or coils [26-27]. These POSS macromers offer a unique opportunity for preparing hybrid organic-inorganic nanocomposites with the inorganic

phase truly molecularly dispersed within the matrix. [26-27] POSS can be thought of as the smallest particles of silica possible having an organic surface. However, unlike silica, silicones or fillers, each POSS molecule contains either nonreactive or reactive organic substituents at the corner silicon atoms, making these nanostructures compatible with polymers or monomers. POSS derivatives are now available with reactive functionalities suitable for polymerization or grafting [17-27]. Hence, polymeric nanocomposites containing POSS nanostructured units are easily prepared via copolymerization, grafting or blending [27-36].

Incorporating POSS cages into polymeric materials often results in dramatic property improvements, including increases in heat distortion temperature, oxidation resistance, surface hardening and improved mechanical properties, as well as reductions in flammability and heat evolution. These enhancements have been reported in a wide range of thermoplastic and a few thermoset systems, i.e., methacrylates [17], styrenes[18-19], norbornenes [21, 30], ethylenes [31], siloxanes [32] and epoxides [20, 33].

Recently, multifunctional POSS chemicals have been designed and incorporated to thermoset resins [33-36]. Pittman et al incorporated a multifunctional POSS, $[(C_6H_5CHCHO)_4(Si_8O_{12})(CH{=}CHC_6H_5)_4]$, with 8 functional groups, including four β-substituted styrenes and four epoxidized β-styryl functions into both epoxy [33] and vinyl ester resins [34]. This isomeric mixture of POSS units dispersed well in the epoxy network [33], probably on the molecular scale, even at a high POSS content (25 wt%) based on TEM observations. The glass transition temperature range was broadened upon incorporating this POSS by curing the epoxy resin at 120 °C and 150 °C, but the T_g (the

tanδ peak temperature from DMTA curves) remained unchanged. Incorporating small amounts of this same multifunctional isomeric POSS mixture (≤10 wt%) into vinyl ester networks had almost no influence on T_g or the glass transition region [34]. The storage moduli, E', of both epoxy/POSS and VE/POSS composites at $T>T_g$ were higher than those of the neat epoxy or vinyl ester resins, respectively, improving their thermal dimensional stabilities [33-34]. Lee reported that multifunctional vinyl POSS cage mixtures (POSS mixtures with cages of 8, 10 and 12 Si atoms) could be used to modify vinyl ester resins [35]. The presence of 15 wt% of the mixed vinyl POSS macromers increased the ignition times of these vinyl ester/POSS resins and also reduced the overall heat release rates. The T_g values of Derakane 441–400 vinyl ester resin (VE) and its 15 wt% mixed cage vinyl POSS composites were 118 °C and 125 °C, respectively. Their heat distortion temperatures were 245 °F, and 257 °F, respectively. The decomposition temperature (T_{dec}) of the neat VE was substantially increased in its 15 wt% POSS composite from 360 °C to 411 °C, and the char% values increased sharply from 8% to 34 %, respectively [35]. This incorporation of vinyl POSS mixture into vinyl ester resins certainly improved the thermal and fire-retardant properties. However, there was very little change in their tensile strengths, tensile moduli, elongations, flexural strengths and flexural moduli [35].

Laine et al studied a new class of nanocomposites containing multifunctional epoxy-POSS, [octaglycidyldimethylsiloxyoctasilsesquioxane (glycidyl-$Me_2SiOSiO_{1.5})_8$] (OG) or octaethylcyclohexenyl-epoxide octasilsesquioxane (OC) [36-37], cured with diaminodiphenylmethane (DDM). A commercial diglycidyl ether of bisphenol A

(DGEBA) resin was used as a reference material. OG/DDM nanocomposites and commercial DGEBA/DDM composites exhibited maximum crosslink densities at N=0.5 (NH_2:epoxy groups = 0.5) whereas the mechanical properties were maximized at N=1.0. The temperatures for 5% mass loss were 344 °C for OG/DDM and 338 °C for DGEBA/DDM composites at N = 1, indicating a slightly better thermal stability for the POSS nanocomposite. However, T_g of OG/DDM nanocomposite at N=1 is about 60 °C, some 50 °C lower than that of DGEBA/DDM composite at N=1 (~110 °C), suggesting that the NH and OH groups in the DEGBA/DDM composite at N=1 hydrogen bond extensively but are constrained from close approach in the OG/DDM nanocomposite at N=1. The glass transition is barely noticeable for OG/DDM composite at N=0.5.

In this dissertation, two multifunctional methacryloxy POSS macromer systems, the multifunctional 3-methacryloxypropyl-POSS cage mixture (T_8, T_{10} and T_{12}) (POSS-**1**) and pure octa(3-methacryloxypropyldimethylsiloxy)POSS (POSS-**2**), were incorporated into a commercial vinyl ester (DERAKANE^{TM} 510C–350 augmented to contain 50 wt% styrene) resin network. The viscoelastic properties and morphology of these nanocomposites were determined by dynamic mechanical thermal analysis (DMTA) and transmission electron microscopy (TEM). The effect of the corner organic substituent structures on viscoelastic properties of the vinyl ester/multifunctional POSS-**1** and POSS-**2** nanocomposites was also considered.

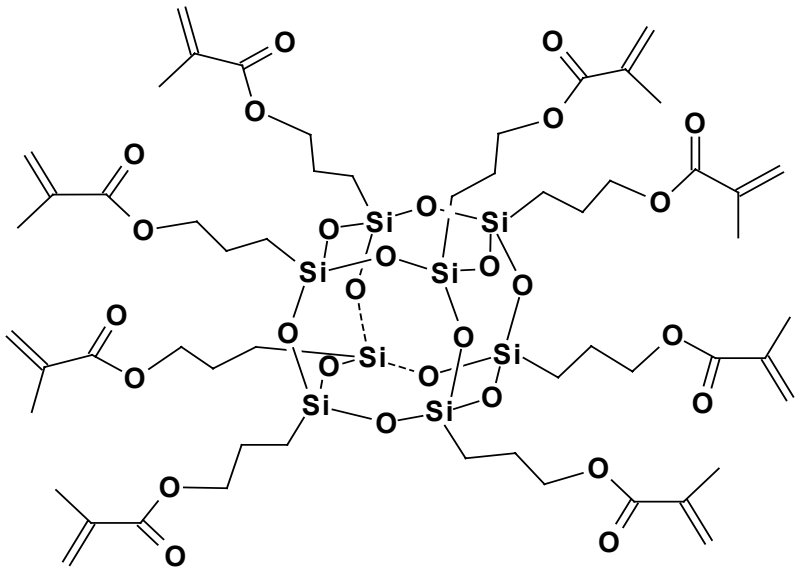

Methacryloxy-POSS Cage Mixture (only T_8 cage is shown.)
$(Methacryloxypropyl)_nT_n$ where n=8 (14mol%), 10 (50mol%) and 12 (36mol%)

POSS-**1**

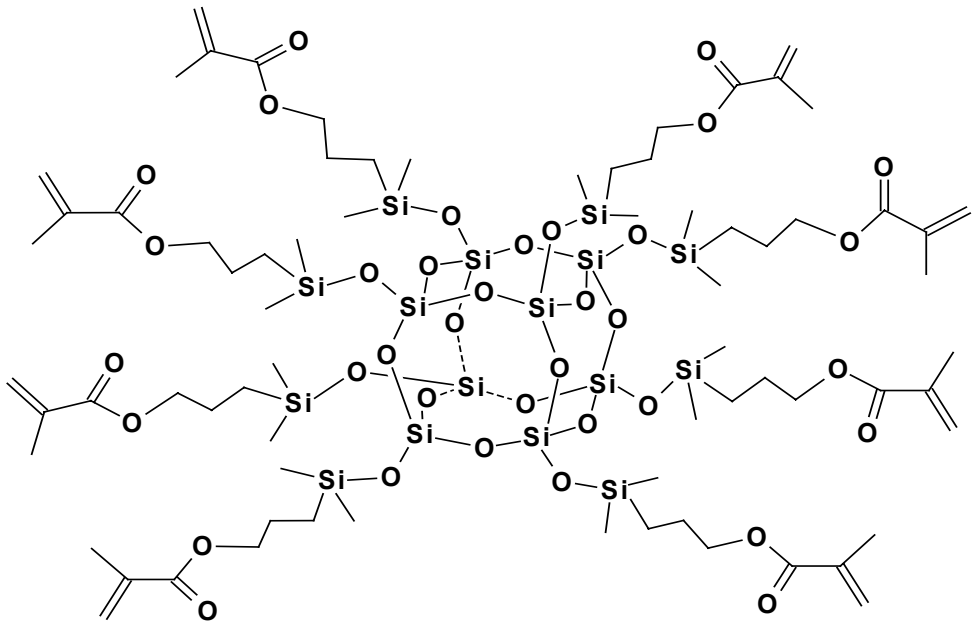

Octa(3-methacyloxydimethylsiloxyl)(T_8)POSS

POSS-**2**

Figure 4.1 POSS chemicals

Experimental

Specimen Preparation

Multifunctional 3-methacryloxy-POSS cage mixtures (average MW: 1871.32 g/mol), containing T_8, T_{10} and T_{12} (14 mol% T_8, 50 mol% T_{10} and 36 mol% T_{12}), POSS-**1**, and octa(3-methacryloxydimethylsiloxyl)(T_8)POSS (MW: 2027.20 g/mol), POSS-**2**, were purchased from Hybrid™ Plastics Co. The commercial vinyl ester (VE) resin, DERAKANE™ 510C-350, containing 35 % (wt) styrene, was purchased from Dow Chemical Co.. Methyl ethyl ketone peroxide (MEKP) and cobalt naphthanate (CoNap), provided by Dow Chemical Co., were employed as the initiator/catalyst curing system. Styrene ($C_6H_5CH=CH_2$, 99%, F.W.104.5, and b.p.145-146 °C) was purchased from Aldrich Chemical Company Inc.

POSS-**1** (0.131 g, 0.402 g, 0.684 g, 1.444 g, 2.294 g, or 3.25 g) was dissolved into styrene (3 g) to produce transparent solutions. Each solution was mixed with VE resin (10 g) to produce clear transparent solutions containing 50 % (wt) styrene with 1wt% or 3 wt% POSS, translucent solutions with 5 wt%, 10 wt% and 15 wt% POSS, or a slightly opaque solution with 20 wt% POSS. Then, 1 wt% MEKP and 0.2 wt% CoNap were added into each solution. Each formulation was placed into a mold, cured at room temperature for 24 h and then postcured in an oven at 90 °C for 24 h and then 160 °C for 5 h. A reference vinyl ester resin was also made by adding 3 g styrene to 10 g DERAKANE™ 510C–350 to bring the styrene wt% to 50 %. This resin was cured using the same protocol. The reference VE resin and the VE(50 wt% styrene)/POSS-**1** 99/1, 97/3, 95/5, 90/10, 85/15 and 80/20 wt/wt specimens were made in 69 mm × 38 mm × 3-4

mm sizes. The cured neat VE resin and the 1 wt% POSS-**1** nanocomposite were transparent. The 3 wt% POSS-**1** nanocomposite was almost transparent. The 5 wt% POSS-**1** nanocomposite was slightly translucent and the 10 wt% POSS-**1** nanocomposite was translucent. The 15 wt% POSS-**1** nanocomposite was almost translucent while the 20 wt% POSS-**1** nanocomposite was opaque.

A series of VE(50 wt% styrene)/POSS-**2** nanocomposites with compositions of 99/1, 97/3, 95/5, 90/10, 85/15 and 80/20 (wt/wt), were made by the same method as the VE/POSS-**1** nanocomposites. The 1 wt% POSS-**2** nanocomposite was transparent. The 3 wt% POSS-**2** nanocomposite was slightly translucent and the 5 wt% POSS-**2** nanocomposite was translucent. As the POSS-**2** content increased to 10 wt%, 15 wt% and 20 wt%, the nanocomposites became opaque.

Measurements

The dynamic storage modulus, E', and loss factor (tanδ) were determined in the dual-level bending mode using a Polymer Laboratories DMTA MK3 instrument. Small amplitude bending oscillations (both 1 and 10 Hz) were used at a gap setting of 8.00 mm. The measurements were carried out from 35 °C to 190-200 °C at a heating rate of 2 °C/min. Nanocomposite samples between 2.3-3.0 mm thick, 5.8-7.6 mm wide and 38 mm long, were used.

The densities of VE/POSS-**1** and VE/POSS-**2** nanocomposites were measured using an Electronic Densimeter (ED-120T) at 25 °C.

Specimens (~0.4 g) of every VE/POSS-**1** and VE/POSS-**2** nanocomposite were immersed into THF at room temperature. Some cracks appeared and these specimens fractured into many small pieces in THF. Thus, swelling volumes couldn't be measured. Small amounts of linear copolymers, with no detectable POSS, were extracted into these THF solutions. After coating onto KBr plates and removal of THF, IR spectra were obtained on an FT-IR instrument (MIDAC Corporation). Specimens (~0.4 cm^3) of each VE/POSS-**1** and VE/POSS-**2** nanocomposite were also immersed in toluene at room temperature. Their weights were measured after reaching equilibrium in toluene. Toluene extracts were also examined by FT-IR. The reference VE resin and the POSS-**1** and POSS-**2** nanocomposites were also examined by FT-IR.

A JEM-100 CXII transmission electron microscope (TEM) (JEOL USA Inc.) was used to characterize phase morphology of the VE/POSS-**1** and VE/POSS-**2** nanocomposites. Specimens for this measurement were microtomed to 70-90 nm thicknesses and set on copper grid. A JSM-6500F field emission scanning electron microscope (FESEM) (JEOL USA Inc.) with an attached X-ray energy dispersive spectrometer (X-EDS) was used to obtain elemental compositions of the aggregated particles and the continuous matrix regions in VE/POSS nanocomposites. The samples for SEM were fractured after immersion in liquid nitrogen and coated with gold before SEM measurements. The electron beam spot at 30 kv is about 1.5 nm. Thus, the spot size was far smaller than the particles being examined, allowing elemental compositions of the particles to be probed specifically. However, the electron beam dislodges electrons which, in turn, dislodge others over a volume which may be in the vicinity of a cubic

micron. Thus, X-ray emissions arise with varying intensities from this volume. This causes the resolution of X-EDS to be considerably less than would be indicated by the spot size. The area resolution depends on many variables but is approximately 1 μm^2.

Results and Discussion

Synthesis of the Nanocomposites

The VE/POSS-**1** and VE/POSS-**2** nanocomposites were prepared by radical initiated polymerization. Synthesis of the VE/POSS-**2** nanocomposites is represented in Figure 4.2. The reactivities of methacryloxy substituents in the POSS macromer are quite similar to those of methacrylyl groups in uncured VE resin. Thus, POSS-bound methacryloxy functions react easily with the VE monomers and with styrene. Therefore, POSS units are easily incorporated into the VE network.

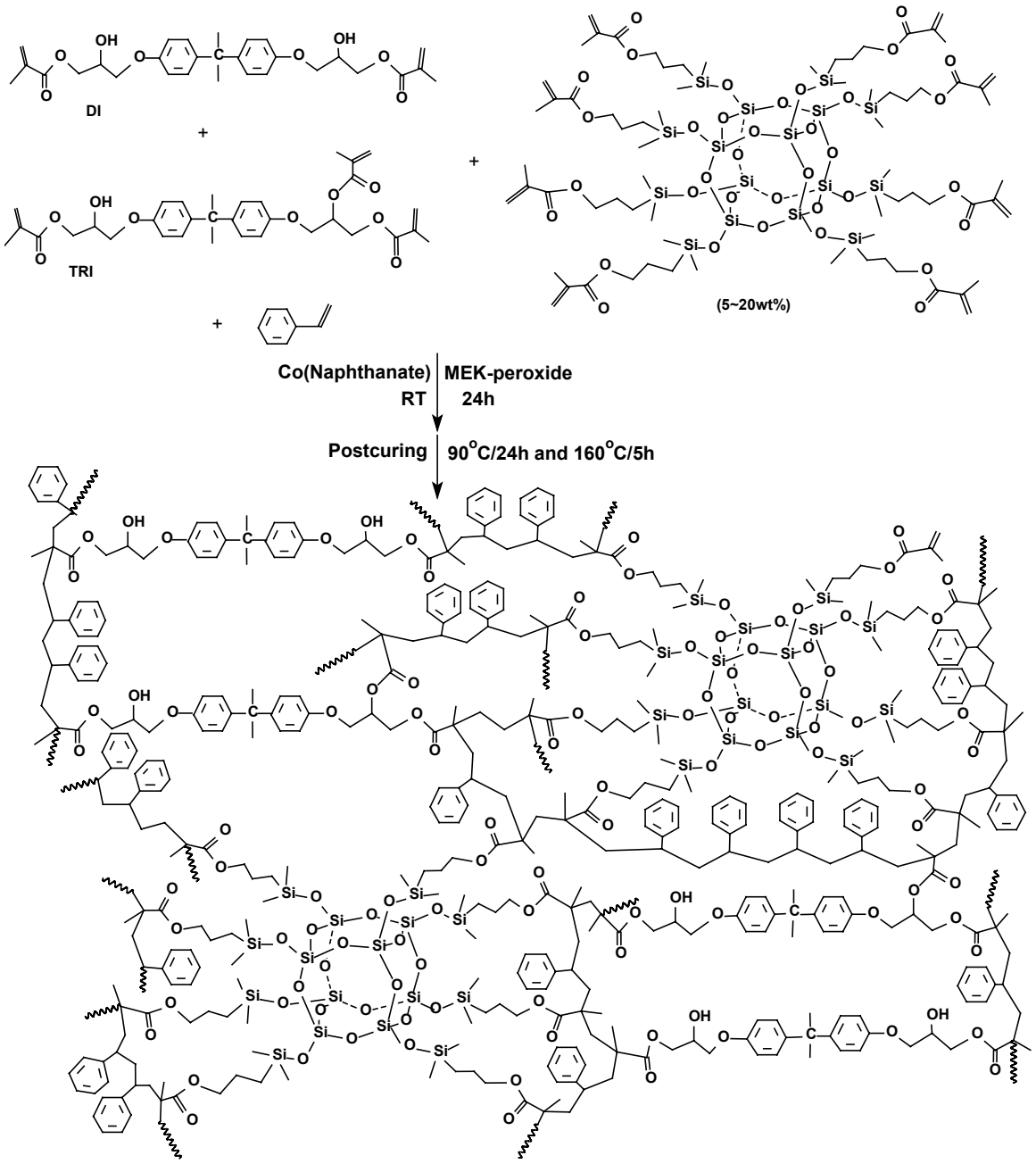

Figure 4.2 Synthesis of VE/POSS-**2** nanocomposites

Viscoelastic Properties of Vinyl Ester (VE)/POSS-1 Nanocomposites

The bending storage moduli, E', versus temperature curves at 1Hz (from DMTA) for the neat vinyl ester and the VE/POSS-**1** (cage mixture) nanocomposites are given in Figure 4.3. Figure 4.3 clearly shows that the E' values of all VE/POSS-**1** nanocomposites are higher than those of the neat VE resin in the rubbery region ($T>T_g$). Furthermore, these E' values increase regularly with an increase in POSS loading. However, in the glassy region ($T<T_g$), the E' values of these nanocomposites are close to those of the neat VE resin. For example, the E' values of neat VE resin and the VE/POSS-**1** 99/1, 97/3, 95/5, 90/10, 85/15 and 80/20 nanocomposites at 40 °C (shown in Table 4.1) are 1.58 GPa, 1.49 GPa, 1.26 GPa, 1.50 GPa, 1.30 GPa, 1.62 GPa and 1.65 GPa, respectively. Only the 15 wt% and 20 wt% POSS-**1** nanocomposites exhibit slightly higher E' values than those of the neat VE resin at $T<T_g$. However, the E' values of neat VE, VE/POSS-**1** 99/1, 97/3, 95/5, 90/10, 85/15 and 80/20 nanocomposites at 175 °C ($>T_g$) are 6.50 MPa, 8.73 MPa, 8.62 MPa, 12.27 MPa, 19.21 MPa, 35.64 MPa and 66.83 MPa, respectively. The E' value for the 80/20 nanocomposite is about 10 times greater than that of the neat VE resin. The VE nanocomposites containing the POSS-**1** cage mixture have better mechanical properties than the neat VE resin above T_g. Their thermal dimensional stabilities are higher than that of the VE resin. This stability increases with increasing POSS-**1** content.

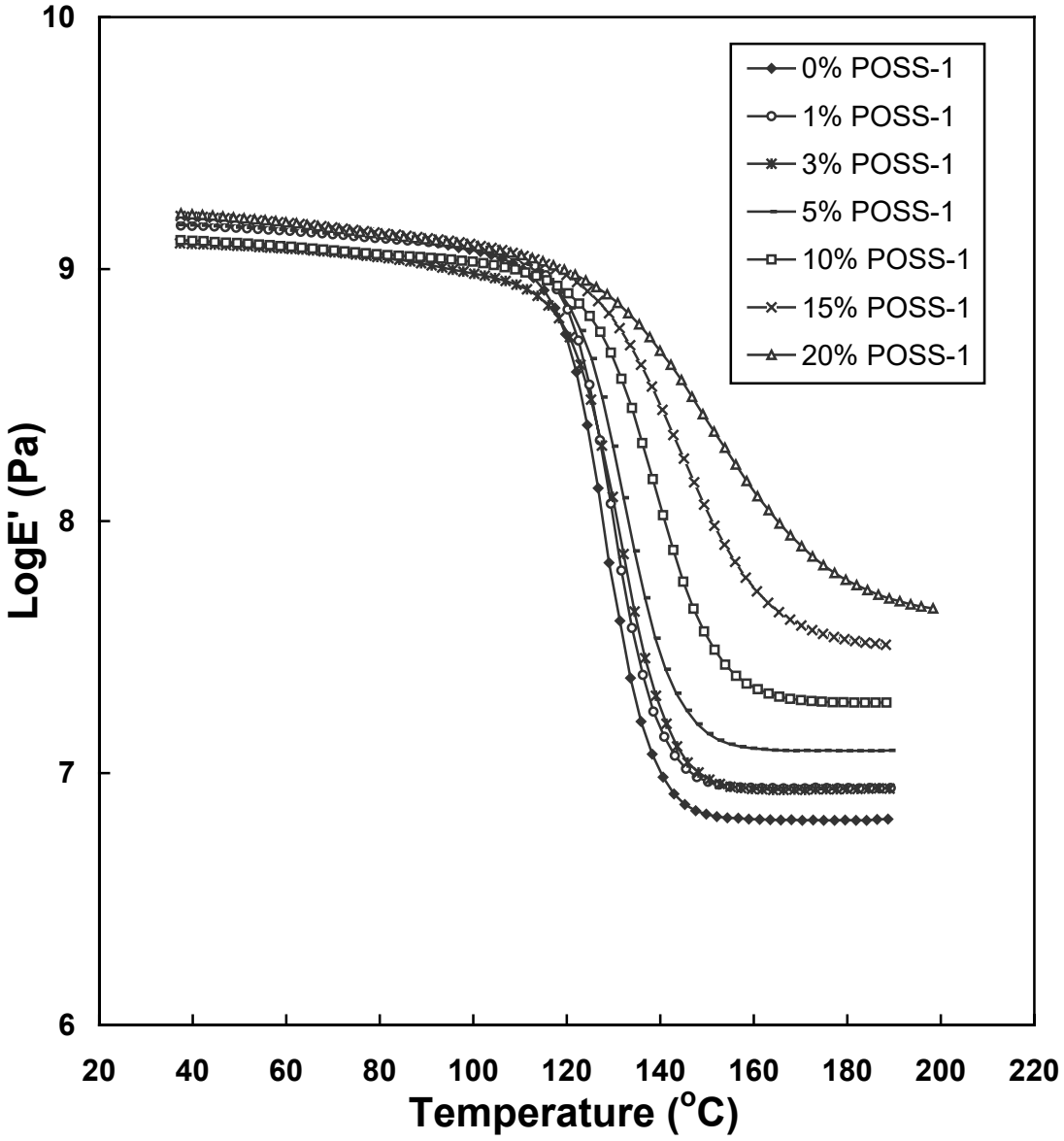

Figure 4.3 Bending storage moduli versus temperature curves at 1Hz for VE (50% styrene)/POSS-**1** nanocomposites at different POSS-**1** loadings

Table 4.1 DMTA Data, density and weight increases after swelling in toluene of neat VE resin and VE/POSS-**1** and VE/POSS-**2** nanocomposites

Samples	T_g (°C)	E' at 40°C (GPa)	E' at 175°C (MPa)	Density(ρ) (g/cm^3)	Weight %increase
VE	131.3	1.58	6.50	1.208	6.78
VE/POSS-**1** 99/1	134.0	1.49	8.73	1.209	1.37
VE/POSS-**1** 97/3	134.5	1.26	8.62	1.212	0.85
VE/POSS-**1** 95/5	136.7	1.50	12.29	1.213	0.50
VE/POSS-**1** 90/10	142.8	1.30	19.21	1.227	0
VE/POSS-**1** 85/15	147.2	1.62	35.64	1.229	0
VE/POSS-**1** 80/20	153.8	1.65	66.83	1.241	0
VE/POSS-**2** 99/1	129.1	1.49	8.43	1.221	4.46
VE/POSS-**2** 97/3	128.6	1.41	7.51	1.211	2.07
VE/POSS-**2** 95/5	129.5	1.53	10.20	1.213	0.89
VE/POSS-**2** 90/10	124.5	1.32	14.26	1.211	0.10
VE/POSS-**2** 85/15	125.0	1.34	19.33	1.216	0
VE/POSS-**2** 80/20	120.2	0.80	18.53	1.214	0

Figure 4.4 displays the bending tanδ versus temperature curves at 1 Hz (from DMTA) for the VE resin and the VE/POSS-**1** nanocomposites. The incorporation of **1** into VE broadens the width of tanδ peak in the glass transition range. Widths of these tanδ peaks increase and their intensities decrease with an increase in the POSS-**1** mixture loading. The VE/POSS-**1** 80/20 composite exhibits a very broad weak tanδ peak. The glass transition temperature (T_g) is defined, herein, as the tanδ peak temperature. The T_g values of the neat VE resin (131.3 °C) and VE/POSS-1 99/1 (134.0 °C), 97/3 (134.5 °C), 95/5 (136.7 °C), 90/10 (142.8 °C), 85/15 (147.2 °C) and 80/20 (158.3 °C) nanocomposites increase with increasing POSS-**1** loadings. Incorporating POSS-**1** into VE network improves its thermal stability.

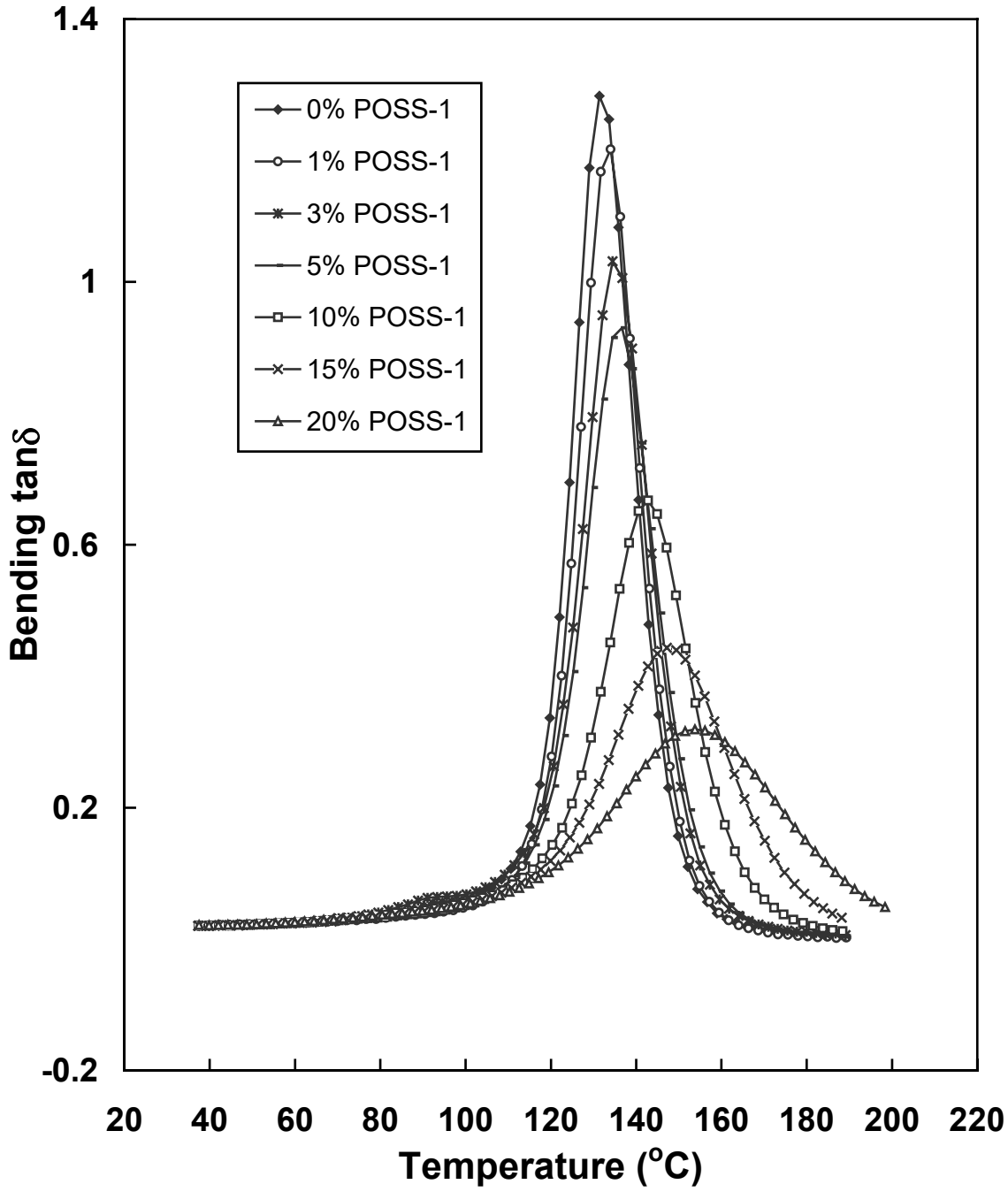

Figure 4.4 Bending tanδ versus temperature curves at 1Hz for VE (50% styrene)/ POSS-**1** nanocomposites at different POSS-**1** loadings

The POSS-**1** mixture contains T_8, T_{10} and T_{12} cages. These are functionalized at every Si atom with methacryloxy functions in the T_8, T_{10} and T_{12} cages, respectively. These macromers easily copolymerize with methacrylyl groups of the VE resin and with styrene. Each POSS cage serves as a network crosslinking site. Since the T_{10} and T_{12} cages are present as 50 and 36 mol% of the POSS units, an increase in the volumetric crosslink density might occur, although each POSS unit occupies a sizeable volume by itself. POSS-**1** cages retard segmental motion in the VE network due to their high masses and the large volume crosslinked hub that each POSS moiety forms upon bonding into the network. Segmental motion will be retarded greatly at these massive crosslinked hubs with 8, 10 and 12 spokes, respectively, radiating from each POSS unit. Therefore, the POSS-**1** nanocomposites exhibit higher T_g values and higher E' values in the rubbery region than those of the neat VE resin.

Viscoelastic Properties of VE/POSS-2 Nanocomposites

The bending storage modulus, E', versus temperature curves at 1 Hz (from DMTA) for the neat VE resin and VE/POSS-**2** nanocomposites, containing 1 wt%, 3 wt%, 5 wt%, 10 wt%, 15 wt% and 20 wt% of POSS-**2**, are shown in Figure 4.5. Below T_g, only small differences exist among the E' values of the neat VE resin and the 1, 3, 5, 10 and 15 wt% POSS-**2** nanocomposites. But, the 20 wt% nanocomposite displays lower E' values than those of the other nanocomposites containing ≤15 wt% POSS-**2**. The bending storage moduli at 40 °C are 1.58 GPa (VE), 1.49 GPa (1 wt% POSS-**2**), 1.41 GPa (3 wt% POSS-**2**), 1.53 GPa (5 wt% POSS-**2**), 1.32 GPa (10 wt% POSS-**2**), 1.34 GPa (15 wt% POSS-**2**) and 0.80 GPa (20 wt% POSS-**2**). The E' value of the 20 wt% POSS-**2**

nanocomposite is only about half that of the neat VE resin. All POSS-**2** nanocomposites exhibit lower E' values than that of the VE at 40 °C ($<T_g$). However, at $T>T_g$, all POSS-**2** nanocomposites exhibit higher E' values than those of the neat VE resin. These E' values increase with an increase of POSS-**2** content to 15 wt%. The E' values of neat VE, and VE/POSS-**2** 99/1, 97/3, 95/5, 90/10, 85/15 and 80/20 nanocomposites at 175 °C ($>T_g$) are 6.50 MPa, 8.83 MPa, 7.51 MPa, 10.20 MPa, 14.26 MPa, 19.33 MPa and 18.53 MPa, respectively. The VE/POSS-**2** nanocomposites containing 15 and 20 wt% POSS exhibit E' values (18-20 MPa) at 175 °C ($T>T_g$), three times greater than the reference VE resin, but much lower than those with 15 and 20 wt% of the POSS-**1** cage mixture (35-67 MPa).

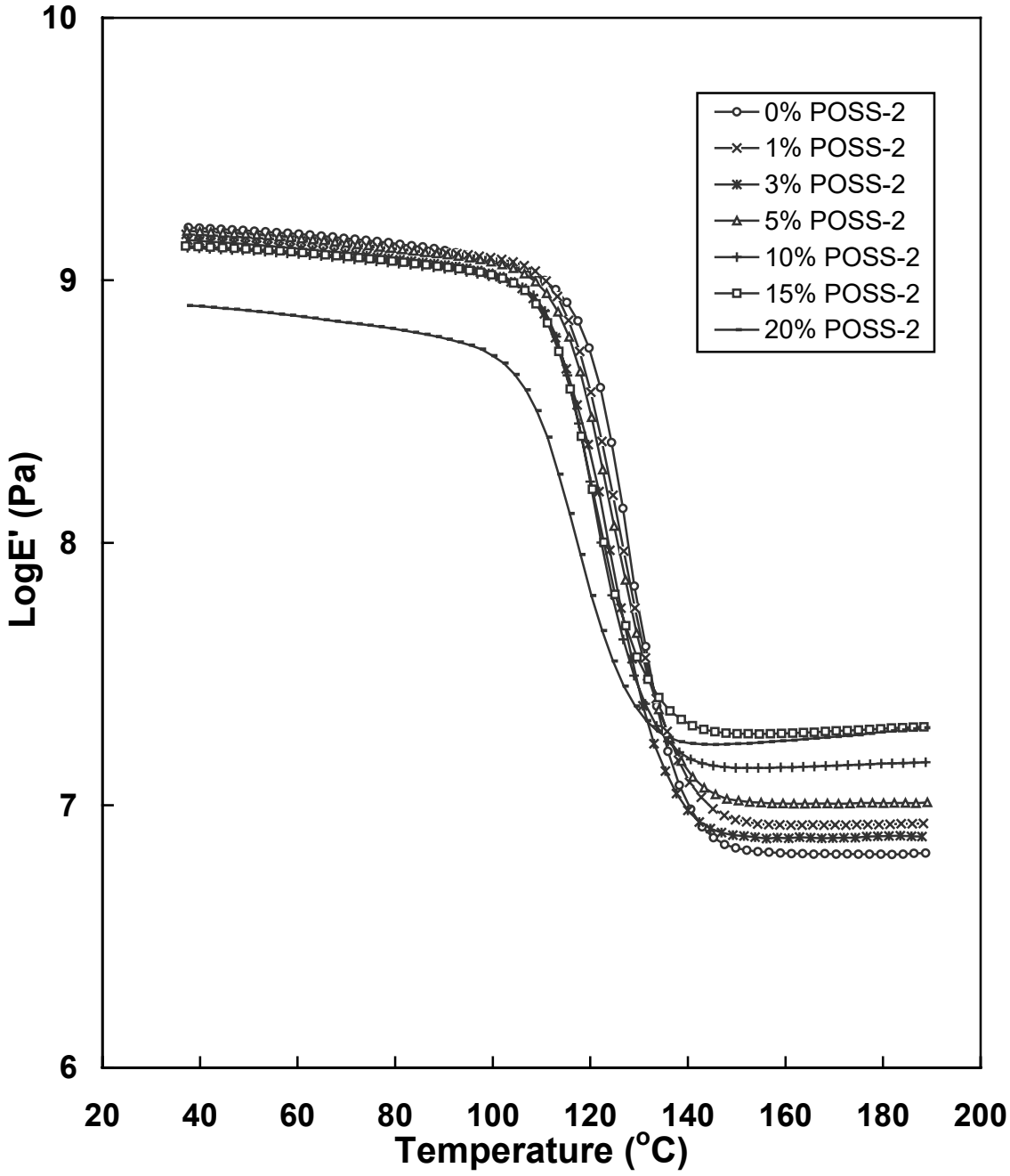

Figure 4.5 Storage moduli, E', versus temperature curves at 1Hz for VE/POSS-**2** nanocomposites

The bending tanδ versus temperature curves obtained at 1 Hz (from DMTA) for the reference VE resin and its POSS-**2** nanocomposites are shown in Figure 4.6. The tanδ peak intensities of these VE resins were lowered and their widths were broadened by incorporation of POSS-**2**, similar to the behavior observed for VE/POSS-**1** nanocomposites. The T_g values (tanδ peak temperatures) are 131.3 °C, 129.1 °C, 128.6 °C, 129.5 °C, 124.5 °C, 125.0 °C and 120.2 °C, for the neat VE resin and the 1, 3, 5, 10, 15 and 20 wt% POSS-**2** nanocomposites, respectively. The T_g values decrease as POSS-**2** is incorporated into the VE resin in greater amounts. This behavior stands in sharp contrast to that observed with the VE/POSS-**1** nanocomposites where T_g increased regularly with increased POSS-**1** contents.

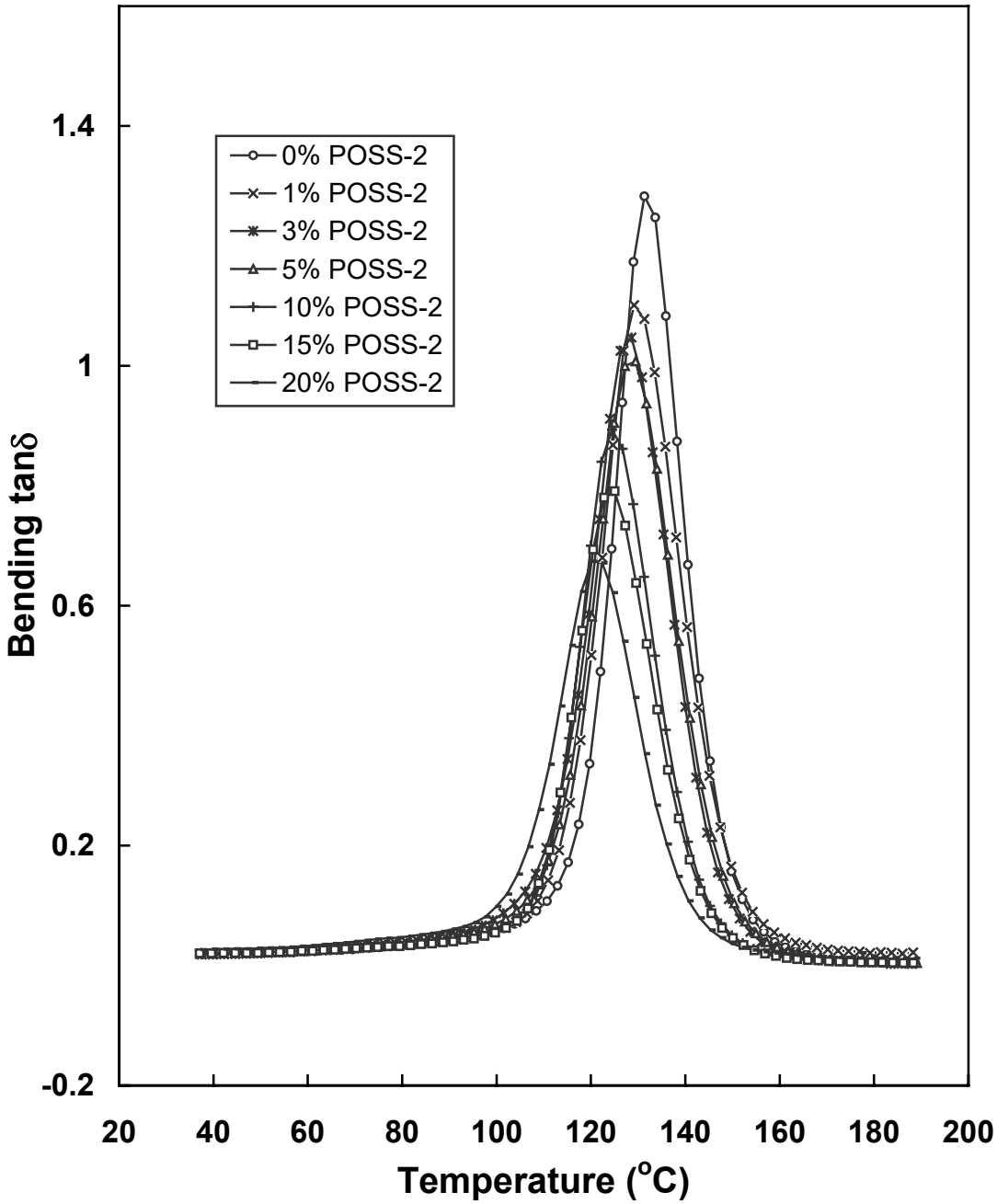

Figure 4.6 Bending tanδ versus temperature curves at 1Hz for VE/POSS-**2** nanocomposites

Why do VE/POSS-**2** nanocomposites exhibit lower T_g and higher E' values in the rubbery region than those of the neat VE resin? This might be due to the more flexible chemical structure of the eight methacryloxy substituents on POSS-**2**, which easily react with styrene or uncured VE methacrylate functions (Figure 4.2). This may give higher network crosslink densities than in neat VE resin, but this POSS macromer occupies a large volume itself. More crosslinks from a single hub location (POSS) might act to raise E' in the rubbery region versus those of the neat VE resin. Increased crosslinking usually results in higher T_g values. However, the substituents on POSS-**2** are longer and more flexible than those of POSS-**1** due to the extra dimethylsiloxyl segment present on all eight POSS-**2** corners. Thus, the segments in the region around POSS-**2** cages move more easily versus those of the POSS-**1** nanocomposites. This factor weakens restrictions on segmental motion of the POSS cages, perhaps decreasing T_g values. This effect counteracts the crosslinking density effect, lowering the T_g values and lowering E' values in the rubbery region versus those of the corresponding VE/POSS-**1** systems.

A second factor also may operate and it complicates any explanation. The T_{10} (50 mol%) and T_{12} (36 mol%) cages in the POSS-**1** mixture have 10 and 12 methacryloxy functions radiating from their cores, respectively. Thus, they can act as hubs with more spokes eminating from each cage to bind the network than do the T_8 cages. The T_{10} and T_{12} cages also have a greater volume than T_8 cages. As we shall see, the POSS-**2** monomer has more propensity to phase-separate as the wt% increases than the POSS-**1** monomer. It is difficult to define the effect of volumetric crosslink density and different crosslink morphologies.

Haddad et al [38] reported the effect which different substituents on the POSS (T_8) cage exerted on the viscoelastic properties of three kinds of thermoplastic poly(styrene-co-styryl-POSS) copolymers. T_g value of polystyrene is 129 °C. The T_g values of three copolymers containing monofunctional styryl-POSS, where the other seven substituents on each monomer were isobutyl, cyclopentyl and cyclohexyl, are 120 °C (4.6 mol% POSS), 131 °C (4.3 mol% POSS) and 138 °C (3.9 mol% POSS), respectively. The E' values for these three styryl-POSS copolymers are also lower than those of pure PS in the glassy region ($T<T_g$) and the E' values of isobutyl styryl-POSS copolymer are slightly lower that those of PS in the rubbery region ($T>T_g$). In contrast, the cyclopentyl and cyclohexyl styryl-POSS copolymers exhibited higher E' values than those of polystyrene in the rubbery region ($T>T_g$). Clearly, the nature of the substituents on POSS has a strong effect on the elastic properties of linear POSS copolymers [38]. Therefore, one might expect a substantial influence by the substituents on the viscoelastic properties in VE/POSS thermoset nanocomposites.

Densities, Solvent Swelling and IR Data

Densities of the neat VE resin, VE/POSS-**1** and VE/POSS-**2** nanocomposites are listed in Table 4.1. The densities for all VE/POSS-**1** nanocomposites are higher than that of the neat VE resin. These densities increase with an increase of POSS-**1** content. However, the VE/POSS-**2** 97/3, 95/5, 90/10, 85/15 and 80/20 nanocomposites all have very similar densities. Only the 1wt% POSS-**2** nanocomposite exhibits a slightly higher density than those of the VE resin and other nanocomposites. These results indicate that

the POSS-**2** nanocomposites might contain more free volume than the POSS-**1** nanocomposites. As a result, the segments in the POSS-**2** nanocomposites might move more easily than those in the POSS-**1** nanocomposites. This is a possible reason why the POSS-**1** nanocomposites exhibited higher T_g and much higher E' values in the rubbery region than those of the corresponding POSS-**2** nanocomposites.

The VE resin, and the VE/POSS-**1** and VE/POSS-**2** nanocomposites specimens were swollen in toluene for 20 days. The weight increments after swelling are shown in Table 4.1. At low POSS content (1 to 5 wt%), the POSS-**1** nanocomposites exhibit lower weight increments (less solvent uptake) than that of the neat VE resin. These values decrease sharply with an increase of POSS content. At POSS-**1** levels above 10 wt%, the POSS-**1** nanocomposites undergo no weight increase after immersion for 20 days in toluene. The nanocomposites were removed and the toluene solutions were evaporated. The extracted portions were studied by FT-IR. Only small amounts of linear copolymer, without any POSS-**1**, were detected in the residue from the neat VE resin and the 1 wt% POSS-**1** nanocomposite. No extractable residue was detected in the toluene solutions from the POSS-**1** nanocomposites containing more POSS (≥3 wt%).

The reference VE and VE/POSS-**1** nanocomposites specimens were also immersed in THF and swollen at the room temperature for 20 days. The VE and the POSS-**1** nanocomposites specimens with ≤10 wt% POSS had fractured into many small pieces. However, only a part of the 15 wt% POSS-**1** nanocomposite specimen fractured and there were no cracks in the 20 wt% POSS-**1** nanocomposite specimen. Thus, the POSS-**1** nanocomposite with 20 wt% POSS-**1** exhibited an extraordinary ability to withstand

solvent. No POSS-**1** was detected in the soluble residues that were extracted into THF from any of these samples. Only a small amount of ungelled VE copolymers were detected in the THF extract. These results are in accord with higher crosslinking densities in the POSS-**1** nanocomposites than that of the neat VE resin and their crosslinking densities increased with an increase of POSS content. Furthermore, all of the POSS-**1** macromers, within our ability to detect, were incorporated into the nanocomposite networks.

The VE/POSS-**2** nanocomposites exhibited somewhat higher weight increases, due to solvent uptake when swollen in toluene, than the POSS-**1** nanocomposites of the same POSS loading. Only the 15 and 20 wt% POSS-**2** nanocomposites showed no weight increase after immersion in toluene for 20days while the 10, 15 and 20 wt% POSS-**1** nanocomposites exhibited no weight increase. The toluene extracts for the 1, 3, 5, 10 and 15 wt% POSS-**2** nanocomposites contained small amounts of ungelled VE copolymers, but no residue was extracted from the 20 wt% POSS-2 nanocomposite by toluene. Furthermore, no POSS-**2** was detected by FT-IR in any of these extracted residues. After 20 days of immersion in THF, the 1, 3, 5, 10 and 15 wt% POSS-**2** nanocomposites had fractured into many small pieces and cracks also appeared on the surface of the 20 wt% POSS-**2** nanocomposite specimen. Like the POSS-**1** nanocomposites, IR spectra of THF solutions for all POSS-**2** nanocomposites showed that small amounts of VE copolymers, without any POSS units, were extracted by THF. Clearly, the VE/POSS-**1** systems are more solvent resistant than their VE/POSS-**2** counterparts, suggesting the POSS-**1** nanocomposites have higher crosslink density than the POSS-**2** nanocomposites. This is

also consistent with higher E' values of the POSS-**1** nanocomposites in the rubbery region versus those of the POSS-**2** nanocomposites with equivalent POSS loadings.

The IR spectrum of uncured VE resin exhibited a sharp carbon-carbon double bond stretching absorption at 1636 cm^{-1} due to the methacrylyl functions. IR spectra for POSS-**1** and POSS-**2** macromers also exhibited a sharp absorption at 1638 cm^{-1} due to their methacryloxy functions. After curing, no absorption could be observed in this region for either the VE resin or the POSS-**1** or POSS-**2**/VE nanocomposites when ≤10 wt% POSS was present. Thus, curing approaches completion for the neat VE resin and the nanocomposites containing ≤10wt% POSS. However, the IR spectra of POSS-**1** and POSS-**2** nanocomposites, containing higher POSS contents (15 wt% and 20 wt%), exhibited a weak absorption around 1636 cm^{-1}. Thus, a small fraction of methacryloxy functions in the 15 wt% and 20 wt% POSS nanocomposites had not reacted.

Phase Morphology for the Nanocomposites

No phase-separation (e.g. POSS particles or aggregates) was observed for the VE/POSS-**1** 99/1, 97/3 and 95/5 nanacomposites by TEM. When the POSS-**1** content was raised to 10 wt%, a few scattered round particles appeared in the VE/POSS-**1** 90/10 sample (Figure 4.7(a)). The particle sizes range from 30 nm to 2.11 μm. At high magnification (Figure 4.7(b)), the particle appears to contain some white regions, quite similar to the continuous phase. As POSS-**1** content increased to 15 wt%, some scattered particles are again observed (Figure 4.7(c)). The biggest particle found after searching many TEMs was 3.11 μm in diameter. The TEM micrograph at high magnification for

the particles in the 15 wt% POSS-**1** nanocomposite (Figure 4.7(d)) exhibits a small difference in contrast between some areas of the particles and the continuous phase. The small particle (near the big particle) has a ~20 nm diameter. As the POSS-**1** content further increased to 20 wt%, only some scattered particles were found, with the biggest particle having a diameter of 8.94 μm (Figure 4.8(a)). At higher magnification, this particle exhibits a low contrast difference versus the continuous phase (Figure 4.8(b)), as was observed in the 10 wt% and 15 wt% POSS-**1** nanocomposites. The particle sizes increase as the POSS-**1** contents increase from 10 wt% to 20 wt%. Furthermore, these particles appear to contain some VE content based on contrast differences and are best considered as POSS-rich particles. In summary, no POSS-rich particles were observed in VE/POSS-**1** nanocomposites containing ≤5 wt% POSS. At ≥10 wt% POSS content, a modest number of POSS-rich particles are found. The number of particles does not vary much as the POSS-**1** content increases from 10 wt% to 20 wt%, but their average size increases.

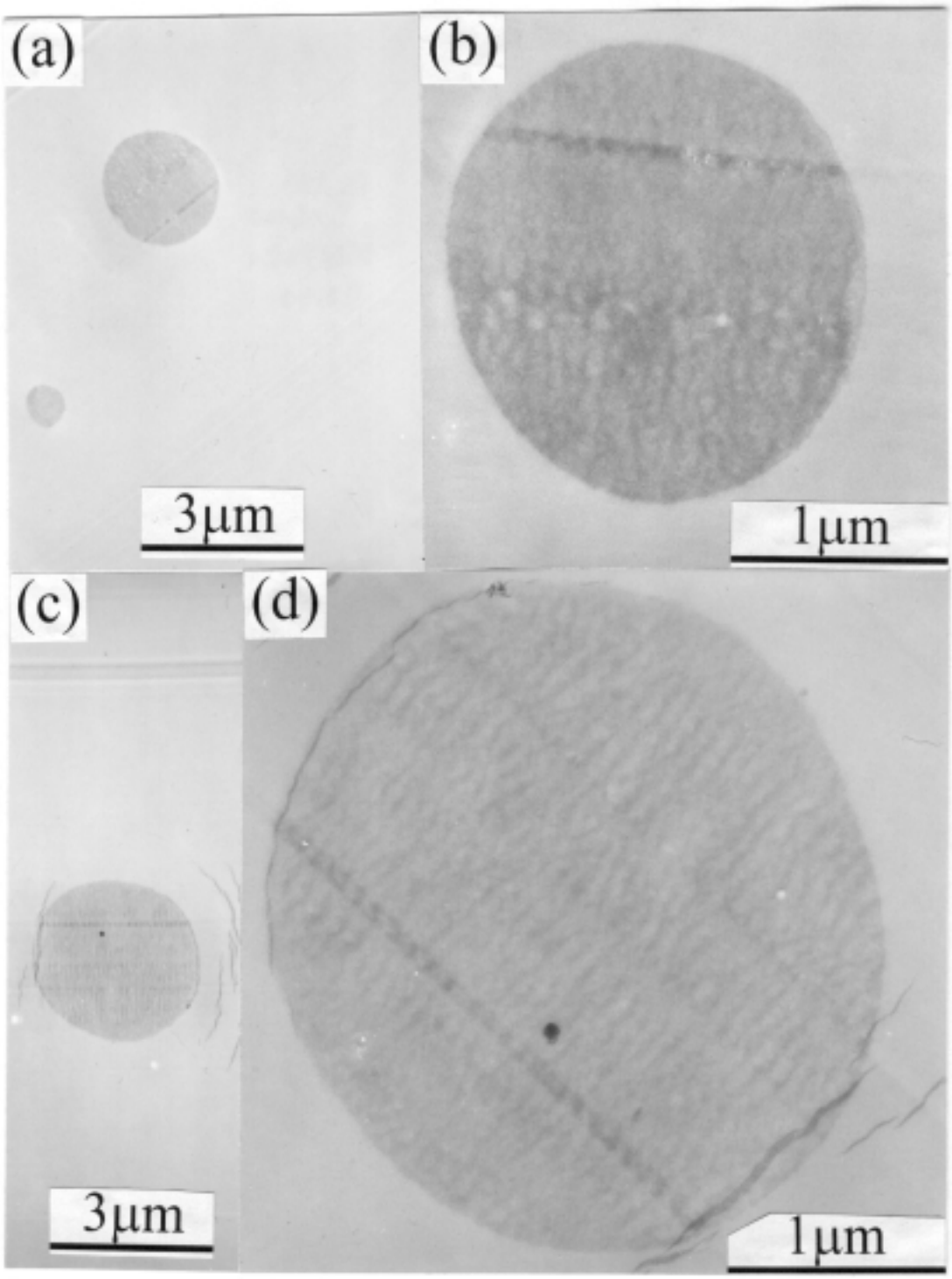

Figure 4.7 TEM micrographs of (1) VE/POSS-**1** 90/10 ((a)×9,000 and (b)×36,000) and (2) VE/POSS-**1** 85/15 ((c)×9,000 and (d)×36,000) nanocomposites

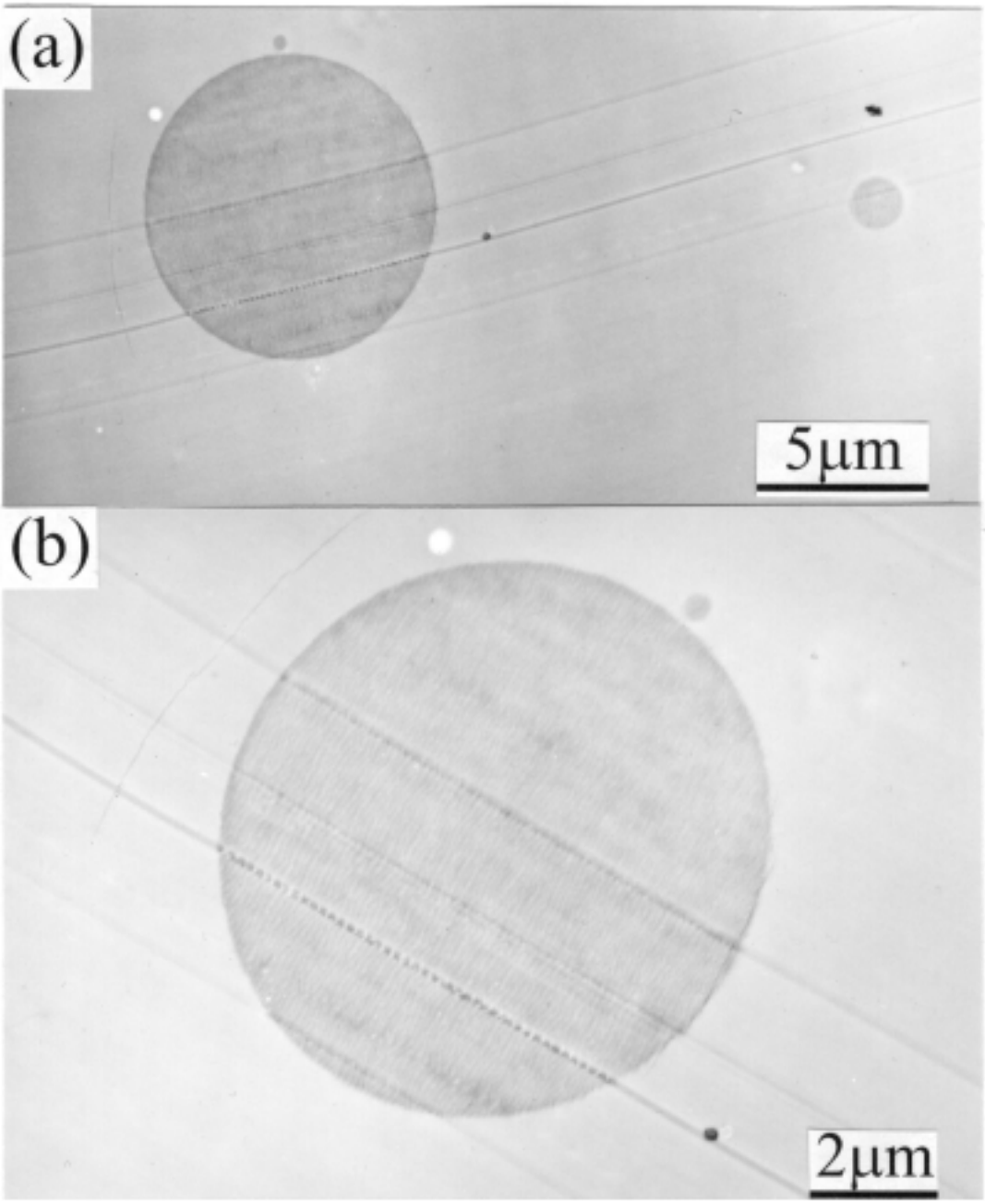

Figure 4.8 TEM micrographs of VE/POSS-**1** 80/20 nanocomposite ((a)×4,860 and (b)×9,000)

In contrast to the VE/POSS-**1** nanocomposites, TEM micrographs of both VE/POSS-**2** 97/3 and 95/5 nanocomposites reveal the presence of several POSS-rich particles (Figure 4.9(a) and (b)). The diameter of the biggest particle found in the 3 wt% POSS-**2** nanocomposite is 1.72 μm. Two small particles lie adjacent (one may be connected) to the biggest particle (Figure 4.9(a)). The biggest particle observed in the 5 wt% POSS-**2** nanocomposite is 1.44 μm in diameter, which is slightly smaller than that in the 3 wt% POSS-**2** nanocomposite. As the POSS-**2** content increased to 10 wt%, more POSS-rich particles per unit volume formed (Figure 4.9(c)) and their sizes increased. The largest was 4.83 μm in diameter, more than twice that of the largest particle observed in the VE/POSS-**1** 90/10 nanocomposite. Moreover, the number of particles in the VE/POSS-**2** 90/10 sample (Figure 4.9(c)) was greater than that in the former (Figure 4.7(a)). Clearly, the compatibility between VE and POSS-**1** is better than that between VE and POSS-**2**.

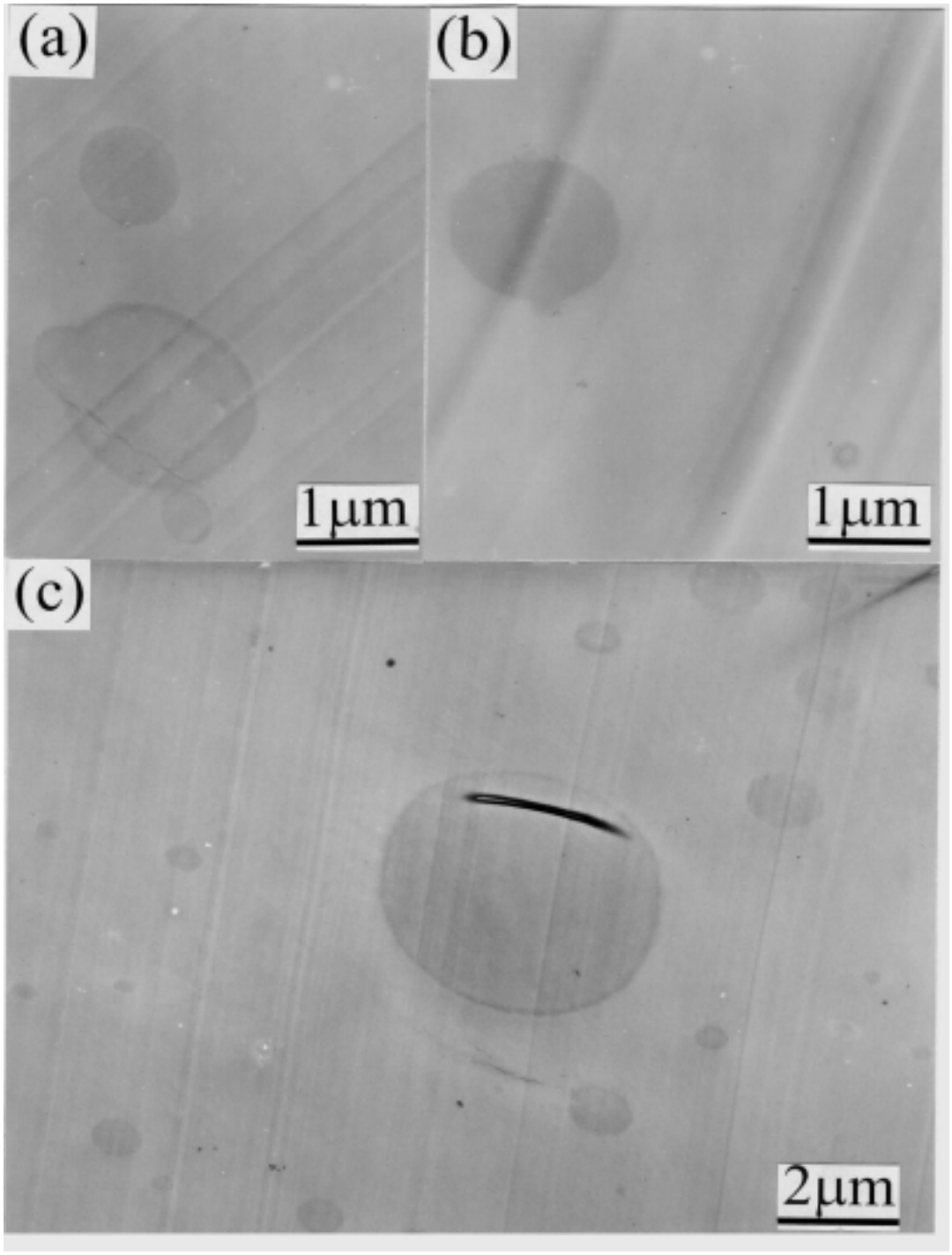

Figure 4.9 TEM micrographs of VE/POSS-**2** nanocomposites with compositions (a) 97/3 (×18,000), (b) 95/5 (×18,000) and (c) 90/10 (×9,000)

The compositions of many particles and the matrix in two VE/POSS-**1** samples (90/10 and 80/20) and one VE/POSS-**2** 90/10 sample were studied by SEM and X-EDS measurements. An SEM micrograph and several X-EDS spectra for the VE/POSS-**1** 90/10 nanocomposite are shown in Figure 4.10. POSS-**1** is the only component which contains Si-atoms. The VE contains the only Br atoms (a fire retardant component). Both VE and POSS contain C, O and H atoms. Thus, X-EDS can be employed to determine if the particles contain matrix polymer and if the matrix contains molecularly dispersed POSS-**1** polymerized into VE by examining the Si and Br elemental compositions of both phases. The big particle in the VE/POSS-**1** 90/10 sample (Figure 4.10) contains a high concentration of Si atoms (Spectrum 1), but it also shows a low Br content. This particle is composed of POSS-**1** with a small fraction of VE resin. The matrix (Spectrum 2) exhibits Si, proving that a portion of the POSS-**1** is incorporated into the continuous phase. The small particle (Spectrum 3) contains substantial Br, showing that this particle has a significant VE resin content. Thus, the particles in the VE/POSS-**1** nanocomposites are composed of both POSS and VE components which are chemically bonded in a crosslinked assembly having a higher POSS-**1** concentration than that in the continuous matrix. Studies of several particles showed different particles contained different fractions of incorporated VE matrix suggesting they phase-separated at different times during cure.

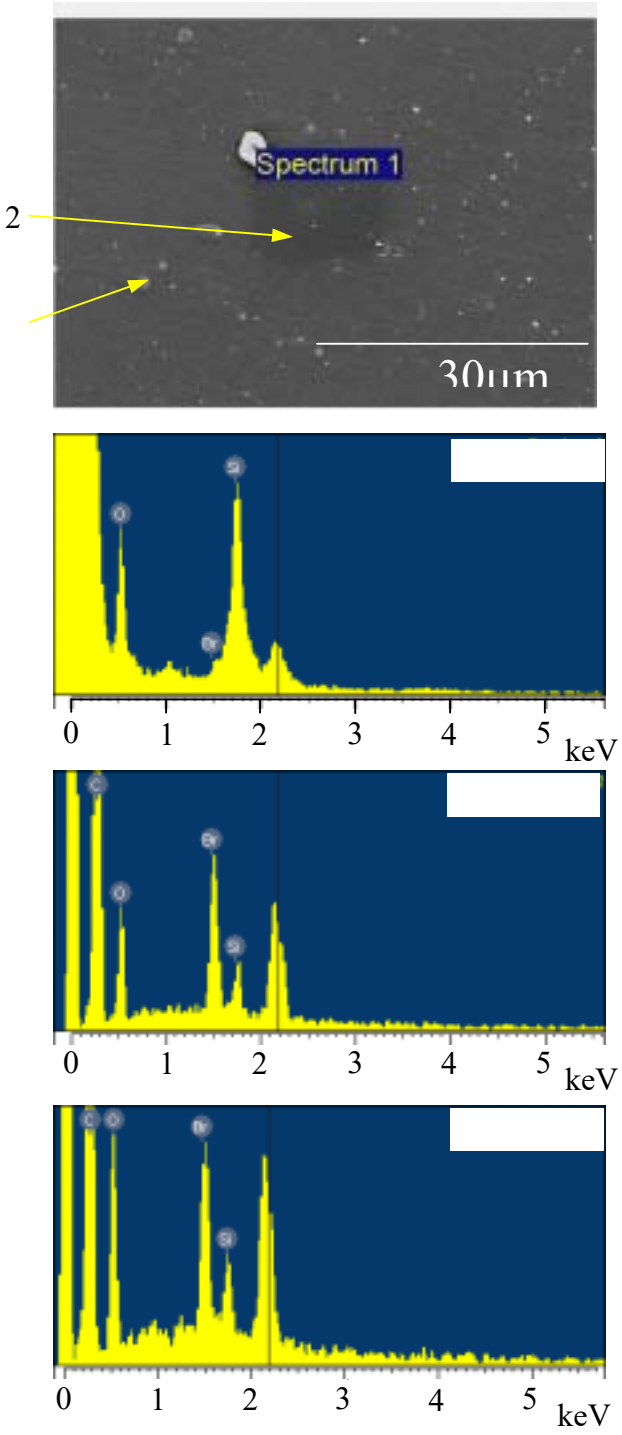

Figure 4.10 An SEM micrograph and X-ray EDS spectra of the VE/POSS-**1** 90/10 nanocomposite. The X-EDX spectra are shown at three locations (spectrum 1 for the big particle, spectrum 2 for the matrix and spectrum 3 for the small particle. These are located in the SEM by arrows.)

The volume fraction of the matrix is far larger than the particle volume fraction. There is a considerable concentration of POSS-**1** distributed throughout the matrix phase as demonstrated in spectrum 2 (Figure 4.10) and in many other matrix locations sampled. Thus, a lot of POSS-**1** was present overall in this matrix phase (all POSS-**1** is in the matrix in the 1, 3 and 5 wt% POSS-**1** samples). Clearly, some POSS-**1** units have aggregated into POSS-rich particles and other POSS-**1** is molecularly dispersed in the continuous phase for the 10, 15 and 20 wt% POSS-**1** samples.

A higher Si concentration exists in the continuous matrix phase of the 20 wt% POSS-**1** composite (Figure 4.11) than is found in the 10 wt% POSS-**1** composite (Figure 3.9). The Si/C atom ratio of 1/86 in the VE/POSS-**1** 90/10 sample's matrix increases to 1/39 in the 80/20 sample's matrix. Thus, the concentration of molecularly dispersed POSS units increases with POSS loading. The X-EDS spectrum indicates a lot of VE is present in the large particle of this 80/20 nanocomposite (Figure 4.11). The large concentration of VE components present in this particle and variation of VE contents observed in several particles show that the phase separation process is very complex. It occurs during certain portions of the curing reaction. A simple solubility limit is not reached where phase separation takes place to form two phases, each having a specific composition. Instead, VE and POSS-**1** polymerize into branched macromolecules and these go on to gel and further polymerize. During this process, POSS solubility decreases, promoting phase separation. POSS moieties incorporated into VE/POSS macromolecules may also aggregate among themselves and with any remaining unpolymerized POSS. As the degree of polymerization increases, POSS mobility steadily decreases. This slows the

aggregation/phase-separation process. Further chain crosslinking and propagation incorporates unpolymerized POSS, present in the separated aggregates or particles, into crosslinked networks within particles. This very complex process takes place with continually changing monomers compositions (monomer drift), changing macromolecular compositions, hyperbranching, gelation and a continuing increase in viscosity.

Similar observations were made with the VE/POSS-**2** composites. SEM micrographs and X-ray EDS spectra (such as that shown in Figure 4.12) for the VE/POSS-**2** 90/10 nanocomposite confirm that phase-separated POSS-rich particles contain some VE resin. Furthermore, POSS-**2** macromers are also molecularly dispersed in the continuous matrix. POSS-**2** (Si/C atom/atom = 2/9) has a higher Si concentration than POSS-**1** (Si/C atom/atom = 2/14). However, the Si/C ratio in the VE/POSS-**2** 90/10 sample's matrix averages 1/91. This value means fewer moles of POSS-**2** are present per unit volume of the matrix than that of the VE/POSS-**1** 90/10 nanocomposite which had a Si/C ratio of 1/86. Thus, the molar concentration of POSS-**1** in the matrix phase is about 1.5 times higher than that of POSS-**2** in the respective 10wt% POSS samples. This demonstrates, in accord with the TEM results, that POSS-**1**/VE miscibility is better than that of POSS-**2**/VE.

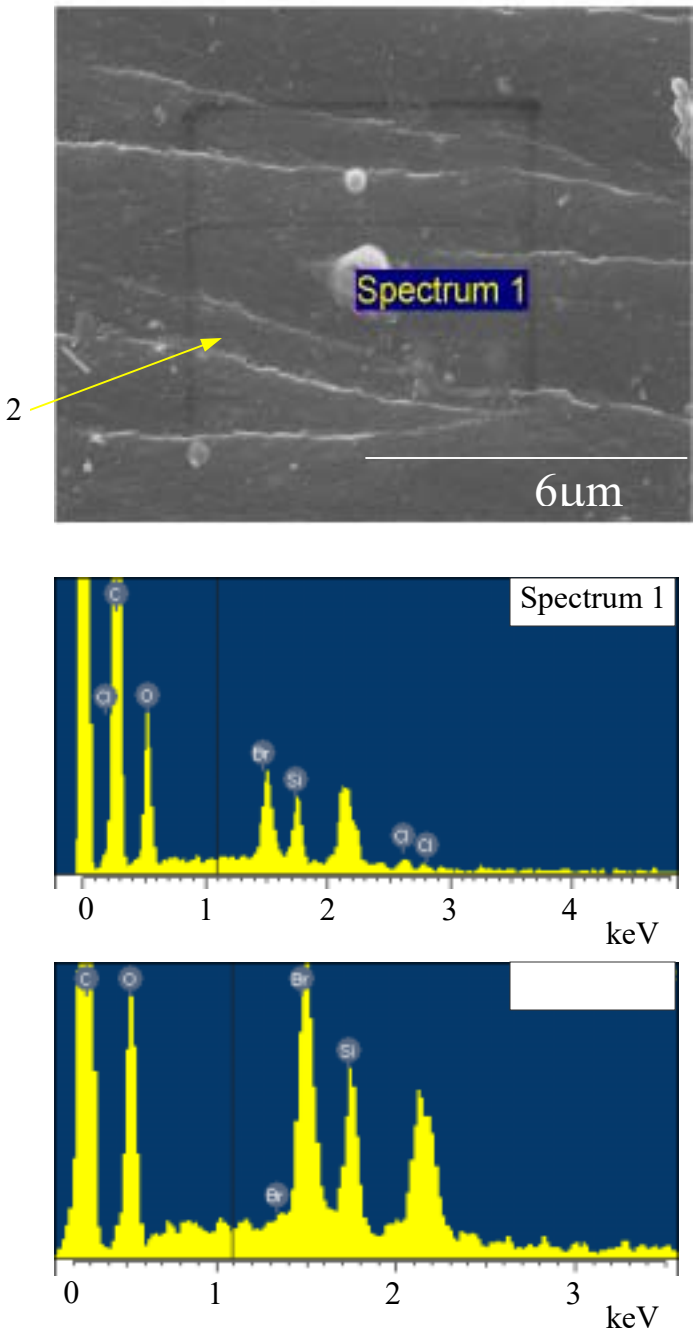

Figure 4.11 An SEM micrograph and X-ray EDS spectra of the VE/POSS-**1** 80/20 nanocomposite. The X-EDS spectra are shown at two locations (spectrum 1 for the particle and spectrum 2 for the matrix)

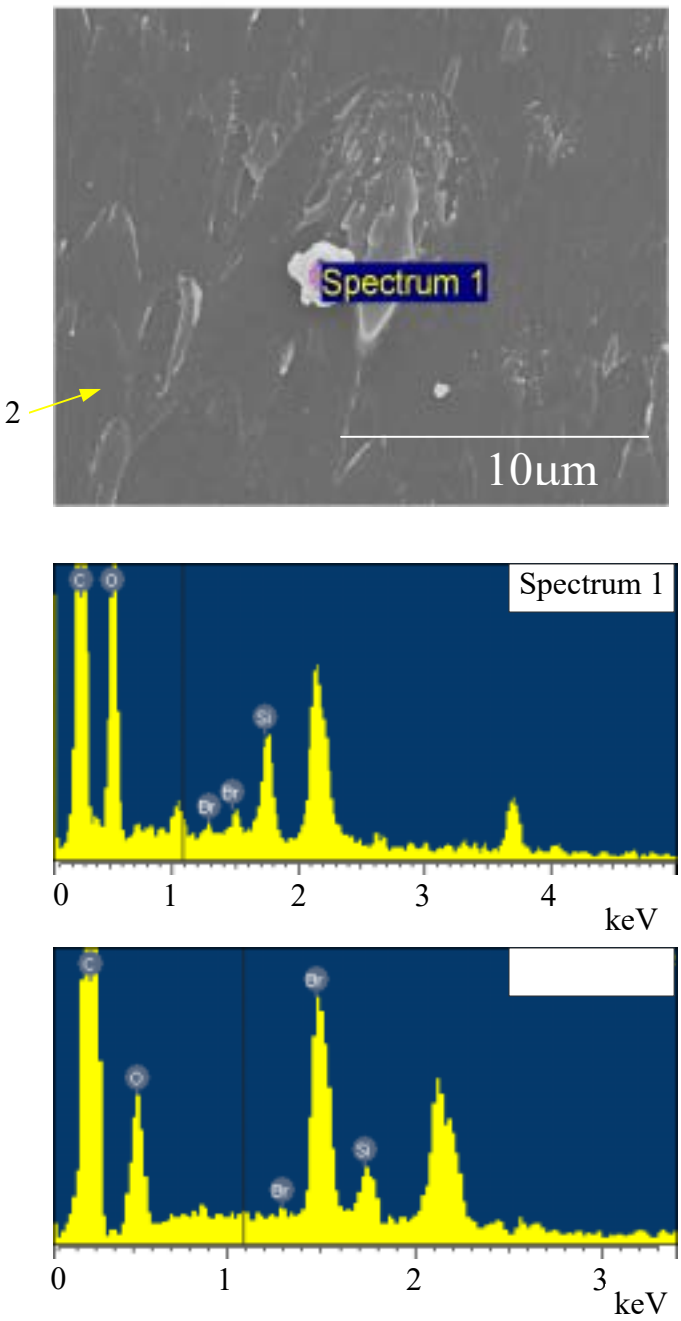

Figure 4.12 An SEM micrograph and X-ray EDS spectra of the VE/POSS-**2** 90/10 nanocomposite. The X-EDS spectra are shown at two locations (spectrum 1 for the particle and spectrum 2 for the matrix)

Conclusions

Two multifunctional methacryloxy-substituted POSS macromers, POSS-**1** and POSS-**2**, were incorporated into VE networks by radical-initiated copolymerization. The VE/POSS-**1** nanocomposites with 1, 3, 5, 10, 15 and 20 wt% POSS exhibit progressively higher T_g and E' values (in the rubbery region) than those of the neat VE resin. Their T_g values and the E' values at $T>T_g$ increase regularly with an increase in POSS-**1** content. The incorporation of the POSS-**1** mixture of T_8, T_{10} and T_{12} cages into the VE network improved greatly its thermal dimensional stability, especially at high POSS content (20wt%). The greater structural flexibility of the corner substituents, induced by the additional dimethylsiloxyl group in POSS-**2**, led to a decrease in T_g values of the VE/POSS-**2** nanocomposites. The VE/POSS-**2** nanocomposites also exhibited higher E' values at $T>T_g$ versus the neat VE resin. However, the E' values of the POSS-**2** nanocomposites in the rubbery region were lower than those of the POSS-**1** nanocomposites of the corresponding POSS composition. Both the structure of the corner substituent on the POSS macromers and the concentration of POSS, which remains molecularly dispersed during the entire curing process, control the viscoelastic properties of thermoset VE/POSS nanocomposites. The VE/POSS-**1** nanocomposites exhibit higher bulk densities than those of the POSS-**2** nanocomposites, perhaps because they may have a higher crosslinking density per unit volume due to the 10 and 12 methacryloxy functions present on the T_{10} and T_{12} cages, respectively. Perhaps the presence of T_{10} and T_{12} cages alone may increase the bulk density relative to the same amount of T_8 cages. The lower substituent flexibility and the higher crosslink density both assist in reducing

solvent swelling in the VE/POSS-**1** versus VE/POSS-**2** nanocomposites. Also, the POSS-**1** systems only show phase separation at ≥10 wt% POSS content while phase separation begins at 3 wt% for POSS-**2** systems. The POSS-**1** molar concentration in the matrix phase is approximately 1.5 times greater than the POSS-**2** concentration in the respective 90/10 samples. Thus, more crosslinking within the continuous resin phase is due to the POSS hubs in the POSS-**1** versus POSS-**2** systems.

Addition of only 1 or 3 wt% of either POSS system sharply increases the solvent resistance. No POSS-containing linear copolymers were extracted from either the POSS-**1** or the POSS-**2** vinyl ester nanocomposites using either toluene or THF. This confirms that the POSS macromers were quantitatively incorporated into the crosslinked network by copolymerization. No POSS particles are observed by TEM for the POSS-**1** nanocomposites containing a small amount of POSS (≤5 wt%). A few POSS-rich particles with diameters ranging from 20nm to several microns were scattered throughout the VE/POSS-**1** 90/10, 85/15 and 80/20 nanocomposites. A majority of the POSS-**1** macromers are dispersed in the continuous matrix phase on the molecular scale in the 10-20 wt% POSS samples. Several POSS-rich particles are detected in the VE/POSS-**2** 97/3 and 95/5 nanocomposites and many particles formed in the 10 wt% POSS-**2** nanocomposites. The molecularly dispersed POSS concentrations in the continuous matrix for the VE/POSS-**2** nanocomposites are lower than that for the corresponding VE/POSS-**1** nanocomposites. This difference probably influences the mechanical properties. The compatibility between VE and POSS-**1** is better than that between VE and POSS-**2**.

References

[1] Nalwa, S.H. Editor, *Handbook of Organic-Inorganic Hybrid Materials and Nanocomposites, Volume 1*, American Scientific Publishers, Stevenson Ranch, Calif., 2003, 382.

[2] Mark, J.E., Lee, C.Y-C., Bianconi, P.A., Editors, *Hybrid Organic-Inorganic Composites*, ACS, Washington, D.C., 1995, 378.

[3] Sanchez, C., de Soler-lllia, G.J., Ribot, F., Lalot, T., Mayer, C.R., Cabuil, V., *Chem. Mater.*, 2001, 13, 3061.

[4] Pyun, J., Matyjaszewski, K., *Chem.Mater.*, 2001, 13(10), 3436.

[5] Gill, I., *Chem. Mater.*, 2001, 13, 3404.

[5] Sanchez, C., Lebeau, B., *MRS Bull.*, 2001, 26, 377.

[6] Gangopadhyay, R., De, A., *Chem. Mater.*, 2000, 12, 2064.

[7] LeBaron, P.C., Wang, Z., Pinnavaia, T., *J. Appl. Clay Sci.*, 1999, 15, 11.

[8] Huang, Q.R., Kim, H., Huang, E., Mecerreyes, D., Hedrick, J.L., Volksen, W., Frank, C.W., Miller, R.D., *Macromolecules*, 2003, 36, 7661.

[9] Lee, K.M., Han C.D., *Macromolecules*, 2003, 36, 7165.

[10] Kim, J., Lee, S., *Polym. Mater. Sci. Eng.*, 2003, 89, 474.

[11] Ren, J., Krishnamoorti, R., *Macromolecules*, 2003, 36.

[12] Chiang, C., Ma, C.M., Wu, D., Kuan, H., *J. Polym. Sci., Part A: Polym. Chem.*, 2003, 41, 905.

[13] Ogoshi, T., Chujo, Y., *Macromolecules*, 2003, 36, 654.

[14] Lee, S., Kim, J., *Polym. Mater. Sci. Eng.*, 2002, 87, 300.

[15] Bharadwaj, R.K., *Macromolecules*, 2001, 34, 9189.

[16] Trimmel, G., Gross, S., Kickelbick, G., Schubert, U., *Appl. Organometal. Chem*., 2001, 15, 401.

[17] Lichtenhan, J. D., Otonari, Y. A., Carr, M. J., *Macromolecules* 1995, *28*, 8435.

[18] Haddad, T. S., Lichtenhan, J. D., *Macromolecules*, 1996, *29*, 7302.

[19] Romo-Uribe, A., Mather, P. T., Haddad, T. S., Lichtenhan, J. D., *J. Polym. Sci., Part B: Polym. Phys*., 1998, *36*, 1857.

[20] Lee, A., Lichtenhan, J. D., *Macromolecules*, 1998, *31*, 4970.

[21] Mather, P. T., Jeon, H. G., Romo-Uribe, A., Haddad, T. S., Lichtenhan, J. D., *Macromolecules*, 1999, *32*, 1194.

[22] Lee, A., Lichtenhan, J. D., *J. Appl. Polym. Sci.*, 1999, *73*, 1993.

[23] Jeon, H. G., Mather, P. T., Haddad, T. S., *Polym. Int.*, 2000, *49*, 453.

[24] Fu, B. X., Hsiao, B. S., White, H., Rafailovich, M., Mather, P. T., Jeon, P. T., Jeon, H. G., Phillips, S., Lichtenhan, J., Schwab, J., *Polym. Int.*, 2000, *49*, 437.

[25] Ellsworth, M. W., Gin, D. L., *Polym. News*, 1999, *24*, 331.

[26] Lichtenhan, J. D., Schwab, J. J., Reinerth, W. A. Sr., *Chemical Innovation*, 2001, 1, 3.

[27] Li, G. Z., Wang, L., Ni, H., Pittman, Jr. C.U., *J. Inorg. and Organometalic Polym.*, 2001, *11*, 123.

[28] Haddad, T. S., Stapleton, R., Jeon, H. G., Mather, P. T., Lichtenhan, J. D., Phillips, S., *Polym. Preprints, (ACS Div. Polymer Chem.)*, 1999, *40*, 496.

[29] Blanski, R. L., Phillips, S. H., Lee, A., *Polym. Preprints, (ACS Div. Polymer Chem.)*, 2001, *42*, 173.

[30] Bharadwaj, B. K., Berry, R. J., Farmer, B. L., *Polymer*, 2000, *41*, 7209.

[31] Tsuchida, A., Bolln, C., Sernetz, F. G., Frey, H., Mulhaupt, R., *Macromolecules*, 1997, *30*, 2818.

[32] Haddad, T. S., Lee, A., Phillips, S. H., *Polym. Preprints, (ACS Div. Polymer Chem.)*, 2001, *42*, 88.

[33] Li, G.Z., Wang, L., Toghiani, H., Daulton, T.L., Koyama K., Pittman Jr C.U., *Macromolecules*, 2001, *34*, 8686.

[34] Li,G.Z., Wang, L., Toghiani, H., Pittman Jr. C.U., Daulton T.L., *Polymer*, 2002, *43*, 4167.

[35] Lee, A., *POSS™ Nanotechnology Conference,* Sept. 25-27, Huntington Beach, CA., 2002. (see website <poss.emedix.org>)

[36] Choi, J., J. Harcup, J., Yee, A. F., Zhu, Q., Laine, R. M., *J. Am. Chem. Soc*., 2001, *123*, 11420.

[37] Laine, R. M., *POSS™ Nanotechnology Conference*, Sept.25-27, Huntington Beach, CA., 2002. (see website <poss.emedix.org>)

[38] Haddad, T. S., Viers, B. D., Phillips, S. H., *J. Inorg. and Organometallic Polym.*, 2001, *11*, 155.

CHAPTER V

PHENOLIC RESIN / POSS INORGANIC-ORGANIC HYBRID NANOCOMPOSITES: SYNTHESIS AND VISCOELASTIC PROPERTIES

Introduction

Inorganic-organic hybrid nanocomposites based on polymers are a relatively new class of materials with ultrafine phase dimensions typically in the range of 1-100 nm [1-3]. These nanocomposites often exhibit unexpectedly improved properties when compared to their micro- and macrocomposite analogs or to the pristine parent polymer matrix [1]. The development of polymer-inorganic hybrid nanocomposites has attracted significant attention in the past few years [1-5] and extensive reviews are available [4]. Phenolic resins are commercially important thermoset resins, widely employed in a huge variety of applications [6]. Recently, phenolic resin/silica hybrid composites prepared by the sol-gel method [7], and phenolic resin/clay nanocomposites [8-10] have been studied. Mechanical properties and thermal stabilities of these systems have been improved.

The silica phases generated by the sol-gel method and well-dispersed clay tactoids and platelets have dimensions that are much larger than the $[SiO_{1.5}]_n$ (n=8, 10, 12) cages of polyhedral oligomeric silsesquioxane (POSS) chemicals. The dispersed silica or clay

phases improve this flammability resistance of phenolic resins by promoting char formation and inhibiting gas transport through the material. Molecular dispersion of POSS macromers will create a far larger surface contact area between the phenolic (organic) and inorganic phases than the equivalent weight fraction of either silica particles or "nanoclays". Therefore, modification of phenolic resins by incorporating POSS derivatives is of great interest.

POSS chemicals are typically from 1 to 3nm in diameter. Their $(SiO_{1.5})_n$ inorganic cage framework, composed of silicon and oxygen, is externally covered (and solublized) by organic substituents. One or more of these substituents can contain reactive functional groups, which can be employed to copolymerize the POSS species with other common monomers. Furthermore, these corner substituents on the silicon atoms of POSS can make the nanostructured molecules compatible with polymers or monomers, offering a unique opportunity for preparing hybrid organic-inorganic nanocomposites with the inorganic phase truly molecularly dispersed within the matrix [11-12]. The development of organic-inorganic hybrid POSS nanocomposites has been accelerated in the past a few years [11-12].

Incorporation of POSS cages into polymeric materials via copolymerization, grafting or blending often results in dramatic property improvements, including increases in use temperature, oxidation resistance, surface hardening and improved mechanical properties, as well as reductions in flammability and heat evolution. These enhancements have been reported for a wide range of thermoplastic and some thermoset systems, i.e.,

methacrylates [13], styrenes [14-15], norbornenes [17, 22] ethylenes [23], siloxanes [24], epoxides [16, 25], and vinyl esters [26].

Three functional POSS macromers and one nonfunctional POSS were incorporated into a commercial phenolic resin (Hitco 134A) in this dissertation. The viscoelastic properties of these nanocomposites were determined by dynamic mechanical thermal analysis (DMTA). How the organic substituents on POSS influence the viscoelastic properties of these nanocomposites was also investigated.

Experimental

Specimen Preparation

Dichloromethylsilylethyl heptaisobutyl-POSS (POSS-**1**, MW: 958.56 g/mol), trisilanol heptaphenyl-POSS (POSS-**2**, MW: 931.34 g/mol), uncured poly(phenylsilsesquioxane) (POSS-**3**, MW: variable), and octaisobutyl-POSS (POSS-**4**, Mw: 873.60 g/mol) were purchased from Hybrid^{TM} Plastics Co. All four POSS derivatives could dissolve in tetrahydrofuran (THF). The commercial phenolic resole resin, Hitco 134A, containing about 30 wt% isopropanol, was purchased from Ashland Specialty Chemical Co.

Specified amounts of each POSS were dissolved in THF, producing transparent 5wt% POSS in THF solutions. Each POSS solution was added to the phenolic resin to produce resin/POSS weight ratios of 99/1, 97/3, 95/5, or 90/10 as transparent solutions. These solutions were put into trays and the solvent was removed in a vacuum oven (500-600mmHg) at low temperature (≤70 °C). The resulting viscous mixtures were

refrigerated and frozen into solids. Each solid was broken and ground into powder. These powders were press-cured in aluminum molds under a pressure of 3.5MPa (508 psi) using the following temperature protocol: 83 °C/10-15 min, 87 °C/45 min, 149 °C/110 min, and 155 °C/180 min. The samples were post-cured at 250 °C for 2 h. Phenolic resin/POSS nanocomposites with compositions (wt/wt) of 99/1, 97/3, 95/5 and 90/10 were prepared for POSS-**1** and **2**. Phenolic resin/POSS-**3** nanocomposites with compositions of 99/1, 97/3 and 95/5 were made. POSS-**4** without functional groups dissolved in THF and a transparent solution was obtained. This solution was then added to the phenolic resin and made a translucent mixture. After removal of solvent in a vacuum oven, a translucent viscous mixture was obtained. POSS-**4**/phenolic resin blend samples with weight ratios of 99/1, 97/3, 95/5 and 90/10 were prepared by using the same curing conditions with those for POSS-**1**, **2** and **3** nanocomposites. A pure phenolic resin control sample was also produced by the same protocol as those used for the POSS nanocomposites.

Measurements

The dynamic storage modulus, E', and loss factor (tanδ) were determined in the dual-level bending mode using a Polymer Laboratories DMTA MK3 instrument. Small amplitude bending oscillations (both 1 and 10 Hz) were used at a gap setting of 8.00 mm. Measurements were carried out from 35 °C to 270-300 °C at a heating rate of 2 °C/min. The nanocomposite sample sizes were used 1.7-3.4 mm thick, 5.5-7.1 mm wide and 38 mm long.

Phenolic resin and phenolic resin/POSS nanocomposite densities were measured using an Electronic Densimeter (ED-120T) at 25 °C.

Specimens of every phenolic resin/POSS nanocomposite (0.67~1.48 g) were immersed into THF at room temperature for 42 days. Only the 10 wt% POSS-**4** composite sample exhibited many cracks on its surface. The other nanocomposite samples and pure phenolic resin exhibited little weight increase due to solvent swelling after 42 days of immersion in THF. Very small amounts of linear copolymers were extracted into these THF solutions. After coating onto KBr plates and removal of solvent, IR spectra were obtained on an FT-IR instrument (MIDAC Corporation). The residues of phenolic resin and its POSS nanocomposites after extraction were also examined by FT-IR.

A JEM-100 CXII transmission electron microscope (TEM) (JEOL USA Inc.) was used to characterize morphology of the selected POSS-**1, 2** and **3** nanocomposites and POSS-**4**/phenolic resin blend. This TEM was operated at 60 KV. Specimens for this measurement were microtomed to 70-90 nm thicknesses and set on copper grid.

Results and Discussion

Synthesis of the Nanocomposites

The chemical structures of four POSS chemicals are shown in Figure 5.1. The phenolic resin/POSS-**1,** phenolic resin/POSS-**2** and phenolic resin/POSS-**3** nanocomposites were prepared by condensation polymerization. No reactive functional groups are present in POSS-**4**. POSS-**4** was blended into the phenolic resin. Synthesis of

the phenolic resin/POSS-**1** nanocomposites is represented in Figure 5.2. The chemical incorporation of POSS-**1** into the phenolic resin was completed by condensation between hydroxyl groups in the uncured phenolic resin and Si–Cl groups attached to POSS-**1** substituent. POSS-**2** and POSS-**3** contain Si-OH functional groups. These groups cannot react as quickly at mild condition with methylol or phenolic hydroxyl groups as the R-$SiMeCl_2$ groups in POSS-**1** can. Thus, the entire sequence of reactions during curing between the phenolic resin and POSS derivatives **2** or **3** would be different from that of POSS-**1** and the phenolic resin (Figure 5.2). Figure 5.3 shows the synthesis of the phenolic resin/POSS-**2** nanocomposite. The reaction chemistry between the Si-OH functions of POSS-**3** and the phenolic resin will be essentially the same as that which occurred between POSS-**2** and the phenolic resin. So, a structural equation for the synthesis of phenolic resin/POSS-**3** nanocomposites is not given. Because POSS-**2** or **3** were well dispersed in the viscous uncured phenolic resin, it was very difficult for POSS macromers to make a contact with each other. Thus, it would be very difficult for these POSS macromers to react with themselves. Trisilanolheptaphenyl POSS-**2** is expected to react with the phenolic and methylol hydroxyl groups to split out water, but the relative rates among these possibilities is not known.

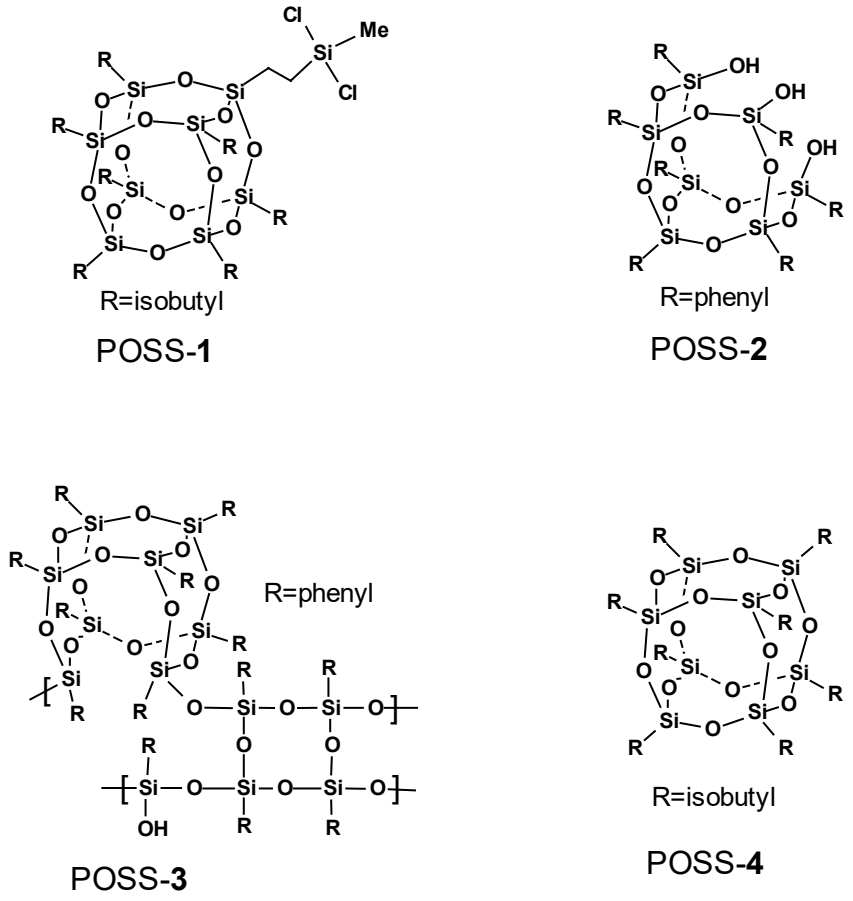

Figure 5.1 Chemical structures of the four POSS derivatives

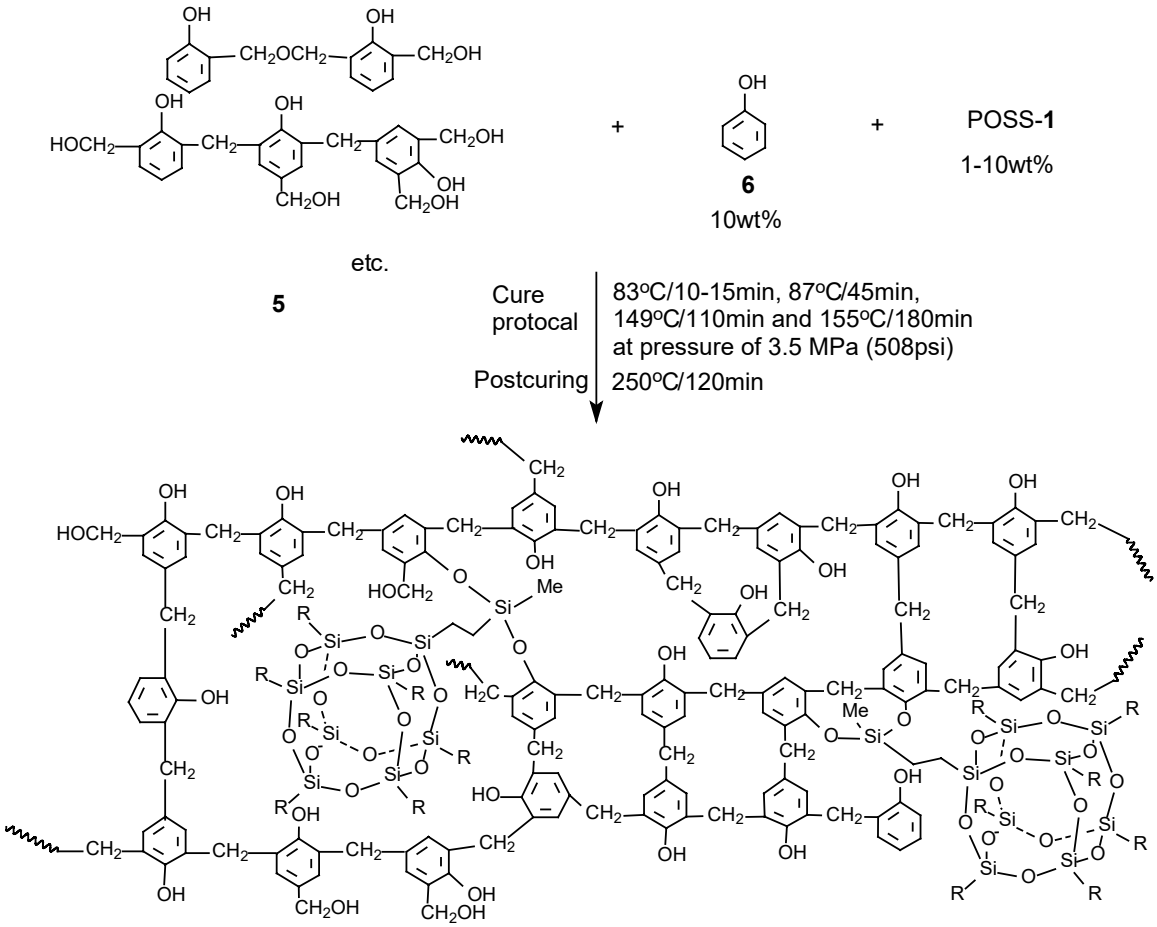

Figure 5.2 Synthesis of phenolic resin/POSS-**1** nanocomposites

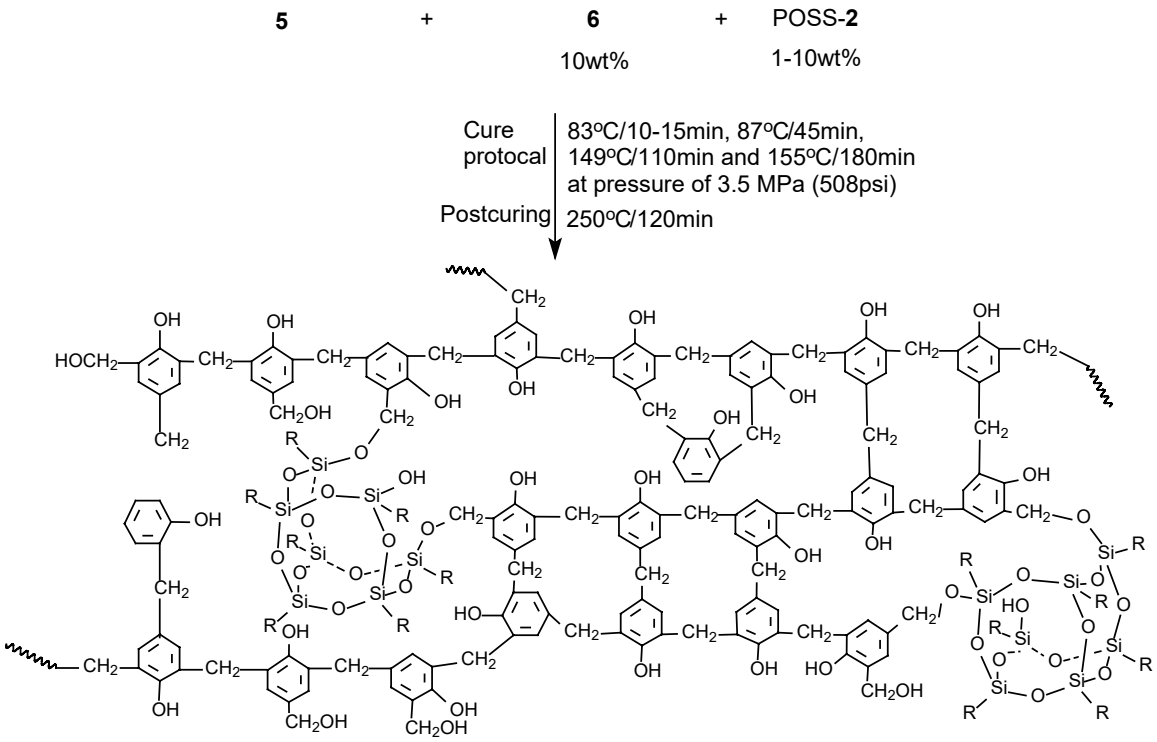

Figure 5.3 Synthesis of phenolic resin/POSS-**2** nanocomposites

Viscoelastic Properties of Phenolic Resin/POSS Nanocomposites

The bending storage moduli, E', versus temperature curves at 1 Hz (from DMTA) for the neat phenolic resin and the phenolic resin/POSS-**1** nanocomposites are given in Figure 5.4. The E' values of all phenolic resin/POSS-**1** nanocomposites are higher than those of the neat phenolic resin in the rubbery region ($T>T_g$). Furthermore, these E' values increase almost linearly with an increase in POSS loading. The E' values of the 1, 3 and 5 wt% POSS-**1** nanocomposites are higher than those of the neat phenolic resin in the glassy region ($T<T_g$), but the 10 wt% POSS-**1** nanocomposite exhibits similar E' values to those of the phenolic resin. The neat phenolic resin and the phenolic resin/POSS-**1** 99/1, 97/3, 95/5 and 90/10 nanocomposites at 40 °C exhibit E' values

(shown in Table 5.1) of 1.37 GPa, 1.68 GPa, 1.79 GPa, 2.01 GPa and 1.34 GPa, respectively. The corresponding E' values at 265 °C (>T_g) are 56.2 MPa (phenolic resin), 65.7 MPa (1 wt% POSS-**1**), 60.8 MPa (3 wt% POSS-**1**), 79.7 MPa (5 wt% POSS-**1**) and 123.5 MPa (10 wt% POSS-**1**), respectively. The E' value for the 90/10 nanocomposite is about twice that for the neat phenolic resin at 265°C. The phenolic resin/POSS-**1** nanocomposites have greater thermal dimensional stabilities than the phenolic resin and this stability increases with increasing POSS-**1** content from 3 wt% to 10 wt%.

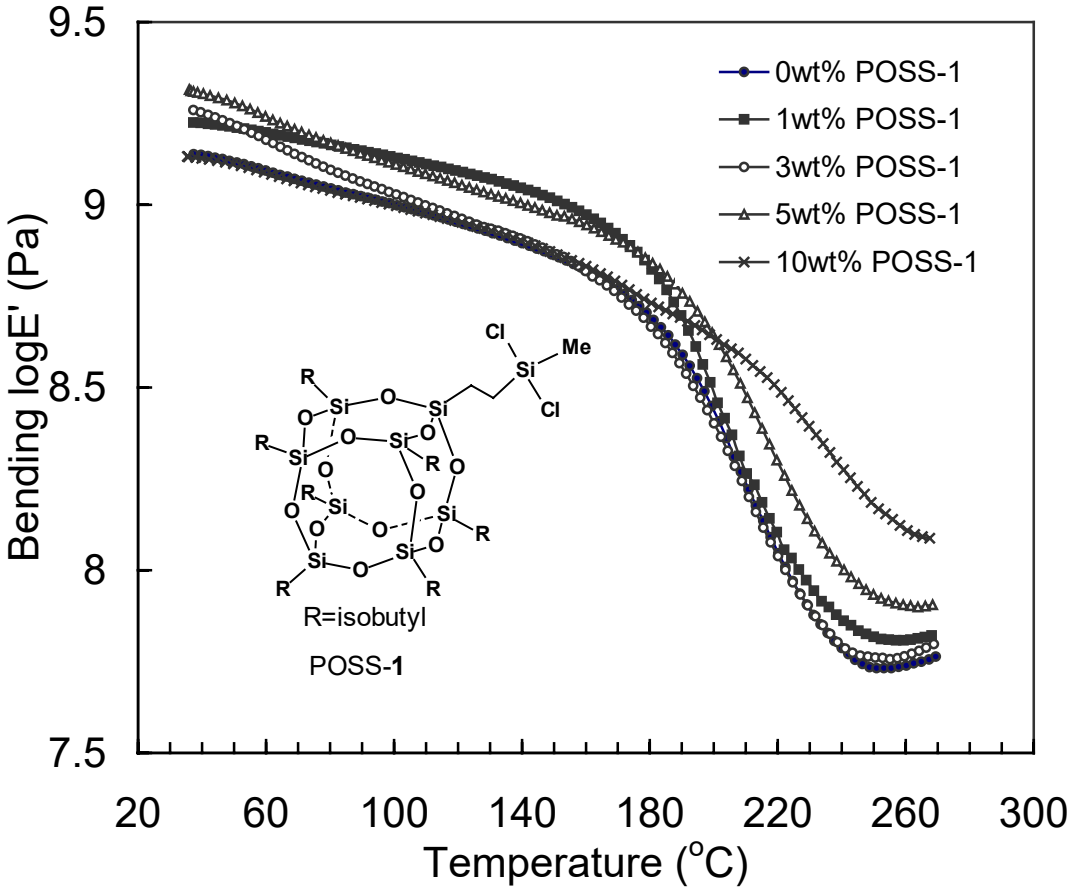

Figure 5.4 Bending E' versus temperature curves at 1 Hz for phenolic resin/POSS-**1** nanocomposites

Table 5.1 T_g, Bending Storage Moduli, Density and Percentages Extracted by THF of the Phenolic Resin Control (PR) and the Phenolic Resin (PR)/POSS-**1**, **2**, **3** and **4** Composites

Composite type	POSS (wt%)	T_g (°C)	E' at 40°C (GPa)	E' at 265°C (MPa)	Density ρ (g/cm^3)	Extraction percentage (%)
PR	0	213.2	1.37	56.2	1.195	0.94
PR/POSS-**1**	1	210.3	1.68	65.7	1.205	0.67
PR/POSS-**1**	3	211.0	1.79	60.8	1.212	0.84
PR/POSS-**1**	5	217.4	2.01	79.7	1.229	1.60
PR/POSS-**1**	10	244.9	1.34	123.5	1.221	2.60
PR/POSS-**2**	1	217.3	1.99	106.2	1.248	0.66
PR/POSS-**2**	3	213.3	2.02	89.1	1.237	0.74
PR/POSS-**2**	5	222.0	2.15	141.1	1.235	5.51
PR/POSS-**2**	10	254.4	1.54	201.0	1.215	8.37
PR/POSS-**3**	1	203.0	1.90	61.5	1.226	0.57
PR/POSS-**3**	3	224.3	1.44	70.4	1.201	0.97
PR/POSS-**3**	5	222.5	1.49	75.3	1.189	2.46
PR/POSS-**4**	1	186.5	1.72	46.6	1.248	0.54
PR/POSS-**4**	3	194.9	1.40	36.1	1.249	1.47
PR/POSS-**4**	5	196.5	1.64	54.6	1.248	5.39
PR/POSS-**4**	10	212.3	1.02	43.2	1.229	14.34

The incorporation of **1** into phenolic resin broadens the tanδ peak (1Hz) in the glass transition range and the intensities decrease with an increase in POSS-**1** loading (shown in Figure 5.5). The glass transition temperature (T_g) is defined, herein, as the tanδ peak temperature. The T_g values of the neat phenolic resin and the phenolic resin/POSS-**1** 99/1, 97/3, 9/5 and 90/10 nanocomposites are 213.2 °C, 210.3 °C, 211.0 °C, 217.4 °C and 244.9 °C, respectively. The 1 and 3 wt% POSS-**1** nanocomposites exhibit T_g values similar to that of the neat phenolic resin. T_g values increase with increasing POSS-**1** loadings. The T_g value of the 90/10 nanocomposite is about 32 °C higher than that of the neat phenolic resin.

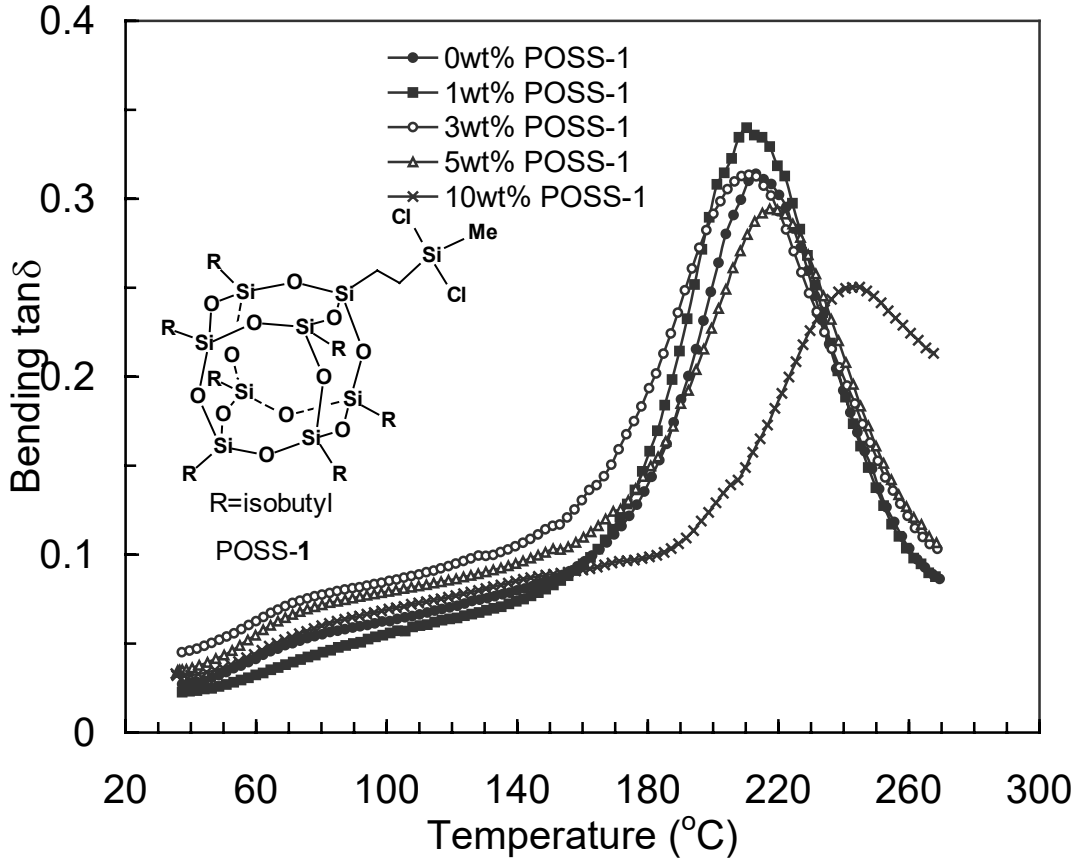

Figure 5.5 Bending tanδ versus temperature curves at 1 Hz for phenolic resin/POSS-**1** nanocomposites

The bending storage moduli, E', versus temperature curves at 1Hz (from DMTA) for the neat phenolic resin and the phenolic resin/POSS-**2** nanocomposites (1wt%, 3 wt%, 5 wt% and 10wt% of POSS-**2**) are shown in Figure 5.6. All POSS-**2** nanocomposites exhibit higher E' values than those of the neat phenolic resin in both glassy and rubbery regions. The bending storage moduli at 40 °C ($<T_g$) are 1.37 GPa (phenolic resin), 1.99 GPa (1 wt% POSS-**2**), 2.02 GPa (3 wt% POSS-**2**), 2.15 GPa (5 wt% POSS-**2**) and 1.54 GPa (10 wt% POSS-**2**), respectively. The neat phenolic resin and the phenolic/POSS-**2** 99/1, 97/3, 95/5 and 90/10 nanocomposites display E' values at 265°C ($>T_g$) of 56.2

MPa, 106.2 MPa, 89.1 MPa, 141.1 MPa and 201.0 MPa, respectively. These values increase steadily with POSS-**2** content from 3 wt% to 10 wt%. The 10 wt% POSS-**2** nanocomposite displays much higher E' values in the rubbery region than those of the neat phenolic resin and the other POSS-**2** nanocomposites (≤5 wt% POSS-**2**). Furthermore, the E' value of the 10 wt% POSS-**2** nanocomposite at 265 °C is about 3.6 times greater than the phenolic resin's at that temperature. Clearly, incorporating 10 wt% POSS-**2** into the phenolic resin greatly improves its T_g and mechanical properties.

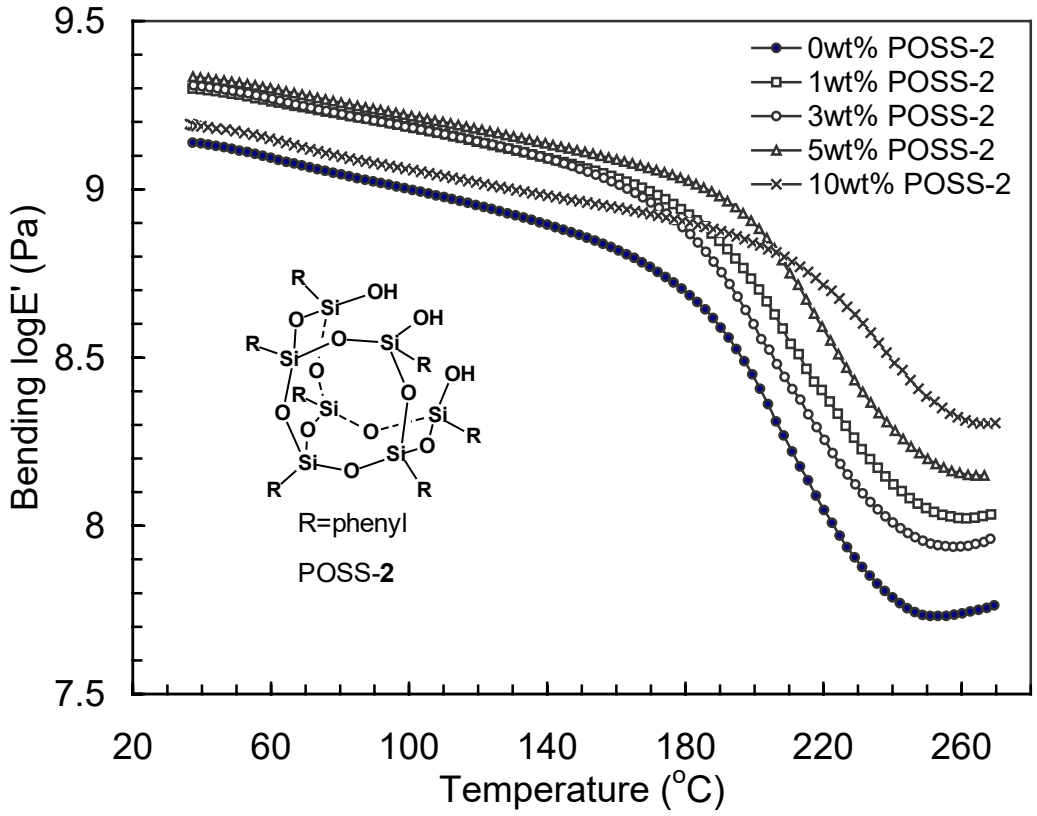

Figure 5.6 Bending E' versus temperature curves at 1 Hz for phenolic resin/POSS-**2** nanocomposites

The bending tanδ versus temperature curves (1 Hz) for the phenolic resin and its POSS-**2** nanocomposites are displayed in Figure 5.7. The 1, 5 and 10 wt% POSS-**2** nanocomposites have broader and less intense tanδ peaks in the glass transition region versus the neat phenolic resin. However, the 3 wt% POSS-**2** nanocomposite exhibits a somewhat more intense and broader tanδ peak than the neat phenolic resin. The T_g values (tanδ peak temperatures) are 213.2 °C, 217.3 °C, 213.3 °C, 222.0 °C and 254.4 °C, for the neat phenolic resin and the 1, 3, 5 and 10 wt% POSS-**2** nanocomposites, respectively. The 1 wt% POSS-**2** nanocomposite exhibits slightly higher T_g value than those of the neat phenolic resin and the 3 wt% POSS-**2** nanocomposite. The T_g values increase as POSS-**2** is incorporated into the phenolic resin from 3 to 10 wt%. Especially, the 10wt% POSS-**2** nanocomposite exhibits much higher T_g value than that of the neat phenolic resin (by 41 °C). Incorporating 10 wt% POSS-**2** into the phenolic resin sharply improves its T_g and the storage moduli in the rubbery region.

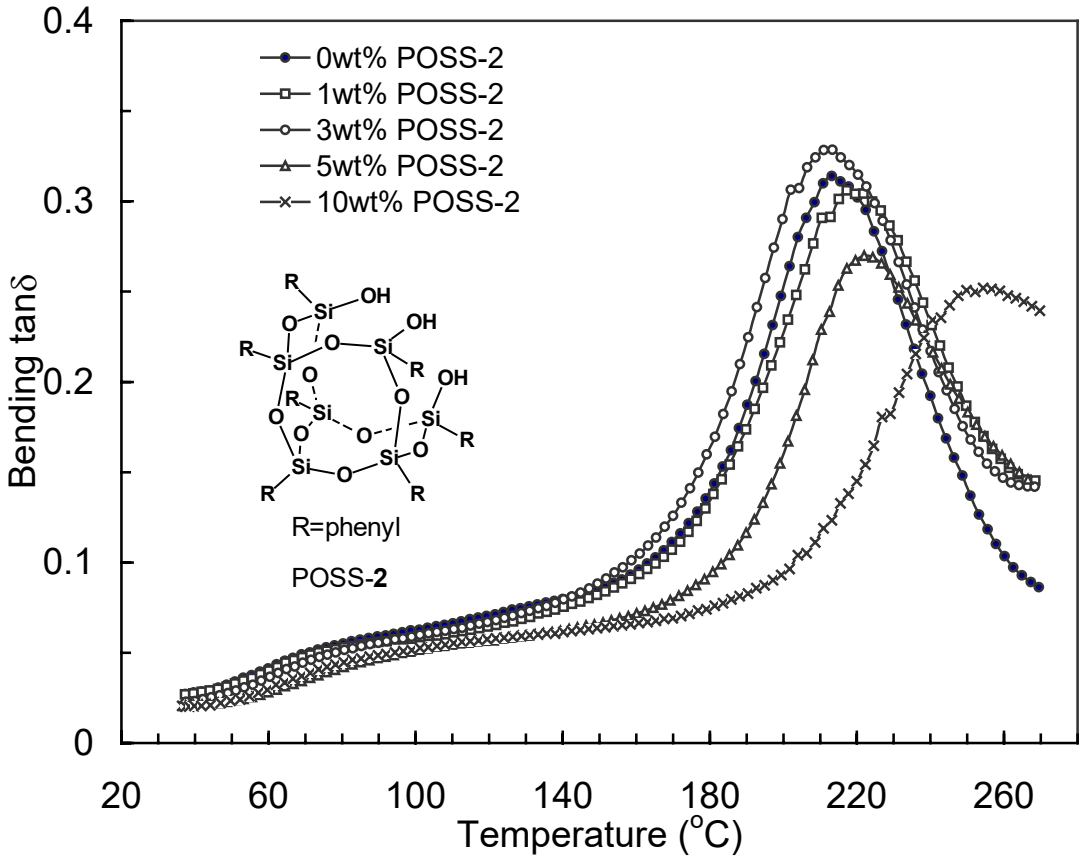

Figure 5.7 Bending tanδ versus temperature curves at 1 Hz for phenolic resin/POSS-**2** nanocomposites

All POSS-**3** nanocomposites containing 1, 3 and 5 wt% POSS have higher E' values (1 Hz) than those of the phenolic resin in the rubbery region and these values increase continuously with an increase of POSS-**3** content (Figure 5.8). For example, the E' values at 265 °C ($T>T_g$) are 56.2 MPa (phenolic resin), 61.5 MPa (1 wt% POSS-**3**), 70.4 MPa (3 wt% POSS-**3**), and 75.3 MPa (5 wt% POSS-**3**). Below T_g, the 3 and 5 wt% POSS-**3** nanocomposites exhibit E' values quite similar to those of the neat phenolic resin while the 1 wt% POSS-**3** nanocomposite has much higher E' values than those of the phenolic resin. At 40 °C, the phenolic resin and its 1, 3 and 5 wt% POSS-**3**

nanocomposites exhibit E' values of 1.37 GPa, 1.90 GPa, 1.44 GPa and 1.49 GPa, respectively. The bending tanδ curves for this POSS-**3** nanocomposite series are given in Figure 5.9. The 1 wt% POSS-**3** nanocomposite exhibits a more intense and broader tanδ peak in the glass transition region than the neat phenolic resin, while the 3 and 5 wt% POSS-**3** nanocomposites exhibit less intense and broader tanδ peaks than the neat phenolic resin. Tanδ peak intensities decreased with rising POSS-**3** contents. The T_g values (tanδ peak temperatures) are 213.2 °C (phenolic resin), 203.0 °C (1 wt% POSS-**3**), 224.3 °C (3 wt% POSS-**3**) and 222.5 °C (5 wt% POSS-**3**). While the 1 wt% POSS-**3** nanocomposite has lower T_g value than the neat phenolic resin, those of the 3 and 5 wt% POSS-**3** are about 10 °C higher. The phenolic resin's T_g and storage moduli ($T>T_g$) were improved by incorporating small amounts (3 to 5 wt%) of POSS-**3**.

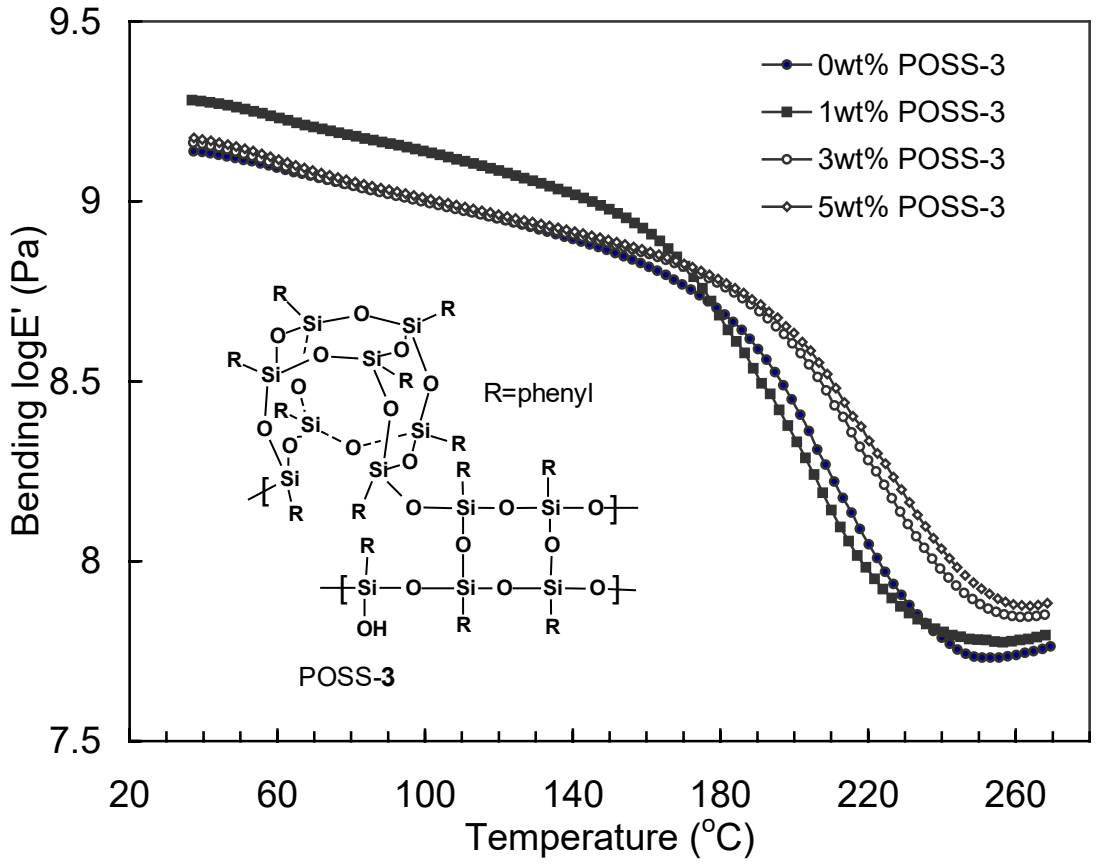

Figure 5.8 Bending E' versus temperature curves at 1 Hz for phenolic resin/POSS-**3** nanocomposites

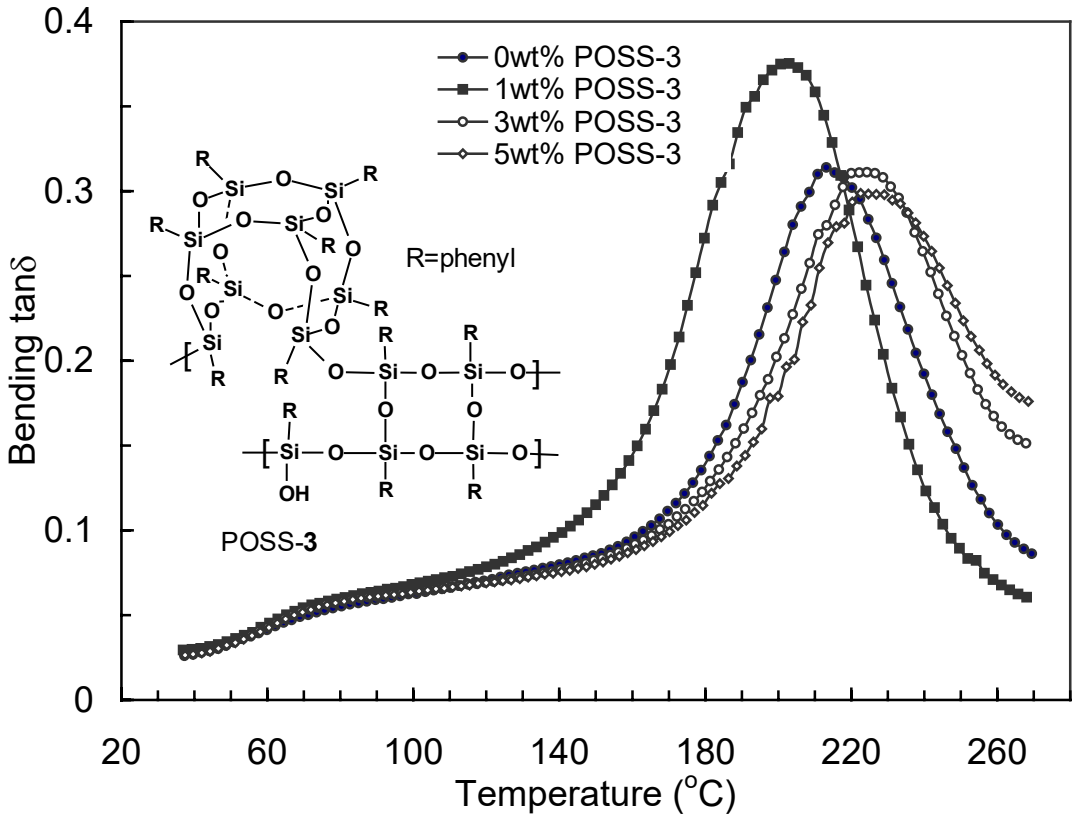

Figure 5.9 Bending tanδ versus temperature curves at 1 Hz for phenolic resin/POSS-**3** nanocomposites

Octaisobutyl POSS (POSS-**4**) has no functional groups present which can react with the phenolic resin components during the cure. Furthermore, the peripheral isobutyl group cannot form π-stacking interactions with phenyl rings of the resins. Thus, POSS-**4** was blended into the phenolic resin and cured in order to compare the effect of chemical incorporation (POSS-**1**, **2** and **3**) with the physical blending of POSS-**4** on the viscoelastic properties. The DMTA curves for 1, 3, 5 and 10 wt% POSS-**4** composites are shown in Figures 5.10 and 5.11. E' values of the 1, 3 and 5 wt% POSS-**4** composites are higher in the glassy region ($T<T_g$) than those of the neat phenolic resin (Figure 5.10), but the 10

wt% POSS-**4** composite exhibits lower E' values at $T<T_g$. At 40°C, these E' values are 1.37 GPa (neat phenolic resin) versus 1.72 GPa, 1.40 GPa, 1.64 GPa and 1.02 GPa for the 1, 3, 5 and 10 wt% POSS-**4** composites, respectively. However, in the rubbery region ($T>T_g$), all POSS-**4** composites exhibit lower bending storage moduli than the phenolic resin. The E' values of the 1, 3, 5 and 10 wt% POSS-**4** composites at 265 °C ($>T_g$) are 46.6, 36.1, 54.6 and 43.2 MPa versus 56.2 MPa for the phenolic resin. This phenomenon contrasts sharply with those observed for the phenolic/POSS-**1**, **2** and **3** nanocomposites, in which the POSS monomers possess functional groups that incorporate into the phenolic resin network by forming chemical bonds (see Figures 5.2 and 5.3).

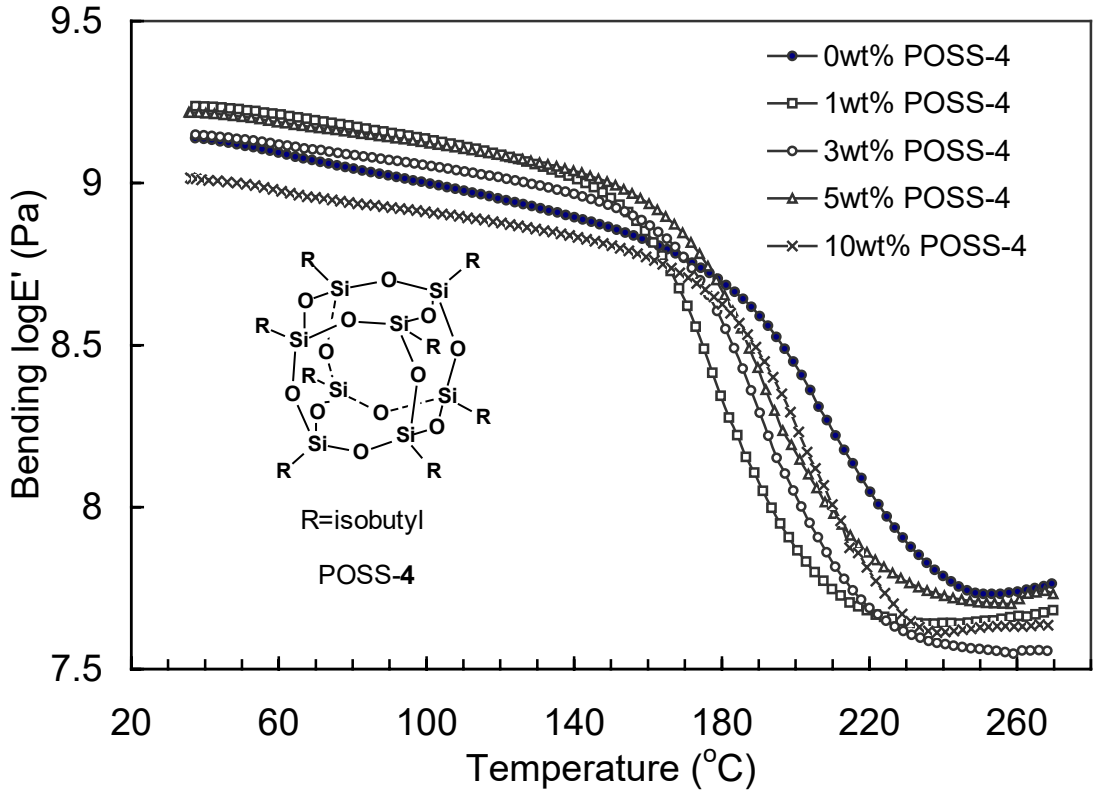

Figure 5.10 Bending E' versus temperature curves at 1 Hz for phenolic resin/POSS-**4** composites

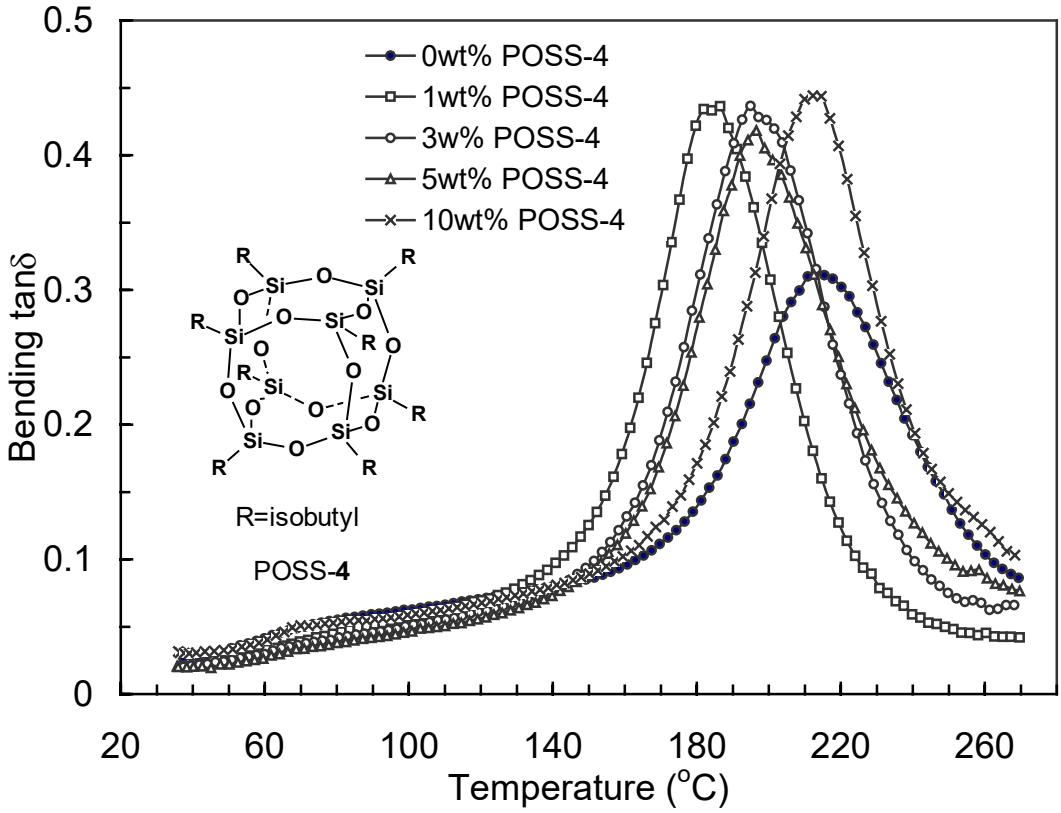

Figure 5.11 Bending tanδ versus temperature curves at 1 Hz for phenolic resin/POSS-**4** composites

The T_g values (tanδ peak temperatures, Figure 5.11) of these POSS-**4** composites are 186.5, 194.9, 196.5 and 212.3 °C for the 1, 3, 5 and 10 wt% POSS-**4** samples, respectively. These T_g values increase with POSS-**4** loadings, but all are lower than that of the neat phenolic resin (213.2 °C). Furthermore, the tanδ peak intensities for the POSS-**4** composites are higher than that of the phenolic resin (Figure 5.11). Thus, unlike POSS derivatives **1**, **2** and **3**, no improvements in the viscoelastic properties or T_g value of the phenolic resin was achieved by blending with POSS-**4**.

POSS-**1**, **2** and **3** contain functional groups which react with functional groups in the uncured phenolic resin, incorporating POSS into the phenolic resin's crosslink network by chemical bonds. No POSS particles were observed for phenolic resin/POSS-**1** nanocomposites with weight ratios of 97/3, 95/5 and 90/10, by TEM at 20,000 times magnification. Furthermore, no particle was observed for phenolic resin/POSS-**2** 90/10 and phenolic resin/POSS-**3** 95/5 nanocomposites. These results indicate that POSS-**1**, **2** or **3** were well dispersed in their phenolic resin nanocomposites. However, POSS-**4**, with no reactive functional groups, formed phase-separated nano- or micro-particles (shown in Figure 5.12), which lowered the phenolic resin's thermal stability and mechanical properties. The POSS-rich particle in Figure 5.12(a) is about 0.5 μm in diameter. Some small irregular particles are observed in Figure 5.12(b), where the small dark particle is about 0.04 μm.

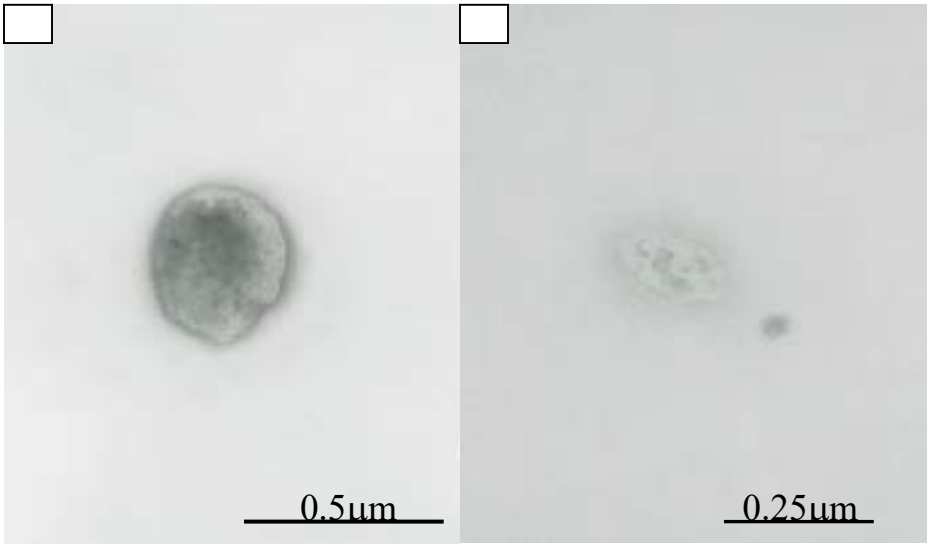

Figure 5.12 TEM micrographs for phenolic resin/POSS-**4** 95/5 composite

THF extraction readily removed POSS-**4** from the phenolic/POSS-**4** composites and the extracted amount increased with an increase of POSS-**4** loadings from 3 wt% to 10 wt% (Table 5.1). In contrast, POSS derivatives **1**, **2** and **3** were not easily removed from their nanocomposites by THF extraction. No POSS monomers or POSS-containing linear copolymers could be extracted from the phenolic/POSS-**1**, **2** and **3** nanocomposites with compositions of 99/1 and 97/3. IR spectra of the THF extracts from the 95/5 phenolic resin/POSS (**1**, **2** or **3**) nanocomposites exhibited very weak absorptions at about 1100-1135 cm^{-1}, attributed to Si-O stretching within POSS units. Even at high (10 wt%) POSS content, only traces of POSS-containing species were extracted. Furthermore, the solid residues which had been extracted (crosslinked network) exhibited Si-O absorptions in their IR spectra, demonstrating these POSS monomers were chemically bound within the resins, after THF extraction for the POSS-**1**, **2** and **3** nanocomposites. This absorption becomes strong at 10 wt% POSS-**1** or **2** content. However, no Si-O absorptions were observed from the phenolic resin/POSS-**4** composite after THF extraction, showing that extraction had moved all of the blended POSS-**4**.

The chemical structures of POSS-**1**, **2** and **3** are different, so their reactivities with phenolic resin during curing would be different. The POSS cages incorporated into the crosslink network in the POSS-**1** nanocomposite are pendant within the network. However, open-cage species POSS-**2** contains three acidic SiOH groups. If all three react, the POSS-**2** framework would be incorporated into the network as a crosslink center. POSS-**3** contains the same type of acidic SiOH groups as trifunctional POSS-**2**. However, they are attached along the ladderlike backbone of POSS-**3** and the Si-OH to Si ratio for **2**

and **3** are different. POSS-**3** is not a discrete single structure, but is a distribution of various molecular weight molecules. All of these factors would have some influence on the extent of cure, free-volume and viscoelasticity of the resulting phenolic resin/POSS nanocomposites.

The weight percentages of solid, which can be extracted by THF from the phenolic resin and its POSS-**1**, **2**, **3** and **4** composites are listed in Table 5.1. The percentage of material extracted from phenolic resin/POSS-**1**, **2** and **3** nanocomposites increased with an increase in POSS loadings. This may result from perturbations in the mechanism and extent of cure due to pH changes, the more acidic nature of the Si-OH groups or other factors. However, the residues extracted contained very little POSS. The extraction percentages from the phenolic resin/POSS-**4** composites, containing 1, 3, 5, and 10 wt% POSS, rise quickly with a rise of POSS-**4** loading due to substantial loss of **4**.

Effect of Thermal History on Viscoelastic Properties of Phenolic Resin/POSS Nanocomposites

Thermal history had an effect on viscoelastic properties of the neat phenolic resin and its POSS nanocomposites. DMTA curves of the first, second, and third heating cycles for the neat phenolic resin are shown in Figure 5.13. T_g values (tanδ peak temperature) increased going from the first to the third heating cycle: 213.2 °C, 233.6 °C and 256.9 °C, respectively. The tanδ peak intensities dropped gradually with successive heating cycles. The storage moduli in the rubbery region ($T>T_g$) increased in the second and third heating cycles. The E' values in the glassy region increased during the second heating and then varied little in the third heating. E' values at 40 °C and 265 °C are listed in

Table 5.2. The E' value at 265 °C in the third cycle is 198.9 MPa, about 3.5 times greater than its value in the first circle (56.2 MPa). Thus, continued phenolic resin curing took place during DMTA heating beyond the cure degree which occurred during the original post-curing at 250 °C/2 h. This increased the phenolic resin's crosslink density. Thus, post-heating cycles can markedly increase the phenolic resin's T_g value and both low and high temperature storage moduli.

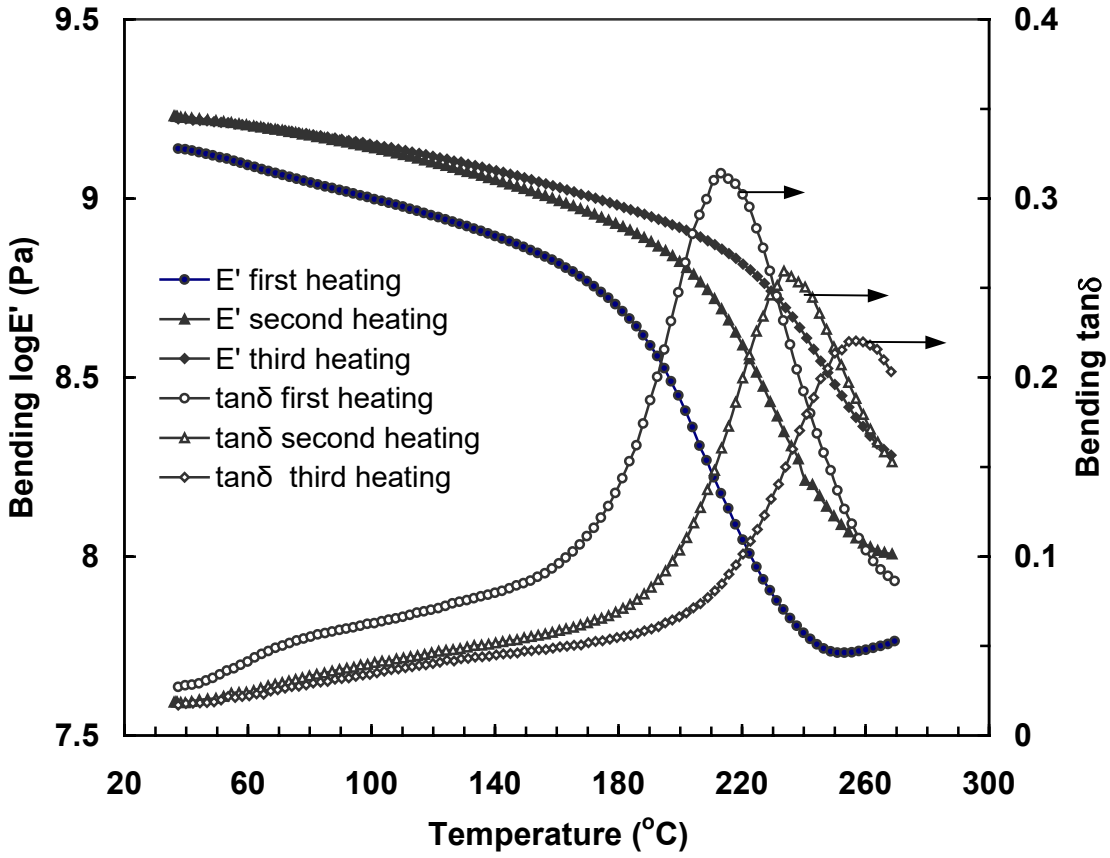

Figure 5.13 DMTA curves of the neat phenolic resin at the first, second, and third heating

Table 5.2 T_g and E' Values at 40 and 265 °C of the Phenolic Resin Control (PR) and Phenolic Resin (PR)/POSS-**1**, **2**, **3** and **4** Composites in the First, Second and Third Heating Cycles

Composite type	POSS (wt%)	Heating cycles	T_g (°C)	E' at 40°C (GPa)	E' at 265°C (MPa)
Phenolic resin (PR)	0	1	213.2	1.4	56.2
		2	233.6	1.7	103.0
		3	256.9	1.7	198.9
PR/POSS-**1**	1	1	210.3	1.7	65.6
		2	229.8	2.1	115.1
		3	256.5	2.1	217.2
PR/POSS-**1**	3	1	211.0	1.8	60.8
		2	237.6	2.0	120.9
		3	262.5	2.2	279.5
PR/POSS-**1**	5	1	217.4	2.0	79.7
		2	234.8	2.4	140.7
		3	252.2	2.6	263.9
PR/POSS-**1**	10	1	244.9	1.3	123.5
		2	272.9	1.6	278.5
		3	>299.6	1.6	593.7
PR/POSS-**2**	1	1	217.3	2.0	106.2
		2	250.0	2.3	253.3
		3	270.8	2.2	502.3
PR/POSS-**2**	3	1	213.3	2.0	89.1
		2	241.0	2.3	217.7
		3	270.4	2.3	401.1
PR/POSS-**2**	5	1	222.0	2.2	141.1
		2	234.0	2.8	269.4
		3	247.1	2.9	412.6
PR/POSS-**2**	10	1	254.4	1.5	201.0
		2	280.2	1.6	581.2
		3	>299.8	1.5	852.9
PR/POSS-**3**	1	1	203.0	1.9	61.5
		2	218.6	2.2	89.2
		3	231.7	2.3	134.2
PR/POSS-**3**	3	1	224.3	1.4	70.4
		2	254.6	1.7	193.1
		3	295.9	1.7	455.6
PR/POSS-**3**	5	1	222.5	1.5	75.3
		2	260.7	1.6	220.8

Table 5.2 (Continued)

		3	>297.8	1.6	471.3
PR/POSS-**4**	1	1	186.5	1.7	46.6
		2	194.4	2.0	61.6
		3	207.1	2.0	73.3
PR/POSS-**4**	3	1	194.9	1.4	36.1
		2	216.2	1.5	55.3
		3	234.0	1.5	87.7
PR/POSS-**4**	5	1	196.5	1.6	54.6
		2	221.9	1.7	125.0
		3	256.7	1.7	248.3
PR/POSS-**4**	10	1	212.3	1.0	43.2
		2	235.2	1.2	118.0
		3	262.9	1.3	310.1

When POSS-**1**, **2** or **3** were present, the storage moduli and thermal stabilities increased for all nanocomposites. Several typical examples are shown in Figures 5.14-5.16. The 90/10 phenolic resin/POSS-**1** nanocomposite exhibited a sharp increase in T_g from 245 °C to ~273 °C and >300 °C in the second and third heating cycles (Figure 5.14). The E' values at 265 °C in the rubbery region were greatly improved from 123.5 MPa in the first cycle to 593.7 MPa in the third cycle, a 4.8 fold increase. The pure phenolic resin's E' value at 265 °C was 198.9 MPa in the third heating cycle, only one-third that of the 10 wt% POSS-**1** nanocomposite. The presence of POSS makes a large difference in high temperature response. The E' values for the 90/10 phenolic/POSS-**1** nanocomposite in the glassy region increased in the second heating cycle and then changed only a small amount thereafter, similar to the behavior of the pure phenolic control resin.

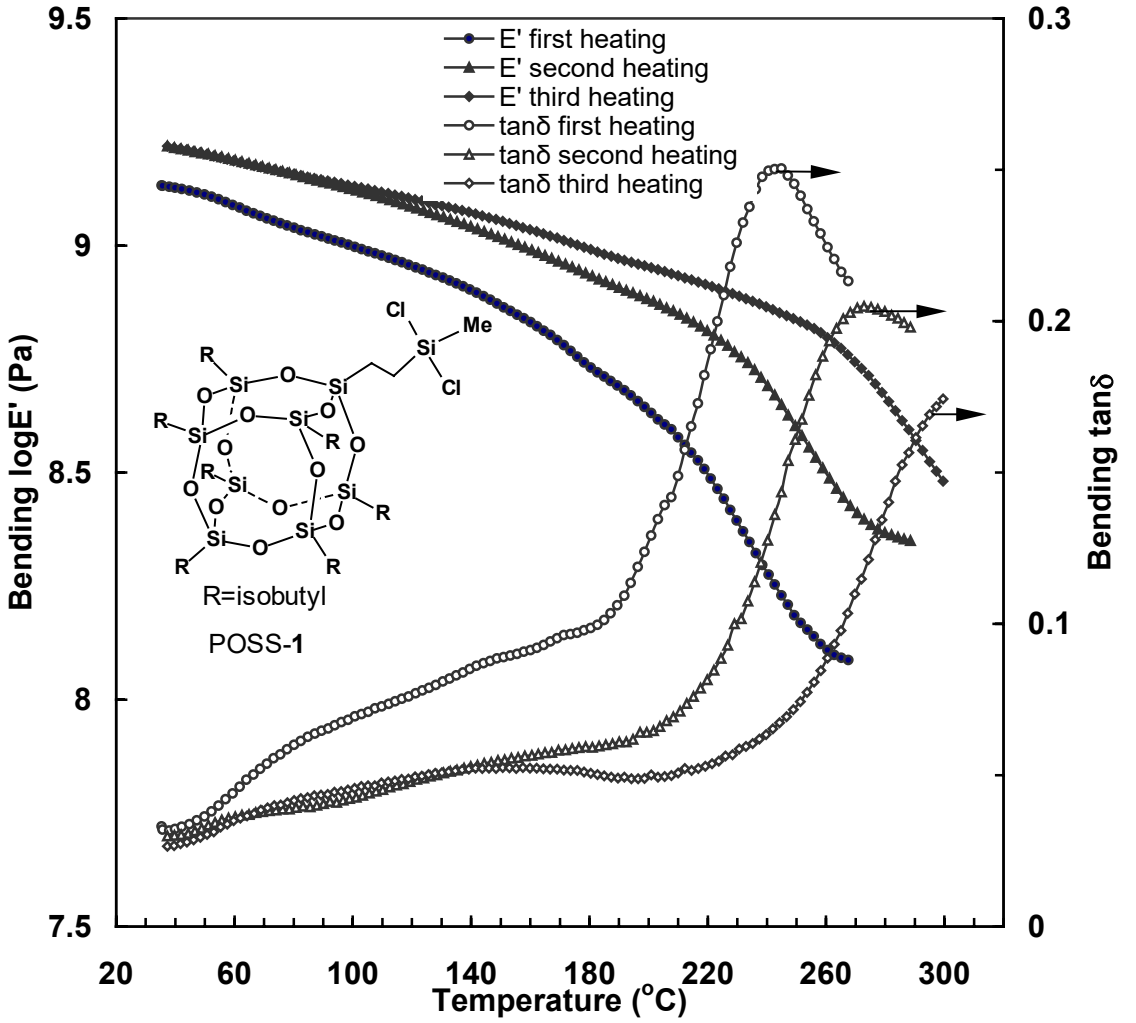

Figure 5.14 DMTA curves of the phenolic resin/POSS-**1** 90/10 nanocomposite in the first, second, and third heating cycles

The 90/10 phenolic resin/POSS-**2** nanocomposite also exhibits great T_g and E' ($T>T_g$) improvements during the second and third heating cycles (Figure 5.15). Its T_g value in the second cycle is ~280 °C with a very large decrease in tanδ intensity. In the third heating cycle, the T_g is much higher than 300 °C. The E' value at 265 °C for this 10wt% POSS-**2** nanocomposite in the third heating was 852.9 MPa, much higher than

that of the 10 wt% POSS-**1** nanocomposite (593.7 MPa) or the phenolic control (198.9 MPa) after the same treatment. The 10 wt% POSS-**2** sample has a higher E' at 40 °C in the first heating cycle than either the phenolic control resin or the 10 wt% POSS-**1** sample. Thus, it does not exhibit as sharp an increase in E' at 40 °C in the second and third heating cycles. However, the values of E' in the glassy region from 100 to 200 °C were substantially increased in the second and third heating cycles (Figure 5.15). Heating the phenolic resin/POSS-**2** nanocomposites has a larger effect on the viscoelastic properties than does heating the POSS-**1**/phenolic systems. The three SiOH groups in **2** may modify the high temperature curing chemistry by promoting further curing where POSS-**2** serves as crosslink sites.

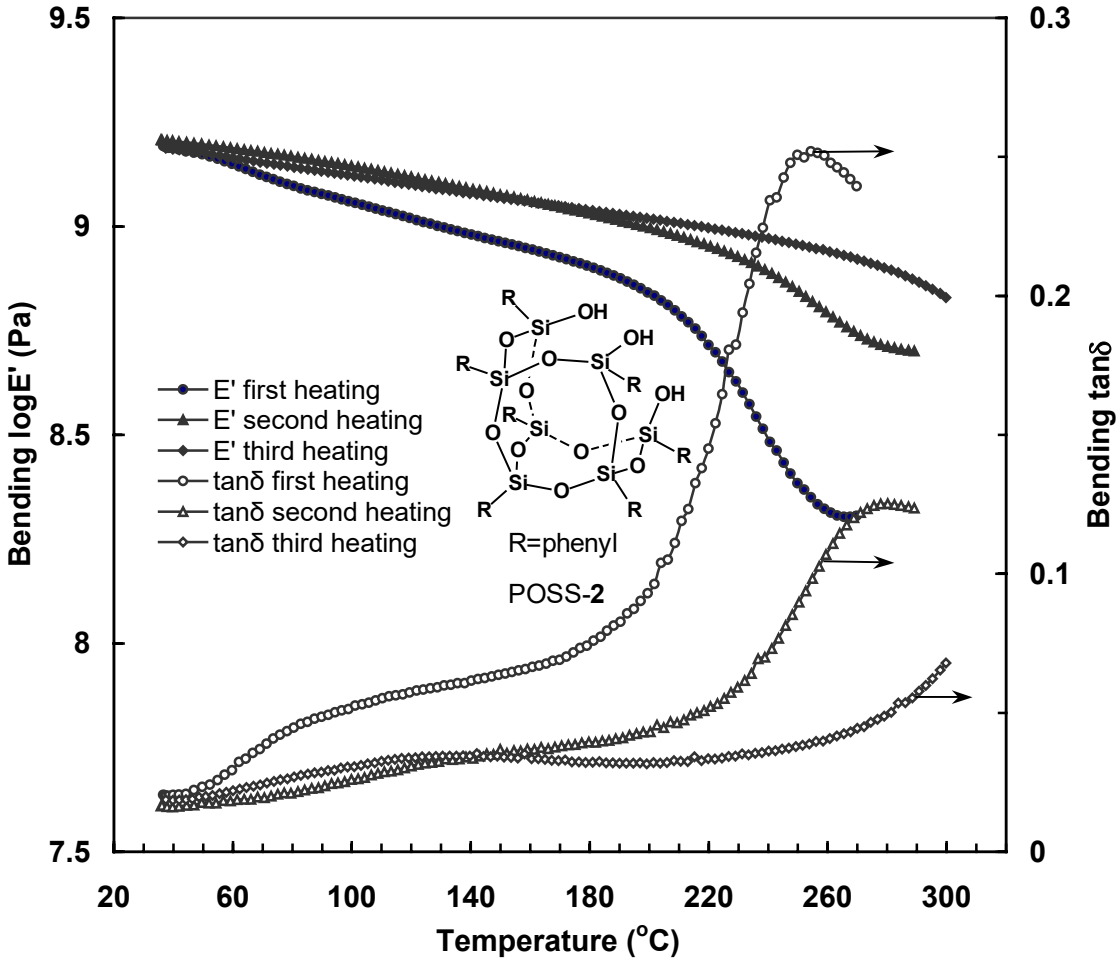

Figure 5.15 DMTA curves of the phenolic resin/POSS-**2** 90/10 nanocomposite in the first, second, and third heating cycles

POSS-**3** also induced enhancements in T_g and E' values on heating (Figure 5.16). The 5 wt% POSS-**3** nanocomposite displayed T_g values of 223, 261 and ~300 °C for the three successive heating cycles, respectively. This sample's E' values were greatly enhanced in the rubbery region, from 75.3 to 220.8 and then to 471.3 MPa (at 265 °C) in the first, second and third heating cycles, respectively. The T_g enhancements upon heating were somewhat less than those induced by 10wt% POSS-**1** and substantially less

than those caused by 10 wt% POSS-**2**. The bending moduli of the POSS-**3** sample in the glassy region from 40 to 180 °C was almost identical to that of the 10 wt% POSS-**1** sample in the second and third heating cycles. The T_g values of the 5 wt% POSS-**3** sample were lower than those of the 10 wt% POSS-**1** composite in each successive heating cycle, but the decrease in the tanδ peak intensity was greater on heating for the POSS-**3** system.

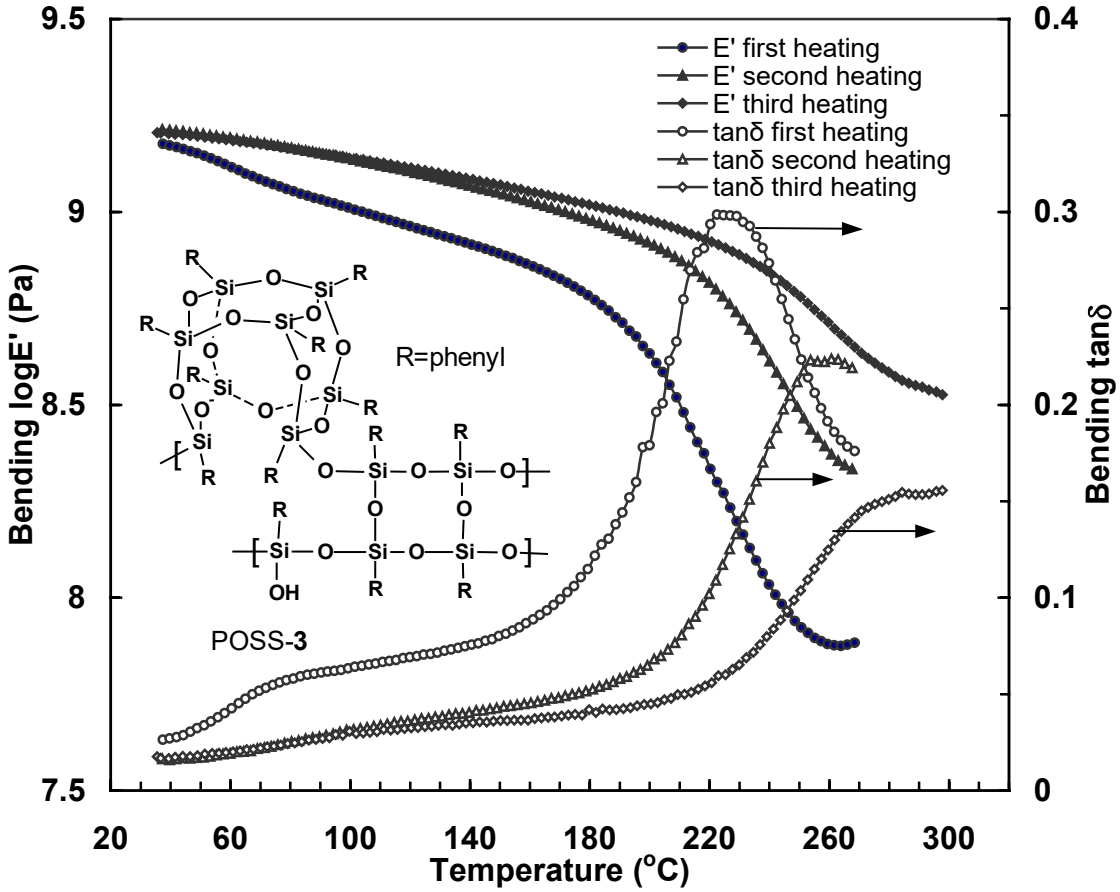

Figure 5.16 DMTA curves of the phenolic resin/POSS-**3** 95/5 nanocomposite in the first, second, and third heating cycles

The DMTA curves for the first, second and third heating cycles of the phenolic resin/POSS-**4** 90/10 composite are given in Figure 5.17. Its T_g values are 212, 235 and 263 °C in the three heating cycles, an improvement similar to that observed for the neat phenolic resin. The E' values in the rubbery region for this 10 wt% POSS-**4** composite were also improved by thermal history. The E' value at 265 °C in the third cycle is 310.1 MPa, which is higher than that of the phenolic resin (198.9 MPa). However, this E' value is much lower that those of the 10wt% POSS-**1** and **2** and 5 wt% POSS-**3** composites (Table 5.2) during the third heating cycle. The 1, 3 and 5 wt% POSS-**4**/phenolic resin composites gave lower T_g values than the neat phenolic resin for the corresponding heating cycles. It is clear that the unfuctionalized POSS-**4** is not effective at enhancing the thermal stability except after several heating cycles. Using 1 and 3 wt% of POSS-**4** sharply degrades the E' values in the rubbery region (265 °C) to values far below those of the phenolic control in all three heating cycles (Table 5.2). In contrast, the T_g and E' values in the rubbery region for the POSS-**1**, **2** and **3** composites were all significantly improved versus the neat phenolic resin during all heating cycles. Thus, chemically incorporating the POSS chemicals into the phenolic resin enhances E' and T_g far more than adding unfunctionalized POSS-**4**. This is found both prior to and after thermal treatments.

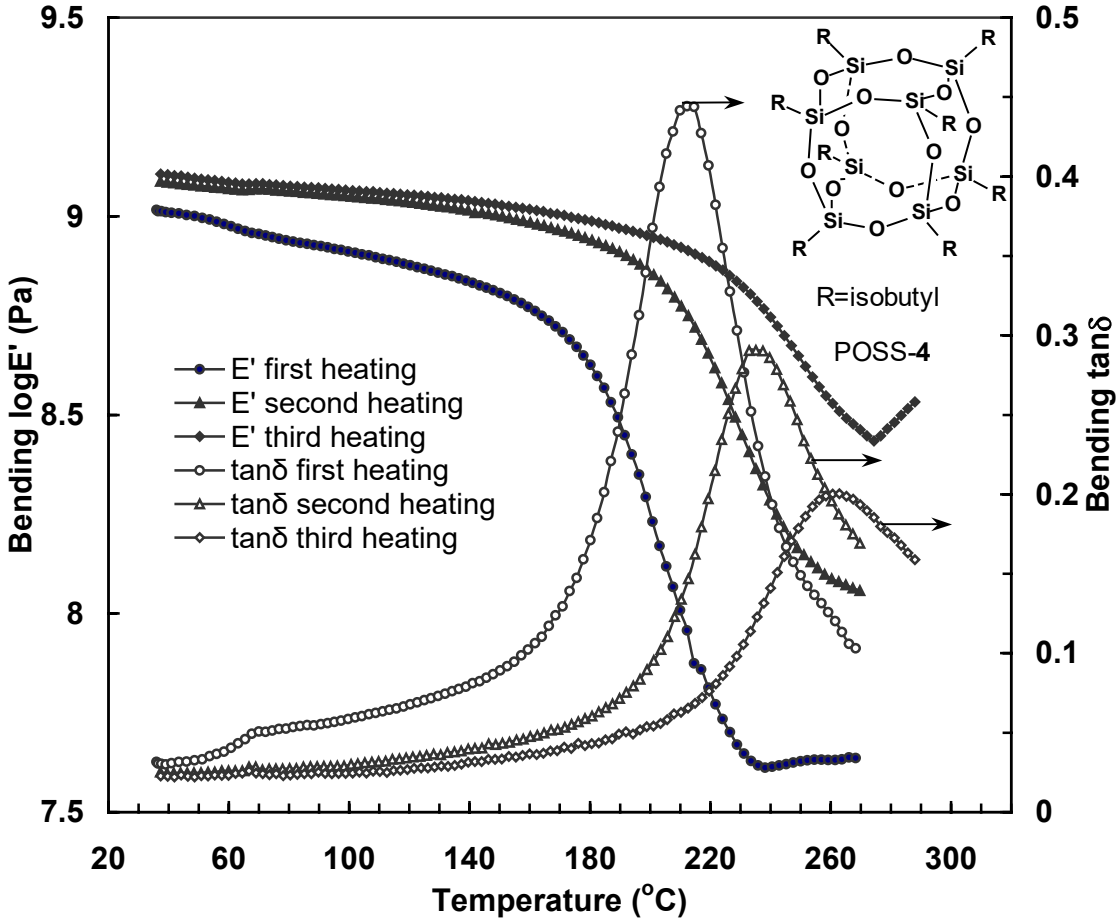

Figure 5.17 DMTA curves of the phenolic resin/POSS-**4** 90/10 composite in the first, second, and third heating cycles

Conclusions

Three multifunctional POSS macromers, POSS-**1**, POSS-**2** and POSS-**3**, were chemically incorporated into the phenolic resin crosslinked networks by thermal condensation curing. For comparison, a fourth nonfunctional compound, POSS-**4**, was blended into the phenolic resin. The phenolic resin/POSS-**1** nanocomposites with 1, 3, 5 and 10 wt% POSS exhibit progressively higher T_g and E' values in the rubbery region versus those of the neat phenolic resin. Their T_g values and the E' values at $T>T_g$ increase

almost in proportion with the increase in POSS-**1** or **2** loading. The incorporation of 10 wt% of either POSS-**1** or POSS-**2** into the phenolic resin leads to high T_g and storage moduli ($T>T_g$). The improvements in T_g and E' values in the rubbery region were also obtained for the phenolic resin/POSS-**3** nanocomposites containing 3 or 5 wt% POSS. However, no improvements in viscoelastic properties or thermal stability of the phenolic resin were observed by physically incorporating the unfunctionalized POSS-**4** into the phenolic resin.

The structural differences in the substituents and the POSS chemical structures also influence the property improvements of the phenolic resin nanocomposites containing POSS-**1**, **2** or **3**. THF extraction of the phenolic resin/POSS-**1**, **2** and **3** nanocomposites removed no measurable POSS residues from the 99/1 and 97/3 samples. Only traces of POSS-containing residues were obtained from the nanocomposites containing 5 or 10 wt% of these three functional POSS monomers. However, POSS-**4**, which is not chemically bound to the phenolic resin, is easily extracted, confirming that the functional monomers, POSS-**1**, **2** or **3**, were chemically incorporated into the crosslinked network during condensation curing.

Heating leads to great improvements of the T_g and E' values in the rubbery region for the neat phenolic resin and all phenolic resin/POSS composites. However, the phenolic resin/POSS nanocomposites containing functional POSS-**1**, **2** and **3**, exhibited much more prominent viscoelastic improvements than those of the neat phenolic resin or the phenolic resin/POSS-**4** composites. POSS-**2** was the most effective POSS derivative

at enhancing the high temperature properties by heating, possibly because it can act directly as a crosslinking site.

References

[1] Giannelis, E.P., *Adv. Mater*., 1996, *8*, 29.

[2] Krishnamoorti, R., Vaia, R.A., editors, *Polymer Nanocomposites: Synthesis, Characetrization and Modeling*, American Chemical Society, Washington, DC, 2003.

[3] Nalwa, H.S. Editor, *Handbook of Organic-Inorganic Hybrid Materials and Nanocomposites, Volume 2, Nanocomposites*, American Scientific Publishers, Stevenson Ranch, Calif., 2003, 385.

[4] Sanchez, C., de Soler-lllia, G.J., Ribot, F., Lalot, T., Mayer, C.R., Cabuil, V. *Chem. Mater.*, 2001, 13, 3061.

[5] Pyun, J., Matyjaszewski, K., *Chem.Mater.*, 2001, 13, 3436.

[6] Gill, I., *Chem. Mater.*, 2001, 13, 3404.

[7] Sanchez, C., Lebeau, B., *MRS Bull.*, 2001, 26, 377.

[8] Gangopadhyay, R., De, A., *Chem. Mater.*, 2000, 12, 2064.

[9] Pomogailo, A.D., *Russian Chemical Reviews*, 2000, 69, 53.

[10] LeBaron, P.C., Wang, Z., Pinnavaia, T., *J. Appl. Clay Sci.*, 1999, 15, 11.

[11] Huang, Q.R., Kim, H., Huang, E., Mecerreyes, D., Hedrick, J.L., Volksen, W., Frank, C.W., Miller, R.D., *Macromolecules*, 2003, 36, 7661.

[12] Lee, K.M., Han C.D., *Macromolecules*, 2003, 36, 7165.

[13] Kim, J., Lee, S., *Polym. Mater. Sci. Eng.*, 2003, 89, 474.

[14] Ren, J., Krishnamoorti, R., *Macromolecules*, 2003, 36, 4443.

[15] Chiang, C., Ma, C.M., Wu, D., Kuan, H., *J. Polym. Sci., Part A: Polym. Chem.*, 2003, 41, 905.

[16] Ogoshi, T., Chujo, Y., *Macromolecules*, 2003, 36, 654.

[17] Lee, S., Kim, J., *Polym. Mater. Sci. Eng.*, 2002, 87, 300.

[18] Bharadwaj, R.K., *Macromolecules*, 2001, 34, 9189.

[19] Trimmel, G., Gross, S., Kickelbick, G., Schubert, U., *Appl. Organometal. Chem*., 2001, 15, 401.

[20] Gardziella, A., Pilato, L.A., Knop, A., *Phenolic Resins: Chemistry, Applications, Standardization, Safety and Ecology*, Second edition, Springer-Verlay, Berlin, Heidelberg, New York, 1999. 1.

[21] Knop, A., Pilato, L.A., *Phenolic Resins*, Springer, Berlin, Heidelberg, New York, 1985.

[22] Haraguchi, K., Usami, Y., Ono, Y., *J. Mater. Sci.*, 1998, *33*, 3337.

[23] Haraguchi, K., Usami, Y., Yamamura, K., Matsumoto, S., *Polymer*, 1998, *39*, 6243.

[24] Choi, M.H., Chung. I.. J., *Chem. Mater.*, 2000, *12*, 2977.

[25] Byun, H.Y., Choi, M.H., Chung, I. J., *Chem. Mater.*, 2001, *13*, 4221.

[26] Wu, Z., Zhou, C., Qi, R., *Polymer Composites*, 2002, *23*, 634.

[27] Lichtenhan, J. D., Schwab, J. J., Reinerth, W. A. Sr., *Chemical Innovation* 2001, 1, 3.

[28] Li, G. Z., Wang, L., Ni, H., Pittman, Jr. C.U., *J.Inorganic and Organometalic Polymers*, 2001, *11*, 123.

[29] Lichtenhan, J. D., Otonari, Y. A., Carr, M. J., *Macromolecules*, 1995, *28*, 8435.

[30] Haddad, T. S., Lichtenhan, J. D., *Macromolecules*, 1996, *29*, 7302.

[31] Romo-Uribe, A., Mather, P. T., Haddad, T. S., Lichtenhan, J. D., *J. Polym. Sci., Part B: Polym. Phys*., 1998, *36*, 1857.

[32] Lee, A., Lichtenhan, J. D., *Macromolecules*, 1998, *31*, 4970.

[33] Mather, P. T., Jeon, H. G., Romo-Uribe, A., Haddad, T. S., Lichtenhan, J. D., *Macromolecules*, 1999, *32*, 1194.

[34] Lee, A., Lichtenhan, J. D., *J. Appl. Polym. Sci.*, 1999, *73*, 1993.

[35] Jeon, H. G., Mather, P. T., Haddad, T. S., *Polym. Int.*, 2000, *49*, 453.

[36] Fu, B. X., Hsiao, B. S., White, H., Rafailovich, M., Mather, P. T., Jeon, P. T., Jeon, H. G., Phillips, S., Lichtenhan, J., Schwab, J., *Polym. Int.*, 2000, *49*, 437.

[37] Ellsworth, M. W., Gin, D. L., *Polymer News*, 1999, *24*, 331.

[38] Bharadwaj, B. K., Berry, R. J., Farmer, B. L., *Polymer*, 2000, *41*, 7209.

[39] Tsuchida, A., Bolln, C., Sernetz, F. G., Frey, H., Mulhaupt, R., *Macromolecules*, 1997, *30*, 2818.

[40] Haddad, T. S., Lee, A., Phillips, S. H., *Polym. Prep. (ACS Div. Polymer Chem.)*, 2001, *42*, 88.

[41] Li, G.Z., Wang, L., Toghiani, H., Daulton, T.L., Koyama K., Pittman Jr C.U., *Macromolecules*, 2001, *34*, 8686.

[42] Li,G.Z., Wang, L., Toghiani, H., Pittman Jr. C.U., Daulton T.L., *Polymer*, 2002, *43*, 4167.

[43] Lee, A., *POSS™ Nanotechnology Conference,* Sept. 25-27, Huntington Beach, CA., 2002.

[44] Choi, J., J. Harcup, J., Yee, A. F., Zhu, Q., Laine, R. M., *J. Am. Chem. Soc*., 2001, *123*, 11420.

[45] Laine, R. M., *POSS™ Nanotechnology Conference*, Sept.25-27, Huntington Beach, CA., 2002.

[46] Mya, K.Y., Huang, J., Xiao, Y., He, C., Siow, Y.P., Dai, J., *Polymeric Materials: Science&Engineering*, 2003, *89*, 757; ACS meeting (preprint), Sept.9-11, Newyork, 2003.

[47] Constable, G.S.; Coughlin, E.B.; Lesser, A.J. *Polymeric Materials: Science&Engineering*, 2003, *89*, 641; ACS meeting (preprint), Sept.9-11, Newyork, 2003.

CHAPTER VI

SYNTHESIS, MORPHOLOGY, THERMAL AND VISCOELASTIC PROPERTIES OF POSS NANOCOMPOSITES WITH EPOXY AND CYANATE ESTER MATRICES

Introduction

The development of hybrid organic matrix-inorganic nanocomposites with a variety of new and improved properties has attracted much research interest in the past few years [1-26]. Example inorganic nanophases include nanoclays [27-32], carbon nanotubes [33-36], vapor-grown carbon nanofibers [37-43], inorganic nanofibers [44-45] and polyhedral oligomeric silsesquioxanes (POSSs) [19-26, 46]. Silsesquioxanes embody a molecular hybrid (inorganic-organic) architecture, which contains an inner inorganic silicon-oxygen $(SiO_{1.5})_n$ framework, that is externally covered by organic substituents. These substituents can be totally hydrocarbon in nature or they can be made of polar structures and functional groups. POSS nanostructured chemicals have diameters from 1 to 3 nm. They can be thought of as analogues to the smallest possible particles of silica. POSS cages can be incorporated into familiar polymers via copolymerization [47-50],

grafting [47, 51], or blending [47, 51-52]. New hybrid inorganic-organic thermoset [46, 53-59] and thermoplastic materials [22, 26, 49-52, 60-61] can be prepared with higher use temperatures [62], oxidation resistances [51], surface hardness [51], and mechanical property modifications [63-64]. Furthermore, reductions in flammability [65], heat evolution [66], and processing viscosity [67] have been reported. Both thermoplastics and thermosets, including methacrylates [68], styrenes [69], norbornenes [70], ethylenes [71], epoxides [72], and siloxanes [50, 73] have been improved.

Laine [74] et al prepared epoxy resin nanocomposites from octaaminophenyl-(T_8)POSS [**1**, $(C_6H_4NH_2)_8(SiO_{1.5})_8$]/diglycidyl ether of bisphenol A (DGEBA) and octa(dimethylsiloxypropylglycidyl ether)(T_8)POSS [$(OSi(CH_3)_2C_3H_6OCH_2CHOCH_2)$-$(SiO_{1.5})_8$, OG]/diaminodiphenylmethane(DDM). The properties of DGEBA/octaamino-phenyl(T_8)POSS, **1** and OG/DDM nanocomposites were compared. They found that tethers with aromatic components increase both char yields and decomposition temperatures in epoxy resin nanocomposites. T_8 POSS loadings were shown to be important in determining the thermal stabilities.

Cyanate ester resin (PT-15, Lonza Corp) composites containing the 1-5wt% of octaaminophenyl(T_8)POSS [**1**, $(C_6H_4NH_2)_8(SiO_{1.5})_8$] were synthesized recently by our group [75]. The glass-transition temperatures (T_g's) rose sharply to maximum values for the composite with 1 wt % **1** versus neat PT-15, and then fell as the content of **1** was raised to 3 and 5 wt %. PT-15/POSS-**1** composites exhibited higher storage moduli (*E'*) than the parent cyanate ester resin at temperatures > T_g with the highest values formed at 1 wt % of **1**. The loss factor peak intensities decreased and their widths broadened upon

the incorporation of POSS. XRD, TEM, IR and extraction data were all consistent with a molecular dispersion of **1** within the cured composites. No phase separation or domains of **1** could be detected. This homogeneity was due to the addition of the POSS-**1** amino groups across the cyanate ester functions to form iminocarbonate functional groups. This reaction chemically bonded **1** to cyanate ester monomers at much lower temperatures (20-60 °C) than the >150 °C temperatures required to thermally cure PT-15 via cyclotrimerization to form triazine rings.

In this dissertation, octaaminophenyl(T_8)POSS, **1** and dodecaaminophenyl(T_{12})-POSS, **2** were synthesized, characterized and then incorporated into two types of resins: (1) epoxy (Epon 828, Shell Chemical Corp.) resin, and (2) the bisphenol-F-based cyanate ester resin, PT-15, respectively, to make two series of nanocomposite materials. The epoxy resins also employed 4,4'-diaminodiphenylmethane (DDM) as a curing agent where the sum of amino groups in DDM an POSS were held in a 1:1 mole ratio to the epoxy groups. Only the pioneering reports of Laine [74, 76] have appeared on the use of octaaminophenyl(T_8)POSS, **1** in thermoset systems. We are unaware of any reports of either the synthesis of dodecaaminophenyl(T_{12}) POSS or its incorporation into thermosets. The morphology, thermal and viscoelastic properties of these composites were determined by transmission election microscopy (TEM), X-ray diffraction (XRD), thermal gravimetric analysis (TGA) and dynamic mechanical thermal analysis (DMTA). Chemical incorporation was demonstrated by extraction and Fourier transform infrared (FTIR) spectroscopy.

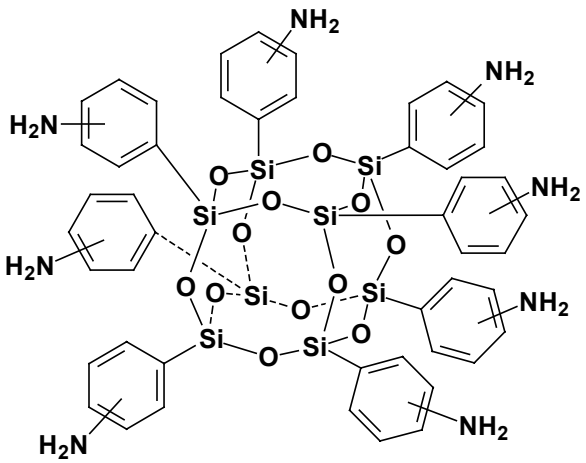

Octaaminophenyl(T_8)-POSS

1

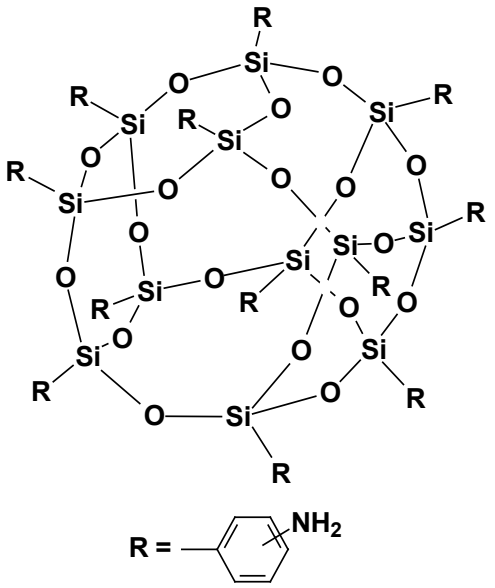

Dodecaaminophenyl(T_{12})-POSS
(D_{2h} cage)

2

Experimental

Materials

The commercial DGEBA-based epoxy resin (EPON® 828) was obtained from the Shell Chemical Company, Houston, TX. It is composed of an undiluted clear difunctional bisphenol-A/epichlorohydrin-derived liquid. Diaminodiphenylmethane (DDM) was purchased from Aldrich Chemical Company, Inc. Both were used as-received.

The bisphenol-F-derived low-viscosity cyanate ester resin PT-15 was used in this work. PT-15, supplied by Lonza, Inc, is a multifunctional, low-viscosity (35 cps at 80 °C and 8 cps at 120 °C) liquid cyanate ester resin. PT-15 also contains a small quantity of some larger oligomers. All the bisphenol-F mixture's phenolic hydroxyls have been converted to -OCN functions by ClCN. PT-15 may be cured via a thermally driven

cyclotrimerization to form triazine rings, each of which serves as a crosslinking site. This reaction can take place readily in the absence of a catalyst at temperatures above 165 °C. This high polymerization temperature allows a large processing window for blending the resin with other components at temperatures from 100 to 130 °C, at which the viscosity is very low (η = 8 cps at 120 °C).

Octaphenyl(T_8)POSS and dodecaphenyl(T_{12})POSS were obtained from Hybrid Plastics Inc. and used as starting materials. Reagents and solvents were purified under N_2 as follows: tetrahydrofuran (THF) was distilled from sodium before use. Formic acid 90% was treated with the drying agent, phthalic anhydride, and then distilled through predried glassware before use. Triethylamine was distilled from calcium hydride before use. Fuming (~90%) nitric acid, Pd/C, ethyl acetate and hexane were obtained from Aldrich and used without purification.

Synthesis of octanitrophenyl(T_8)POSS

Octaphenyl(T_8)POSS**,** 50 g (48.4 mmol) was added in small portions to 300 mL of fuming nitric acid with stirring at 0 °C. After the addition was complete, the solution was stirred for an additional 30 min and then at room temperature for 20 h. After filtration through glass wool, the solution was poured onto 250 g of ice. A faintly yellow precipitate was collected, washed with water (~100 mL × 5 until pH = 6.0) and then with ethanol (~100 mL × 2). The powder obtained was dried at ambient temperature to remove residual solvent to yield 60.8 g (43.6 mmol, 90.1%) of octanitrophenyl(T_8)POSS as a faintly yellow solid. mp: >350 °C; ^{1}H NMR (acetone-d_6, ppm): 8.6 (*t*, 1.0H), 8.4-8.1 (*m*,

4.1H), 7.8 (*m*, 2.7H); ^{13}C NMR (acetone-d_6, ppm): 154.0, 148.2, 141.0, 138.2, 136.5 (small), 135.3, 134.1, 132.3 (small), 130.8, 129.4, 127.0, 125.2, 123.6 (small); ^{29}Si NMR (THF, TMS, acetone-d_6, ppm): -79.1, -83.0; FTIR (cm-1) 3167–2870 (*v*C–H), 1615 (*v*C–C), 1529, 1349 (*v*N-O), 1268–975 (*v*Si–O–Si), 730, 505 (*v*C–H).

Synthesis of dodecanitrophenyl(T_{12})POSS (DNPS)

Dodecanitrophenyl(T_{12})POSS was synthesized under the same conditions used to make octanitrophenyl(T_8)POSS above. Dodecaphenyl(T_{12})POSS, 50 g (32.3 mmol) was added slowly to 300 ml of fuming nitric acid in small portions at 0 °C, followed by the work-up described above. Residual ethanol was removed from the powder obtained at ambient temperature to yield 60.3 g (28.8 mmol, 90%) of a faintly yellow solid. mp: >350 °C; ^{1}H NMR (acetone-d_6, ppm): 8.6 (*t*, 1.0H), 8.3-8.0 (*m*, 4.1H), 7.8 (*m*, 2.7H); ^{13}C NMR (acetone-d_6, ppm): 154.0, 148.9, 141.0, 138.6, 136.5 (small), 135.3, 134.1, 132.3 (small), 130.8, 129.5, 127.0, 125.2, 123.6 (small); ^{29}Si NMR (THF, TMS, acetone-d_6, ppm): -78.9, -82.5; FTIR (cm-1) 3166–2872 (*v*C–H), 1612 (*v*C–C), 1529, 1350 (*v*N-O), 1270–978 (*v*Si–O–Si), 735, 505 (*v*C–H).

Synthesis of octaaminophenyl(T_8)POSS, 1

POSS-**1** was prepared by introducing octanitrophenyl(T_8)POSS (10.0 g, 7.16 mmol, -NO_2 57.4 mmol) and 5 wt % Pd/C (1.22 g, 0.574 mmol) into a 250-mL Schlenk flask equipped with a condenser under N_2. Distilled THF (80 mL) and triethylamine (80.0 mL, 0.574 mmol) were then added. The mixture was heated to 60 °C, and distilled formic acid (10.4 mL, 0.230 mol) was added slowly at 60 °C. Carbon dioxide evolved, and the

solution separated into two layers. After 5 h, the THF layer was separated. Then THF 50 mL and 50 mL water were added until the slurry formed a black suspension. The suspension and the THF solution, separated previously, were mixed and filtered through Celite. More THF (20 mL) and water (20 mL) were added to the flask to dissolve the remaining black slurry. Then the suspension was filtered again. All of the filtrates were combined with 50 mL ethyl acetate and washed 4 times with 100 mL H_2O. The organic layer was dried over 5 g anhydrous $MgSO_4$ and precipitated by addition to 2 L hexane. A light yellow precipitate was collected by filtration, redissolved in 30:50 THF/ethyl acetate and reprecipitated into hexane (1 L). The resulting slightly brown powder obtained was dried under vacuum. Yield 6.80 g (5.89 mmol, recovery 82%). mp: >350 °C; ^{1}H NMR (acetone-d_6, ppm): 7.7-6.2 (*b*, 4.0H), 5.1-3.7 (*b*, 2.0H); ^{13}C NMR (acetone-d_6, ppm): 154.0, 148.5, 136.4, 132.8, 129.3, 123.4, 120.8, 117.3, 115.8, 114.4; ^{29}Si NMR (THF, TMS, acetone-d_6, ppm): -73.3, -77.2; FTIR (cm-1) 3345 (νN–H), 3120–2820 (νC–H), 1598 (νC–C), 1439 (δC–H), 1230–970 (νSi–O–Si), 698, 493 (νC–H).

Synthesis of dodecaaminophenyl(T_{12})POSS, 2

POSS-**2** was synthesized and worked up using the same procedure and conditions used to make POSS-**1** from its nitro precursor described above. Dodecanitophenyl(T_{12}) (10.0 g, 4.2 mmol) and 5 wt% Pd/C (0.71 g, 0.48 mmol) were added to a 250 ml Schlenk flask. Distilled THF (80 ml) and triethylamine (80.0 mL, 0.574 mmol) were added under nitrogen. Distilled formic acid (10.4 mL, 0.230 mol) was added slowly at 60 °C in the same manner described above to make POSS-**1** above. Yield 6.3 g (3.65 mmol, recovery 87%). mp: >350 °C; ^{1}H NMR (acetone-d_6, ppm): 7.7-6.2 (*b*, 4.0H), 5.1-3.5 (*b*, 2.0H); ^{13}C

NMR (acetone-d_6, ppm): 153.8, 148.0, 136.6, 132.8, 129.3, 123.4, 120.8, 117.3, 115.8, 114.4; FTIR (cm-1) 3353 (νN–H), 3105–2824 (νC–H), 1596 (νC–C), 1440 (δC–H), 1230–970 (νSi–O–Si), 697, 495 (νC–H).

Preparation of composites

Five EPON-828/**1**/DDM and EPON-828/**2**/DDM composite compositions were made for each series with 1:1 epoxy/amino group ratios. These compositions employed EPON-828/POSS/DDM wt/wt/wt ratios of 78.63/0/21.37, 77.48/5/17.52, 76.34/10/13.66, 74.05/20/5.95 and 72.28/27.72/0 for both series. These components were blended in solution. POSS and DDM were dissolved in THF, giving transparent solutions. The liquid epoxy resin, which was previously dissolved into a separate THF solution, was then added to the POSS/DDM/THF solution. THF of the resulting solution was removed in a vacuum (400-450 mm Hg) at 40-50 °C for 12 h. One equivalent of epoxy groups was employed per equivalent of the amino groups present in the combined POSS and DDM reagents as the amount of POSS was varied. These blends were thermally cured in Al containers according to the following temperature/time protocol: 55 °C/12 h, 100 °C/6 h and 150 °C/6 h. Post-curing was conducted at 200 °C for 3 h and then 250 °C for 1 h to enhance the crosslinking of residual DGEBPA epoxy groups.

PT-15/**1** and PT-15/**2** composites (99/1, 97/3 and 95/5 wt/wt compositions for both types) were also prepared by solution blending, solvent removal and thermal curing. POSS-**1** or **2** was dissolved in THF to give a transparent solution (0.5 g/mL). Then, the liquid cyanate ester components were also dissolved in this THF solution. THF was

removed in vacuum oven (300-350 mmHg) at 50 °C for 16 h. The resulting cyanate ester/POSS-**1** liquid blends were transparent in each case. These blends were cured by (1) heating to 188 °C and maintaining this temperature for 120 min, (2) ramping the temperature to 250 °C at 5 °C/min, and (3) holding the samples at 250 °C for 180 min. Periodic examination showed that the samples remained transparent at all stages during the cure, and they remained transparent after being cured and postcured. No phase separation was visually apparent.

Measurements

TEM was employed to characterize phase separation morphology in these POSS-**1** and **2** composites. A JEM-100 CXII transmission electron microscope (JEOL USA, Inc.) operating at 60 KV was used. The samples were ultramicrotomed to a thickness of approximately 70-90 nm and mounted on carbon-coated Cu TEM grids.

The dynamic storage modulus (*E'*) and loss factor (tanδ) were determined in the bending mode versus the temperature with a Rheometrics Scientific model MK III DMTA instrument. A dual-level bending mode was employed. Small-amplitude bending oscillations (both 1 and 10 Hz) were used at a gap setting of 8.00 mm. All measurements were carried out from 35 to 350 °C. The test samples were approximately 3.0-4.0 mm thick, 4.5-5.5 wide, and 38 mm long. Other DMTA runs were made at Michigan State University by A. Lee.

XRD measurements were performed to examine the potential POSS alteration of the solid-state polymer microstructure in the POSS-**1** and **2** composites. XRD can probe ordered POSS aggregates formed by phase separation. The samples were examined with

a Statton X-ray diffractometer. Cu Kα radiation (λ = 1.54 Å) was employed at a generator tension of 40 kV and a current of 45 mA. Scans were taken over the 2θ range of 5-35^{o} with a step size of 0.05^{o} at 1 s per step.

A TA Hi-Res TGA 2950 thermogravimetric analyzer was used to investigate the thermal stability of the nanocomposites. The samples (about 10 mg) were heated in nitrogen atmosphere from ambient temperature to 850 ^{o}C at a rate of 20 ^{o}C/min.

Specimens (1.0 g) of every composite were ground into a powder and immersed into a large excess of THF at room temperature for 2 months to determine if any POSS could be extracted by THF. The extraction of **1** or **2** would indicate that the extracted POSS had not been chemically bonded to the resin matrix. Concentrated residue/THF solutions from extractions were coated onto KBr plates, and THF was removed. IR spectra were obtained on an FTIR instrument (MIDAC Corp.). Residues were weighed after the removal of THF.

Results and discussion

Two comparative studies are reported. The first compares the structure-property relationships of POSS-**1** (T_8) and **2** (T_{12}) in epoxy/DDM nanocomposites. The second compares cyanate ester nanocomposites prepared with either POSS-**1** or POSS-**2**. The two macromonomers, POSS-**1** and **2**, were first synthesized and characterized followed by preparation of the composites (see experimental section and Figure 6.1). Then the epoxy/POSS-**1**/DDM and epoxy/POSS-**2**/DDM nanocomposites were compared using TEM, DMTA, FTIR and solvent extraction analysis. The comparison of the properties of PT-15/POSS-**1** and PT-15/POSS-**2** nanocomposites is described below.

The multifunctional monomers octaaminophenyl(T_8)POSS, $(C_6H_4NH_2)_8(SiO_{1.5})_8$ (Mw: 1153.63 g/mol), **1** and dodecaaminophenyl(T_{12})POSS, $(C_6H_4NH_2)_{12}(SiO_{1.5})_{12}$] (Mw: 1767.03 g/mol), **2** (Figure 5.1) were prepared by the nitration of octaphenyl(T_8)POSS and dodecaphenyl(T_{12})POSS, respectively, in fuming (98 wt%) nitric acid to produce their octanitro (yield = 90%) and dodecanitro (yield = 90%) derivatives. This was followed by nitro group reduction in dry formic acid/triethyl amine catalyzed by 5% Pd/C to POSS-**1** and POSS-**2**. Laine previously reported the application of this method to the synthesis of octaaminophenyl(T_8)POSS[76] but the experimental description was very sparse. The formic acid reductions of octanitrophenyl(T_8)POSS and dodecanitrophenyl(T_{12})POSS gave 82% and 87% isolated yields of POSS-**1** and POSS-**2**, respectively. It is essential that all water be removed from the $HCOOH/Et_3N$ solution when following this procedure. Hydroxide ions can react with the POSS cages. The amino group's positional distribution is approximately 80% meta, 15% para, and 5% (maximum) ortho, which is consistent with the electron-withdrawing nature of the Si_8O_{12} cage substituent. Thus, each of these POSS products is a complex isomer mixture. The overall structure was confirmed by ^{1}H, ^{13}C, and ^{29}Si NMR spectroscopy[77].

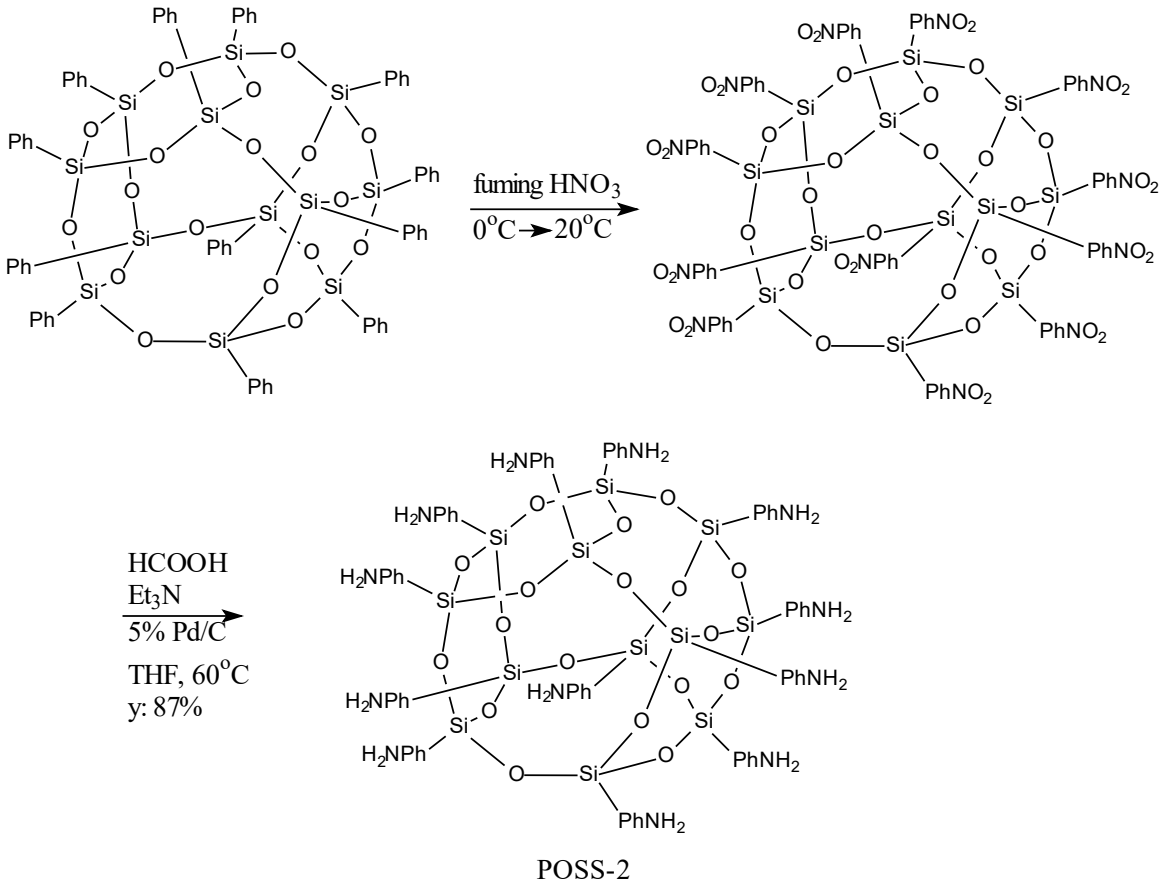

Figure 6.1 Synthesis of dodecaaminophenyl(T_{12})POSS (eg POSS-**2**)

Synthesis of epoxy nanocomposites

DGEBA was thermally cured via S_N2 substitution-ring opening by DDM to generate crosslinked resins. Aromatic amino POSS derivatives **1** or **2**, blended with DDM, were also used to cure DGEBA (see Figure 6.2 and experimental section).

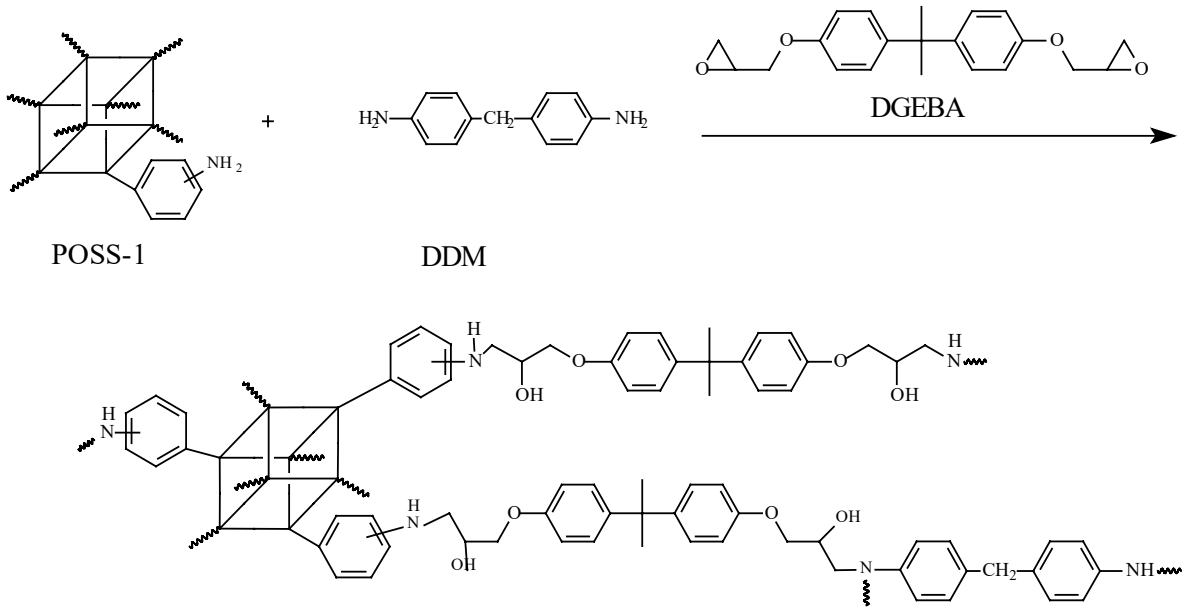

Figure 6.2 Synthesis of EPON-828/POSS-**1**/DDM composites

Synthesis of the PT-15 nanocomposites

The thermal curing of the PT-15 resin generates solid, crosslinked resins via cyclotrimerization of the OCN functions. This process forms trisubstituted triazine rings. The triazine rings serve as thermally stable crosslinking hubs throughout the resin. Amine groups add across the cyanate ester function upon mild heating or in the presence of base catalysts ($R\text{-}NH_2$ + Ar-OCN → RNHC(=NH)OAr) [78]. This addition product is primarily of importance as a catalytic intermediate in triazine ring formation [79-80]. Thus, the amino groups on POSS-**1** or **2** react easily by adding across the CN triple bond of the cyanate ester groups of PT-15 [79] which chemically bonds both **1** and **2** to cyanate ester monomers at temperatures below 60 °C. Then, at temperature above 165 °C, the cyanate ester cures without any POSS phase separation since POSS moieties are now part of a fraction of the cyanate ester monomers, which are curing (Figure 6.3). The reaction

of **1** and **2** with the cyanate ester monomers at low temperatures permits both **1** and **2** to become part of the liquid PT-15 solution prior to curing.

At 188-250 °C, PT-15 cures, incorporating **1** or **2** molecularly throughout the resin. The initial amino group addition to -OCN functions generates RNHC(=NH)OR groups [81]. However, the detailed fate of these functional groups during the subsequent 188-250 °C cure or 300 °C postcure is unknown. The presence of aminophenyl functional groups promotes the cyanate ester cure as will be demonstrated in the DMA studies discussed in a later section. The idealized final resin structure is shown in Figure 6.3. The structure shown for the resin is only suggested because the fate of the RNHC(=NH)OR functions at high temperatures is not known fully [see reference [81] for a partial description of this chemistry]. The imino-carbamate functions likely react further with –OCN functions and in other undefined ways at the 200 °C and 250 °C stages of cure.

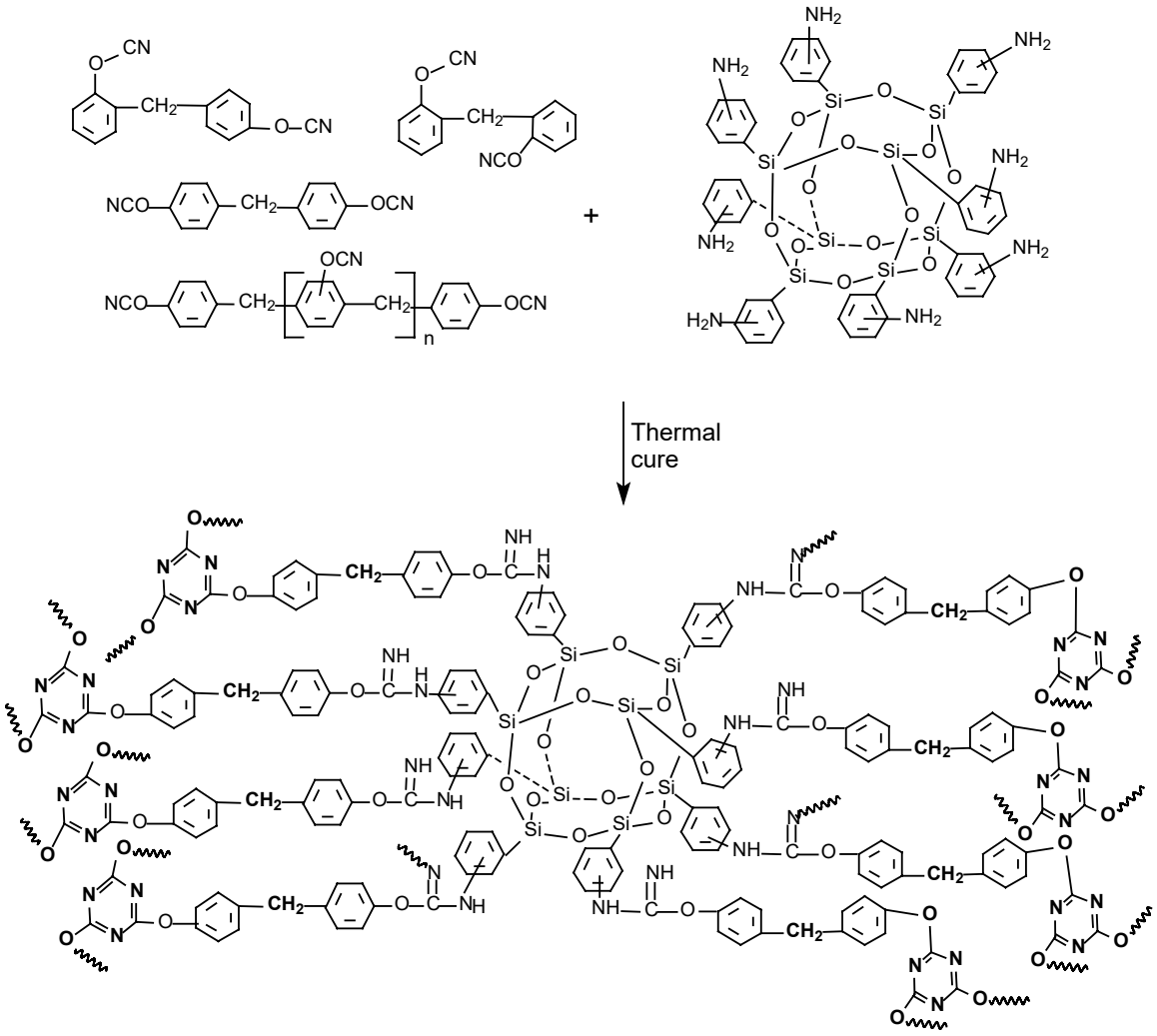

Figure 6.3 Synthesis of PT-15/POSS-**1** composites. Analogous incorporation of POSS-**2** also occurs

Morphology of epoxy/POSS-1/DDM and epoxy/POSS-2/DDM nanocomposites

POSS-**1** or -**2** and DDM were dissolved completely in THF, giving transparent solutions. After adding epoxy resin and then removing THF and curing, both epoxy/POSS-**1**/DDM and epoxy/POSS-**2**/DDM nanocomposites remained transparent.

The wide-angle X-ray diffraction (WAXD) patterns of the cured epoxy and the EPON-828/**1**/DDM composites with compositions of 5, 10, 20 and 27.72 wt% of POSS-**1**

are in Figure 6.4. The diffraction pattern of POSS-**1** is also shown for comparison. One weak amorphous peak was observed at 2θ ≈ 19° in the diffraction pattern of the neat amorphous epoxy resin.

The XRD patterns of all the EPON-828/1/DDM composites overlap almost exactly with that of neat epoxy resin. Therefore, the morphology of epoxy resin does not change significantly by adding POSS-**1**. The intensity of the 2θ ≈ 19° peak decreases as the **1** content increases. Figure 6.4 shows the diffraction pattern for POSS-**1**, which has a broadened peak at approximately 2θ ≈ 7.5°, corresponding to lattice spacing of about 11.85 Å. Since POSS-**1** is a complex isomer mixture with approximately 80 % *meta*-amino groups, 15 % or more *para*-amino groups, and about 5 % ortho amino groups, sharp narrow peaks, indicative of exact crystalline lattice spacing, were not observed for this material. This 2θ ≈ 7.5° peak was absent in the diffraction patterns of all the EPON-828/1/DDM composites. This suggests that **1** is molecularly dispersed into the epoxy network at loadings of **1** up to 27.72 wt%. No aggregation or particles of POSS-**1** with crystalline order could be detected. This is constent with molecular dispersion (no significant aggregation) of POSS-**1** due to its incorporation into cyanate ester monomer components prior to the cure. Thus phase separation could not occur during the cure.

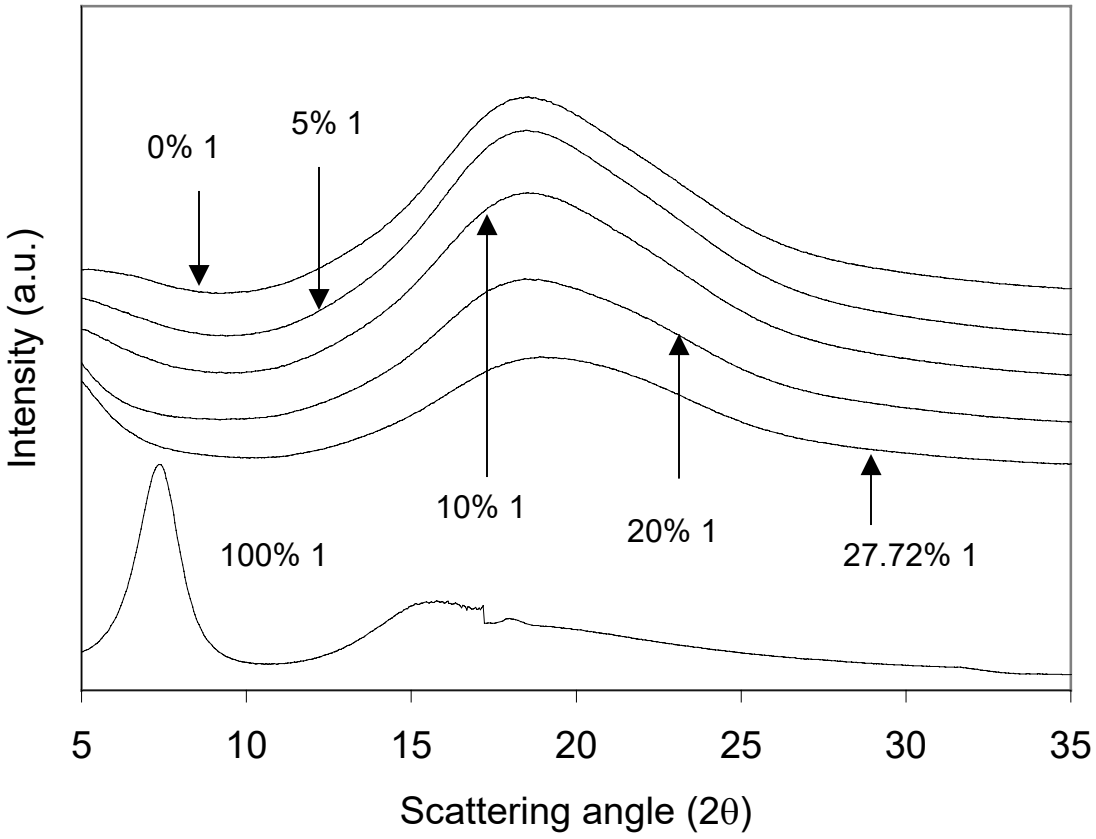

Figure 6.4 XRD patterns of the neat cured epoxy resin, its EPON-828/**1**/DDM composites, and octaaminophenyl(T_8)POSS, **1**

The wide-angle X-ray diffraction (WAXD) patterns for the epoxy resin, POSS-**2** and the 5, 10, 20 and 27.72 wt% POSS-**2** epoxy nanocomposites are displayed in Figure 6.5. POSS-**2** is also an isomer mixture. It exhibits a broadened peak at $2\theta \approx 8.1°$ corresponding to a lattice spacing of 10.85 Å. The neat epoxy resin gives a broad amorphous peak with a maximum intensity at $2\theta \approx 19°$. Similar to the behavior observed for epoxy/1/DDM nanocomposites, the $2\theta \approx 8.1°$ POSS-**2** peak was not present in any of the diffraction patterns of the EPON-828/**2**/DDM composites. No evidence for aggregation of POSS-**2** into ordered lattice was detected. The resin's amorphous peak at

$2\theta \approx 19°$ is observed in all the EPON-828/**2**/DDM composites and the intensity of this peak decreases when 5 wt% POSS-**2** is present and then increases as the content of **2** increases. These observations show **2** does not crystallize but instead is dispersed into the epoxy network as compatible POSS units.

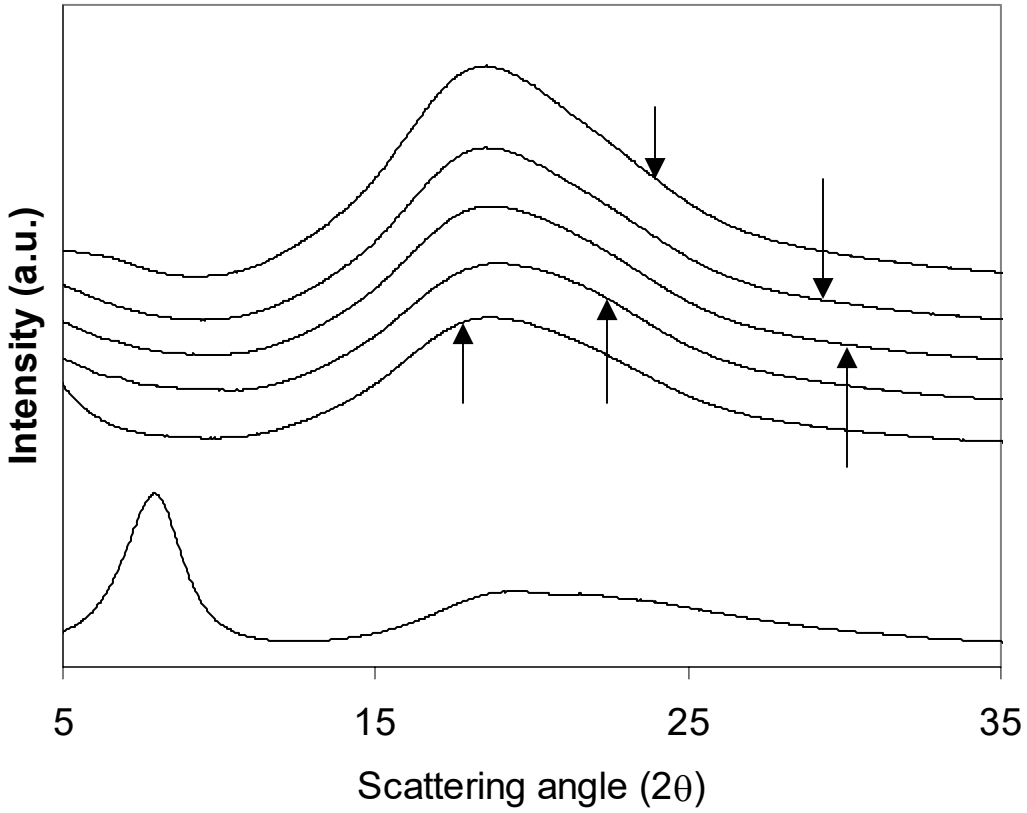

Figure 6.5 XRD patterns of the neat cured epoxy resin, its EPON-828/**2**/DDM composites, and dodecaaminophenyl(T_{12})POSS, **2**

No phase-separation (e.g. POSS particles or aggregates) could be observed for any of the transparent EPON-828/**1**/DDM and EPON-828/**2**/DDM composites with POSS contents between 5-27.72 wt% by TEM at magnifications as high as 20,000X. This indicates that POSS-**1** or **2** has been molecularly dispersed within the epoxy matrix. The

TEM observations are consistent with XRD studies that show that the POSS-**1** at 2θ ≈ 7.5° or POSS-**2** at 2θ ≈ 8.1° disappear in all the diffraction patterns of both EPON-828/**1**/DDM and EPON-828/**2**/DDM composites, even those with high weight percents of POSS.

Morphology of PT-15/POSS-2 nanocomposites

POSS-**2** completely dissolved in THF, giving transparent solutions. After adding cyanate ester resin, PT-15, and then removing the THF and curing, the PT-15/POSS-**2** composites remained transparent.

Figure 6.6 displays the wide-angle X-ray diffraction (WAXD) patterns for the PT-15 resin, POSS-**2** and the 1, 3 and 5 wt% POSS-**2** PT-15 nanocomposites. The POSS-**2** lattice peak at 2θ ≈ 8.1° from POSS-**2** are not present in any of the diffraction patterns of the PT-15/**2** composites. The PT-15 resin's amorphous peak at 2θ ≈ 20.0° is observed in all the PT-15/**2** composites. The intensity in this region increases as the **2** content increases. These observations suggest that **2** is molecularly dispersed into the PT-15 network. Crosslinking of the network occurs so that the POSS-**2** moieties, which are chemically bonded into the polymer chains, cannot aggregate during the cure. Indeed, each POSS-**2** molecule is a crosslinking hub within the network.

TEM examinations of the 1, 3 and 5 wt% POSS-**2** nanocomposites exhibited no particles or aggregate phase separation. These observations agree with XRD measurements in which the XRD peak for POSS-**2** at 2θ ≈ 8.1° disappears in all the diffraction patterns of PT-15/**2** composites.

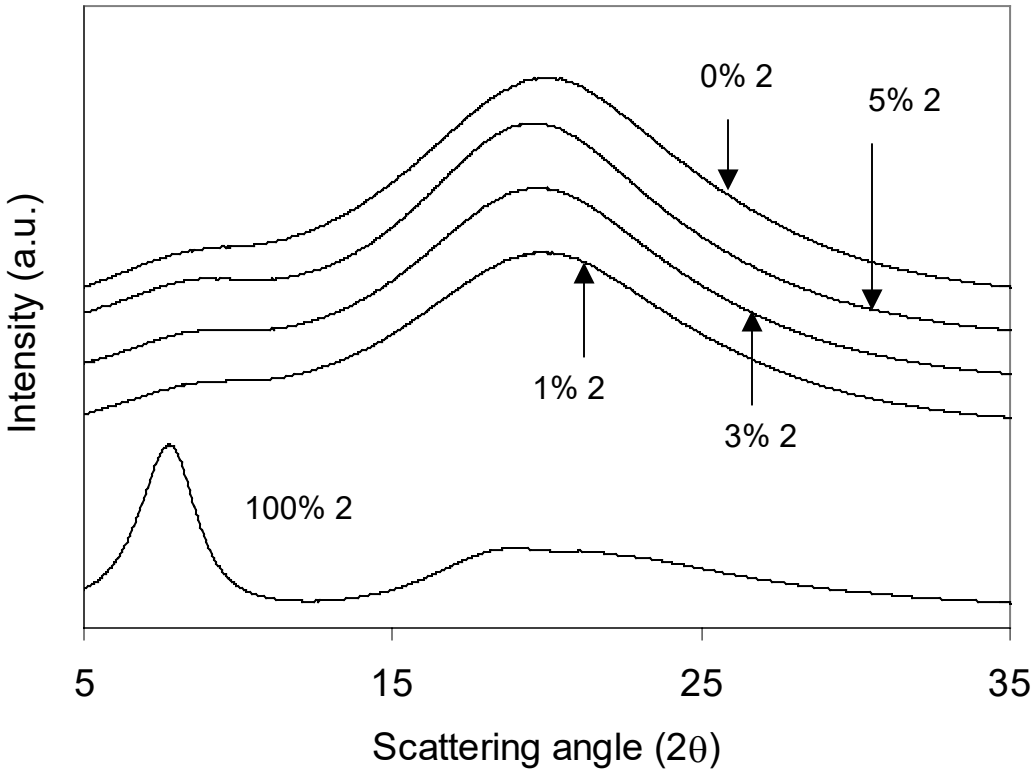

Figure 6.6 XRD patterns of the neat cured PT-15 resin, its PT-15/POSS-2 composites and dodecaaminophenyl(T_{12})POSS, **2**

POSS and DDM were dissolved completely in THF, giving transparent solutions. After the removal of THF and curing, both epoxy/POSS-**1**/DDM and epoxy/POSS-**2**/DDM nanocomposites remained transparent.

No particle formation or phase separation could be observed for the transparent EPON-828/**1**/DDM and EPON-828/**2**/DDM composites (78.63/0/21.37, 77.48/5/17.52, 76.34/10/13.66, 74.05/20/5.95 and 72.28/27.72/0 wt/wt/wt compositions for both series) with TEM at magnifications as high as 20,000X.

Viscoelastic Properties of epoxy/POSS-1/DDM nanocomposites

The bending storage moduli, E', versus temperature curves at 10Hz (from DMTA) for the neat epoxy resin and epoxy/**1**/DDM nanocomposites, containing 78.63/0/21.37, 77.48/5/17.52, 76.34/10/13.66, 74.05/20/5.95 and 72.28/27.72/0, (wt/wt/wt) EPON-828/**1**/DDM, are given in Figure 6.7. The E' values of all epoxy resin/**1**/DDM nanocomposites are higher than those of the neat epoxy resin in the rubbery region ($T>T_g$). The E' values of the 76.34/10/13.66 and 74.05/20/5.95 (wt/wt/wt) EPON-828/1/DDM nanocomposites are higher than those of the neat epoxy resin in the glassy region ($T<T_g$), but the 72.28/27.72/0 and 77.48/5/17.52 (wt/wt/wt) EPON-828/**1**/DDM nanocomposites exhibit smaller E' values than those of the epoxy resin. The neat epoxy resin and the EPON-828/**1**/DDM 77.48/5/17.52, 76.34/10/13.66, 74.05/20/5.95 and 72.28/27.72/0 (wt/wt/wt) nanocomposites at 40 °C exhibit E' values (shown in Table 6.1) of 2.47 GPa, 2.37 GPa, 2.96 GPa, 3.17 GPa and 1.32 GPa, respectively. The corresponding E' values at 200 °C ($>T_g$) are 46.3 MPa (epoxy resin), 50 MPa (5 wt% **1**), 60.3 MPa (10 wt% **1**), 52.3 MPa (20 wt% **1**) and 168 MPa (27.72 wt% **1**), respectively. The E' value for the 27.72 wt% POSS-**1** sample is about four times of that for the neat epoxy resin at 200 °C. EPON-828/**1**/DDM nanocomposites have greater load-bearing capability at high temperatures than the epoxy resin. This stability increases with increasing POSS-**1** contents.

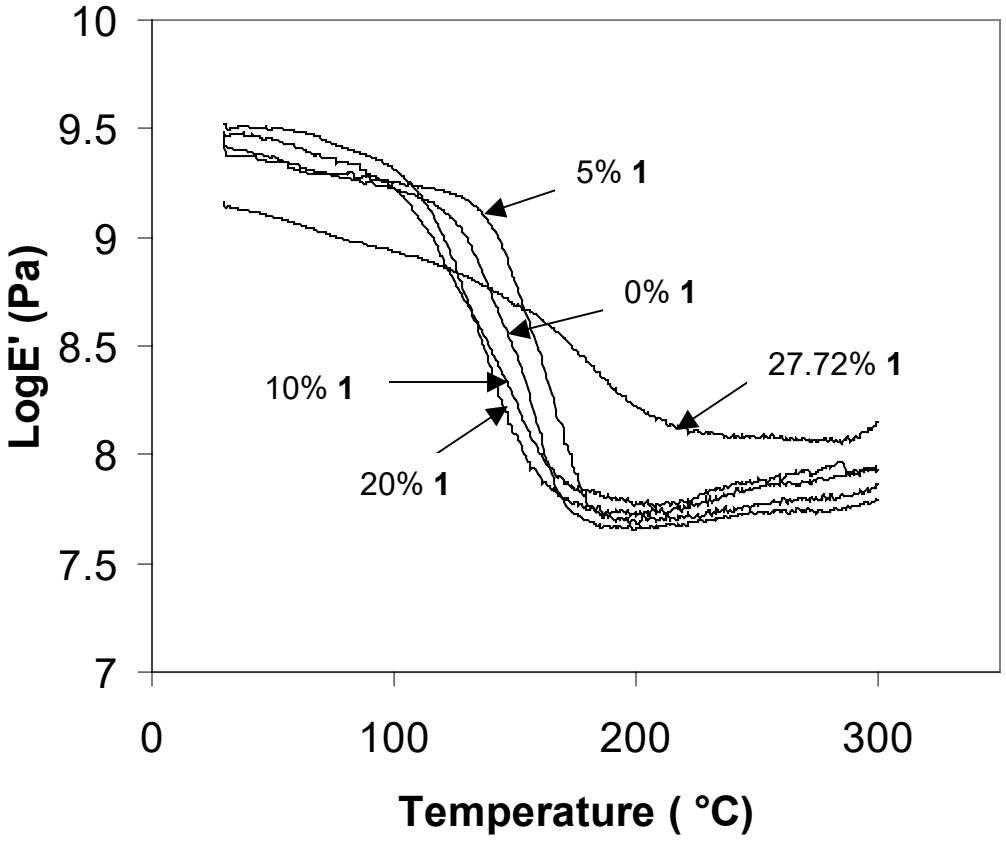

Figure 6.7 Bending storage moduli versus temperature curves at 10Hz for EPON-828/**1**/DDM nanocomposites (First heating cycle)

Table 6.1 Bending storage moduli (E'), T_g values, densities and extraction percentages of neat epoxy resin and EPON-828/POSS-**1**/DDM and EPON-828/POSS-**2**/DDM nanocomposites

Samples	T_g[a, b] (°C)	E'at 40°C[a] (GPa)	E'at 200°C[a] (MPa)	Density ρ (g/cm^3)	Weight loss (%)
Epoxy resin	157 (153)	2.47 (2.5)	46.3 (86.4)	1.186	0.31
EPON-828/**1**/DDM (77.48/5/17.52)	169 (165)	2.36 (2.36)	50 (160)	1.19	0
EPON-828/**1**/DDM (76.34/10/13.66)	162 (155)	2.96 (3.17)	60.3 (104)	1.195	0
EPON-828/**1**/DDM (74.05/20/5.95)	152 (155)	3.17 (3.14)	52.3 (134)	1.228	0.23
EPON-828/**1**/DDM (72.28/27.72/0)	180 (195)	1.32 (1.32)	168 (238)	1.233	0.11
EPON-828/**2**/DDM (77.48/5/17.52)	162 (155)	3.01 (2.87)	59.2 (96.2)	1.189	0
EPON-828/**2**/DDM (76.34/10/13.66)	164 (158)	3.24 (3.1)	73.3 (130)	1.195	0
EPON-828/**2**/DDM (74.05/20/5.95)	170 (174)	2.09 (2.01)	86.8 (115)	1.218	0.21
EPON-828/**2**/DDM (72.28/27.72/0)	185 (193)	2.04 (2.17)	190 (244)	1.22	0.12

[a] Values from the first heating cycle and second heating cycle (in parentheses) are given. The T_{max} reached in these heating cycles was 300 °C at a heating rate of 2 °C/min.
[b] T_g defined as tan δ peak temperatures

The bending tan δ (10 Hz) peak intensities drop and the peaks broaden in the first heating cycle as the content of **1** increases (Figure 6.8). The T_g values (tan δ peak temperatures) are 157, 169, 162, 152 and 180 °C, respectively, for the epoxy resin and the 5, 10, 20 and 27.72 wt% POSS-**1** epoxy nanocomposites. T_g increases as the **1** content is raised to 10 wt%. However, the T_g drops after 20 wt% of **1** was incorporated and this value increases again upon 27.72 wt% **1** addition.

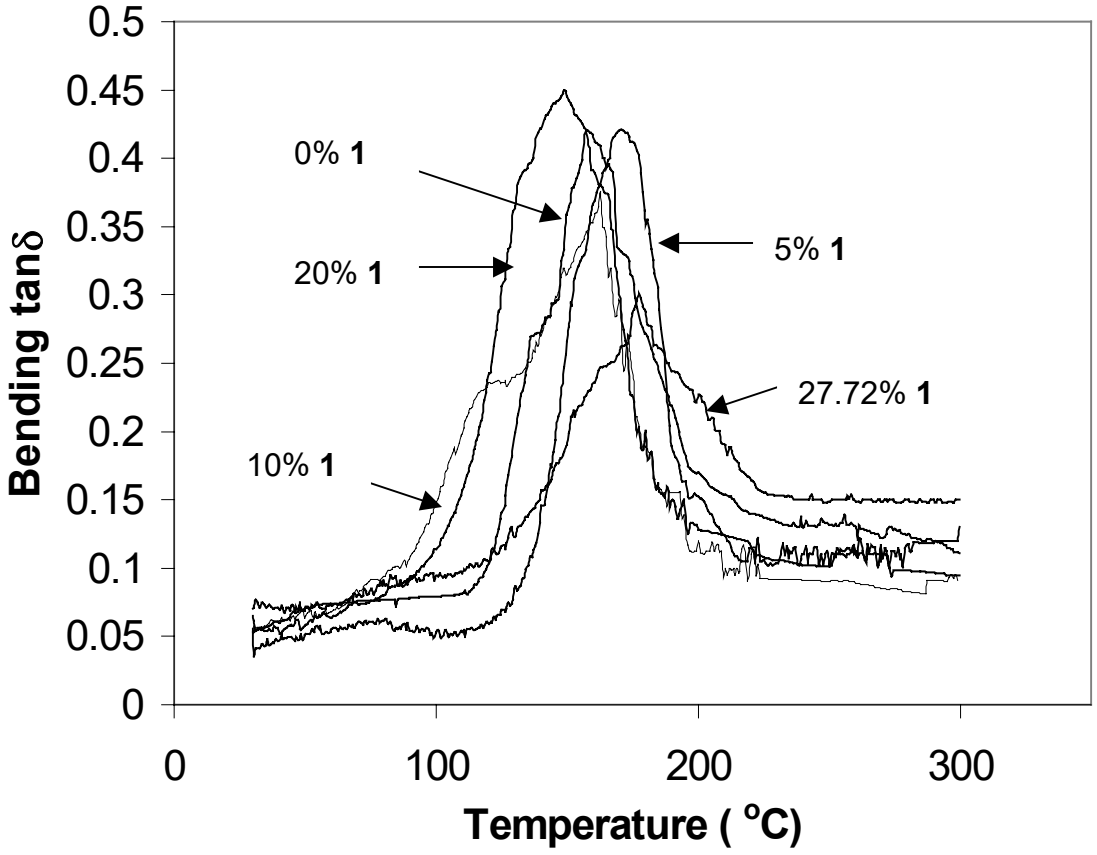

Figure 6.8 Bending tanδ versus temperature curves at 10 Hz for EPON-828/**1**/DDM nanocomposites (First heating cycle)

The effect of thermal history on the viscoelastic response of the 20 wt% POSS-**1** epoxy nanocomposite is shown in Figure 6.9. The E' values increase upon its second heating cycle over the 80-300 °C temperature range but the T_g values change little (152 and 155 °C in the first and second cycles). However, the bending tan δ peaks broaden and their peak intensities weaken during the second heating.

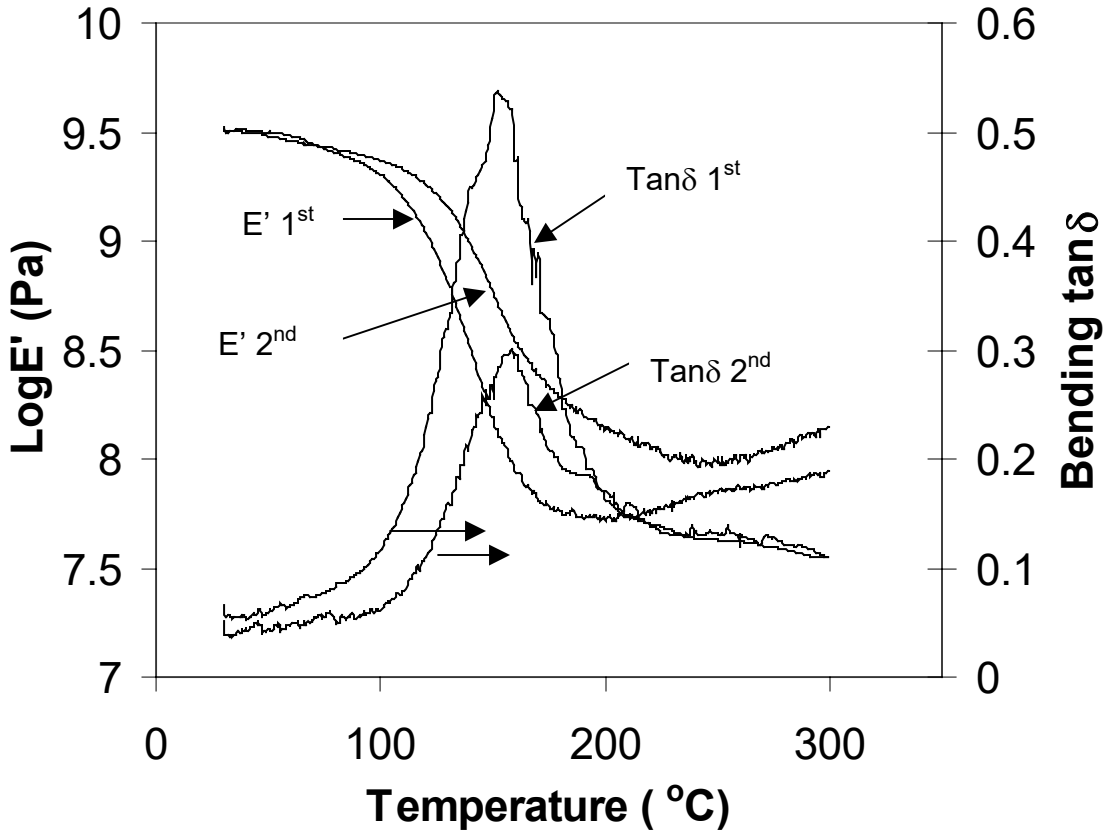

Figure 6.9 Bending storage moduli (E') and tanδ versus temperature curves at 10Hz for EPON-828/**1**/DDM 74.05/20/5.95 nanocomposite for two successive heating cycles (represented as 1st and 2nd)

The aminophenyl functions of the POSS-**1** T_8 cage easily copolymerize with the resin's epoxide functions. Each POSS cage serves as a network crosslinking site. POSS-**1** cages retard segmental motion in the epoxy network due to their high masses and the large volume crosslinked hub that each POSS moiety forms upon bonding into the network. Therefore, the POSS-**1** nanocomposites can exhibit higher T_g values and higher E' values in the rubbery region than those of the neat epoxy resin. Thus, the question arises: why is the 20 wt% POSS-**1** sample the only one in the series to exhibit a lower T_g

than that of the neat epoxy? This sample still exhibits higher E' values in the rubbery region than those of the neat epoxy resin. One tentative suggestion is that this lower T_g value might be due to a reactivity race between amino functions on POSS-**1** and DDM. The DDM amino functions have a higher reactivity than those of the POSS-**1** amino groups due to the electron withdrawing effects of the O_3Si groups on the aryl rings in **1**. Thus, the POSS-**1**/DDM amine group ratio increases during the cure (monomer drift). Also, the DDM amino groups promote more curing at lower temperature. Thus, changes in network structure might reduce the fraction of POSS amino groups bound into the epoxy, lowering the number of restrictions on segmental motion within the matrix. However, the fraction of epoxy segments to which POSS-**1** is bound would help resist deformation at high temperature ($T>T_g$).

Viscoelastic Properties of epoxy/POSS-2/DDM nanocomposites

The bending storage moduli, E', versus temperature curves at 10 Hz (from DMTA) for the neat epoxy resin and EPON-828/**2**/DDM nanocomposites, containing 5, 10, 20 and 27.72 wt% POSS-**2** are shown in Figure 6.10 (first heating cycle). Below T_g, differences exist among the E' values of the neat epoxy resin and the 5, 10, 20 and 27.72 wt% POSS-**2** nanocomposites. The EPON-828/**2**/DDM nanocomposites with 20 and 27.72 wt% **2** display lower E' values than those of the other nanocomposites containing ≤10 wt% **2**. The bending storage moduli at 40 °C are 2.47 GPa (epoxy resin), 3.01 GPa (5 wt% **2**), 3.24 GPa (10 wt% **2**), 2.09 GPa (20 wt% **2**), 2.04 GPa (27.72 wt% **2**). However, at $T>T_g$, all nanocomposites containing **2** exhibit higher E' values than those of the neat epoxy resin. These E' values increase with an increase of **2** loading. These E' values at

200 °C (>T_g) are 43.63 Mpa (neat epoxy resin) and 59.2, 73.3, 86.8 and 190 MPa for the systems with 5, 10, 20 and 27.72 wt% of **2** respectively. These E' values are higher than those of the POSS-**1** series when compared at equal wt% of POSS.

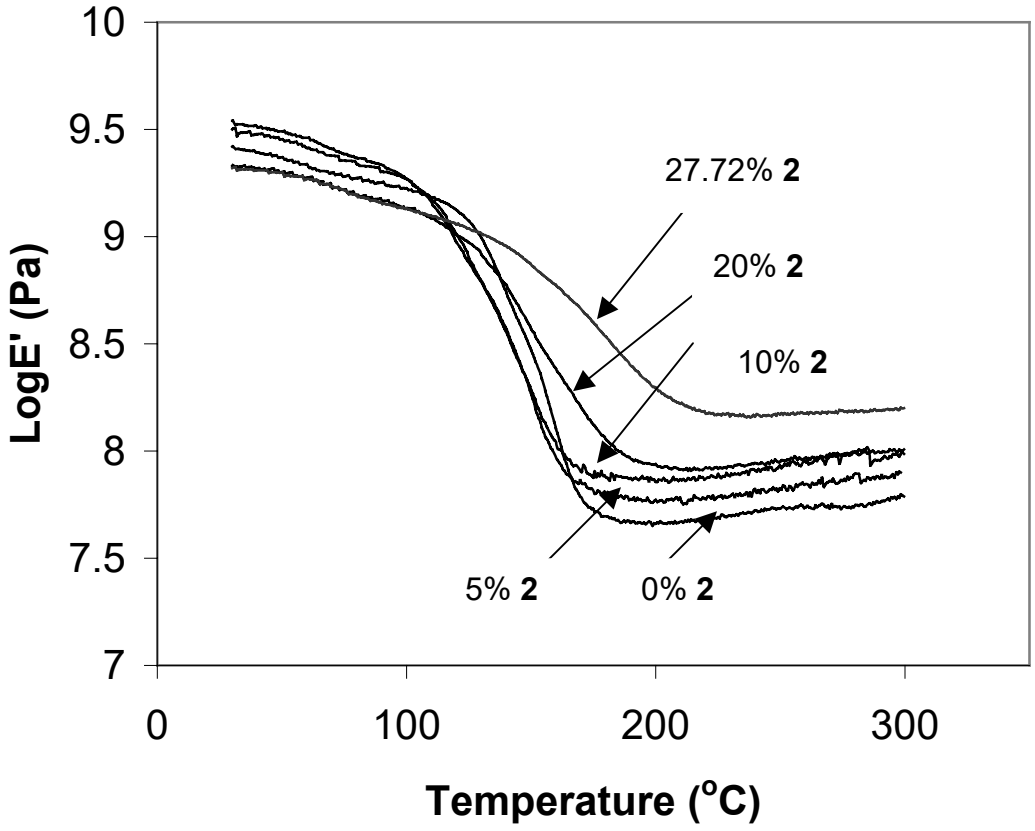

Figure 6.10 Bending storage moduli (E') versus temperature curves at 10Hz for EPON-828/**2**/DDM nanocomposites (First heating cycle)

The bending tanδ versus temperature curves (10 Hz) for the epoxy and its epoxy/**2**/DDM nanocomposites are shown in Figure 6.11 The tanδ peak intensities are lowered and their widths are broadened by incorporation of POSS-**2** in the first heating cycle, similar to the behavior observed for epoxy/**1**/DDM nanocomposites. The T_g values (tanδ peak temperatures) increase with increasing POSS-**2** content. They are 157 °C, 162

°C, 164 °C, 170 °C, 185 °C, for the neat epoxy resin and the 5, 10, 20 and 27.72 wt% **2** nanocomposites, respectively. This regular behavior contrasts with that observed with the epoxy/**1**/DDM nanocomposites.

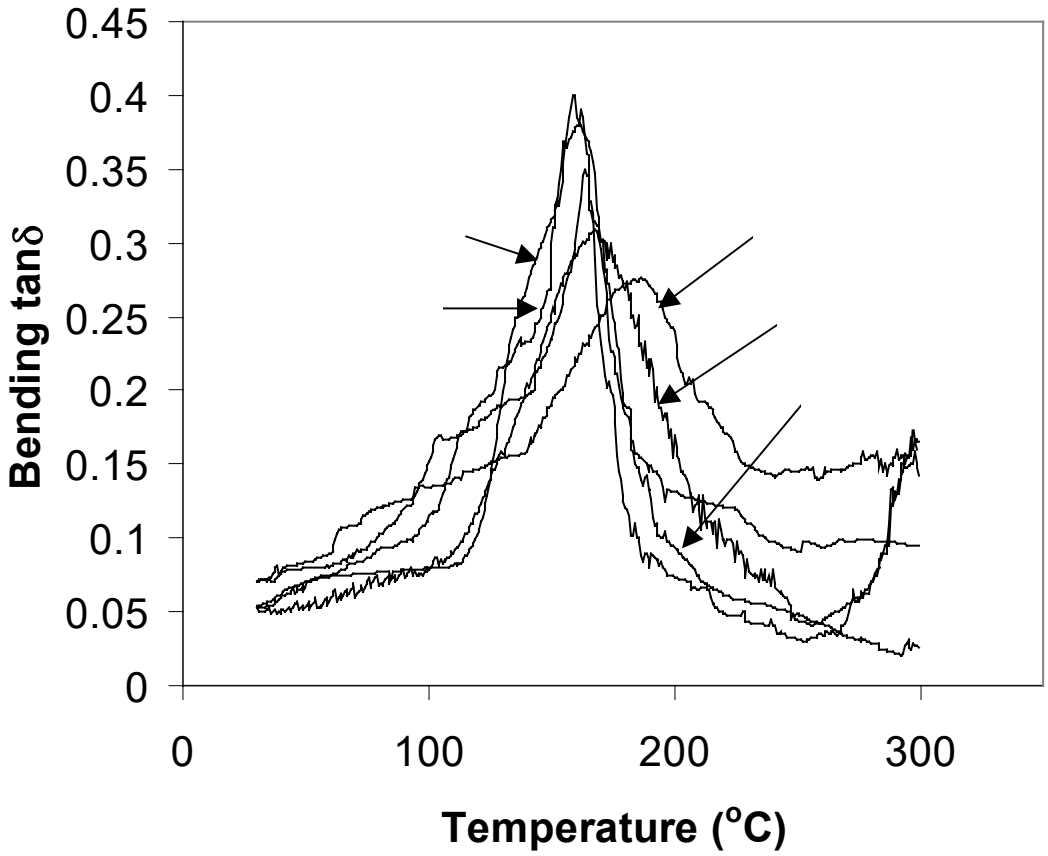

Figure 6.11 Bending tanδ versus temperature curves at 10 Hz for EPON-828/**2**/DDM nanocomposites (First heating cycle)

The effect of thermal history on the viscoelastic properties of the 74.05/20/5.95 (wt/wt) EPON-828/**2**/DDM nanocomposite was studied through two heating cycles (Figure 6.12). The E' values increase over the entire 30-350 °C range in the second heating cycle. T_g values increased going from 170 °C in the first heating cycle to 173.5 °C in the second heating cycle. Furthermore, the tanδ peaks broaden and their intensities

decrease in the second cycle. The most pronounced effects are the large increases in E' at T>T_g in the second heating cycle. For example, E' at 200 °C goes from 50 to 160 MPa for the 5 wt% POSS-**1** sample and from 73 to 130 MPa for the 10wt% POSS-2 sample (see Table 5.1). Large E' values were observed at 200 °C for POSS-**1** and **2** systems after heating through the first DMA cycle which went to a maximum of 300°C. The 27.72 wt% samples of **1** and **2** exhibited E' values of 238 and 244 MPa, respectively.

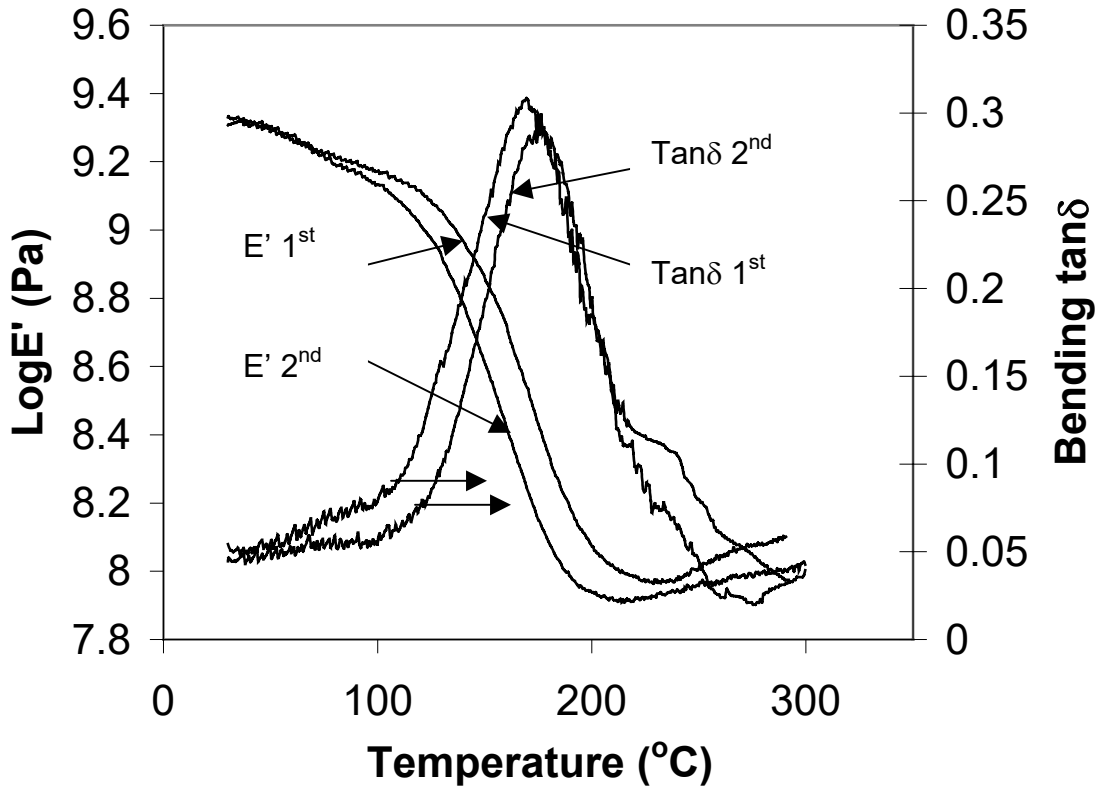

Figure 6.12 Bending storage moduli (E') and tanδ versus temperature curves at 10 Hz for EPON-828/**2**/DDM 74.05/20/5.95 nanocomposite for two successive heating cycles

The POSS-**2** monomer contains a D_{2h} T_{12} cage. There are twelve aryl amino substituents on POSS-**2**, which can react with the epoxide functions of the epoxy resin. Thus, more spokes eminate from each T_{12} cage to bind the network than are present in the T_8 cages. Segmental motion will be retarded greatly at these massive crosslinked POSS hubs with 8 and 12 spokes respectively. POSS-**2** nanocomposites exhibit higher T_g values and higher E' values in the rubbery region than those of the neat epoxy resin.

Viscoelastic Properties of PT-15/POSS-2 nanocomposites

Samples which had only been cured previously at 188 °C were selected for DMA studies. The pure PT-15 sample exhibited a large initial drop in E' when heating to over 200 °C. However, the magnitude of E' as the temperature was steadily raised to 300 °C recovered due to further curing. The first heating of the 1 wt% POSS-**2** sample showed a similar drop in bending storage modulus (E') at ~200-250 °C due to further curing followed by a rise in E' as the temperature was increased to 300 °C (Figure 6.13). However, subsequent heating cycles exhibited a T_g = 310 °C and E' ≈ 176 MPa at 360 °C. Both values are lower than that of the pure PT-15 resin (T_g = 325-330 °C, E' ≈ 287 MPa at 360 °C). The first and second heating cycles of the 5 wt% POSS-**2** system looked similar because this system was more fully cured at lower temperatures than the 1wt% POSS-**2** sample due to catalysis by the higher concentration of POSS-**2** amine groups present. No further curing seemed to occur on the second heating of the 5 wt% POSS-**2** sample. The T_g value (~240 °C, 2nd heating) was much lower than that of the neat PT-15

resin or the 1 wt% POSS-**2** composite. The E' vs temperature plots for these three fully cured systems are compared in Figure 6.14.

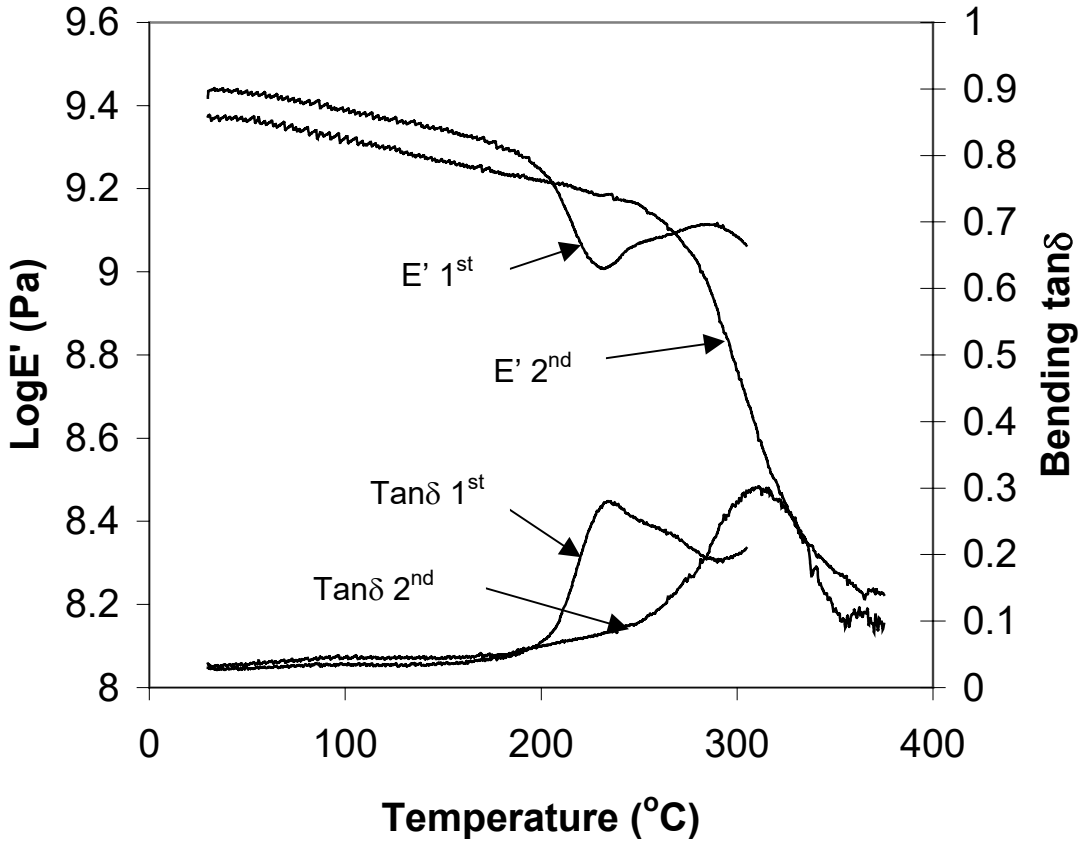

Figure 6.13 Bending storage moduli (E') and tanδ versus temperature curves at 10 Hz for PT-15/1wt% POSS-**2** nanocomposite for two successive heating cycles

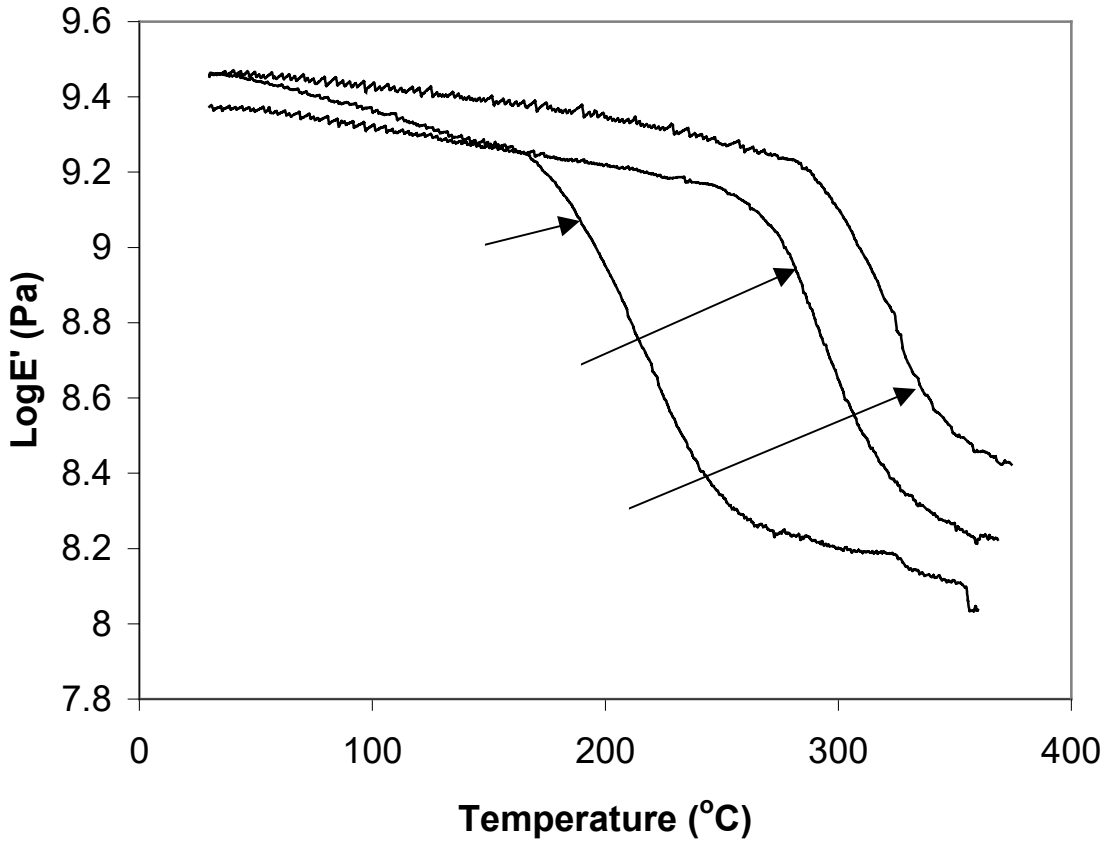

Figure 6.14 Bending storage moduli (E') versus temperature curves at 10 Hz for PT-15/POSS-**2** nanocomposites (Second heating cycle)

It is clear that progressive addition of POSS-**2** catalyzes the cure at lower temperatures. When 5 wt% POSS-**2** was used, the cure was close to complete after holding at 188 °C. Further heating to 300 °C produced little change in the E' curves. However, a large amount of further curing occurred with pure PT-15.

Thermal Stability of epoxy/POSS/DDM nanocomposites

Thermogravimetric analysis (TGA) was used to investigate the thermal stability of the POSS-containing epoxy and cyanate ester nanocomposites. The improvement in

thermal stability for two composite systems by incorporating POSS-**1** or **2** was observed from the rates of weight loss from segmental decomposition and from the ceramic yields.

The TGA curves of the neat cured epoxy resin, POSS-**1** and EPON-828/**1**/DDM nanocomposites recorded at 20 ^{o}C/min in a nitrogen atmosphere are shown in Figure 6.15. All the TGA curves displayed similar degradation profiles over the entire temperature range. The presence of POSS-**1** did not significantly change the degradation pattern of the epoxy matrix polymers. The temperatures of degradation (T_{10} and T_{50}) were taken as the initial thermal decomposition temperature (T_{10}) at which a 10 wt% of mass loss occurred and the mid-point thermal decomposition temperature (T_{50}) where 50 wt% of the total original composite mass loss occurred. The initial decomposition temperatures (T_{10}) of the 77.48/5/17.52 and 76.34/10/13.66 (wt/wt/wt) EPON-828/**1**/DDM nanocomposites are lower than that of the neat epoxy resin, but the 74.05/20/5.95 and 72.28/27.72/0 (wt/wt/wt) EPON-828/**1**/DDM nanocomposites exhibit higher T_{10} values than that of the neat epoxy resin. The neat epoxy resin and the EPON-828/**1**/DDM 77.48/5/17.52, 76.34/10/13.66, 74.05/20/5.95 and 72.28/27.72/0 (wt/wt/wt) nanocomposites exhibit T_{10} values of 368, 360, 357, 371, and 397 ^{o}C, respectively.

The mid-point decomposition temperatures (T_{50}) of all epoxy resin/**1**/DDM nanocomposites are higher than that of the neat epoxy resin. The corresponding T_{50} values are 394 ^{o}C (epoxy resin), 401 ^{o}C (5 wt% **1**), 416 ^{o}C (10 wt% **1**), 426 ^{o}C (20 wt% **1**) and 449 ^{o}C (27.72 wt% **1**), respectively. These T_{50} values increase progressively with an increase of **1** loading.

The ceramic yields of all epoxy resin/**2**/DDM nanocomposites are higher than that of the neat epoxy resin. The ceramic yields at 850 °C rise with higher POSS-**1** contents. These ceramic yields at 850 °C are 14 % (neat epoxy resin) and 22, 27, 28 and 33 % for the systems with 5, 10, 20 and 27.72 wt% of **1** respectively.

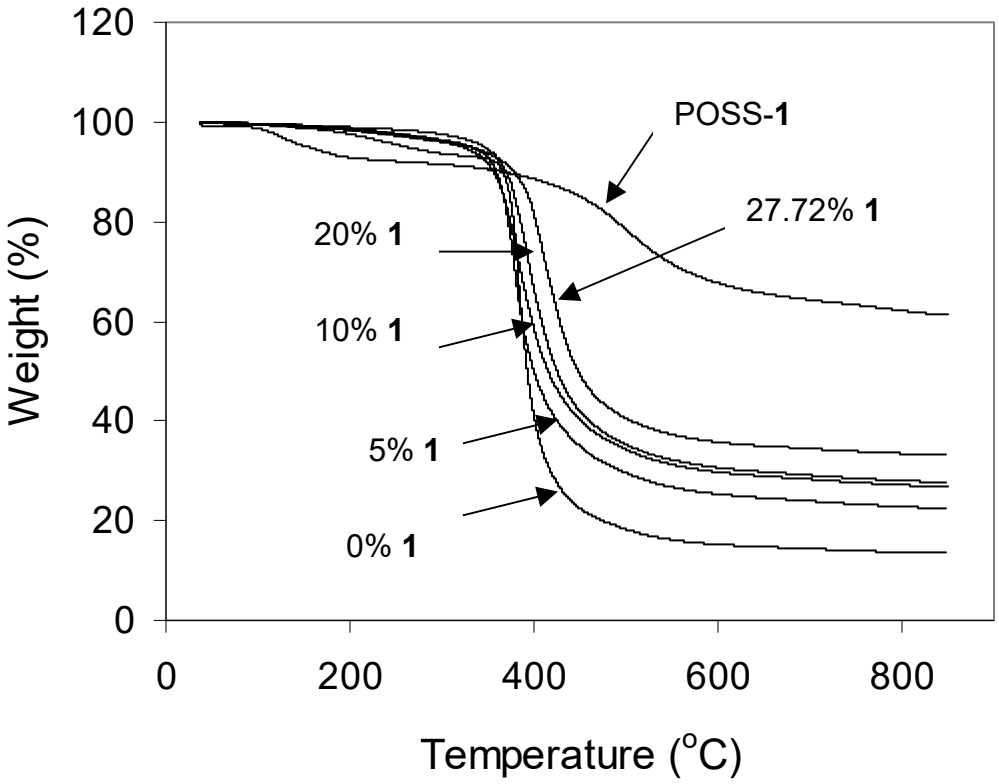

Figure 6.15 TGA thermograms of the neat cured epoxy resin, its EPON-828/**1**/DDM composites, and octaaminophenyl(T_8)POSS, **1**

The TGA curves of the neat cured epoxy, POSS-**2** and EPON-828/**2**/DDM nanocomposites recorded at 20 °C/min in a nitrogen atmosphere are shown in Figure 6.16. The thermal behavior of the POSS-**2** composites versus POSS loading differs from somewhat that of the POSS-**1** systems. The initial decomposition temperatures (T_{10}) of

the 5 and 10 wt% POSS-**2** nanocomposites (374 and 384 °C, respectively) are higher than that of the neat epoxy resin (368 °C). The T_{10} values of the 20 and 27.72 wt% **2** nanocomposites remained almost unchanged (366 and 368 °C). The mid-point decomposition temperatures (T_{50}) of all epoxy resin/**2**/DDM nanocomposites are higher than that of the neat epoxy resin. These T_{50} values are 394 (neat epoxy resin) and 431, 446, 406 and 418 ^{o}C for the systems with 5, 10, 20 and 27.72 wt% of **2** respectively. Adding more than 10 wt% **2** begins to lower thermal stability. The ceramic yields of all the °C epoxy resin/**2**/DDM nanocomposites are higher than that of the neat epoxy resin. These ceramic yields at 850 °C are 14 (neat epoxy resin) and 33, 28, 21 and 25 % for the systems with 5, 10, 20 and 27.72 wt% of **2** respectively. It is not clear why the ceramic yield doesn't continue to rise as the POSS-**2** content increases.

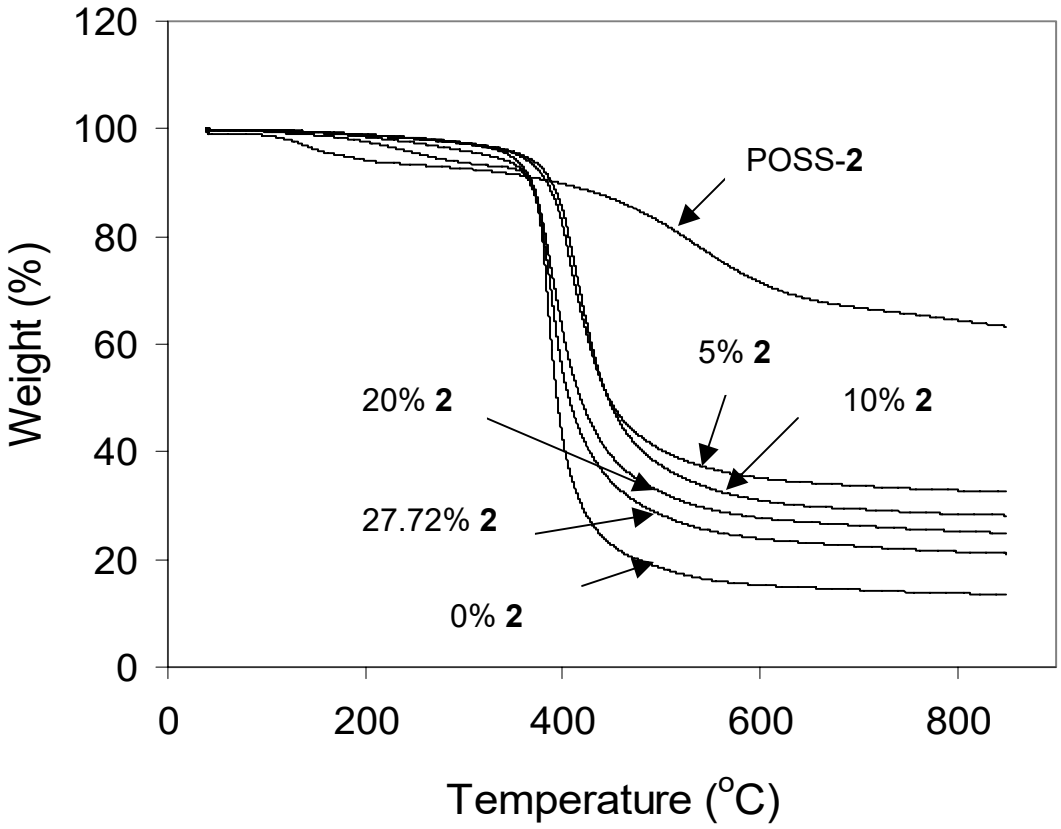

Figure 6.16 TGA thermograms of the neat cured epoxy resin, its EPON-828/**2**/DDM composites, and dodecaaminophenyl(T_{12})POSS, **2**

The incorporation of POSS-**1** or **2** into epoxy resin network generally leads to lower rates of mass loss and enhanced char yields at high temperatures. This effect was increasingly pronounced with increasing the content of **1** in EPON-828/**1**/DDM systems. The high thermal stability of epoxy nanocomposites containing POSS-**1** or **2** may result from the nano-scaled dispersion of POSS molecules into the epoxy matrices and a strong POSS-epoxy covalent bond network, which hinders the continuous decomposition of the epoxy matrix as organic decomposition occurs. Some carbon and oxygen from the epoxy combines with the inorganic $(SiO_{1.5})_n$ cores to form CSiO-containing chars. The high

aromatic contents of the POSS molecules probably assist the thermal stability of these epoxy nanocomposites.

Thermal stability of PT-15/POSS-2 nanocomposites

Figure 6.17 displays the TGA curves of the neat PT-15, POSS-**2** and PT-15/POSS-**2** nanocomposites recorded at 20 ^{o}C/min in the nitrogen atmosphere. The 1 and 3 wt% POSS-**2** nanocomposites exhibit T_{10} values quite similar to that of the neat PT-15 resin while the 5 wt% POSS-**2** nanocomposite has a lower T_{10} value than that of the PT-15 resin. These T_{10} temperatures are 429 ^{o}C (PT-15), 431 ^{o}C (1 wt% **2**), 427 ^{o}C (3 wt% **2**), and 417 ^{o}C (5 wt% **2**), respectively. The mid-point decomposition temperatures (T_{50}) of all PT-15/**2** nanocomposites are lower than that of the neat epoxy resin. The corresponding T_{50} values are 573 ^{o}C (epoxy resin), 566 ^{o}C (1 wt% **2**), 535 ^{o}C (3 wt% **2**) and 471 ^{o}C (5 wt% **2**), respectively. All nanocomposites containing **2** exhibit lower char yields than that of the PT-15 resin. At 850°C, these yields are 60 (PT-15) and 59, 57 and 52% for the systems with 1, 3 and 5 wt% of **2** respectively. The weight loss rates increased and char yield decreased upon increasing the POSS-**2** content in the PT-15 resin. No improvement in the thermal stability was achieved adding POSS-**2**. Furthermore, thermal properties decreased with increased POSS-**2** loading in these nanocomposites. This might result from an increase in unreacted POSS-**2** amino groups as the POSS loading goes up.

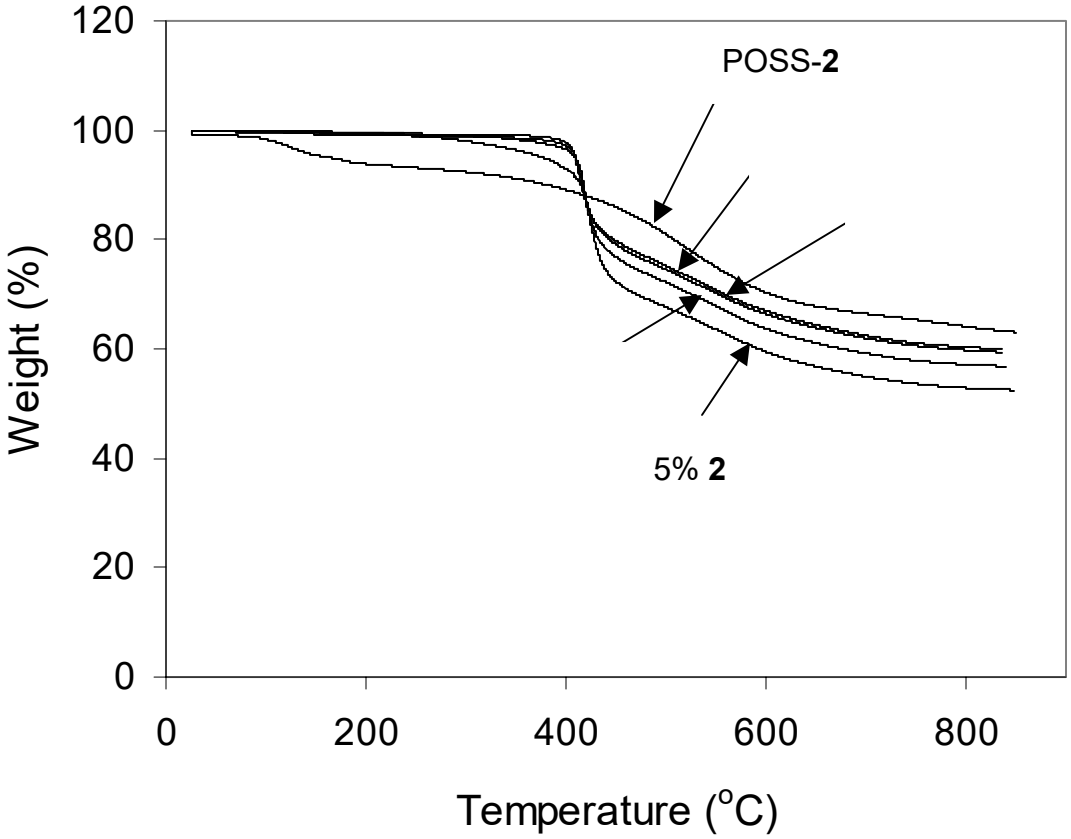

Figure 6.17 TGA thermograms of the neat cured PT-15 resin, its PT-15/**2** composites, and dodecaaminophenyl(T_{12})POSS, **2**

Densities, Solvent Swelling/extraction and IR Data for epoxy/POSS/DDM nanocomposites

Densities of the neat epoxy resin, EPON-828/**1**/DDM and EPON-828/**2**/DDM nanocomposites are listed in Table 6.1. The densities for all EPON-828/**1**/DDM and EPON-828/**2**/DDM nanocomposites are higher than that of the neat epoxy resin. These densities increase with an increase of POSS-**1** and **2** content. None of these systems swelled after being submerged in THF for 3 months. The resulting THF solutions were evaporated after removing the samples. The extracted residues were studied by FT-IR. Only very small amounts of epoxy resin oligomers (0.15-0.31 wt %) were extracted

(Table 6.1). No **1** or **2** was detected in these residues. Both sets of resins were ground into powders and extracted for 48h in refluxing THF. No extracted POSS-**1** or **2** could be found after filtration and evaporation of the THF. The FT-IR spectra of **1** and **2** exhibit strong SiO cage absorptions at 1115-1107 cm^{-1} and a NH stretch at 3455 cm^{-1}. These bands were not present in the extracted residues. Thus, all of the macromers **1** or **2** had been chemically incorporated into the nanocomposite networks.

Solvent Swelling/extraction for PT-15/POSS nanocomposites

Extraction of powdered cyanate ester/POSS-**1** and POSS-**2** resins with excess refluxing THF for periods up to 20 h did not generate any POSS-containing soluble residues upon filtering and removal of solvent. Thus, both of these monomers have been chemically bounded into the resin matrix.

Conclusions

Two multifunctional monomers octaaminophenyl(T_8)POSS [**1**, $(C_6H_4NH_2)_8(SiO_{1.5})_8$] and dodecaaminophenyl($T_{12}$)POSS [**2**, $(C_6H_4NH_2)_{12}(SiO_{1.5})_{12}$] were synthesized, characterized and then incorporated into two types of thermoset resins: (1) Cyanate ester resin, PT-15, and (2) epoxy/4,4'-diaminodiphenylmethane (DDM) resin.

The epoxy resin/DDM nanocomposites containing POSS-**1** or POSS-**2** exhibit higher E' values than those of the neat epoxy resin in the rubbery region ($T>T_g$). The E' values at $T>T_g$ are very large in the second DMA heating cycle as POSS loading increases. The tan δ peak intensities decrease and the peaks broaden in the first heating cycle as the content of **1** or **2** increases. The T_g increases as the content of **1** or **2** is raised.

The E' values continue to increase upon its second heating cycle over the 80-300 °C temperature range for the 20 wt% POSS-**1** EPON-828/DDM nanocomposite. Also, the bending tan δ peaks broaden and their peak intensities decrease during the second heating. These nanocomposites exhibit better high temperature properties versus those of the neat epoxy resin. Their T_g and E' values at T>T_g increase with an increase of **2** loading over the entire 30-350 °C range increase in the second heating cycle.

Incorporation of POSS-**1** and **2** into cyanate ester, PT-15, serves to catalyze the curing reaction. In contrast to the epoxy systems, the cyanate ester itself has a very high T_g and progressive incorporation of POSS-**2** lowers the T_g.

TGA indicates that the presence of POSS-**1** and **2** did not significantly change the degradation pattern of the epoxy matrix polymers, whereas the properties of oxidation resistance of the materials were significantly enhanced. The improved thermal stability of epoxy nanocomposites containing POSS-**1** or **2** may result from the nano-scaled dispersion of POSS molecules into the epoxy matrices and a strong POSS-epoxy covalent bond network.

No improvement in the thermal stability was achieved adding POSS-**2** into cyanate ester, PT-15. Furthermore, thermal properties decreased with increased the POSS-**2** loading in these nanocomposites. This might result from an increase in unreacted POSS-**2** amino groups as the POSS loading goes up. Also, the normal packing of the highly crosslinked cured PT-15 resin would be disrupted in the vicinity of the ponderous T_{12}-POSS cages. This could interfere with cohesive chain-chain interactions among neighboring segments, lowering the cohesive energy density in these regions.

XRD, TEM, extraction and IR data all show that all of the POSS-**1** or POSS-**2** is molecularly dispersed and chemically bonded into the continuous matrix phase on a molecular scale in all of the epoxy and cyanate ester systems.

References

[1] Giannelis, E. P., *Adv. Mater.* 1996, 8, 29.

[2] Jog, J. P., Hambir, S., Bulakh, N., *Polym. Eng. Sci.*, 2002, 42, 1800.

[3] Kim, D. S., Lee, K. M., *J. Appl. Polym. Sci.*, 2003, 90, 2629.

[4] Liu, Z. J., Chen, K. Q., Yan, D. Y., *Eur. Polym. J.*, 2003, 39, 2359.

[5] Priya, L., Jog, J. P., *J Polym Sci Part B: Polym. Phys.*, 2002, 40, 1682.

[6] Wang, Y. Z., Zhang, L. Q., Tang, C. H., Yu, D. S., *J. Appl. Polym. Sci.*, 2000, 78, 1879.

[7] Bureau, M., Denault, N. J., Cole, K. C., Enright, G. D., *Polym. Eng. Sci.*, 2002, 42, 1897.

[8] Wan, C.Y., Qiao, X. Y., Zhang, Y., Zhang, X. Y., *Polym. Test.*, 2003, 22, 453.

[9] Wu, S. H., Wang, F. Y., Ma, C. C. M., Chang, W. C., Kuo, C. T., Kuan, H. C., Chen, W. J., *Mater. Lett.*, 2001, 49, 327.

[10] Burnside, S. D., Giannelis, E. P., *Chem. Mater.*, 1995, 7, 1597.

[11] Agag, T., Koga, T., Takeichi, T., *Polymer*, 2001, 42, 3399.

[12] Kodgire, P., Kalgaonkar, R., Hambir, S., Bulakh, N., Jog, J. P., *J. Appl. Polym. Sci.*, 2001, 81, 1786.

[13] Chen, Z., Gong, K., *J. Appl. Polym. Sci.*, 2002, 84, 1499.

[14] Gilman, J. W., *Appl. Clay. Sci.*, 1999, 15, 31.

[15] Lepoittevin, B., Devalckenaere, M., Pantoustier, N., Alexandre, M., Kubies, D., Calberg, C., Jerome, R., Dubois, P., *Polymer*, 43, 4017.

[16] Gu, A. J., Liang, G. Z., *Polym. Degrad. Stab.*, 2003, 80, 383.

[17] Bourbigot, S., Devaux, E., Flambard, X., *Polym. Degrad. Stab.*, 2002, 75, 397.

[18] Gilman, J. W., Kashiwagi, T., Lichtenhan, J. D.,*SAMPE J*, 1997, 33, 40.

[19] Romo-Uribe, A., Mather, P. T., Haddad, T. S., Lichtenhan, J. D., *J. Polym. Sci. Part B: Polym. Phys.*, 1998, 36, 1857.

[20] Mather, P. T., Jeon, H. G., Romo-Uribe, A., Haddad, T. S., Lichtenhan, J. D., *Macromolecules*, 1999, 32, 1194.

[21] Lee, A., Lichtenhan, J. D., *J. Appl. Polym. Sci.*, 1999, 73, 1993.

[22] Jeon, H. G., Mather, P. T., Haddad, T. S., *Polym. Int.*, 2000, 49, 453.

[23] Fu, B. X., Hsiao, B. S., Pagola, S., Stephens, P., White, H., Rafailovich, M., Sokolov, J., Mather, P. T., Jeon, H. G., Phillips, S., Lichtenhan, J. D., Schwab, J., *Polymer*, 2001, 42, 599.

[24] Gonzalez, R. I., Phillips, S. H., Hoflund, G. B., *J. Spacecraft Rockets*, 2000, 37, 463.

[25] Lichtenhan, J. D., Otonari, Y. A., Carr, M. J., *Macromolecules*, 1995, 28, 8435.

[26] Haddad, T. S., Lichtenhan, J. D., *Macromolecules*, 1996, 29, 7302.

[27] Simon, S. L., Gillham, J. K., *J. Appl. Polym. Sci.*, 1993, 47, 461.

[28] Yeh, J. M., Chin, C. P., *J. Appl. Polym. Sci.*, 2003, 88, 1072.

[29] Wang, Z., Pinnavaia, T. J., *Chem. Mater.*, 1998, 10, 1820.

[30] Alexandre, M., Dubois, P., *Mater. Sci. Eng. Rep.*, 2000, 28, 1.

[31] Gangun, S., Dean, D., *Polymer*, 2003, 44, 1315.

[32] Ganquli, S., Dean, D., Vaia, R., *Polym. Mater. Sci. Eng.*, 2002, 87, 94.

[33] Dufresne, A., Paillet, M., Putaux, J. L., Canet, R., Carmona, F., Delhaes, P., *J. Mater. Sci.*, 2002, 37, 3915.

[34] Penumadu, D., Dutta, A., Pharr, G. M., Files, B., *J. Mater. Res.*, 2003, 18, 1849.

[35] Thostenson, E. T., Chou, T. W., *J. Phys. D: Appl. Phys.*, 2002, 35, L77.

[36] Bai, J. B., Allaoui, A., *Compos. A*, 2003, 34, 689.

[37] Kuriger, R. J., Alam, M. K., Anderson, D. P., Jacobsen, R. L., *Compos. A*, 2002, 33, 53.

[38] Shofner, M. L., Rodriguez-Macias, F. J., Vaidyanathan, R., Barrera, E. V., *Compos. A*, 2003, 34, 1207.

[39] Kuriger, R. J., Alam, M. K., *Polym. Compos.*, 2001, 22, 604.

[40] Gordeyev, S. A., Ferreira, J. A., Bernardo, C. A., Ward, I. M., *Mater. Lett.*, 2001, 51, 32.

[41] Lakshminarayanan, P. V., Toghiani, H., Pittman, Jr, C. U., *Carbon*, 2004, 42, 2433.

[42] Patton, R. D., Pittman, Jr, C. U., Wang, L., *Int. SAMPE Technol. Conf.*, 1997, 29, 77.

[43] Patton, R. D., Pittman, Jr, C. U., Wang, L., Hill, J. R., Day, A., *Compos. A*, 2001, 33, 243.

[44] Yamamoto, K., Otsuka, H., Takahara, A., Wada, S. I., *J. Adhes.*, 2002, 78, 591.

[45] Xu, H. Kong, Y.H., Yang, Z. B., *Chin. J. Mater. Res.*, 2003, 17, 127.

[46] Lee, A., Lichtenhan, J. D., *Macromolecules*, 1998, 31, 4970.

[47] Lichtenhan, J. D., Schwab, J. J., *Int. SAMPE Technol. Conf.*, 2000, 32, 185.

[48] Mather, P. T., Jeon, H. G., Haddad, T. S., *Polym. Prepr.*, 2000, 41, 528.

[49] Haddad, T. S., Choe, E., Lichtenhan, J. D., *Mater. Res. Soc. Symp. Proc.*, 1996, 435, 25.

[50] Haddad, T. S., Stapleton, R., Jeon, H. G., Mather, P. T., Lichtenhan, J. D., Phillips, S. H., *Polym. Prepr.*, 1999, 40, 496.

[51] Phillips, S. H., Blanski, R. L., Svejda, S. A., Haddad, T. S., Lee, A., Lichtenhan, J. D., Feher, F. J., Mather, P. T., B. S. Hsiao, B. S., *Mater. Res. Soc. Symp. Proc.*, 2000, 628, CC4.6.1.

[52] Blanski, R.L., Phillips, S. H., Chaffee, K., Lichtenhan, J. D., Lee, A., Geng, H. P., *Polym. Prepr.*, 2000, 41, 585.

[53] Haddad, T. S., Lee, A., Mather, P. T., Phillips, S. H., *Polym. Prepr.*, 2000, 41, 584.

[54] Lu, S., Martin, G. C., *Conf. Proc/Annu. Tech. Conf.*, 2003, 2, 1893.

[55] Constable, G. S., Coughlin, E. B., Lesser, A. J., *Conf. Proc/Annu. Tech. Conf.*, 2003, 2,1663.

[56] Li, G., Wang, L., Toghiani, H., Pittman, Jr, C. U., Daulton, T. L., Koyama, K., *Macromolecules*, 2001, 34, 8686.

[57] Li, G., Wang, L., Toghiani, H., Daulton, T. L., Pittman, Jr, C. U., *Polymer*, 2002, 43, 4167.

[58] Gupta, S. K., Schwab, J. J., Lee, A., Fu, B., Hsiao, B. S., *Int. SAMPE Symp. Exhib.*, 2002, 47, 1517.

[59] Feher, F. J., Lucke, S., Schwab, J. J., Lichtenhan, J. D., Phillips, S. H., Lee, A., *Polym. Prepr.*, 2000, 41, 526.

[60] Haddad, T. S., Mather, P. T., Jeon, H. G., Romo-Uribe, A., Farris, A. R., Lichtenhan, J. D., *Mater. Res. Soc. Symp. Proc.*, 1998, 519, 381.

[61] Mantz, R. A., Jones, P. F., Chaffee, K. P., Lichtenhan, J. D., Ismail, M. K., Burmeister, M., *Chem. Mater.*, 1996, 8, 1250.

[62] Xu, H. Y., Kuo, S. W., Lee, J. Y., Chang, F. C., *Polymer*, 2000, 43, 5117.

[63] Pellice, S. A., Fasce, D. P., Williams, R. J. J., *J. Polym. Sci. Part B: Polym. Phys.*, 2003, 41, 1451.

[64] Lee, A., *Mater. Res. Soc. Symp. Proc.*, 1999, 576, 343.

[65] Philips, S.H., Gonzalez, R. I., Chaffee, K. P., Haddad, T. S., Hoflund, G. B., Hsiao, B. S., Fu, B. X., *SAMPE*, 2000, 45, 1921.

[66] Huang, J. C., He, C. B., Xiao, Y., Mya, K. Y., Dai, J., Siow, Y. P., *Polymer*, 2003, 44, 4491.

[67] Fu, B. X., Namani, M., Lee, A., *Polymer*, 2003, 44, 7739.

[68] Lichtenhan, J. D., Otonari, Y. A., Carr, M. J., *Macromolecules*, 1995, 28, 8435.

[69] Haddad, T. S., Lichtenhan, J. D., *Macromolecules*, 1996, 29, 7302.

[70] Bharadwaj, R. K., Berry, R. J., Farmer, B. L., *Polymer*, 2000, 41, 7209.

[71] Tsuchida, A., Bolln, C., Sernetz, F. G., Frey, H., Mulhaupt, R., *Macromolecules*, 1997, 30, 2818.

[72] Lee, A., Lichtenhan, J. D., *Macromolecules*, 1998, 31, 4970.

[73] Pan, G., Mark, J. E., Schaefer, D. W., *J. Appl. Polym. Sci. B*, 2003, 41, 3314.

[74] Choi, J., Kim, S. G., Laine, R. M., *Macromolecules*, 2004, 37, 99.

[75] Liang, K., Toghiani, H., Pittman, Jr, C. U., *J. Polym. Sci. Part A*, 2005, 43, 3887.

[76] Tamaki, R., Tanaka, Y., Asuncion, M. Z., Choi, J., Laine, R. M., *J. Am. Chem. Soc.*, 2001, 123, 12416.

[77] Cho, H. S., Mississippi State University, MS. Ph.D. dissertation research (following a modification of the procedure of Tamaki, R., Tanaka, Y., Asuncion, M. Z., Choi, J., Laine, R. M., *JACS*, 2001, 123, 12416).

[78] Grigat, E., Putter, R., *Angew. Chem. Int. Ed.*, 1967, 6, 206.

[79] Shimp, D. A., Christenson, J. R., Ising, S. J., *AroCy Cyanate Ester Resins: Chemistry, Properties and Applications*; Rhone-Poulenc: Louisville, KY, (1991).

[80] Bauer, J., Bauer, M., *Macromol. Chem. Phys.*, 2001, 202, 2213.

[81] Liang, K., Mississippi State University, MS. Ph.D. dissertation research.

CHAPTER VII

SUMMARY AND CONCLUSIONS

Recent advances in generating nanostructured materials with novel material properties have stimulated research to create macroscopic materials by designing structures at the nanometer scale. Development of nanocomposites is one of the rapidly evolving areas of composites research.

The specific creation of controlled nano-scale sized phases in nanocomposites has been, and still is, a major synthetic challenge. Nano-biotechnology, nano-electronics and nano-structured materials represent areas where this challenge needs to be solved to prepare structures for architecture-property studies.

Nano-structured materials can be made using a bottom-up approach where materials will be made by building larger structures from atoms or molecules. This differs from all previous manufacturing processes which have used the top-down approach, where raw materials get pressed, cut or ground to smaller sized phases and then combined into products.

Our work with POSS nanoparticles fits into the bottom-up approach. Nanocomposites have been constructed from individual POSS molecules with molecular diameters in the ~1 to 2 nm range. The properties of nanostructured composites are highly structure/size dependent. Therefore, understanding how to make polymer/POSS

systems, where individual POSS molecules constitute the dispersed phase, constitutes a way to prepare the smallest of all phase sizes. In fact, it is a fair question to ask if a POSS/organic copolymer or a curd POSS/organic resin system is a nanocomposite or not if the POSS monomer unites are molecularly dispersed. In this dissertation, such systems are considered nanocomposites at the borderline of composites and homogeneous molecular materials.

Can POSS nanophases be dispersed or chemically bonded into materials as single molecules, small groups of POSS or larger groups of POSS with aggregate diameters from 3-100 nm or more? Larger phase-separated aggregates, ranging into the micron diameter region, might also be designed. Various classes of aggregates can be envisioned including crystallized POSS, various chemically bonded POSS functions within aggregates or aggregates with chemical bonds between the phase-separated POSS molecules and the resin (Figure 7.1). Such phases may be envisioned with high to no crystalline order and sizes form a single POSS molecule up to micron sized phases.

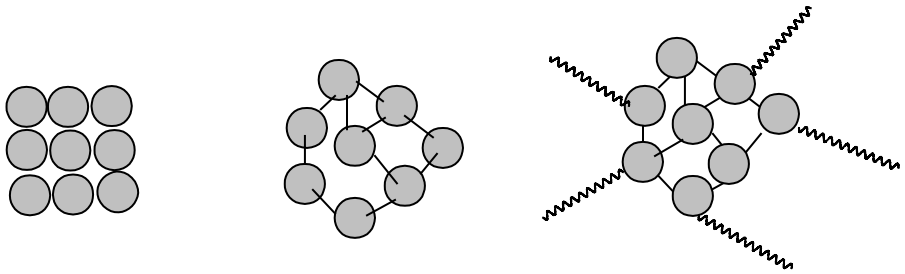

Figure 7.1 Types of POSS aggregations: (1) crystallized POSS (2) chemical linkages between POSS (3) chemical bonds of the phase separated POSS to the resin

Nonfunctional POSS molecules (octamethyl(T_8)POSS for example) can be dispersed physically into organic polymer matrices without any covalent bonding developed during physical blending. POSS-POSS interactions almost always dominate. Therefore, this results in various states of POSS aggregation (crystallized POSS) forming separate phases instead of dissolution. However, monofunctional or multifunctional POSS compounds can form covalent bonds with organic monomers of the thermoset or thermoplastic systems to become part of the polymer during copolymerization. POSS aggregation can occur in thermoplastic polymers containing pendant POSS groups. Pendant POSS groups, randomly incorporated in thermoplastic, could aggregate to form the high POSS domains (Figure 7.2).

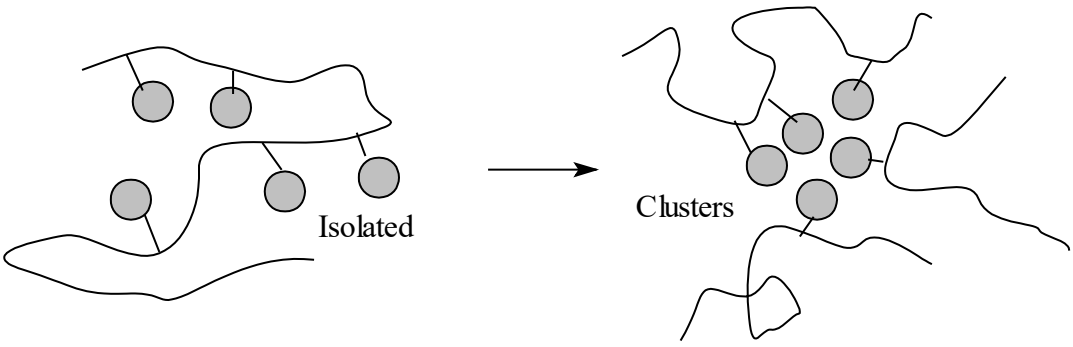

Figure 7.2 POSS aggregation in the thermoplastic polymer

A major theme of this research was to find ways to molecularly disperse POSS in thermoset and thermoplastic systems or to define the size of larger aggregates which might form instead. What combination of factors compete and which dominate? Then, properties were compared after different systems were characterized.

In order to investigate how the type of morphology and the size of aggregated POSS particles affect the properties of nanostructured composites, both monofunctional and multifunctional POSS monomers were incorporated into crosslinked resin matrices (acrylics, vinyl esters, phenolics and epoxides) to make POSS nanocomposites by using the bottom-up syntheses. The wt% of POSS in each polymer system has been changed to see if aggregation had an onset loading and if phase size could be controlled.

The monofunctional 3-methacrylylpropylheptaisobutyl-T_8-polyhedral oligomeric silsesquioxane (MA-POSS) was used to generate poly(isobutyl methacrylate-co-butanediol dimethacrylate). Thus, a series of resins were prepared where the amount of MA-POSS was one variable and the crosslink density was another variable. The MA-POSS wt% (5-30 wt%) was varied and the BDMA wt% (1-5 wt% of BDMA) was varied to change the crosslinking density of these networks. Several nm to micro-sized POSS aggregations were observed in the P(iBMA-co-BDMA-co-MA-POSS) with 3 and 5 wt% BDMA. The average size of POSS-rich particles increased from 1.3 to 2.9 μm with an increase in POSS contents from 5 to 30 wt% at the constant higher crosslink density (5 wt% BDMA). The interaction between the functional group on the POSS cage and the iBMA and BDMA segments is weak in the MA-POSS. Therefore POSS aggregates form. However, the modulus still increased because the POSS aggregates acted like noncovalent crosslinks (Figure 7.2). This explains why the P(iBMA-co-5wt%BDMA-co-MA-POSS) nanocomposites exhibited slightly higher storage modulus values at $T>T_g$ than those of pure P(iBMA-co-5wt%BDMA), whereas the reverse was found at lower BDMA contents (1 or 3 wt%).

The multifunctional 3-methacryloxypropyl-POSS cage mixture (T_8, T_{10} and T_{12}) and the single octa(3-methacryloxypropyldimethylsiloxy)(T_8)POSS system were incorporated into a vinyl ester networks. Since each methacrylate function on every POSS molecule should have a reactivity similar to the VE methacrylates, we might expect all POSS monomers would have a high probability of reacting with the VE monomers early in the polymerization. Therefore, even though the gel point will be reached early, the phase-separation of POSS would be retarded. In agreement with this expectation, most POSS molecules were molecularly dispersed into the VE resin matrices. However, POSS-rich particles from 20 nm to several microns were still detected in the VE nanocomposites containing from 10 to 20 wt % of POSS. These POSS aggregations were bonded to each other also to the VE resin. The resulting particles were composed of POSS molecules which contained a small fraction of VE resin (X-EDS). These POSS/VE nanocomposites exhibited progressively higher T_g and E' values (in the rubbery region) as the POSS loading increased. The nanocomposites' properties increased with an increase of POSS content even when POSS aggregation-phase separation increased. These mutifunctional POSS derivatives can form several covalent bonds with the matrix, becoming a hub for cosslinking "spokes" into the resin. This crosslinking enhances T_g and modulus. But several other effects (dispersed phase generation by aggregation, for example) must be operating.

One difunctional and two multifunctional POSS macromers, dichloromethylsilylethylheptaisobutyl(T_8)POSS, trisilanolheptaphenyl-POSS, and poly(phenylsilsesquioxane) uncured POSS were chemically dispersed into a phenolic

resin. Curing generated crosslinked networks. In addition, the nonfunctional octaisobutyl(T_8)POSS was physically blended into the phenolic resin. The phenolic resin nanocomposites containing each one of these three functional POSS monomers exhibited viscoelastic improvements versus those of the neat phenolic resin or the phenolic resin/ octaisobutyl(T_8)POSS composites. Each of these three POSS monomers was dispersed molecularly within the crosslinked phenolic resin. However, the phenolic resin/POSS nanocomposites containing the octaisobutyl POSS exhibited phase-separated, crystalline POSS particles. The size of these POSS aggregates increased from 30 nm to 1μm with an increase of octaisobutyl POSS content from 3 to 5 wt%.

Octaaminophenyl(T_8) and dodecaaminophenyl(T_{12})POSS were incorporated into the epoxy (EPON-828)/4,4'-diaminodiphenylmethane (DDM) resin. The epoxy resin/DDM nanocomposites containing T_8 POSS or T_{12} POSS exhibit higher E' ($T>T_g$) and T_g values than those of the neat epoxy. Both of these multifunctional aminophenyl POSSs systems are molecularly dispersed and chemically bonded into the epoxy systems as either single POSS molecules or small groups of POSS. The aminophenyl functions of these POSSs easily copolymerize with resin's epoxide functions. Each POSS cage can serve as a network crosslinking site. Therefore, both multifunctional aminophenyl POSSs might become part of the polymer during the polymerization, providing the increase in T_g and modulus.

The control of POSS aggregation dispersed phase size by the variation of POSS wt% led to substantial changes in the mechanical and thermal properties of the POSS nanocomposites. Several features that favor molecular dispersion were demonstrated.

However, a detail fundamental understanding of how to control dispersion size level of POSS nanostructured chemicals into the resin matrices remains elusive. Gaining such control is critical to create macroscopic materials with specifically-tailored and nanometer-sized dispersed POSS phases. Are single POSS molecule dispersions created or are POSS aggregates on the scale of 2 to 5-10 nm present? This is a difficult question to answer without high resolution TEM and small angle neutron scattering studies. There are no model studies to answer this question yet. Therefore, future research is required in order to learn how to prepare specific and narrow sized POSS aggregate dispersions in a variety of thermoset and thermoplastics. This is even more challenging if the goal is extended to each of the types of aggregates shown in Figure 7.1.

Studies of the effect of POSS aggregation size on the properties of POSS nanocomposites will need to be greatly expanded with precise size control of the aggregation size. For example, studies need to be performed on the mechanical properties of composites having (1) the same POSS wt% but specific controlled aggregate sizes over a range of sizes (2) several different POSS wt% with the same particle sizes (3) varying the particle sizes in item (2) and various POSS aggregate sizes where the particle surface area is held constant by varying wt% of POSS. In order to do these studies, more research must be done to learn how to gain the synthetic control to achieve the above series.